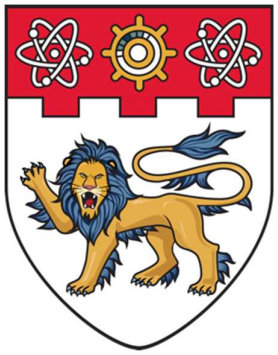

NANYANG TECHNOLOGICAL UNIVERSITY
SINGAPORE

LAND RECLAMATION AND SOIL IMPROVEMENT USING DREDGED SLURRY AS FILL

LAM KOK PANG

School of Civil and Environmental Engineering

2017

LAND RECLAMATION AND SOIL IMPROVEMENT USING DREDGED SLURRY AS FILL

LAM KOK PANG

School of Civil and Environmental Engineering

Final Report submitted to

the Nanyang Technological University

in partial fulfilment of the requirements for the degree of

Doctor of Philosophy

2017

ACKNOWLEDGEMENTS

The pursue of Ph.D. is never easy for part-time candidate. For me, this was a constant struggle for time, focus and energy between work, family, social life and putting the thesis together. There are many wonderful people whom I am hugely indebted to, who in their own kind ways assisted and supported me in this journey to attain one of my childhood dreams.

First and foremost, I would like to express my gratitude to my supervisor Professor Chu Jian for his guidance, patience, support and encouragement to complete this dissertation. His grit, energy, positivity, enthusiasm and perservance is truly infectious. He is a great role model that I look up upon and I am truly blessed for him to be my mentor and I am eternally grateful for that.

I am also grateful to have Associate Professor Tan Soon Keat for his kind support and guidance as my co-supervisor.

Special thanks to my wife, Dr. Zheng Sha, for encouraging me to embark on the Ph.D. journey which have enriched our lives together with great lessons. Time is absolutely precious and we shall never take time for granted. Sacrifices, tradeoffs and adjustment of priorities had to be made. I am thankful for her kind reminders that I should work on my thesis whenever I have pockets of free time and indebted eternally for her companionship, support, understanding, and her unwavering beliefs that I can complete what I started.

I and also greatly grateful to my fellow researchers, Dr. Wu ShiFan, Dr. Hailei, Dr. He Jia, Dr. Guo Wei, Dr. Vu Thu Chan, Dr. Li Bing, Cheng Hao, Hao Jie and Joseph for their generous sharing and contributions. The completion of this thesis would not be possible without them.

Finally, I would like to thank my family, friends, employers, colleagues, contractors, consultants who had provided me their kind supports, encouragement and the space I need to complete this thesis.

TABLE OF CONTENTS

SUMMARY

Dredged seabed materials are proposed as an alternative reclamation fill for sand depleted cities. Hydraulic dredging and infilling are identified as the most efficient and cost-effective ways to place large quantities of dredged materials at shallow depth when dump barges cannot be used. However, the intermixing of the dredged materials with seawater in hydraulic dredging will destroy its soil fabrics forming slurry with poor engineering properties. These will bring about many site challenges affecting project costs, schedule and meeting the specified technical requirements. A series of laboratory model tests and two field trials were carried out.

Laboratory model tests were carried out to examine the behaviors of natural and flocculants treated sedimentation process of dredged slurries. Findings showed that the inclusion of flocculents although could bring faster settling by forming larger focs in the dredged slurry suspension, they also modified the sediments fabrics causing larger consolidations to occur. Laboratory model tests were also carried out to evaluate the performance of vacuum preloading techniques to improve different types of marine clays with very high water content. The model tests concluded that vacuum preloading technqiues are effective in enhancing the engineering properties of different high water-content marine clay samples. However, the degree of improvement in the marine clay samples were observed to reduce with increasing distance from the prefabricated drains transmitting the vacuum.

In the first field trial, a combined membraneless vacuum and embankment preload field trial was carried out over a newly reclaimed land. Site observations concluded that the performance of this technique were largely affected by vacuum pump's reliability and the accuracy of the soil profiles obtained. In the second field trial, hydraulic dredged slurries were used as the main infill. Key site challenges in using dredged slurries as infill were described and illustrated.

A new land reclamation method of applying vacuum through horizontally placed prefabricated horizontal drains was proposed. Laboratory studies and numerical

analysis were carried out to examine the feasibilities of this method. The results showed positive outcomes in addressing the key site challenges while improving operational productivity and increase infill capacity when dredged seabed slurry are used as reclamation infill. Several recommendations are proposed for further study to develop the new land reclamation method.

LIST OF PUBLICATIONS

Submitted (First Author)

1. Lam, K.P.[1], Kou, H.L.[2], He.J.[3] and Chu, J.[4] (2017) Use of a waste-based binder for high water content soil treatment. Journel of Materials in Civil Engineering

2. Lam, K.P.[1], Wu, S.F.[2], and Chu, J.[3] (2017) A field trial of BeauDrain-S vacuum preloading for soil improvement in Singapore. Ground Improvement

Published (Not as First Author)

3. Li, B.[1], Wu, S.F.[2], Chu, J.[3], and Lam, K.P.[4] (2011). Evaluation of Two Vacuum Preloading Techniques Using Model Tests. Geo-Frontiers 2011: Advances in Geotechnical Engineering**:** 636-645.

4. Chu, J.[1], Yan, S.W.[2], and Lam, K.P.[3] (2012). "Methods for improvement of clay slurry or sewage sludge." Proceedings of the Institution of Civil Engineers-Ground Improvement **165**(4): 187-199.

5. He, J.[1], Chu, J.[2], Tan, S.K.[3], Vu, T.T.[4], and Lam, K.P.[5] (2017). "Sedimentation behavior of flocculant-treated soil slurry." Marine Georesources & Geotechnology **35**(5): 593-602.

LIST OF TABLES

LIST OF FIGURES

LISTS OF SYMBOLS

a	Width of band-shaped drain
b	Thickness of band-shape drain
c	Cohesion
c_h	Horizontal coefficient of consolidation
c_r	Reduced Cohesion
D_{50}	Particle diameter for which 50 % of the soil particles are smaller
D_C	Diameter of equaivlent cylinder
dQ_1 , dQ_2	Infinitesimal volume flow
d_e	Diameter of influence area
d_m	Diameter of a circle with an area equal to the cross sectional area of mandrel
d_w	Equivalent diameter of drain
d_s	Diameter of smear zone
δ_{ult1}	Ultimate Settlement
E_{ref}	Young modulus
$F(n)$	Drain spacing factor
F_s	Smear effect
F_r	Well resistance
k_h	Horizontal permeability

k_w	Reduced permeability in the smear zone
k_v	Vertical permeability
n	Spacing Ratio
O_{50}	Apparent Opening Size, 50% of the opening in the geotextile are smaller
P_a	Atmospheric Pressure
q_w	Discharge capacity
r	Radical coordinate
r_e	Radius of influence area
S	Vertical drain spacing
S_n	Settlement observations
S_u	Undrained shear strength
S_{ult}	Ultimate primary settlement
U_{avg}	Average degree of consolidation
u	Excess pore pressure
u_0	Initial pore water pressure or hydrostatic pore water pressure
u_t	Excess pore pressure at time, t
u_s	Suction line
z	Depth of soil
z_n	Depth below which all soil is normally consolidated

γ_w	Unit weight of water
γ'	Unit weight of soil
γ_{sat}	Unit weight of saturated soil
γ_{unsat}	Unit weight of unsaturated soil
σ_T	Total stress
σ'_i	Effective stress before vacuum
σ'_f	Final Effective stress during vacuum
$\Delta\sigma'$	Efficiency of vacuum pump
ϕ	Friction Angle
Φ_r	Internal Friction Angle
Ψ	Dilatancy Angle

CHAPTER 1 INTRODUCTION

1.1 Background

Growing demand for land reclamation

Land reclamation is espoused by many countries worldwide as a key strategy to expand their coastal land mass to drive, support and protect economic and population growth. It has been regarded as an effective measure to resolve land shortages to accommodate infrastructure, industrial, commercial, residential, military and parks developments.

Difficulties in obtaining granular fill (sand)

Land reclamation is a process of using large amount of fill materials to form new land mass from shorelines, riverbanks and water bodies such as the sea and lakes. Sand is considered as the best materials to be used for fill as they are easy to transport and can be handled efficiently and cost effectively in large quantities by specially developed vessels and machineries. The reclaimed land using sand fill can be densified quickly and would have little or no long-term consolidation and settlement problems.

However, with increasing numbers of land reclamation projects, demand and competition for sand has risen significantly. Thus, sand become costlier as its availability depletes quickly. Today, sand is an important strategic resource that is not necessarily available for coastal cities like Singapore who has already exhausted its own sand and land fill resources and must rely on fill imported to continue their reclamation works.

Singapore's dependence on imported sand was deeply felt when both Indonesia and Malaysia instituted ban against sand export to Singapore. The sand ban caused stagnation to many on-going reclamation projects and could have led to pull out of promised investments. To overcome the situation, Singapore diversified its imported sand to multiple distant sources such as Vietnam, Cambodia, Myanmar, Philippines and etc. such that reclamation works could continue. Despite this diversification

strategy and paying a premium for the distant sand, the supply of sand remains highly volatile and uncertain to allow timely and consistent sand supply due to protests from environmental groups, changes in political policies and natural elements at the source countries.

Need for alternative fill to replace sand fill

The Ministry of National Development has projected that Singapore could have a population of between 6.5 to 6.9 million by 2030 (MND, Population White Paper, 2013). To accommodate for this larger population growth, Singapore will require 76,600 ha of land, an increase from the current supply of 71,000 ha (MND, Land Use Plan, 2013) and land reclamation will be one of the key strategies to provide the additional 5,600 ha of land needed.

It is inevitable that the difficulties faced in sand supply and increasingly costlier sand fill will become a major limitation to the future reclamation in sand depleted coastal cities like Singapore. This foreseeable demand for considerable amount of fill materials has articulated the motivation to explore alternative fill that could be available in large quantities cheaply and readily to replace some, if not most of the sand needed for future reclamation.

Dredged seabed slurry as fill materials

Extensive deposits of soft marine clay in the territorial waters of Singapore have been reported and could be a possible reclamation fill source for future reclamation works (Yong, 1989). These deposits of soft marine clay were also reported to be available in large quantities in the coastal regions of many expanding coastal cities that need large amount of fill materials to satisfy their reclamation works.

The used of dredged seabed slurry as reclamation fill is not a new idea. However, the primary motives for using them as fill is not to replace sand but to fulfill contractual obligations and avoid costly tariffs imposed for their disposal into regularized dumping sites. This is because, the use of dredged seabed slurry as fill is not popular

as they are difficult to handle and have poor engineering properties due to their high water and fines content.

Current paradigm

Generally, the available literature shows that reclamation using mainly dredged seabed slurry as fill and the subsequent soil improvement on the deposited slurry fill although is not infeasible, but is conceivable to be cluttered with operational, technical and engineering challenges that need to be addressed and overcome. As a consequence, it will take more time and costs to complete while producing a reclaimed land mass of perceived lower quality when comparing to a typical reclamation project using sand fill.

1.2 Research objectives

The aim of this thesis is to help narrow the gaps in knowledge and share practical experiences in the use of dredged seabed slurry. This was done by examining, identifying and understanding the problems associated when dredged seabed slurry are used as land reclamation fill and the subsequent soil improvement works through the conduct of laboratory model tests, field trials and simple numerical model analysis. With new and better understanding, appropriate planning provisions, land reclamation methodology and engineering solutions can be developed in a more cost-effective, time-efficient and technically sound ways to meet and satisfy the quality and other requirements of a reclamation project. The key research objectives established for this thesis are as follows:

i. To review existing land reclamation and soil improvement techniques and to identify and understand the key technical challenges associated with the use of dredged seabed slurry as fill for land reclamation

ii. To examine the sedimentation process and consolidation behavior of hydraulically placed soil slurry and the consolidation behavior of lumpy soil under different vacuum or other preloading methods

iii. To carry out large-scale field trials to evaluate and validate the technical and operational feasibility of:
   a. the proposed vacuum technique to improve soft marine clay deposits in existing reclaimed land, and
   b. the proposed land reclamation technique for using dredged seabed slurry as reclamation fill.

iv. To propose practical, cost-effective and time-efficient engineering solution to overcome the operational and technical challenges associated with the use of dredged seabed slurry as fill for land reclamation.

1.3 Scope of works

The scope of works for this thesis include:

i. Review existing literatures on land reclamation and soil improvement techniques to identify and understand the key technical challenges associated with using dredged seabed slurry as fill materials for land reclamation.

ii. Examine the sedimentation process of the dredged slurry and the time needed for the suspended particles to settle and form sediments under the action of gravity. Study how the sedimentation process and soil formation can be expedited through the applications of selected commercial available flocculants.

iii. Examine and compare the consolidation behavior and the effectiveness of vacuum preloading technique in treating soil samples using a highly instrumented single PVD consolidation tank.

iv. Assess the field performance of the membraneless vacuum preloading technique in treating marine clay layer in reclaimed land.

v. Study the viability in using the dredged seabed slurry as reclamation fill and examine the design and construction process of a load bearing platform over the dredged seabed slurry deposits through large-scale field trials and numerical analyses.

vi. Examine and validate the proposed new reclamation method of using vacuum with horizontal prefabricated drains to overcome the constraints and challenges in using dredged seabed slurry as fill for land reclamation.

Observations, analysis and learning lessons of the laboratory model tests and field trials are shared and discussed. It is the hope of the author that this information can provide reference and new ideas to inspire further research works, opening up new possibilities and creating innovative capabilities in using dredged seabed slurry fill for land reclamation in more cost-effective and time-efficient ways.

1.4 Outline of thesis

This thesis is organized into nine chapters.

Chapter One gives a quick glimpse on the dilemma faced by sand scarce cities such as Singapore and their dependence and risks faced in adopting imported sand as key strategy to sustain their land reclamation projects. This backdrop defined the purpose of this thesis where dredged seabed slurry is proposed as the alternative reclamation fill.

Chapter Two reviews existing literatures on land reclamation demand, materials and methods applied. Soil improvement techniques such as reinforced soil and vacuum

preloading to treat and improve soft marine clay and dredged slurry with high fines are also discussed.

Chapter Three examines the behavior of natural and flocculant acelerated sedimentation process from dredged seabed slurry through the conduct of multiple column tests.

Chapter Four examines consolidation behavior of different types of clay samples treated by vacuum preloading and compares the results of two different vacuum preloading techniques

Chapter Five presents the setup, field observations and challenges encountered in using the membraneless vacuum preloading technique to treat marine clay layer with varying thickness.

Chapter Six presents the field observations and lessons learnt in the field trial to use dredged seabed slurry as reclamation fill. The technical difficulties in forming the load bearing platform over the dredged seabed slurry using geotextile inclusions are discussed.

Chapter Seven proposes the application of the newly developed land reclamation method of using vacuum with horizontal prefabricated drain as the solution to help overcome the technical and operation challenges encountered in the laboratory and field trials.

Chapter Eight concludes the major findings of this PhD thesis and the recommendations of possible areas for further research.

CHAPTER 2 LITERATURE REVIEW

2.1 Introduction

With the diminishing supply and increasing demand of granular fill, it will be inevitable to look for alternative fills that are readily available, cheap and in abundant supply to meet the demand for future reclamation projects. Dredged seabed is proposed in this thesis as it fulfills these criterions. However, seabed materials are usually high in water content and fines. They can appear to exists either in lumpy, semi-solid or slurry form when they are dredged. This make them difficult to handle and transport efficiency in large quantities. The land mass formed using dredged seabed as infill are highly compressible, soft with poor engineering properties.

To overcome these constraints, a good understand on the existing reclamation fill materials and their properties are reviewed, in particularly the characteristics of clay. This is because, even in small amount, clay will significantly affects the engineering properties of the dredged seabed materials when used as reclamation fill. Reclamation methods and equipment are also presented in this chapter to examine the feasibility to handle large quantity of dredged seabed hydraulically in slurry form for efficacy, productivity and cost effectiveness. Finally, different soil improvement techniques are studied to evaluate the best methodology to improve the dredged seabed fill.

2.2 Land reclamation fill

All land reclamation projects will require considerable amount of fill materials. Therefore, the type of fill materials used will have significant impacts to the cost, time and quality of the reclamation projects. The fill materials' cost and their extraction, transportation, re-handling and final placement will be the major costs in a reclamation project which will also affect the ground improvement method implemented to satisfy the project's requirement and timeline. Hence, fill material selection is an extremely important decision-making process. In this section, the most common types of fill materials namely sand, soil and clay will be discussed.

2.2.1 Sand fill

Sand is granular, cohesionless and nonplastic materials. They are the most popular and suitable land reclamation fill materials for the following reasons:

i. They are easy to extract, transport and re-handle. Hydraulic filling is very efficient in re-handling large quantities of granular fill.
ii. Form soil mass with high permeability. No drainage problems during and after reclamation.
iii. The reclaimed land has high bearing capacity after compaction,
iv. They can be compacted quickly by well-developed densification methods to satisfy reclamation requirement
v. There is no long-term consolidation and settlement of sand fill after compaction.

2.2.1.1 Quality and control

Sand used for land reclamation shall be well-graded with a good representation of sand particles over a wide range of sizes. The grain size distribution will affect the engineering behavior (Bo and Choa, 2004, Grim, 1959) and relative density (Chang et al., 2006) of the sand fill. Generally, a well-graded sand fill will give better compaction than a poor-graded or uniformly-graded sand fill.

The friction angle of the sand fill is recommended to be at least 30° corresponding to a relative density of 35% to ensure the provision of adequate shear strength for bearing capacity and slope stability of the reclaimed sand fill. The inner surface of the steel pipes that are used to transport hydraulically pumped sand will wear off faster when conveying sand with higher friction angle than sand with lower internal friction angle.

Sand used for reclamation fills shall not have high contents of clay, peat, or organic materials. Clay and peat when more than 10% by weight, will lead to difficulty in densifying the granular material. High shell contents in sand fills shall also be avoided as they they will lead to immediate settlement upon application of static and dynamic

loads. Chemical and heavy metal content of the sand shall be tested to ensure that they are within the stipulated regulatory limits such that the use of future reclaimed land will not be limited.

2.2.1.2 Compaction

Different sand sources and sand placement methods will lead to variations in the density of the sand fill. The determination of relative density either by void ratio or dry density, provides a measure of the compactness, strength and compressibility characteristics of sand fill and is used to evaluate their engineering behavior and adequacy to provide the desired properties (Chang et al., 2006, Van Impe et al., 2015).

Placement of sand by hydraulic filling will form loose granular fill with low shearing resistance and high compressibility which can be subjected to bearing capacity failure and large settlements (Bo et al., 2009). Bearing capacity failure can be prevented by improving the peak angle of shear strength of granular fill and minimizing settlement by enhancing the modulus of elasticity of the soil through deep densification treatment.

2.2.2. Earth fill

Earth fills are mixtures of heterogeneous materials. The key sources of the earth fill materials are usually from hill cuts and excavations of construction projects. It is the next popular fill material after sand. They are considered for reclamation fill for the following reasons:

i. They are easy to handle and transport in dry condition.
ii. Form soil mass with some permeability. Some drainage problem during and after reclamation are anticipated but can be resolved with proper planning and sequencing of works.
iii. They are compactable and can form stable fill with good load bearing capacity quickly in dry condition.
iv. The settlement of the reclaimed soil is very dependent on the compressibility of the heterogeneous soil fill.

The properties of earth fill can vary widely depending on the geological formations and soil layers where they are extracted. In Singapore, earth suitable for filling works are generally classified into two categories:

i. Coarse-grained soils. They shall include all passing through 63mm British Standard (BS) sieve. A percentage by weight retained on the 0.063mm BS sieve shall be at least 65%. The remaining 35% passing through the 0.063mm BS sieve shall contain a liquid limit not exceeding 70% and a plasticity index not exceeding 40%. Coarse-grain soils shall exclude all forms of rocks.

ii. Fine-grained soils. They shall include silt and clay that have a fraction of more than 35% passing through a 0.063mm BS sieve. The fraction of particle size passing through less than 2μm BS sieve should not be more than 80%. The liquid limit shall not exceed 60% and plasticity index not more than 30%. The moisture content of the soil shall be 40% or less.

Similar to sand fill, the chemical and heavy metal content of the soil fill shall be determined to ensure that they are within the stipulated regulatory limits and will not limit the use of the reclaimed land.

2.2.3 Clay fill

In civil engineering, clay often means clayey soils which are fine-grained, have plasticity and are cohesive (Holtz and Kovacs, 1981). The presence of even a small amount of clay minerals in a soil mass can noticeably affect the engineering properties. As the content of clay in the soil increase, the soil's behaviors will be increasingly governed by the properties of the clay. When the clay content is about 50% by weight, sand and silt grains are essentially floating in a clay matrix and have little effects on the soil's engineering behaviors.

The presences of water in clay will greatly affects their engineering response. Clay is usually not the preferred choice for reclamation fill for the following reasons:

i. They are difficult to handle.
ii. There are limited transportation options. Most are with low transport efficacy.
iii. Form soil mass of very low permeability causing drainage problems during and after reclamation.
iv. Form soil mass with little or no bearing capacity.
v. Soil mass formed will a take long time to settle.

This thesis proposes the use of dredged seabed slurry as fill to overcome the crunch in sand supply. Typically, most seabed is assumed to contain significant portion of clayey sediments. It is therefore important to understand the characteristics of these clayey materials and their interaction with water by examining the properties of clay and the soil formation process by sedimentation and self-weight consolidation of the dredged slurry.

2.2.3.1 Clay mineral structures

Clay minerals have very tiny crystalline substances, colloidal-sized crystals (diameter less than 1 um). They can only be seen with an electron microscope. They are formed primarily from chemical weathering of certain rock-forming minerals and are very active electrochemically. Chemically they are hydrous aluminosilicates plus other metallic ions. Water has great influence on the engineering behavior of clay minerals.

The individual clay crystal looks like tiny plates or flakes as shown in Figure 2.1. From X-ray diffraction studies, these flakes consist of many crystal sheets, which have a repeating atomic structure. There are two fundamental crystal sheets, the tetrahedral or silica, and the octahedral or alumina sheets. The ways in which these sheets are staked together with different bonding and different metallic ions in the crystal lattice, constitute the different clay minerals with different characteristics.

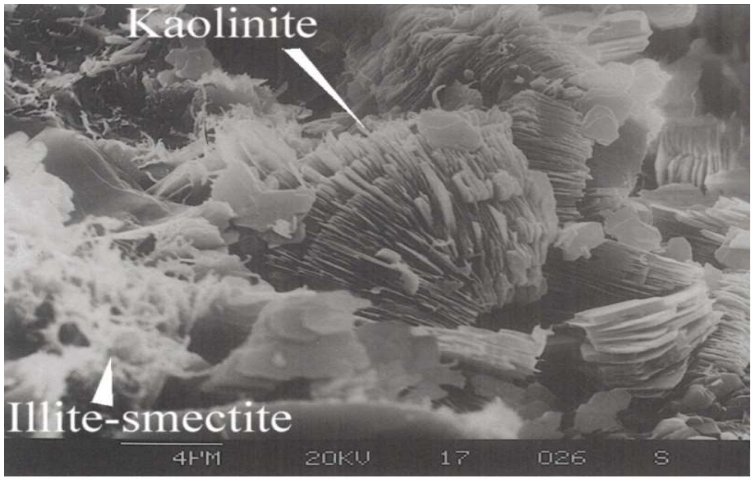

Figure 2.1 Scanning electron microscope (SEM) image of kaolinite and small amount of illite-smetite clay (Higley et al., 1997)

The tetrahedral sheet is basically a combination of silica tetrahedral units. A tetrahedral unit is composed of silica tetrahedral in which four oxygen atoms surround a single silicon atom. Figure 2.2(a) shows a single silica tetrahedron; Figure 2.2(b) shows how the oxygen atoms at the base of each tetrahedron are combined to form the tetrahedral sheet structure. Figure 2.2 (c) illustrates the common schematic representation of the tetrahedral sheet.

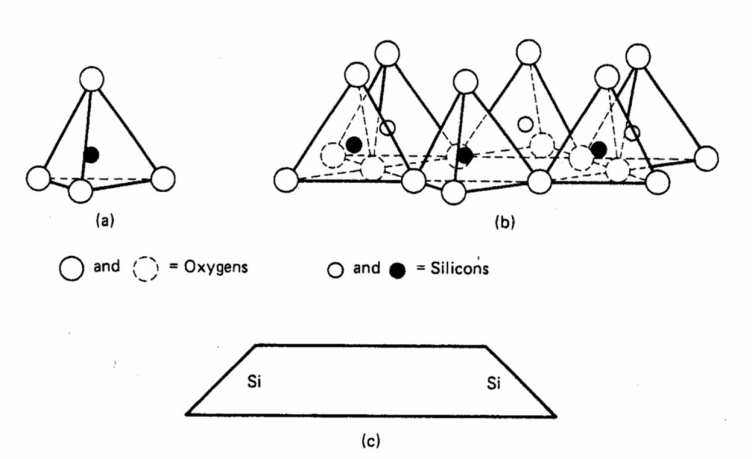

Figure 2.2 Clay mineral with tetrahedral sheet structure (Grim, 1959, Lambe, 1958)

The octahedral sheet composed of octahedral units consisting of six oxygen or hydroxyls enclosing an aluminum, magnesium, iron, or other atom. As single

octahedron is shown in Figure 2.3(a) and Figure 2.3(b) shows how the octahedrons combine to form a sheet structure. The rows of oxygens or hydroxyls in the sheet are in two planes. Figure 2.3(c) is a schematic representation of the octahedral sheet.

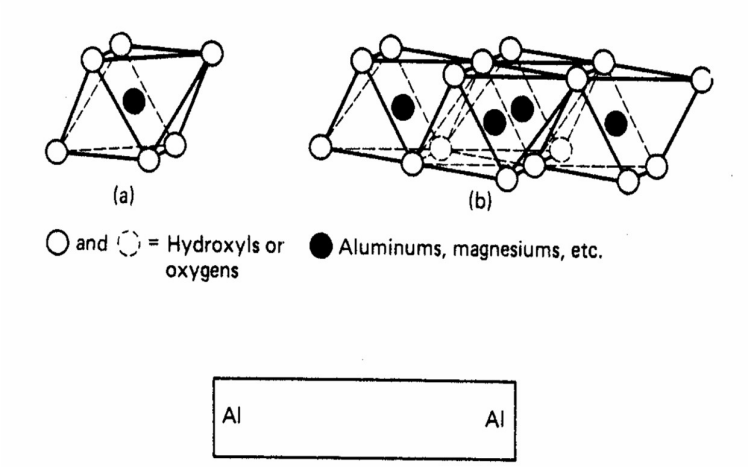

Figure 2.3 Clay mineral with octahedral sheet structure (Lambe, 1958, Grim, 1959)

Substitution of different cations in the octahedral sheet is rather common and leads to different clay minerals and affects their behavior. Since the ions substituted are approximately the same physical size, such substitution is called isomorphous. Common cation replacement includes aluminum (Al^{+3}) for silicon (Si^{+4}), magnesium (Mg^{+2}) for aluminum (Al^{+3}), and ferrous iron (Fe^{+2}) for magnesium (Mg^{+2}) in the ideal tetrahedral and octahedral sheets. Isomorphous substitution in clay minerals results in a charge deficiency in the crystal structure and a net negative charge on the mineral's surface.

Clay minerals are small particles with large specific surfaces which are very active. The surface activity of clay is defined as:

$$Activity, A = \frac{Plastic\ Index, PI}{clay\ fraction} \tag{2.1}$$

The clay fraction is usually taken as the percentage of the sample less than 2 μm. The relative sizes and specific surfaces of four common clay minerals and their specific surface are illustrated in Figure 2.4

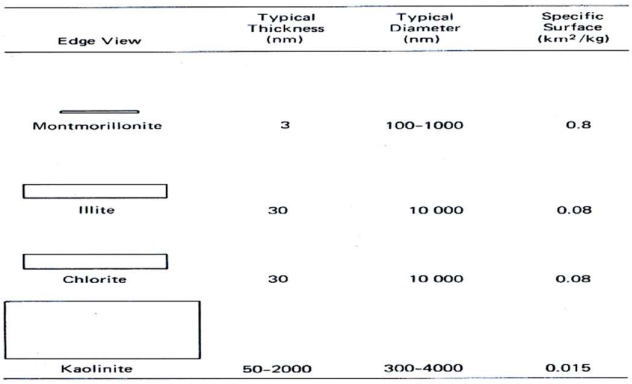

Figure 2.4 Relative sizes & specific surfaces of clay minerals (Holtz and Kovacs, 1981)

2.2.3.2 Interactions between water and clay minerals

Clay particles are usually hydrated in nature. In such state, there are layers of water surrounding each clay crystal. These layers of water are called adsorbed water, which greatly influence the structure of the clay soils and their engineering properties. The association of clay minerals and their adsorbed water layer provides the physical basis for soil structure. In general, water is adsorbed on the surface of the clay particles in the following ways:

i. Electrostatic attraction

Water molecule is electrostatically attracted to the surface of the clay crystal. The attraction of water to the clay surface is very strong near the surface and diminishes with distance from that surface. Gordon (Gordon and Mitchell, 1976) reported that some thermodynamic and electrical properties of the water next to the clay surface are different than that of "free water".

ii. Hydrogen bonding

Water is held to the clay crystal by hydrogen bonding whereby hydrogen of the water is attracted to the oxygen of hydroxyls on the clay surface.

iii. Negative charge surface

The negatively charged clay surface attracts cations present in the water. Since all cations are hydrated to some extent, they also contribute to the attraction of water to the clay surface. The source of negative charge at the surface of the clay crystal results from both isomorphous substitution and imperfections in the crystal lattice, especially at the surface. “Broken” edges contribute greatly to unsatisfied valence charges at the edges of the crystals. Since the crystal wants to be electrically neutral, cations in the water may be strongly attracted to the clay, depending on the amount of negative charge present.

Figure 2.5 shows a sodium montmorillonite and kaolinite crystal with a layer of adsorbed water on its surface. The thickness adsorbed water thickness is about the same. However, because of different particle size, the montmorillonite crystal will have much greater activity, plasticity, swelling, shrinkage, and volume change when loaded.

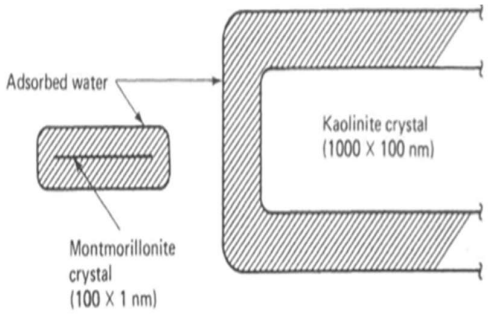

Figure 2.5 Adsorbed water layers on different clay crystal (Lambe, 1958)

2.2.3.3 Sedimentation of clayey soil slurry

Wang (Wang et al., 2015) reported that the water content of typical hydraulic dredged seabed materials would be ranging between 200% to 900%. The dredged slurry of seawater-soil mixture exists in flow state and will be pumped and deposited in a containment pond/structure. Therefore, a good understanding of its sedimentation

and consolidation process will enable us to appreciate and optimize the sediment formation process and predict their engineering behaviors.

The sedimentation and self-weight consolidation of slurry have been extensively studied as they have great importance in the mining and chemical industries. In civil engineering, it has practical importance in the management of dredged materials from capital and maintenance dredging for ports and waterways in terms of maximizing the Confined Disposal Facilities' (CDF) storage capacity (US, 2015) and reducing the cycle time needed for sedimentation. Research and experimental works in these field are typically carried out in the laboratories using settling columns.

The formation of the sediments from slurry would typically go through two stages. The first stage is known as the sedimentation stage which involves the conversion of discrete soil particles in a suspension into loose sediments and begins at the top of the slurry suspension while the second stage is the self-weight consolidation stage where the process starts usually after the sediments are formed. (Bo, 2008).

2.2.3.3.1 Sedimentation theories

Sedimentation is the process where the suspended solids in a fluid settle under the action of gravity. It is complex process and easily influenced by factors such as size, shape and densities of the suspended particles. The first scientific discussion on sedimentation process is by George Gabriel Stokes in 1851 where he proposed the terminal (or settling) velocity equation that he used for describing the relationship between settling velocity, densities, radius of particles, gravity and fluid viscosity. Kynch (Kynch, 1952) presented the well-known paper " A theory of sedimentation" where he proposed a kinematical theory of sedimentation based on the propagation of concentration waves in the suspension using only the continuity equation. In his theory, Kynch assumed that velocity of settling as a function of local concentration, one-dimensional and the particles are of the same size and shape. This simple model has great influence in the field of chemical and environmental engineering, particularly contributing to the development of thickening (Tory et al., 2013).

Kynch assumed that the aggregate of settled particles never consolidates in his sedimentation theory. Figure 2.6 provides a clear-cut illustration of the interrelation between settling and sediment formation. Uniformly dispersed particles settle and form a sharp interface between the dispersion and clear water with time. When the suspended particles in the dispersion reach the bottom surface, they form into sediments. The sediments are formed at the boundary between the dispersion and sediments. This boundary will change over time, tracing a "sediment formation line" until the dispersion has been fully converted to sediments. The uniform settling of particles and the lack of consolidation in the sediment make the sediment formation line straight.

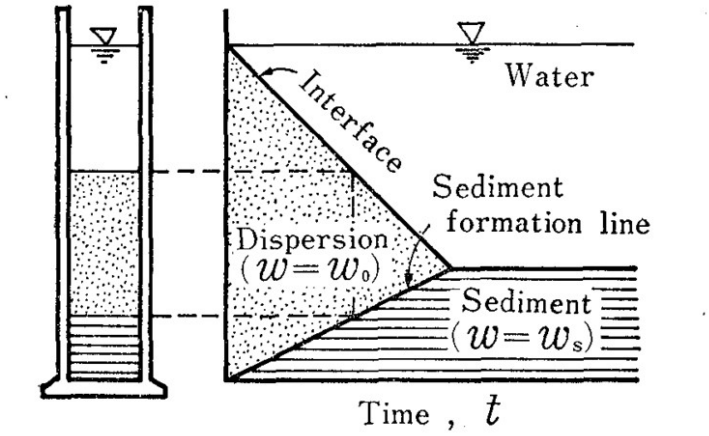

Figure 2.6 Idealized settling in Kynch's sedimentation theory (Imai, 1981)

While Kynch's theory gives a clear-cut concept of sediment formation, it is not adequate to describe the self-weight consolidation process of the sediment. McRoberts and Nixon (McRoberts and Nixon, 1976) extended Kynch's theory to investigate the sedimentation of silty soil slurry by taking into account of the consolidation effect. They concluded that Kynch's sedimentation theory is too simple to describe the complex phenomenon of the sedimentation of clayey-like slurries.

Modifications to Kynch's theory was first proposed by Fitch (Fitch, 1966) to account for a wide range of inexplicable sedimentation behaviors. In Fitch's modification (Fitch, 1979), he theorized that all steps of the sedimentation process are profoundly

affected by interfacial phenomena. Van der Waals or London forces if not over-powered by electrostatic repulsion (zeta potentials) or fluid-dynamic shear, will cause particles to cohere on contact. These give rise to three different modes of sedimentation: (i) Clarification in which flocculates are separated and settled independently; (ii) zone settling in which flocculates are incorporated into some solid structure so that they are all constrained to subside at more or less the same rate; and (iii) compression or compaction in which the solid structure is strong enough to exhibit a compressive yield value. The type of sedimentation that will occur in suspensions depends largely on the solids concentration and the relative tendency of the particles to cohere. The types of sedimentation are illustrated in Figure 2.7. The left side represent particles with little tendency to cohere, the right side represents particles for which the interparticle cohesion is strong. The vertical axis represents particle concentration with more concentrated suspension at the top.

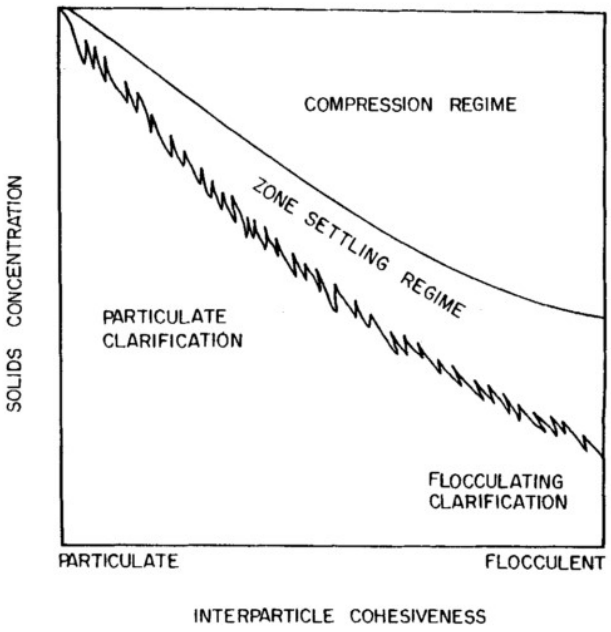

Figure 2.7 Types of Sedimentation (Fitch, 1979)

Clarification occurs at low solid concentration. Particles are generally far apart and free to settle independently resulting in free settling of isolated particles as every particle in theory falls freely with no interaction with other particles. These settling rates are governed by Stoke's law. However, when solid concentration becomes

slightly higher, “hindered settling” will be observed (Imai, 1980). In these cases, the fall of the large size particles are interrupted by collisions with the smaller particles falling at slower rates. These will result in the collision of particles. The collided particles will cohere to each other forming into clumps, or flocculate, resulting in increased settling rates. Then again, if the solid particles do not cohere, they will bump downward at their characteristic rates. Hence, there are two types of settling in clarification, namely the flocculent and the particle setting. There is no sharp boundary between the two as one grades gradually into the other. Clarification behavior is easily recognized as slower settling particles string out behind faster settling ones. The upper layers gradually thin out, or clarify. The settled solids will collect at the bottom in layers whose upper boundary rises as solid particles settle into it.

In slurry where the particles are more concentrated and crowded closer together, the particles will have tendency to cohere and form into some sort of floc structure. The mutual interactions among the flocs restricted their free fall forming sharp interface between the dispersion and clear water (Imai, 1980). This type of settling is usually called zone-settling and exhibits line-settling behaviors.

The final type of settling occurred when the concentration of the solid concentrating is higher than that of the zone-settling regime. This regime is termed “compression” or “compaction” settling where the pulp structure becomes so firm it develops compressive strength. Each layer of solid particles is able to transmit mechanical support to the layers above. In order to compact the structure to a higher solids concentration, a solid stress or squeeze must be exerted on it.

2.2.3.3.2 Sedimentation stages in clayey slurry

Imai (Imai, 1980, Imai, 1981) examined the sedimentation and sediment formation characteristics using dilute clay-water mixtures and concluded that the process of soil sedimentation can be divided into three stages as illustrates in Figure 2.8.

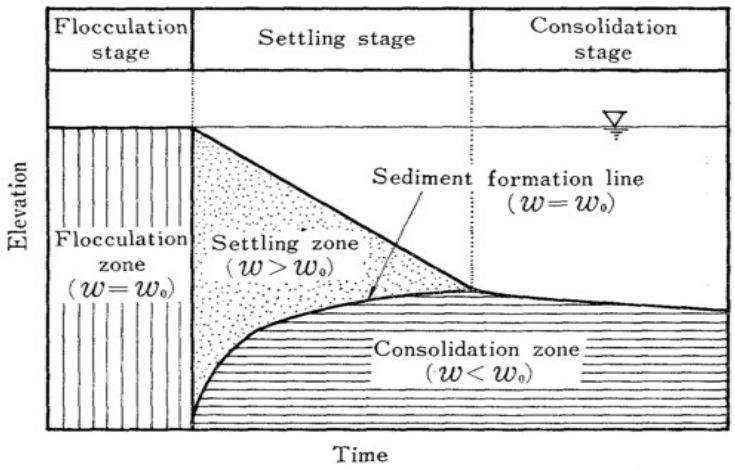

Figure 2.8 Sedimentation stages of clay-water mixture (Imai, 1981)

The process begins with flocculation. At this stage, only flocculation of the soil particles occurs throughout the entire depth and flocs are formed. The flocs will remain suspended in the dispersion where no settling can be observed.

The flocculation stage will transit into the settling stage when the newly formed flocs and solid particles gradually settle in the settling zone and form a layer of sediments at the bottom. Figure 2.8 illustrates the co-existence of the three different zones in the clay-water mixture in the settling stage. The most upper zone contains clarified water as flocs in the dispersion settled. The middle settling zone contains the diminishing dispersion of flocs and solid particles and the bottom most zone contains the gradually increasing consolidation zone. The boundary between the settling zone and the consolidation zone is the sediment formation line.

When the settling zone vanishes, the sedimentation process transits to the consolidation stage. In this stage, the whole sediment layer undergoes self-weight consolidation. Reduction of the sediment elevation will be observed over time as presented in the convex line. The decreasing gradient of the sediment formation line indicates that compression is taking place even at very low stresses until an equilibrium state is reached.

There are several notable differences between Imai's sedimentation mechanism and Kynch's sedimentation theory. Imai has considered flocculation zone at the early stage, non-uniformity of particle sizes in the settling zone which resulted in the non-linearity of the sediment formation line, non-uniformity of the consolidation zone and volume reduction during the consolidation stage in his studies.

2.2.3.3.3 Self-weight consolidation of sediments

When focs settle, the spacings and gaps at the bottom of the dispersion will be filled up and new layers of flocs will be formed on top of the existing sediments. The top flocs layers will press their weight agaisnt the bottom floc layers by the actions of gravity. Self-weight consolidation will occur as pore water from the bottom floc layers are being expulsed. This will result in the increase in effective stresses and stiffness in the sediments. However, the newly formed soil structures are extremely weak, compressible and will experience large strains deformation when loaded. As such, traditional soil consolidation theories such as Terzaghi's infinitesimal strain theory are inadequate and inappropriate to explain its consolidation process (Been and Sills, 1981, Schiffman et al., 1984).

Large strain consolidations are generally associated with thick layers of compressible soils with high moisture content (Bo, 2008). It is first proposed by Gibson (Gibson et al., 1967) who use the continuum theory to describe large strain consolidation of a soil layer under its own weight. Gibson's theory consists of the continuity equations for the fluid and solid phase, momentum balance, Darcy-Gersevanov's flow relationship, and the assumption of the validity of the effective stress. A solution of the equations requires knowledge of material properties for deformations and flow. Both properties are assumed to be monotonic functions relating density or void ratio to the effective stress and permeability. Since Gibson's publication, experimental and numerical issues of large-strains consolidation have been reported in numerous papers (Znidarcic et al., 1984, Tan et al., 1990, Boer et al., 1996, Sills, 1998, Toorman, 1999) and has been widely used for the management of dredged materials (Bartholomeeusen et al., 2002) and mining tailing for compliance with regulatory requirement (Townsend and McVay, 1990).

2.3 Land reclamation methods

The implemenation of land reclamation methods depend on several factors. They include the types of fill material, foundation soils, topography of the seabed, sea waves, current speed, the availability of the equipment, the tolerance of the siltation and etc. In this section, common types of land reclamation methods and case studies in Singapore are discussed.

2.3.1 Dry filling method

This method is usually adopted for earth movement. It is suitable for shallow foreshore areas where deployment of marine vessels for reclamation filling works are not feasible. Dry earth fill usually come from land sources such as hill cut and excavations. Trucks are used to transport the earth fill from source to the reclamation site. Bulldozers, excavators and roller compactors are deployed to spread, grade and compact the deposited fill to form stable land the required platform level. This method is sutiable for areas with firm seabed soils. If the seabed soil is weak, mud waves will be created due to displacement of the weak seabed. The displacement will push the seabed in uncontrolled manner until equilibrum is reached resulting in greater quantities of earth fill used.

2.3.2 Direct dumping method

2.3.2.1 Dump barges

Direct dumping method by dump barges are employed when there are sufficient water depths to carry out the dumping operations and sea spaces for the maneuverig of the dump barge in the reclamation site. This method can be implemented for all types of fill materials. Clayey soils are usually dredged from the seabed in semi-lumpy form illustrated in Figure 2.9 and loaded into the dump barges by the use of backhoe as shown in Figure 2.10 or grabbing using a grab or clamshell dredger as shown in Figure 2.11. It should be noted that dumping of clayey materials at deeper seabed is not encourage as the risk of dispersion of the clayey soils' fines in the seawater may have environment impact and affects the quality of the seawater.

Figure 2.9 Semi-lumpy mechanical dredged seabed sediments (Welp, 2006)

Figure 2.10 Scooping of seabed materials using backhoe dredger (Welp, 2006)

Figure 2.11 Grabbing of seabed materials using grab dredger (Boskalis, 2017)

The loaded dump barges will sail from the loading location to the final dumping location either by self-propelled or pushed by tugboats. The dump barges will be guided to the exact dumping position with the help of the global positioning system before dumping. Figure 2.12 shows the photo of a split-bottom barge and the schematic diagram in Figure 2.13 illustrates the dumping operations of a typical hopper barge. The dump barges usually have a capacity of a few hundreds to a few thousand cubic meters depending on vessel's size. The production rate by this method is largely dependent upon the number of the barges used and the distance between the fill loading sources and the reclaimed land.

Figure 2.12 Split-bottom barge (US, 2015)

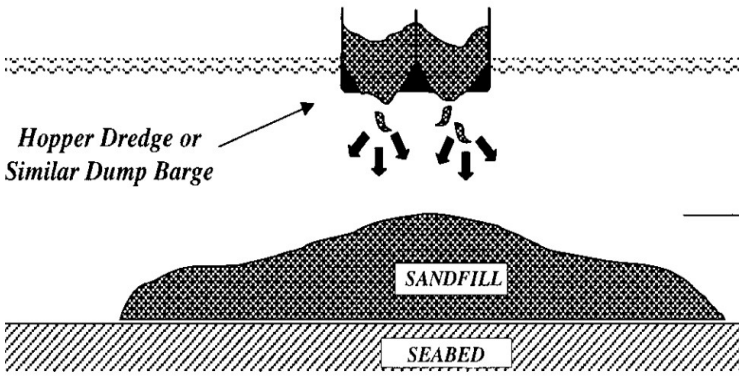

Figure 2.13 Direct dumping operation by hopper barge (Lee et al., 1999)

2.3.2.2 Conveyor belt barges

Generally, a fully loaded dump barges will need a 2-3m clearance from the keel to carry out its dumping operations. Due to this limitation, direct dumping reclamation methods by the use of other equipment such as the reclaimer barge and pelican barge are required to continue the filling works to the final design platform level. Both the reclaimer and pelican barges employed the use of conveyor belt system which can help to extend its reach above shallow water and on land allowing them to transfer and place the fill materials in controlled manner as illustrated in Figure 2.14 and Figure 2.15.

Figure 2.14 Reclaimer barge placing of fill at shallow waters (Kanmon, 2017)

Figure 2.15 Pelican barge discharge fill materials in shallow waters (Kwt, 2015)

2.3.3 Hydraulic filling method

Hydraulic filling is most suitable for granular fill as this method can handle large amount of granular fill efficiently quickly. It is usually implemented in large infrastructure reclamation projects such as airports, harbors and industrial land. Van Vant't Hoff (Van't Hoff and Van der Kolff, 2012) defines hydraulic filling as the creation of new land following the consecutives activities:

i. Dredging of fill in an area by specialized floating equipment.
ii. Transporting of the dredged fill to the reclamation site.
iii. Discharging and placing of fill material hydraulically as a mixture of fill and water in the reclamation site as illustrated in Figure 2.16.

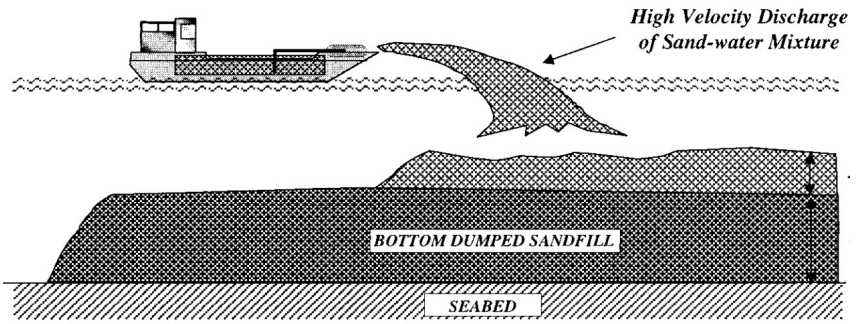

Figure 2.16 Discharging of sand-water mixture hydraulically (Lee et al., 1999)

2.3.3.1 Production rate

2.3.3.1.1 Specialized vessels

Specialized and powerful equipment and vessels like the Trailer Suction Hopper Dredger (TSHD) and Cutter Suction Dredger (CSD) has been developed to carry out dredging works at very high production rate. With the growing demand of completing larger land reclamation projects within a shorter time frame over the years, the capacity of TSHD has increased from 5,000m^3 in 1965 to 46,000m^3 today. The loading and unloading of fill material for these mega vessels can be carried out within

three to four hours. Figure 2.17 illustrates the relative size of a 33,000m^3 Mega TSHD *Vasco Da Gama*. Figure 2.18 show the lowering of the long trailing suction arm of the TSHD which can extend its reach to deep seabed to mine fill materials. Table 2.1 categorized the different types of TSHD based on their hopper capacity.

Figure 2.17 Relative size of 33,000m3 mega TSHD Vasco Da Gama berthing at St Johns Newfoundland (Fitzsimons, 2017)

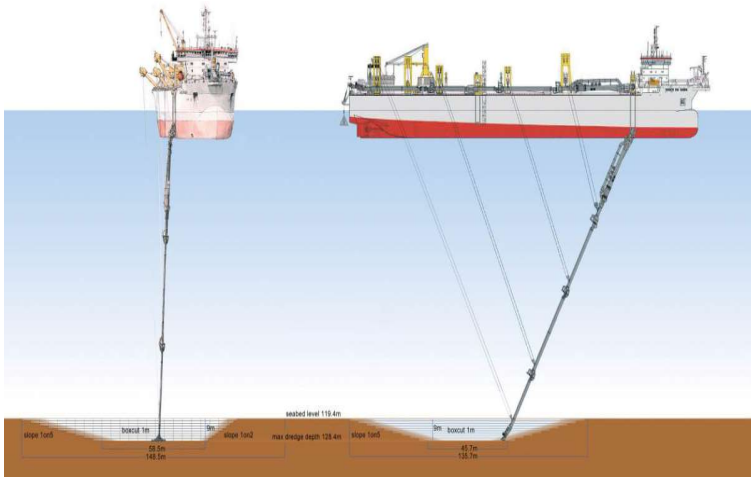

Figure 2.18 Illustration on the extended long trailer suction arm of mega TSHD to mine fill materials at deeper seabed during dredging operations (Fitzsimons, 2017)

Table 2.1 Classification of TSHD vessels by hopper capacity (Fitzsimons, 2017)

Type	Hopper capacity [m^3]	Inboard pump power [kW]
Small	700	350
Medium	4,500	2,500
Large	10,000	5,500
Jumbo	23,000	10,500
Mega	35,000	16,000

With increasing demand globally, more powerful CSD have been developed over the years from the 5kW vessels in 1965 to the 41 MW CSD today. The increase in CSD power allows mining of fill materials in harder and deeper seabed and also the conveyance of dredged materials by pumping over longer distance. Figure 2.19 illustrates and compare the increase in power and capability of a CSD modern built in 2003 and that being built in 2017. Table 2.2 classified the CSD types based on their available total power that the vessel can deliver.

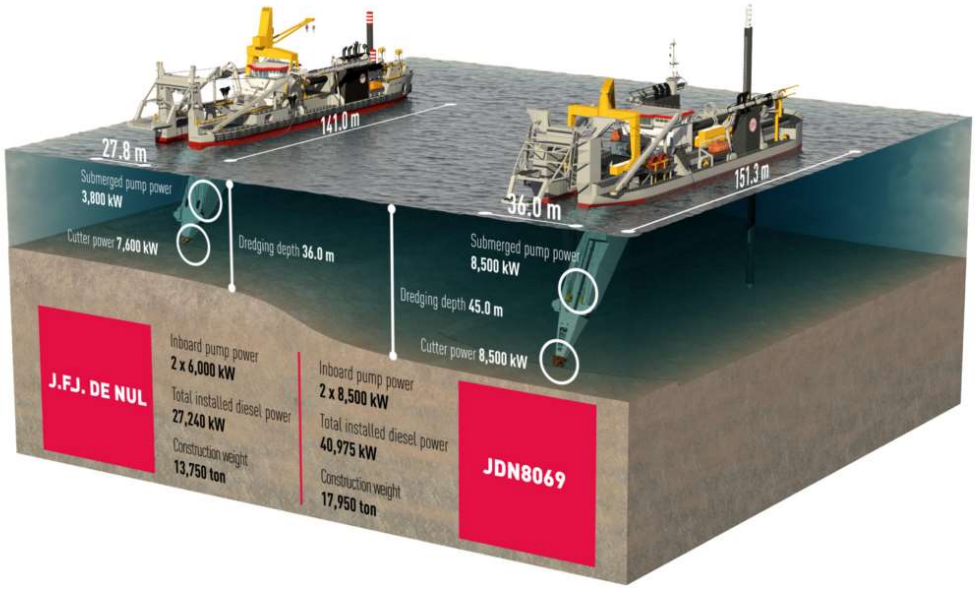

Figure 2.19 Capacity of CSD built in 2003 and latest CSD being in 2017 (Fitzsimons, 2017)

Table 2.2 Classification of CSD by total power (Fitzsimons, 2017)

Type	Length [m]	Pumping Power [kW]		
		Inboard	uwp	total
Small	62	2,000	750	2,750
Medium	95	5,500	1,350	6,850
Large	115	7,500	2,350	9,850
Mega	130	12,000	3,400	15,400
Today	150	17,000	8,500	25,500

2.3.3.1.2 Fill material to water ratio

For hydraulic filling using granular fill, the ratio of fill material to water is adjusted according to the grain size of the fill material. A larger ratio of material to water would lead to increase wearing of the inner walls of the steel pipes transporting the sand. On the other hand, a small ratio of material to water will reduce the production rate.

2.3.3.1.3 Transportation of dredged materials

The time taken to transport fill materials is dependent on the distance between the reclamation fill mining source and the reclamation site. When the fill mining source is far to the reclamation area, more vessels can be deployed to meet the production rate. However, when the distance is less than 10km, direct pumping through connecting floating steel pipes with the help of the intermediate booster pumps will be more efficient and cost-effective. Figure 2.20 illustrates the transportation and placement of hydraulic fill through connecting floating steel pipes.

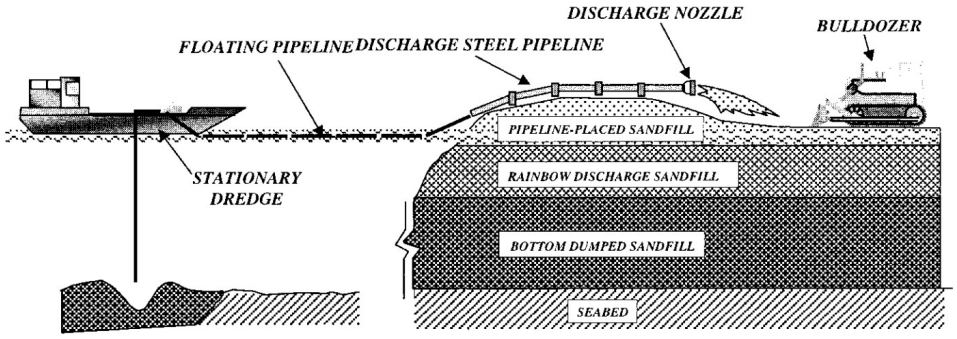

Figure 2.20 Transporting and placement of fill materials hydraulically through floating steel pipes (Lee et al., 1999)

2.3.4 Confined disposal facility (CDF)

According to Van't Hoff (Van't Hoff and Van der Kolff, 2012), hydraulic filling may not have to be restricted to only granular fill. With proper technical measures under the right conditions, cohesive and fine-grained materials such as clay and silt can also be used. Direct hydraulic deposition of clayey soils dredged slurry using pipeline in CDFs is one of the most common method employed today (US, 2015).

A CDF is an engineered structure for containment of dredged materials. They may be constructed as upland sites, nearshore sites with one or more sides in water, or island containment areas as illustrated in Figure 2.21.

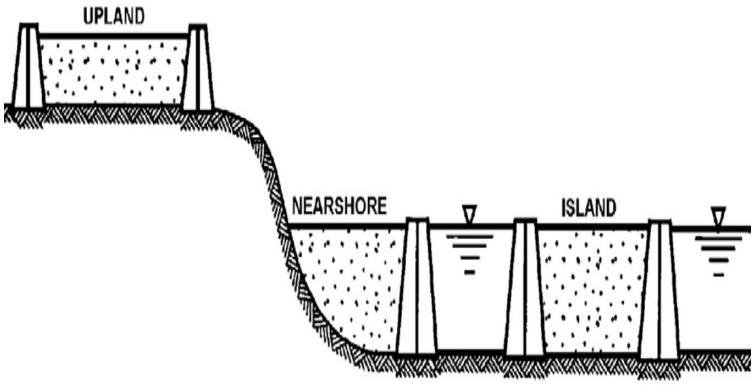

Figure 2.21 Schematic diagram of upland, nearshore and island CDFs (US, 2015)

A CDF must be designed to provide adequate initial storage volume and surface area to hold the dredged material solids during active hydraulic filling operation. It must be able to retain the suspended and settled solids and allow the discharge of the clarified water. Hydraulic filling of fine-grained materials general adds several volumes of water for each volume of sediment. The excess clarified water is normally discharged as effluent from the CDF during filling operation. The amount of water added depend on the design of the dredged fill, the physical characteristics of the sediments, and operation factor such as pumping distance.

The required initial storage capacity, water depth, and surface area of the CDF are governed by the sedimentation processes that occur during and after the hydraulic placement of fine-grained dredged materials. Settling tests of dredged slurry are needed to define their settling behaviors as they provide the required information to determine the optimal design criteria, capacity and filling cycles for the CDF.

The key components of CDF are illustrated schematically in Figure 2.22. Dikes are constructed to form the containment. The dredged sediments are pumped into the CDF hydraulically. Both the influent dredged slurry and effluent clarified water can be characterized by suspended solids concentration, suspended particle size gradation, type of carrier water (fresh or saline), and rate of flow. The clarified water is usually discharged from the containment area over a weir. Effluent flow rate is approximately equal to influent flow rate for continuously operating placement areas. Flow over the weir is controlled by the static head and the weir length provided. To promote effective sedimentation, ponded water is maintained in the area with the depth of water controlled by the elevation of the weir crest. The thickness of the sediments will increase with time until the hydraulic filling is completed. Minimum freeboard requirements and mounding of coarse-grained material result in a ponded surface area smaller than the total surface area enclosed by the dikes. Dead spots in corners and other hydraulically inactive zones will reduce the surface area for flow to considerably less than the total CDF's surface area.

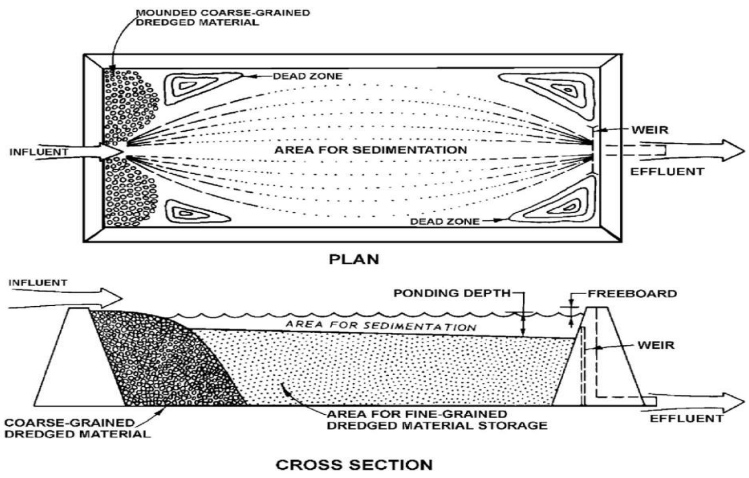

Figure 2.22 Schematic concept of hydraulic fill placement in CDF (US, 2015)

2.3.5 Case studies on reclamation methods

Land reclamation are complex construction projects. The type of land reclamation methods applied will depend on the reclamation fill, the project site conditions, constraints, project needs and the completion timeline given. The reclamation methods of two large-scaled reclamation projects in Singapore are discussed in this section.

2.3.5.1 East Coast reclamation project

In the East Coast reclamation project (Singapore), hill cuts were the main fill materials used. The fill materials were extracted from inland by bucket wheel excavators and transported by belt conveyors to a loading jetty. They were then loaded and transported by dump barges and placed on the reclaimed area. For inland reclamation, the dry fill material from the transfer barge was loaded to a reclaimer barge which re-handle the dry fill onto a land conveyor belt that conveyed the dry fill to the inland deposition area as illustrated in Figure 2.23. Bulldozers and dump trucks were then deployed to spread, grade and compact the reclaimed land to its final level.

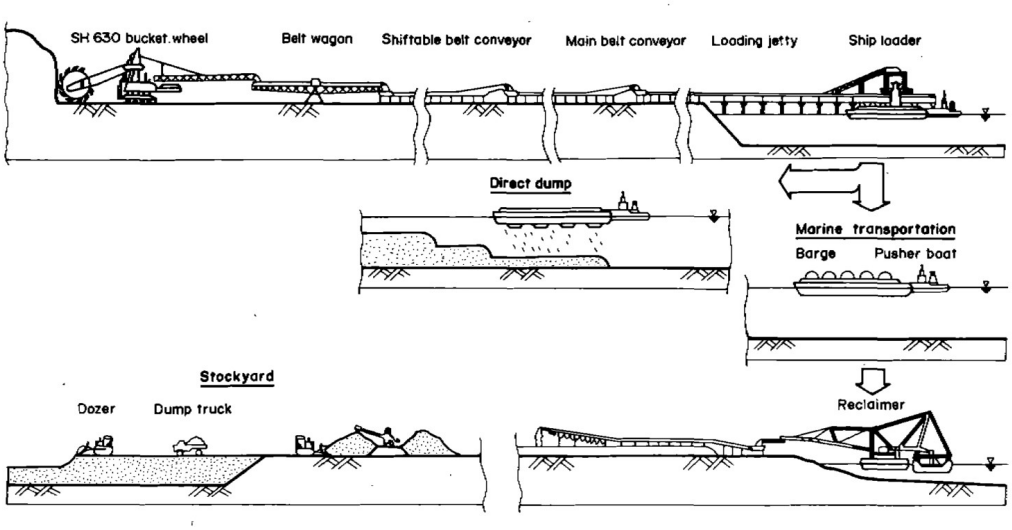

Figure 2.23 Reclamation methods implemented at East Coast reclamation (Yong, 1989)

2.3.5.2 Tuas reclamation project

In the Tuas reclamation project (Singapore), the main reclamation fills were imported sand from neighboring countries. The sequence and the reclamation methods deployed are illustrated in Figure 2.24.

The reclamation works begun with the dredging of the soft seabed clay using grab dredgers to form the foundation sandkey for the containment bund. The sandkey were then filled with sand by hopper barges while the dredged materials were placed within the reclamation site as part of the fill materials.

Sand containment dikes were constructed by direct sand placement using reclaimer barges. After completion, placement of sand over the deposited dredged soft clay was carried out by a sand spreader barge. The imported sand were spread in thin layers to form a sand blanket to minmise the intermixing of the sand and clay. A cutter suction dredger was used to transfer the imported sand deposited in an interim re-handing area to the sand spreader barge via floating steel pipes.

After the placement of sand blanket was completed, full scale hydraulic sand filling was carried out using the cutter suction dredger until the final reclamation platform level was reached.

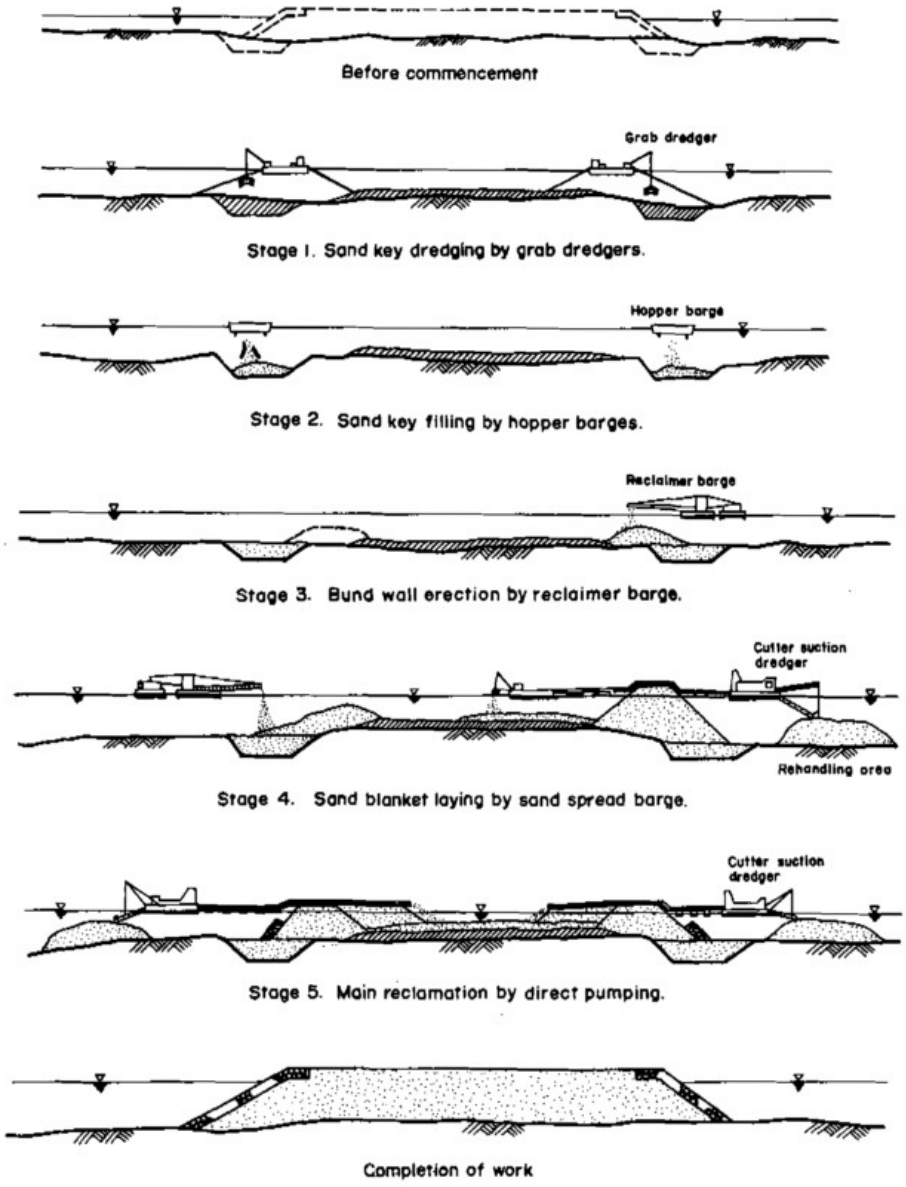

Figure 2.24 Sequence of the reclamation works and reclamation methods implemented for the Tuas reclamation project (Yong, 1989)

2.4 Soil improvement methods for ultra soft fill

After the sedimentation process, settled soil particles in the hydraulic fill will form sediments and undergo self-weight consolidation. These sediments are highly compressible materials with little or no shear strength due to its high water content. To enable the use of the sediments to form future land mass, soil improvement will be required to further consolidate and improve the sediments so that the excess pore water can be dissipated. This will increase the effective stress and reduce future settlement of the infilled sediments. Several suitable soil improvement methods to treat the ultra soft sediment are discussed in this section.

2.4.1 Surface desiccation

Surface desiccation is a time-dependent and climate-dependent soil improvement method commonly adopted to consolidate the dredged slurry deposited in CDFs to further increase their storage capacity by evaporative drying as illustrated in Figure 2.25.

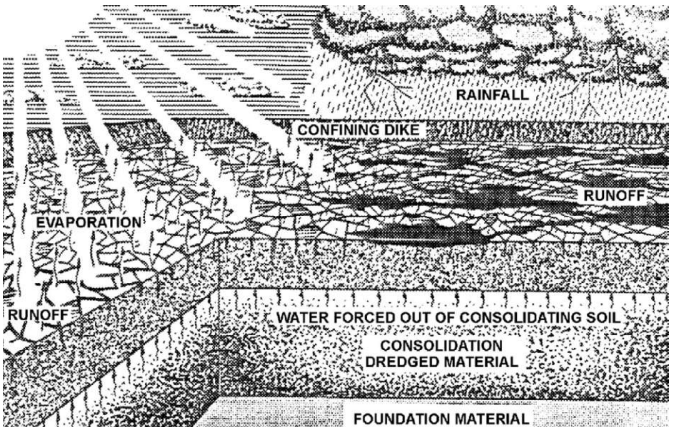

Figure 2.25 Surface desiccation to consolidate dredged slurry in CDFs (US, 2015)

The exposed surface of the deposited sediments will exhibit an overconsolidated zone that is represented by the crust development as a result of in-situ modifications by desiccation (Lutenegger, 1995). For practical reasons, it is important to identify the extent of the crust development to predict and determine its engineering properties if they are to be considered for bearing capacity, settlement and stability design.

2.4.1.1 Surface desiccation process

The different stages of surface desiccation are briefly described in Figure 2.26. In the initial stage, free water on the surface of the sediments would be removed by evaporation. At this time, the pore water pressure is positive everywhere in the sediment with no capillary suction and strain on the soil skeleton.

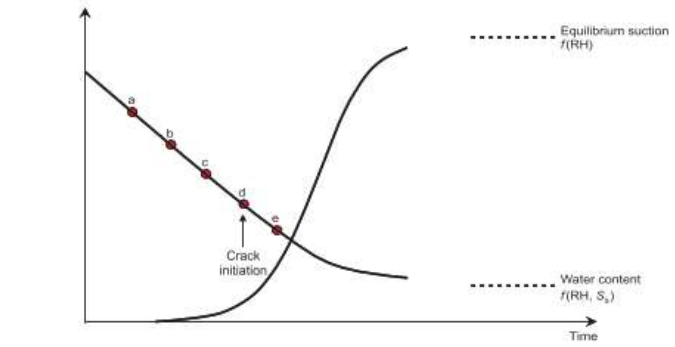

Stages	(a)	(b)	(c)	(d)	(e)
Global view					
Particle scale view					
Comments	Evaporation of supernatant water No suction No strain in the soil skeleton	Air–water interface membrane reaches the soil surface	Membrane forms around soil particles Suction increases Consolidation of soil skeleton and increase in stiffness	Air invades the largest pores The air–water interface membrane pushes particles away from the invaded pore Pore size increase at the tip and crack grows	Crack propagation and formation of polygons Vertical deformation ceases Eventually, the soil mass becomes unsaturated

Figure 2.26 Different stages of surface desiccation (Shin and Santamarina, 2011)

Over time, the water level above the deposited sediment will lower until the free surface water are evaporated. This brings the air-water interface membrane against the grain surface, mobilizing the tensile membrane as suction develops on the top

layers of the sediments. This air-water interface membrane grabs on to soil particles and resist invading the deposits matrix.

Capillary suction then develops in the pore fluid causing the pore water pressure above the receding water table to decrease to negative value while the total stress in the deposit remains constant. The effective stress and stiffness in the granular skeleton increase as consolidation takes place on the surface sediment while the sediments remain saturated throughout this stage.

The developed negative pore water pressure acts isotopically in all directions. This further reduce the water content and cause settlement at the upper layer of the sediments until the increased stiffness of the deposit skeleton hinders further consolidation. If evaporation continues, capillary suction will cause the air-water interface to invade the sediments further. Air intrusion will start at the largest pores in the sediments. The air-water interface pushes the sediment particles away from the invaded pores, further increasing their sizes until cracks are formed at the sediment's surface.

These cracks with continuing membrane invasion, will propagate deeper into the surface of the sediments. As the process repeats itself, the capillary actions will extend deeper dehydrating, consolidating and densifying the sediments which eventually will form a layer of unsaturated crust of higher shear strength over the saturated deposits. Figure 2.27 illustrates the profile of negative pore-water pressure in unsaturated soil.

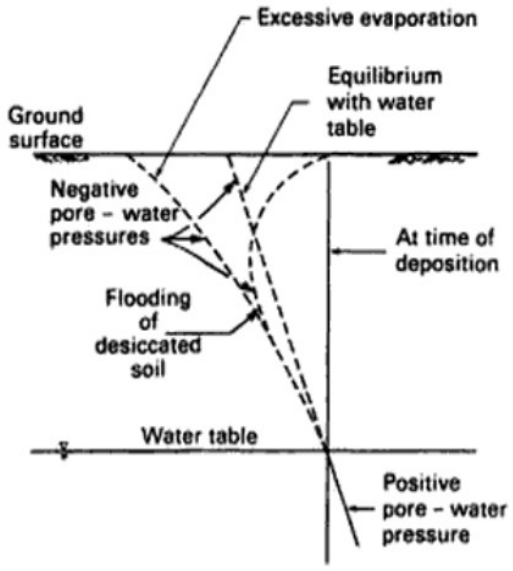

Figure 2.27 Pore-water pressure of unsaturated soil (Fredlund and Rahardjo, 1993)

2.4.1.2 Fractured surface patterns

Over multiple cycles of wetting and drying, extensive fracture patterns can develop on the crusted sediment's surface. Figure 2.28 shows the crack patterns after each wetting and drying (W-D) cycle. After the first W-D cycle, the shape of the clods are relatively regular and the crack segments are clearly defined and perpendicular to each other. Morris (Morris et al., 1992) explained this observation using the maximum stress release criterion and crack propagation criterion. With more W-D cycle, the shapes of the separated clods become more irregular and the crack segment shapes become cruder. The formed clods were observed to be smaller and will degrade significantly with increase in porosity after each W-D cycle. This can be explained by the progressive increase in pore volume and the average diameter of the pores with the increase of W-D cycles (Zemenu et al., 2009).

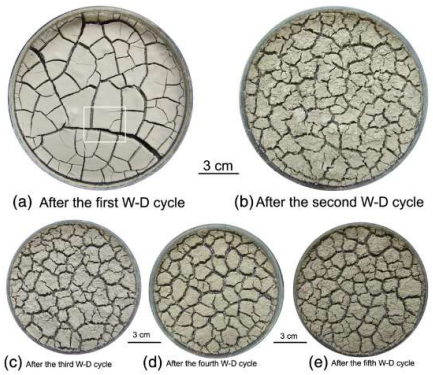

Figure 2.28 Crack patterns in crust after several W-D cycles (Tang et al., 2011)

2.4.1.3 Positive effects of surface desiccation

The desiccation of the sediment surface can have many functional benefits. According to Blight (Blight, 1988), surface drying helps reduce the void ratio of the sediments considerably. The densification of the sediments can also maximize the storage capacity for CDFs, stabilize the containment dike structure and increase the sediment's shear strength, bearing capacity and reduce long-term settlement (Abu-Hejleh and Znidarčić, 1995).

2.4.1.4 Method to accelerate surface desiccation

Often, reclamation sites will require the development of desiccated crust surface over the saturated sediments to provide adequate bearing capacity and shear strength to support workers and equipment to carry out construction activities (Johnson et al., 1977, Carrier and Bromwell, 1983). Active dewatering operations such as surface trenching as shown in Figure 2.29 can help to speed up and deepen the extend of surface desiccation. Park (Park et al., 2014) reported that Progressive Trenching Method (PTM) have been developed by Korean contractor solely for the purpose to accelerate and deepen surface desiccation to allow early accessibility of construction equipment and activities. Park reported that a stiff desiccated crust layer with thickness of 0.6m and an average field vane shear strength of 10kPa can be achieved using PTM.

Figure 2.29 Cut trench on clayey sediment surface by rotatory trencher (US, 2015)

2.4.2 Geosynthetics

Geosynthetics is the collective term applied to thin, flexible, sheets of material incorporated with soil to enhance it engineering properties (Ingold, 2013). The oldest historical examples of the use of fabrics as an aid to road construction over soft ground include the use of woven reed mats by the ancient Romans (Shukla, 2011). The modern concept of soil reinforcement using synthetic membrane was proposed by Casagrande, who idealized the problem in the form of a weak soil reinforced by high-strength membrane laid horizontally in layers (Westergaard, 1939).

Today, geosynthetics are well-accepted construction material. They offer numerous practical applications, quick and easy to install and are cost-effective alternatives to conventional civil engineering solutions. Jewell (Jewell, 1996) reported that savings up to 30% are possible for projects when compared with conventional solutions. Geosynthetics are made from polymeric materials or nature fibers (jute, cotton, wool, silk and etc.) are used to perform at least one of the following major or secondary functions describe in Table 2.3 when used in conjunction with soil, rocks and other civil engineering materials.

Table 2.3 Primary and secondary functions of geosynthetics (Shukla, 2011)

S/N	Function	Details
1.	Separation	Prevents intermixing of adjacent soil layers with different properties during construction
2.	Reinforcement	Increase the strength of a soil mass by carrying the tensile loads as a result of its inclusion and thus maintains the stability of the soils.
3.	Filtration	Function as a filter that allows for adequate flow of fluids across its plane while preventing the migration of soil particles, along with the flow
4.	Drainage	Allows adequate flow of fluids within the plane from the surrounding soil mass to various outlets
5.	Fluid Barrier	Prevent the infiltration of liquids

2.4.2.2 Geotextiles

Geosynthetics contain a broad range of products each serving single or multiple purposes. The typical geosynthetics products include geotextiles, geogrids, geonets, geomembranes, geofoams, geo-composites and etc. Of the wide range of geosynthetics products, geotextiles are of particular interest in this thesis as they are adopted in the pilot field trial to provide a geosynthetic-reinforced soil to form a load bearing working platform over the ultra soft sediments to allow construction activities.

Geotextiles are permeable, polymeric textile products in the form of flexible sheets. Currently available geotextiles are classified into different categories as summarized in Table 2.4 based on the manufacturing process.

Table 2.4 Types of geotextiles and their production methods and structure

S/N	Type of geotextile	Production methods	Structure
1.	Woven	Made from yarns by conventional weaving process with a regular textile structure	Variations of weaving structure have major influence on the physical, mechanical and hydraulic properties of the resulting geotextiles
2.	Non-Woven	Made from directionally or randomly oriented fibers in a loose web other than weaving and are relatively thick 0.5 to 5mm	Fibers are joined together by mechanical bonding (needle punching), thermal bounding (partial melting) and or chemical bounding (using cementing medium such as glue)
3.	Knitted	Produced by interloping one or more yarns together	Interlocking a series of loops of one or more yarns together to form a planar structure
4.	Stich-bonded	Formed by the stitching together of fibers or yarns	

The most common raw materials for the manufacturing of the geotextile are polypropylene, polyester, polyamid and polyethylene. Each type of polymer has their unique characteristics and properties. John (John, 1987) compared the properties of polymers used in the manufacturing of geosynthetics. The key polymers and their unique characteristics properties are described in Table 2.5.

Table 2.5 Characteristics and properties of polymers used in manufacturing geotextiles

S/N	Raw Materials	Characteristics and Properties
1.	Polypropylene (PP)	Low cost, for non-critical structures, excellent chemical and pH resistance, carbon black gives give PP ultraviolet light resistance, unsuitable for long-term sustained load due to poor creep deformation characteristics
2.	Polyester (PET),	High cost, high strength, resistance to creep, excellent chemical resistance, not suitable for high pH environment, stable to ultraviolet light
3.	Polyamid (PA),	Medium cost, medium strength, medium resistance to creep, medium resistance to ultraviolet light, good chemical resistance,
4.	Polyethylene (PE)	Low cost, low strength, low resistance to ultraviolet light, high creep, high resistance for high pH environment

2.4.2.3 Reinforced soil mechanism

The main purpose of the reinforcement is to prevent the development of the tensile strains in the soils. However, if it does develop, the composite soil system will provide strengthening effect, greater extensibility and smaller losses of post peak strength (McGown et al., 1978). The reinforcement improves the soil mechanical properties by reducing the shear stress that has to be carried by the soil and by increasing its available shearing resistance, as the normal stress acting on potential shear surface increases. The reinforcement will be most effective when aligned in a direction of tensile strain in the soil in which the tensile reinforcement stress develops (Jewell, 1996, Jewell and Wroth, 1987).

Shukla (Shukla, 2011) summed up that the behaviors of the reinforced soil depend on the following factors:

i. Soil and reinforcement mechanical characteristics.
ii. Soil-reinforcement interactions mechanism and properties.
iii. Geometry of the reinforced system.
iv. Shape, number, location and alignment of reinforcements.
v. Construction sequence and process.

Although factors such as the geometry of a reinforced soil system and process of its construction can be influence the soil-reinforcement interaction properties, they are strongly determined by the interaction mechanism, the physical mechanical properties of soil (density, grain shape, grain size distribution, water content and etc.) and the mechanical properties, shape and geometry of reinforcements. Three mechanisms of interaction can be identified in the reinforced soil systems namely:

i. Skin friction along the reinforcement.
ii. Soil-soil friction.
iii. Passive thrust on the bearing members of the reinforcement.

2.4.2.4 Increased bearing capacity with geotextile

The inclusion of geotextile with foundation soils, forming the soil-geotextile system, would help to improve the load bearing capacity and reduce the settlement in the following ways as illustrated in Figure 2.30.

2.4.2.4.1 Changing failure mode

The geotextiles reduces the outward shear stresses transmitted from the top soil to the underlying foundation. This changes the failure mechanism from local shear failure to a general-shear failure. This is known as the shear stress reduction effect, thereby increasing the load-bearing capacity of the foundation soil. (Bourdeau et al., 1982, Love et al., 1987, Guido et al., 1985, Espinoza, 1994, Adams and Collin, 1997, Espinoza and Bray, 1995, Hausmann, 1990).

2.4.2.4.2 Redistribution of applied force

Geotextiles reduces the maximum applied stress by spreading and redistributing the applied surface load to a wider area below the geotextiles. This is referred as the “slab effect” or “confinement effect” of the geotextiles. The frictions mobilized between the soil and the geosynthetic layer play an important role in confining the soil (Bourdeau et al., 1982, Giroud et al., 1984, Madhav and Poorooshasb, 1989, Sellmeijer, 1990).

2.4.2.4.3 Membrane effect

Supplementary support given by the deformed geotextile provides an equivalent opposite vertical support that resist the applied loads. The membrane effect of the geotextiles causes an increase in the load-bearing capacity of the foundation soil below the loaded area, with a downward loading on its surface at either side of the loaded area, thus reducing heave potential (Giroud and Noiray, 1981, Bourdeau et al., 1982, Sellmeijer et al., 1982, Love et al., 1987, Madhav and Poorooshasb, 1988, Sellmeijer, 1990, Shukla and Chandra, 1994).

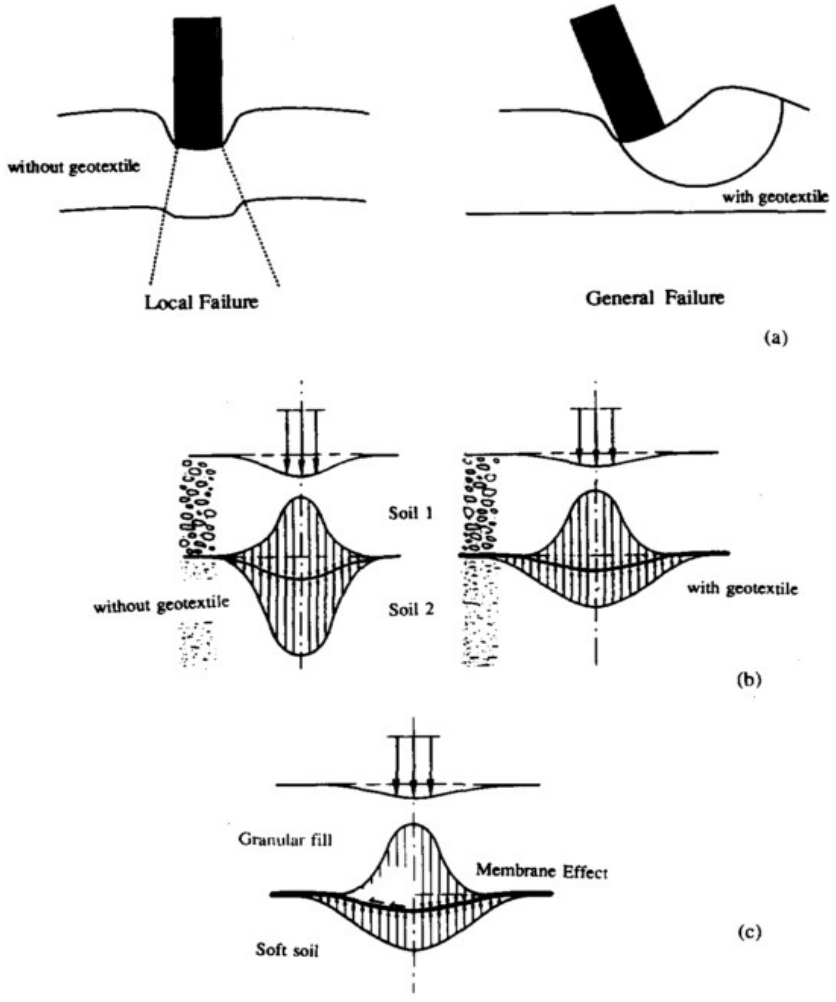

Figure 2.30 Influence of geotextiles inclusion on a two-layer soil system. (a) change of failure mode; (b) redistribution of applied surface load; (c) membrane effect (Bourdeau et al., 1982)

2.4.2.5 Soft soils stabilization using berms

The soil improvement technique of placement of geotextiles on top of ultra-soft soils to allow placement of sand layer has been applied in some land reclamation and CDF projects obligated to use these weak and highly compressible dredged materials from maintenance and capital dredging (Yamauchi and Kitamori, 1985, US, 2015).

Such preliminary soil improvement would allow access, trafficability and subsequent soil improvement works and construction activities to be carried out over these soft deposits with little or no bearing capacity.

Broms (Brons, 1987) proposed the placement of narrow berms simultaneously at regular spacing across the geotextile to active its tensile force to stabilize the soil. The narrow berms are then widened until the whole area is covered. The height of the fill can be raised in layer where the same procedure should be followed to avoid overloading the soft soils underneath the woven geotextile. Figure 2.31 shows the cross section and Figure 2.32 shows the proposed construction sequence of Broms proposed soil stabilization methods during construction using berms.

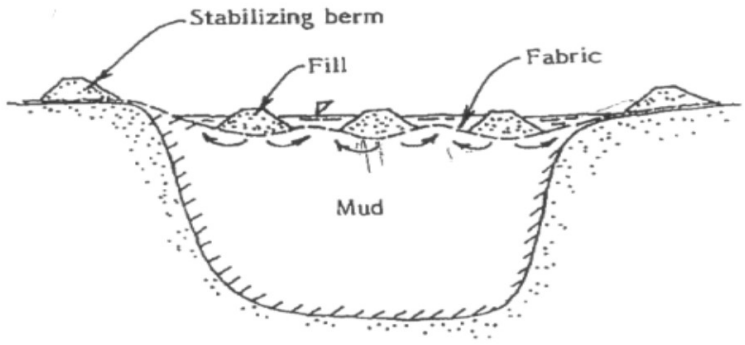

Figure 2.31 Cross section of soft soil stabilization using berms (Brons, 1987)

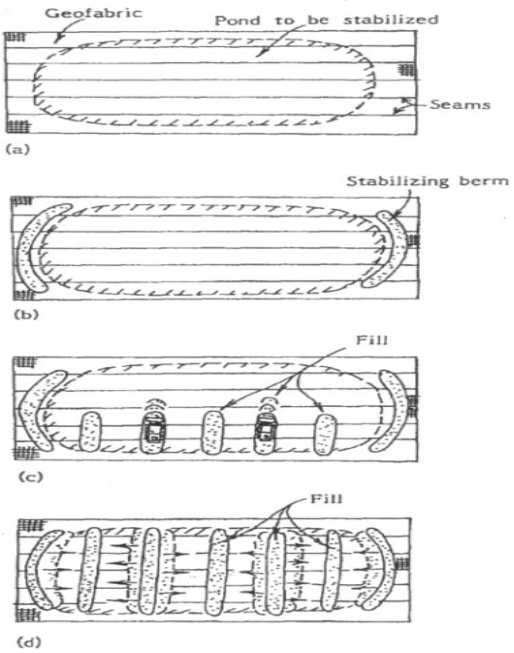

Figure 2.32 Construction sequence of soft soil stabilization using berms (a) placement of geofabric; (b) placement of stabilizing berms; (c) placement of fill; (d) widening and spreading of berms (Brons, 1987)

2.4.3 Preloading

In the past, the problems of consolidation settlement were usually overcome by preloading the ground. By preloading the ground beyond the future load until most of the primary consolidation has occurred will enable the underlying soil to increase its effectiveness stress. However, most clays are usually characterized by very low permeability, as the time needed for the desired consolidation can be very long, even with very high surcharge load. As such, the application of preloading alone may not be feasible for projects with tight schedule.

The simplest solution of preloading is the introduction of an embankment that serves as an additional load acting of the ground as illustrated in Figure 2.33. When the load is placed on the soft soil, it is initially carried by the pore water in the soil mass. When the soil is not very permeable, the pore water pressure will dissipate very slowly in the vertical direction. Not to create any instability problems, preloads are added in layers stage by stage to allow the soil mass to gain shear strength slowly. When the

temporary load exceeds the final construction load, the excess material is referred as surcharge.

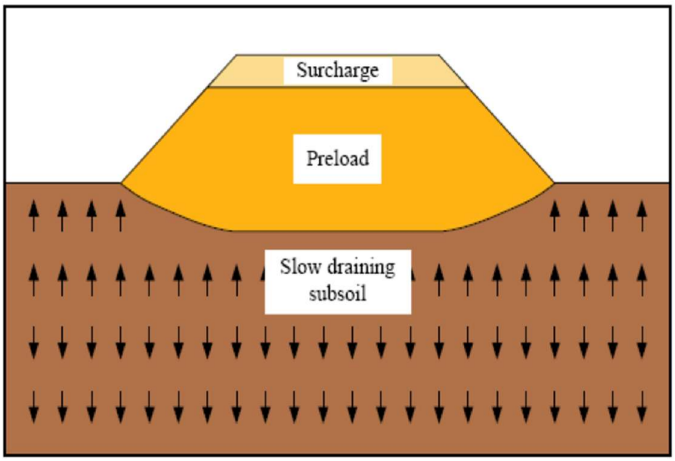

Figure 2.33 Preloading of subsoil (Stapelfeldt, 2006)

Figure 2.34 illustrates the settlement of the soil mass under preloading. The introduction of surcharge is to induce further consolidation beyond the design load and thus bringing more settlement in the soil mass.

When the surcharge is removed, the settlement curve will rebounded but the settlement will remain below the "design loading". More consolidation can be achieved by lengthening the preload time and increasing the preload magnitude.

The soil will be in an over-consolidated state when the apply surcharge is greater than the design workload. This will benefit greatly the subsequent geotechnical design (Chu et al., 2004) as the subsequent secondary compressions for over-consolidated soil will be smaller than that of normally consolidated soil. A portion of the preload material will remain in place as compensation fill to top up the settled/consolidated soil volume.

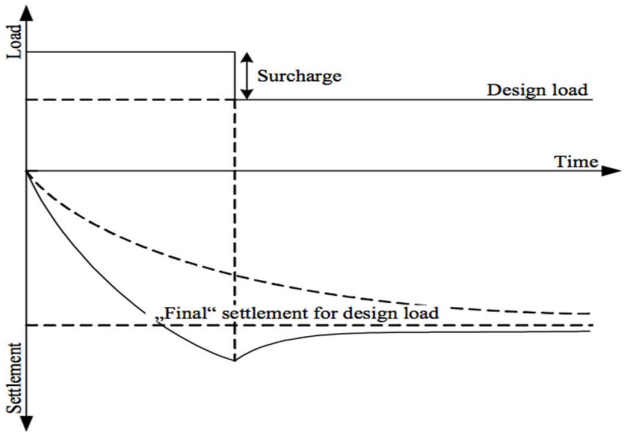

Figure 2.34 Settlement curves of preloading and surcharging (Stapelfeldt, 2006)

The duration of the preload is governed by soil consolidation characteristics, permeability, pore water travel distance and surcharge height. Consolidation characteristics of soil particles are challenging to enhance and there are limits to the surcharge height due to safety reasons. For soil mass without vertical drainage, the pore water travel distance is taken to be equal to the entire soil for single drainage and one-half of the soil thickness for double drainage for soil strata undergoing consolidation..

2.4.4 Sand drains

Vertical sand drains are basically vertical boreholes filled with sand. The distribution and diameter of sand drains depends on soil properties and on how quick the maximum settlement is expected to be reached. Usually, the vertical sand drains will have diameters between 250mm and 600mm and the distance between drains between 2m and 5m. They are usually distributed in the form of a network as illustrates in Figure 2.35.

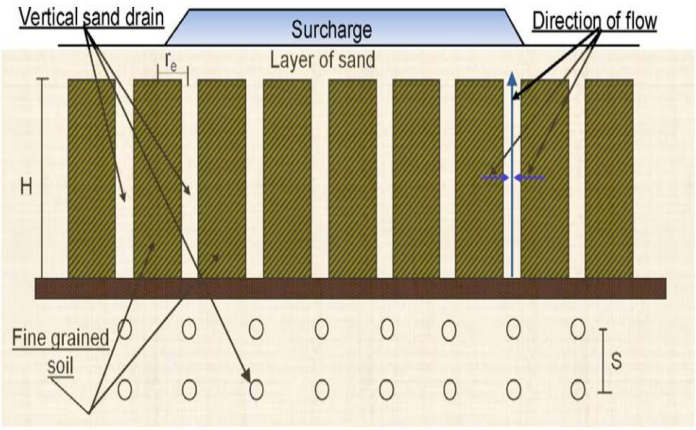

Figure 2.35 Sand drains system (Covo-Torres et al., 2015)

Installation of vertical sand drains will result in displacement of the soil mass in both the vertical and the horizontal directions. This will result in disturbances, especially in soft and sensitive clays soil mass, which will further reduce the shear strength and horizontal permeability. Yeung (Yeung, 1997) listed the disadvantages of using the sand drains. They include:

- Sand used for sand drains should have adequate drainage properties. They usually have to be procured separately from reclamation fill.
- Sand drains might become discontinuous because of careless installation or horizontal soil displacement during the consolidation and construction process.
- Disturbance of the soil mass surrounding each drain (smear zone) caused by installation will reduce the permeability the flow of water of water to the drain and thus the efficiency of the system.
- The reinforcing effects of sand drains as columns may reduce the effectiveness of preloading the subsoil.

Layered clay-sand scheme is another approach that was studied by Singapore in the early 1980s as an alternative reclamation-soil improvement method. This method use sand as both fill and also drainage to facilitate the consolidation of the soft clay slurries when they are used as reclamation fill (Lee et al., 1987). In this method, a

thin sand layer is sandwiched between hydraulically placed marine clay to form a layered clay-sand fill as illustrated in Figure 2.36. Special attention is necessary when spreading the intial seam of sand on top of the hydraulically placed clay which has extremely low shear strength. The sand layer shall not be excessively thick so as to cause local shear failure. Sand particles are expected to sink in at the surface of the clay and to form a crust to prevent penetration of subsequent sand

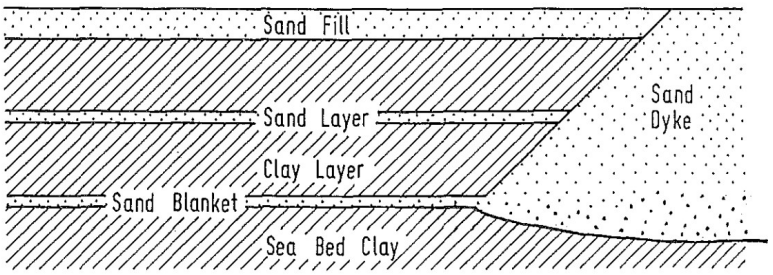

Figure 2.36 Schematic representation of layered clay-sand reclamation scheme (Tan et al., 1992)

In this scheme, less sand would be needed. This result in cost savings on imported sand for Singapore. The layered clay-sand fill would consolidate and gain strength more rapidly as compared to a full clay fill owing to the shorter drainage path provided by the sand layer where a full clay reclamation of practical depths may take several years to consolidate and gain sufficient strength to support machineries for construction (Watari, 1984).

2.4.5 Prefabricated vertical drains

With so many constraints and challenges in applying sand drains, synthetic drains have been developed to replace sand drains. Kjellman introduced the first prototype of a prefabricated vertical drain made entirely of cardboard (Jamiolkowski, 1983). Subsequently, several types of Prefabricated Vertical Drains (PVDs) were developed which basically consist of a plastic core with a longitudinal channel wick functioning as a drain and a sleeve of paper of fibrous material as a filter protecting the core. By

the mid-1980s, PVDs had significantly replaced sand drains, which have been rendered almost obsolete in the United States.

PVDs provide relatively low cost, practical, easy to apply and effective means of expediting consolidation settlement in fine-grained soils. Soils suitable for PVDs include clays, silts, organic layers, peat, clayey and silty sands, dredge spoils, and wastes such as mine tailings and industrial sludge.

Today, soil improvement projects using PVDs with surcharge are common in infrastructure, construction and land reclamation projects. This soil improvement method serves to accelerate construction works and reduce the magnitude of post-construction settlement. The scale of PVDs applications can range from a few hundred to several million square meters.

In addition to expediting settlement for ground improvement project, PVDs have been used to reduce potential down drag on piles, increase storage capacity for future landfills and waste containment sites, and for collection and extraction of contaminated groundwater. Since undrained soft clay can undergo high lateral displacement at or close to failure, an important role of PVD is to stabilize the soft clay and reduce lateral soil movement by promoting initial compression and reinforcement to the soft clay layers.

2.4.5.1 Types of PVD

A variety of PVDs types are available in the market today as shown in Figure 2.37. The most common of which consists of a polypropylene core wrapped in a spun-bond polypropylene fabric. These highly durable drains are designed to resist rotting, tearing, clogging, cracking, and chemical degradation. Typical lightweight drains are approximately 100mm wide by 4mm thick. Drain discharge capacity varies with the amount of head that is applied, but typically ranges from approximately 1.5 to 2.5 gallons per minute. As fill is placed, pore water pressure in the soil mass increases and is dissipated into the PVDs resulting in increased flow of water in the core.

Figure 2.37 Different types of PVDs in the market (Systemindo)

2.4.5.2 PVD installation

A crawler excavator fitted with an installation rig and mandrel can carry out the installation of the PVDs. Following the initial set up and feeding of the PVDs, the drains are installed by pushing a hollow, steel mandrel into the soil mass. The mandrel houses the PVD and protects it from damage as the mandrel is inserted into the ground and pushed to the termination depth. At the base of the mandrel, the wick material is looped through an anchor plate that holds the drain securely in place as the mandrel is extracted. The anchor plate also prevents soil from entering the mandrel and plugging it during penetration.. Once the mandrel has been extracted from the ground, the PVD is cut and the next drain is installed. The installation sequence of PVDs is shown in Figure 2.38.

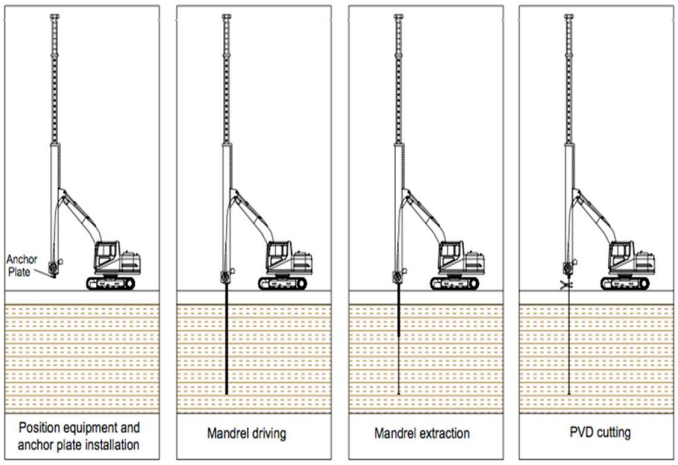

Figure 2.38 Installation sequences of PVDs (Seafco)

2.4.5.3 PVDs layout configurations

PVDs are installed in square or triangular patterns as shown in Figure 2.39. A square pattern of drains may be easier to set up in the field and control during installation in the field, however, a triangular pattern is usually preferred since it can provide a more uniform consolidation between drains than the square pattern (Holtz et al., 1991). The influence zone of the drain (R) is a function of drain spacing (S) as given by:

$$R = 0.546S \tag{2.1}$$

for drains installed in a square pattern and

$$R = 0.525S \tag{2.2}$$

for drains installed in a triangular pattern

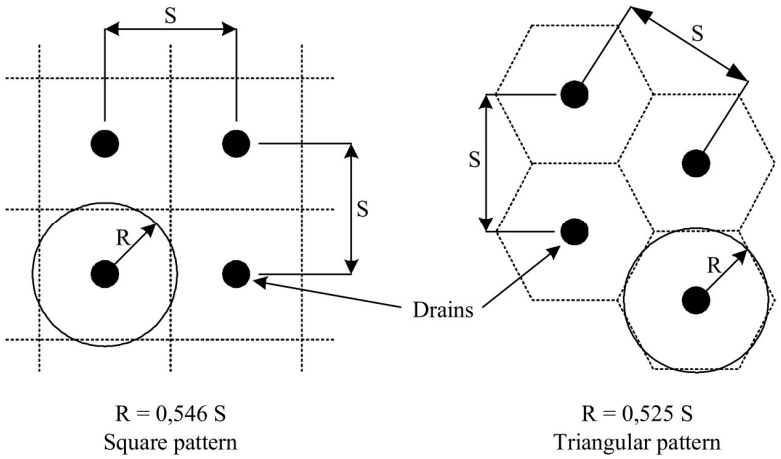

Figure 2.39 PVDs installation patterns and their zone of influence (Stapelfeldt, 2006)

2.5.5.4 PVD properties

2.5.5.4.1 Equivalent diameter for band drains

The cross-section of band-shaped PVD is rectangular. , Therefore it must be converted into an equivalent cylindrical shape. Hansbo (Hansbo, 1976) suggested that both band and circular drains lead to practically same degree of consolidation if their circumferences are equal. The equivalent diameter (dw) of a band-shaped drain with width (a) and thickness (b) as shown in Figure 2.40 can be expressed by:

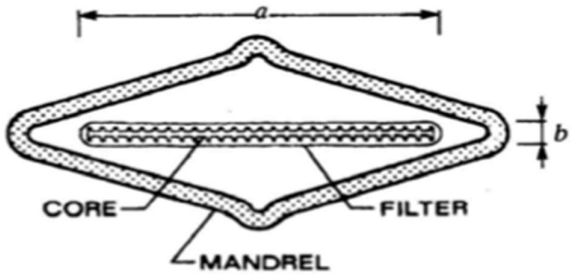

$$d_w = [2(a + b)]/\pi$$

Figure 2.40 Equivalent diameter of band drains (Holtz et al., 1991)

2.5.5.4.2 Discharge capacity

Discharge capacity measures the water flow capacity within the PVD and is required to analyze the drain (well) resistance factor. Bergado (Bergado et al., 1996) reported that the discharge capacity depends on the following factors:

- Lateral earth pressure*:* discharge capacity decrease as lateral earth pressure reduce the cross-sectional area available for flow.

- Large settlements*:* discharge capacity decrease as the deformation from settlement caused bending and folding of PVDs as shown in Figure 2.41

- Clogging of drain: discharge capacity decrease as the fine particles may be deposited in the PVD core channels, blocking the flow of the drain.

- Time: discharge capacity decrease over time due to aging of PVDs caused by physical wearing and biological and chemical activities.

- Hydraulic gradient: discharge capacity decrease with higher hydraulic gradient due to possibly loss of flow energy from turbulent flow at a high hydraulic gradient.

Figure 2.41 Folded PVD in soil with large settlement (Stapelfeldt, 2006)

2.4.5.5 Factors influencing PVD's efficiency

The mandrel will cause significant remolding to the adjacent subsoil during PVDs installation. A smear zone with reduced permeability and increased compressibility is formed surrounding the PVD. Barron (Barron, 1948) reported that in clayey soils, finer and more impervious layers will be dragged down and smeared over the more pervious layers which create additional resistance of the excess water to dissipate, retarding the rate of consolidation.

The remolded soil has different behavior when compared to the undisturbed soil in terms of permeability and compressibility. Essentially, the behaviors of soil stabilized with vertical drains cannot be predicted accurately if the effect of smear is ignored. Both Barron (Barron, 1948) and Hansbo (Hansbo, 1981) modeled the smear zone by dividing the soil cylinder dewatered by the central drain into two zones. The smear zone is the zone in the immediate vicinity of the drain and the other is the undisturbed zone as shown in Figure 2.42.

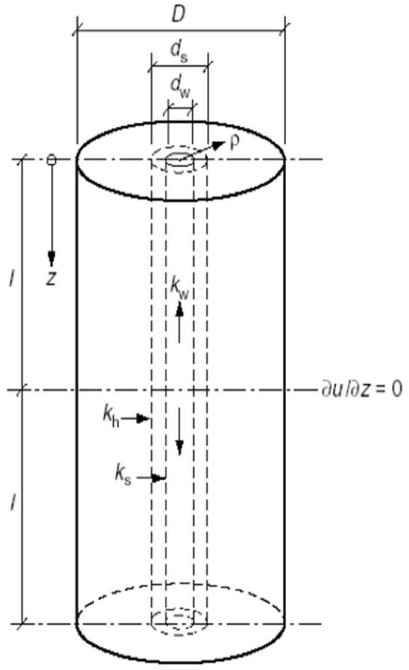

Figure 2.42 Smear effect (Hansbo, 1994)

The degree of disturbance by the smear zone depends on the following:

i. Installation procedure:

To determine the size of the smear zone, different relationships were suggested. Jamiolkowski (Jamiolkowski, 1983) proposed that the diameter of the smear zone (d_s) and the cross sectional area of the mandrel can be related as:

$$d_s = \frac{(5-6)d_m}{2} \tag{2.10}$$

where (d_m) is the diameter of a circle with an area equal to the cross-sectional area of the mandrel or the cross-sectional area of the anchor at the tip, whichever is greater. At this diameter, the theoretical shear strain is approximately 5 % as shown in Figure 2.43. Based on laboratory investigations, (Indraratna and Redana, 1998) estimated the ratio of (d_s / d_m) to be four to five.

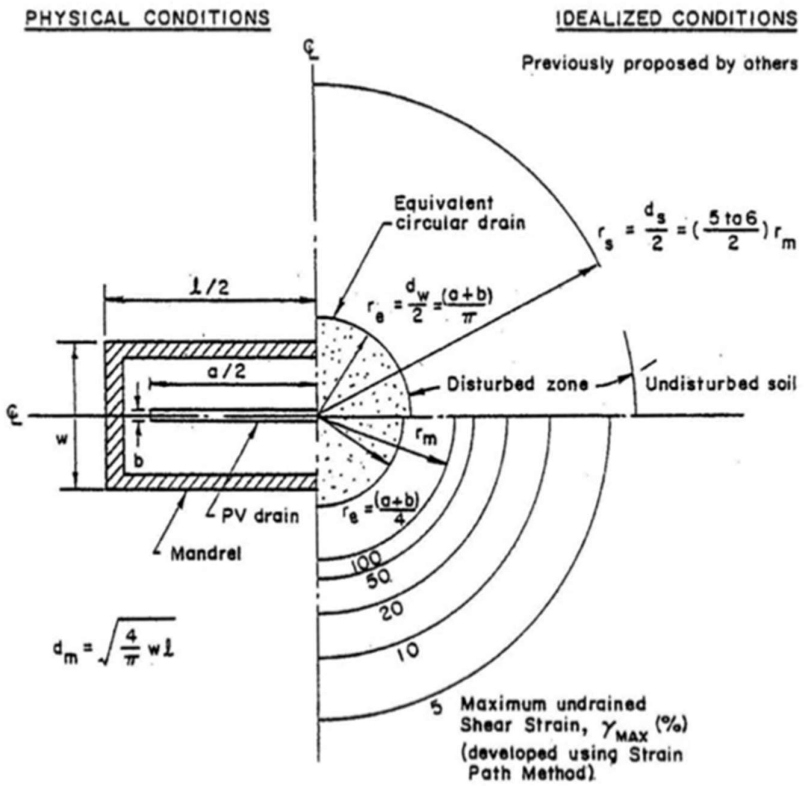

Figure 2.43 Estimate disturbed zone around mandrel (Bergado et al., 1996)

ii. Soil structure:

The ratio of horizontal permeability to vertical permeability (k_h / k_v) can be very high for soil with noticeable anisotropy. However, within the disturbed smear zone, this ratio (k_h / k_v) approach unity as it is closer to the drain according to Indraratna's study on the ratio of horizontal to vertical permeability. Indraratna reported that the measured coefficient of horizontal permeability becomes smaller towards the drain but the coefficient of vertical permeability remains nearly unchanged as illustrated in Figure 2.44.

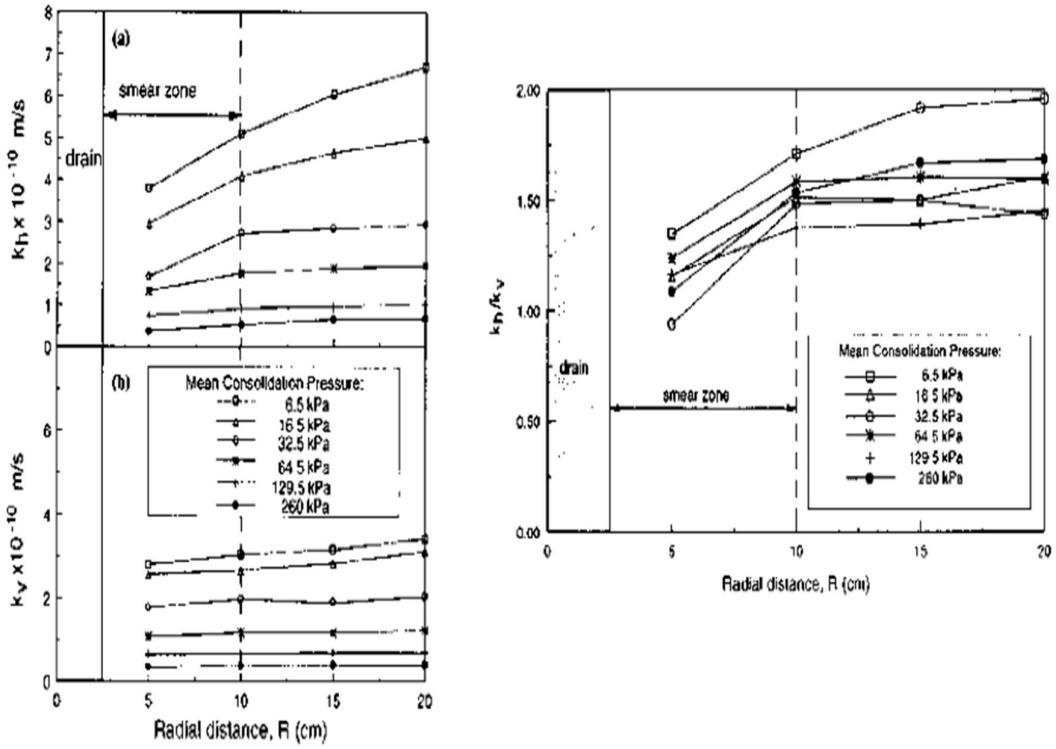

Figure 2.44 Left upper graph (a) Horizontal permeability, Left lower graph (b) vertical permeability. Right Diagram: Ratio of (kh/kv) along radial distance from central drain (Indraratna and Redana, 1998)

iii. Size and shape of mandrel:

In a case study where different mandrel sizes were used, Bergado (Bergado et al., 1996) reported that the areas installed PVDs with smaller mandrel experienced faster settlement rate and higher compression when compared to areas where larger mandrel was used. This case study verified the importance of the mandrel sizing and to minimize the effects of smear zone, mandrel size should be designed to be as close as possible to the PVD size.

2.4.5.6 Well resistance

The performance of a PVD is influenced by their discharge capacity and filter permeability. When the discharge capacity is reached, the PVD will exhibit a resistance to water flow known as well resistance, slowing down the consolidation process. It is proposed to use PVD with a working discharge capacity that exceed

100-150 m^3 / year. Well resistance can be ignored when the discharge capacity is sufficiently large.

2.4.6 Vacuum preloading

Vacuum Preloading was first introduced by W. Kjellman in 1952 who is also the inventor of PVD. Simply put it, vacuum preloading is a system of vertical drains to transmit the negative suctions generated from the vacuum pump to remove the excess pore water and increase effective stress in the applied soil mass. Vacuum preloading has been researched extensively and was applied in many construction projects worldwide to treat extremely soft soils where conventional PVD with surcharge preloading are deemed to be slow or inappropriate due to site constraints such as space limits, unsafe or obstructing embankment height, highly unstable underlying soil conditions, no access to large volume of surcharge fill materials and etc.

2.4.6.1 Mechanism of vacuum preloading

The principles of surcharge preloading and vacuum preloading have been discussed extensively (Kjellman, 1952, Holtz and Wager, 1975, Qian et al., 1992, Chu et al., 2000, Chu and Yan, 2005a). Both the consolidation under fill surcharge and vacuum pressure can be explained by the spring analogy as illustrated in Figure 2.45.

When the surcharge load is applied, it is the excess pore water pressure that will take the applied load. As the excess pore water pressure dissipates, the load is gradually transferred from the water to the spring that represents the soil skeleton. The amount of effective stress increased equals to the amount of pore water pressure dissipated. At the end of the consolidation, the total gain in the effective stress shall be the same as the surcharge applied.

When vacuum load is applied, the effective stress increase directly as the pore water pressure in the soil system reduces due to the suction (negative pressure), while the total stress remains the same. The spring gradually compresses as the pore pressure gradually reduces indicating the soil skeleton is gradually gaining effective stress. It should be noted that the amount of effective stress increased will be equal to the

amount of pore water pressure reduced which is estimated to be around 80kPa and will not exceed the atmospheric pressure of 101.3kPa.

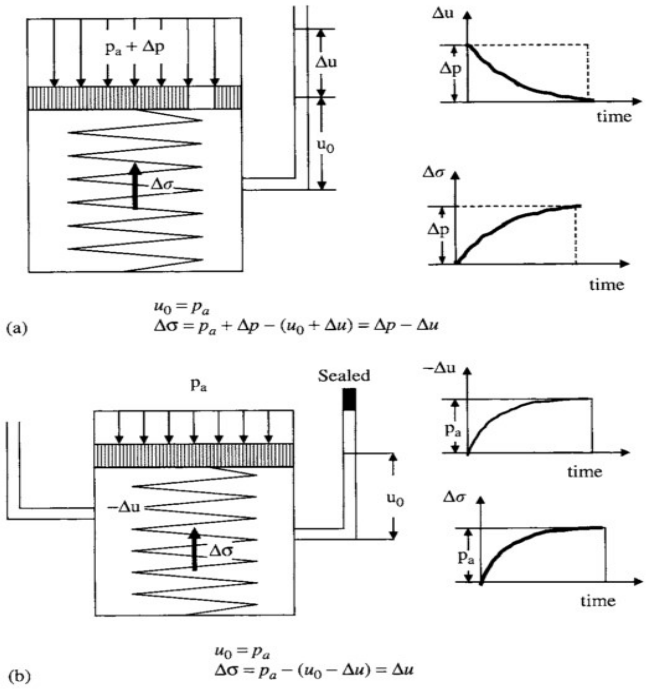

Figure 2.45 Spring analogy of consolidation process (a) under fill surcharge; (b) under vacuum pressure (Chu and Yan, 2005a)

2.4.6.2 Lateral soil displacement

Surcharge loading by an embankment will not only cause settlement of the soft subsoil but also generally outward lateral displacement. This lateral displacement is mainly caused by the shear stresses induced by the embankment load, and if these shear stresses are big enough they may potentially lead to shear failure.

By contrast, the vacuum pressure technique tends to apply an isotropic consolidation pressure to the soft subsoil. The isotropic consolidation will induce settlement and inward lateral displacement of the soil. However, the amount of lateral displacement will depend on the relative depth below the ground surface and distance from the neighboring vertical drains. Figure 2.46 shows the measured inclinometer of the inward lateral displacements caused by vacuum loading. It can be seen that the lateral

displacements were greatest at the ground level and reduced with depth. This kind of inward deformation may cause some surface tension cracks around the perimeters of the treated soil, but without potential risks of shear failure (Chai et al., 2005).

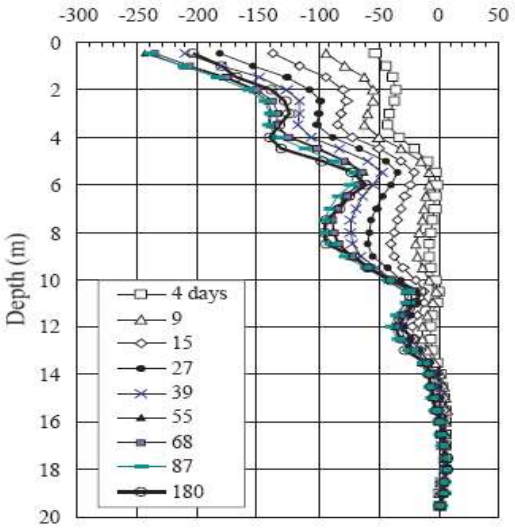

Figure 2.46 Example of lateral soil displacements by vacuum preload (Yan and Chu, 2005)

Both the inward and the outward lateral displacement can cause problems to structure adjacent to the area undergoing soil improvement works. However Indraratna (Indraratna and Rujikiatkamjorn, 2008, Indraratna et al., 2011) reported that for combined vacuum-surcharge preloading, the net lateral soil displacement can be reduced and in theory, prevented from occurring. Figure 2.47 illustrates the lateral deformation of soil under different loading conditions.

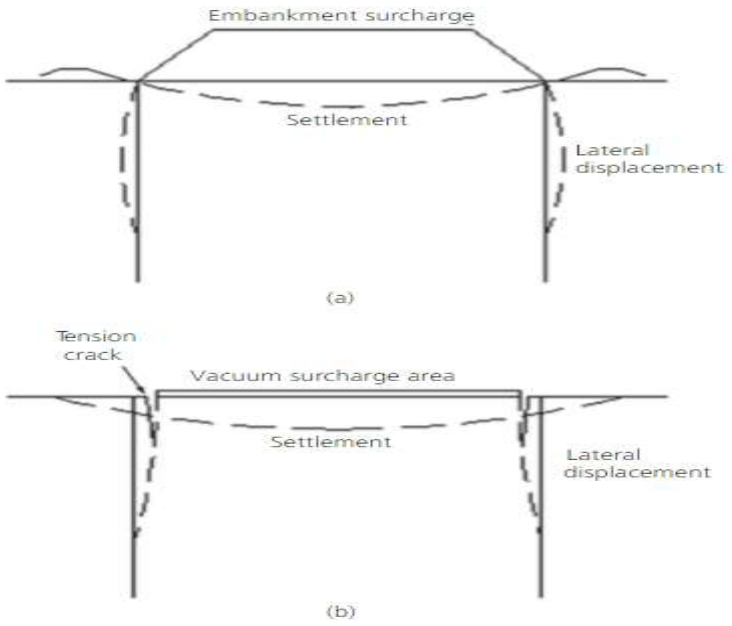

Figure 2.47 Lateral deformation of soil under (a) embankment surcharge and (b) vacuum preloading (Griffin and O'Kelly, 2014)

2.4.6.3 Effective depth of vacuum treatment

There are conflicting views on the depth where vacuum can be effective applied to treat the soil mass. A common industry concern is that vacuum pressure only be effectively applied to a depth of about 10m below ground level regardless of installed drain depth (Griffin and O'Kelly, 2014). In a vacuum preloading pilot test, Choa (Choa, 1989) observed that the vacuum consolidation diminished in its effect at about 14m below ground level. Later in a vacuum assisted consolidation field trial conducted at the Second Bangkok International Airport (SBIA), Bergado (Bergado et al., 1998) reported that measured vacuum pressure reduced with depth. At 15m below ground level, the measured vacuum pressure was about 25% of that applied at ground level.

Chu (Chu et al., 2000) reported contradictory findings for a very soft soil deposits for about 20m deep. Vacuum pressure was found to be fully developed at 14m below ground level and for deeper level, about 80% vacuum pressure were developed. Later,

Masse (Masse et al., 2001) explained that, in theory, the vacuum pressure effectiveness shall not vary and limited by depth.

2.4.6.4 Instrumentation monitoring

A comprehensive instrumentation program is required to monitor settlement, lateral soil displacement, pump pressure and dissipation of pore water pressure to assess the progress of the soil improvement works by vacuum preloading.

2.4.6.5 Membrane vacuum consolidation technique

The membrane based vacuum consolidation technique consists of installing vertical and horizontal draining system and vacuum pumping system under single or multiple airtight impervious membrane as illustrated in Figure 2.48. The treatment area is sealed by the impervious membrane into a network of peripheral trenches to prevent leakages of the applied vacuum pressure in the soil mass. These trenches are continuously recharged and filled with water to maintain full saturation of the soils and to avoid a general lowering of the ground water table within the treatment area.

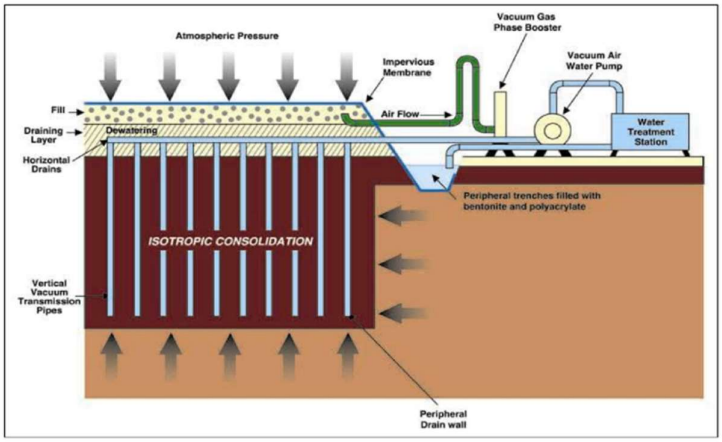

Figure 2.48 Schematic diagram of typical membrane vacuum consolidation system (Masse et al., 2001)

An air-water pumping system is installed to produce suction in the soil mass below the impervious membrane via the PVDs. Typically, an effective vacuum pressure range between 60-80 kPa which is approximately 75% of the atmospheric pressure,

and at the right conditions higher vacuum pressure of about 90 kPa can be achieved. The effective vacuum pressure achieved would depend mainly on the workmanship (leakages) and overall efficiency of the pumping systems. This pressure of 60-80 kPa is equivalent to that exerted by a 3-4m high of surcharge embankment. This preloading through the application of an atmospheric pressure creates an isotropic accelerated consolidation for the compressible soils. Settlement in this case can be achieved with reduced time without surcharge load.

Including setup and installation, and depending on the soil mass and site condition, a typical membrane vacuum consolidation technique would take 4 to 6 months to improve the target soil mass to the stipulated requirement. During this period, all risky activities that could puncture the membrane must be avoided and controlled and the sealed membrane must be properly protected from damages and deteriorations.

Unsuccessful attempts by others in applying the membrane vacuum preloading technique have been recorded. This is probably due to the lack of understanding of its basic principles and proper setting up technique and operation management.

Operational and technical problems associated with the membrane vacuum preloading technique includes:

i. Maintaining an effective drainage under the membrane to expel water and air during vacuum pumping.
ii. Maintaining an effective level of vacuum of the atmospheric pressure.
iii. Maintaining a leak-proof system at the pumps, connections and the membrane area.
iv. Anchoring and sealing of the system at the periphery.
v. Reducing lateral water flow towards the vacuum area.

2.4.6.6 Membraneless vacuum consolidation technique

The vacuum consolidation technique can generally group into two categories, namely the membrane technique and the relatively newer membraneless technique. The membraneless technique has been applied for the construction of the new Bangkok

International Airport (Seah, 2006) and also has been used in China coast reclamation as part of a vacuum assisted solution to treat very soft clay (Chu et al., 2012).

In this technique, each installed vertical drain is joined to a single vertical watertight tubing/hose by an interface cap as illustrated schematically in Figure 2.49(a). The joining between the PVD and the interface cap is establishing by simply stapling them together as shown in Figure 2.49(b).

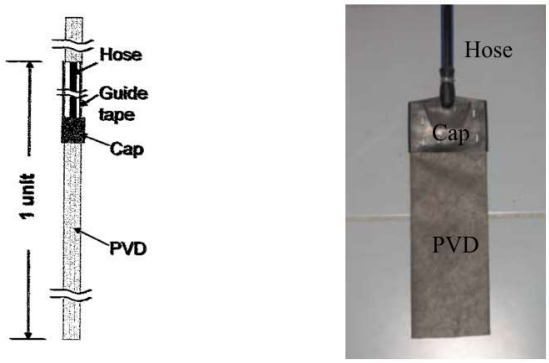

(a) Illustration (b) Actual BeauDrain-S PVD

Figure 2.49 PVD connection to vertical tubing/hose in a typical membraneless vacuum consolidation system

The vertical tubing/hose will extend to the ground surface and is then connected to the horizontal tubing leading to the manifolds of the vacuum pump. This line of connections from the PVD to the tubing and to the pump forms the vacuum line which transmit the vacuum pressure from the vacuum pump to the soil mass and drain out the excess pore water from the soil mass to the vacuum pump for discharge.

The purpose of the vertical watertight tubes is to prevent leakage of vacuum pressure and are installed in the permeable layer of the stratified soil mass just above the soft compressive soil layers as illustrated in the schematic diagram in Figure 2.50 (a). Ideally, all the connections of the vacuum line should be sealed completely.

Figure 2.50 (b) shows the situation where an interim sand layer is present in the soil mass. This interim sand layer could reduce the performance and efficacy of any vacuum consolidation treatment significantly. To resolve this issue, a sealing sheet can be applied onto the affected PVD at the elevation of the sand layer to prevent vacuum loss.

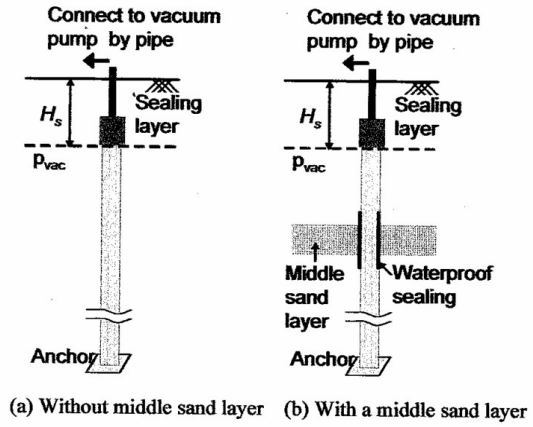

Figure 2.50 Modified PVD installation into stratified soil of different permeability in the membraneless vacuum consolidation technique (Bergado et al., 2006)

The membraneless vacuum consolidation technique is more suitable for a site with undulating thickness of stratified soil layers with high permeability where the installation of the cut-off trenches, impervious membrane, sand blanket may not be practical due to technical difficulty, prohibited costs and non-availability of sand for the drainage layer underneath the sealed membrane.

2.4.6.6.1 Low vacuum pressure in soil

For the membraneless vacuum consolidation system, each drains act independently (Indraratna et al., 2011). However, this set up also make it difficult to ensure that every drain work effective to provide the required vacuum pressure unless the system is under perfect airtight condition.

Literature review shows that the vacuum pressure achieved at applied sites using the membraneless vacuum methods were usually around or below -60 kPa. Chai (Chai et al., 2008) reported a case study using a membraneless technique. As shown in

Figure 2.51, the measured vacuum pressure is nearly zero at the ground surface and at the tip of vertical drain that was next to the bottom impervious layer, whereas the maximum vacuum pressure achieved elsewhere was less than -60 kPa.

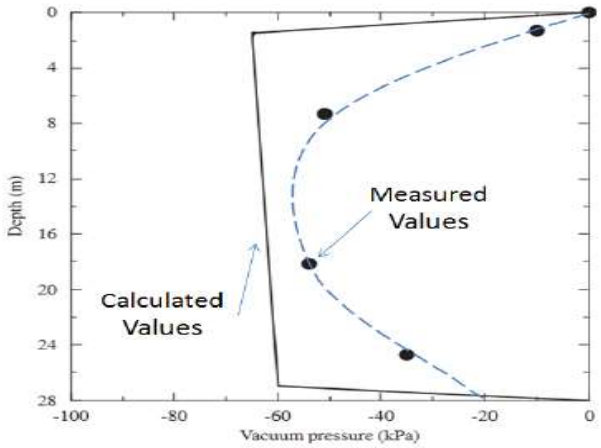

Figure 2.51 Vacuum pressure vs. depth in Yamaguchi Prefecture, Japan (Chai et al., 2008)

2.4.6.6.2 Considerations for scalability

For large-scaled soil improvement project, thousands of drains would be required The significant number of tubing connecting parts and modifications required for each membraneless vacuum consolidation technique drain can be labor intensive, costly and time-consuming and should be taken into account in the planning (Indraratna et al., 2011, Seah, 2006).

2.5 Conclusion

In this chapter, different types of reclamation fill, reclamation methods and soil improvement methods are presented and discussed.

The use of dredged seabed as fill materials is not at all a new idea as it has been implemented in the disposal management of dredged materials for port and waterway capital and maintenance dredging.

With the development of specialized vessels, large amount of dredged seabed materials can be efficiently handled and transport hydraulically in slurry form. However, the dredged seabed materials are high in water content and low in low solid content. When used as reclamation fill, the long time taken for sedimentation process must be taken into account in the project planning.

Application of surface desiccation and use of geotextile to form reinforced soil as a means to provide a stable working platform over the ultra soft soils and their subsequent soil improvement using vacuum consolidation technique seemed promising.

CHAPTER 3 SEDIMENTATION BEHAVIOURS OF FINE-GRAINED SOIL SUSPENSIONS

3.1 Introduction

Large amount of sand can be transported, re-handled and deposited quickly at reclamation site hydraulically as sand can settle almost instantaneously. However, this is not the case for dredged seabed slurry as it contains fine-grained materials like silt and clay which stay suspended for a while before settling down as sediments. The high water-low solid content of the dredged slurry coupled with long settling time for the suspended particles to form sediments greatly limit the attractiveness and potential to using dredged seabed slurry as reclamation fill despite their abundance in sand scarce coastal cities.

To overcome this constraint, a good understanding on the sedimentation process and behaviours of the fine-grained soil suspensions will be needed to help improve the design and sizing of the containment facilities and also develop more appropriate material planning and project management strategies. In Chapter 3, the sedimentation and behaviour of clayey slurry was studied and the viability of using commercially available flocculent to expedite the sedimentation process was examined using laboratory model tests.

3.2 Settling column model tests

Settling column tests were carried out using 2 metres tall columns with 7.05cm diameter as shown in Figure 3.1. The purpose is to understand the settling behaviour of dredged slurry with varying compositions of seabed materials namely marine clay (MC) and silt from Jurong Formation (JF). Five variations of samples were prepared using different mixed of MC and JF to represent the possible seabed compositions. The mixed slurries of 1200kg/m^3 design density were allowed to settle in the glass columns for up to 3668 hours. The interfaces between the dispersion and clear water were measured over time.

Dredged mixture samples S1, S2, S3 and S4 were classified as clay and S5 as silt under the Unified Soil Classification System (USCS) developed by Professor A. Casagrande (1948). Table 3.1 shows that the Plasticity Index (Ip), which describes the range of water content overwhich a soil is in plastic state. Plasticity Index was found to decrease with reduced MC content. The samples before and after settlement behaved as very viscous slurry with Liquidity Index (IL) greater than 1. The Liquidity Index of the different soil samples reduced significantly as they settled down to formed sediments. Most sediments after settlement have decreased water content, reduced void ratios and higher bulk and dry density when compared to the mixed slurry before as shown in Table 3.2.

Figure 3.1 Photo showing the settlement of the columns at the 3668hrs

Table 3.1 Atterberg's limit & consistency indices of soil samples

Atterberg's Limit & Consistency Indices	**S1 100% MC**	**S2 70% MC 30% JF**	**S3 50% MC 50% JF**	**S4 30% MC 70% JF**	**S5 100% JF**
Soil Classification	CH	CL	CL	CL	ML
Liquid Limit, LL [%]	61	46	45	43	42
Plastic Limit, PL [%]	22	22	21	22	27
Plasticity Index, I_p [%]	39	24	24	21	15
Liquidity Index, I_L					
Before Settlement	6.18	9.88	9.46	10.57	13.87
After Settlement	2.38	3.71	3.67	3.52	2.33

Table 3.2 Density, water content & void ratio of soil samples before and after settlement

Parameters	**S1 100% MC**	**S2 70% MC 30% JI**	**S3 50% MC 50% JI**	**S4 30% MC 70% JI**	**S5 100% JI**
Bulk Density, $\gamma_{bulk,}$ [Mg/m^3]					
Before Settlement	1.20	1.20	1.20	1.20	1.20
After Settlement	1.42	1.44	1.40	1.48	1.62
Dry Density, $\gamma_{dry,}$ [Mg/m^3]					
Before Settlement	0.33	0.33	0.34	0.35	0.36
After Settlement	0.66	0.68	0.67	0.76	1.00
Water Content, *w* [%]					
Before Settlement	263	259	248	244	235
After Settlement	115	111	109	96	62
Void Ratio, e_0					
Before Settlement	7.35	7.35	7.09	6.91	6.40
After Settlement	3.18	3.10	3.17	2.65	1.64

Figure 3.2 illustrates the measurement of the interface settlement of the floc dispersions (settlement curves) and their associated bulk density of settlement column tests over the entire column test duration of 3668 hours. The curves are presented in logarithmic time scale to emphasize the behaviours during the earlier time of settling process and the entire settling process. Generally, settling columns with pure MC materials (S1: 100% MC & S5: 100% JF) exhibited clear S-shape curves showing

distinct Flocculation, Settling and Consolidation Stages while settlement curves of mixed clay and silt compositions are mostly linear with constant settling rate. The boundaries of the different sedimentation stages are also indicatively marked on Figure 3.2.

It is noted that the flocculation time of the larger suspended silt particles in Column S5 was lesser and with steeper interface settling rate when compared with the finer suspended clay particles in Column S1. Overall, Column S5 achieved the largest settlement with the highest sediment bulk density while Column S1 achieved the least settlement and lowest sediment bulk density. This clearly shows that the weightage of fines composition in the hydraulic dredged materials will have significant influence on the sedimentation process. This observation is further supported by the mixed soil samples where Column S2 & S3 (with 70% & 50% MC respectively) with higher weightage of fines than Column S4 (30% MC) were found to have settled less with lower sediments bulk density at the end of the column tests.

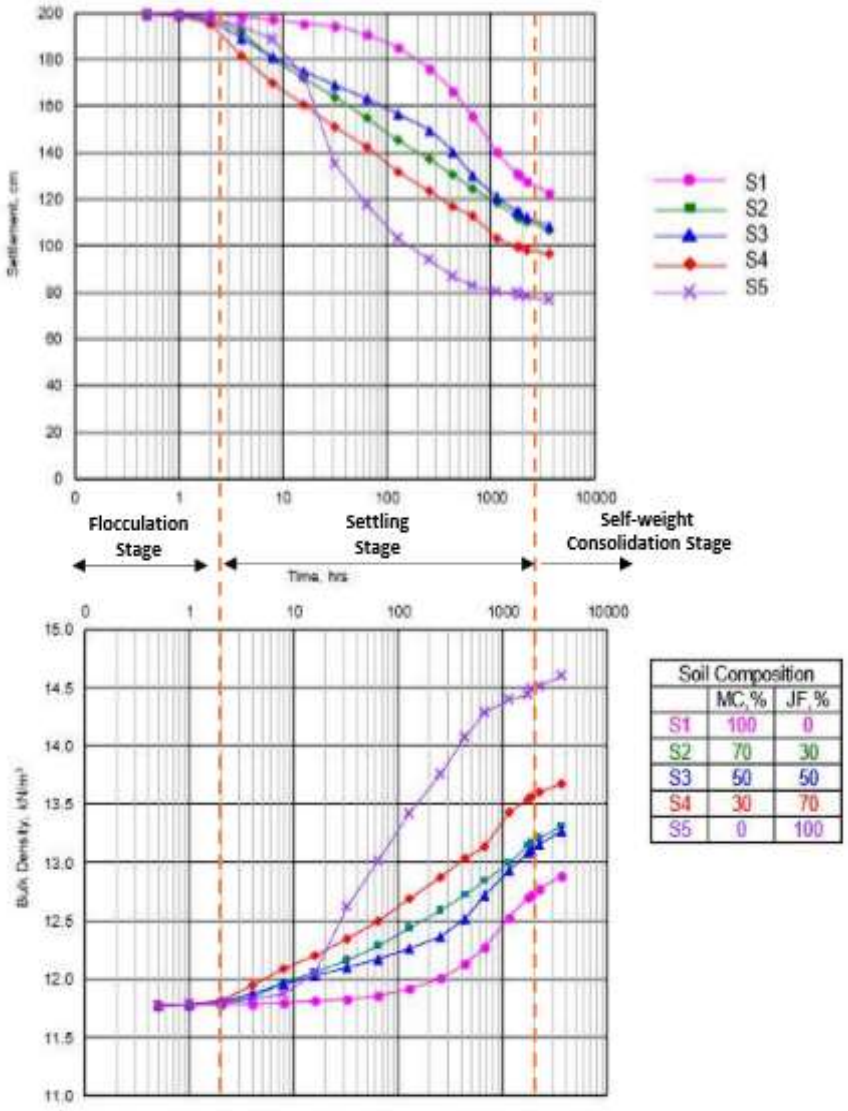

Figure 3.2 Settlement & bulk density curves of the 2m column tests

The settlement curves of Column S2, S3 and S4 show that mixed the MC-JF samples had a slower settling rate when compared to Column S5 with 100% JF after the flocculation stage. The could be due to the "hindered settling" phenomenon as the fall of the larger JF particles was interrupted by the collisions of the smaller MC particles with lower settling rate.

During the settling stage, the settling of the suspended particles and self-weight consolidation of the newly formed sediment layers were taking place concurrently which formed the “settling zone” and “consolidation zone” shown in Figure 2.8. The boundary between these two zones is termed as the “sediment formation line”. Generally, at the early part of the settling stage, settling zone will dominate the whole settling column, but it will gradually decrease and vanish at the end of the settling stage as the “consolidation zone” increases (Imai, 1981). This subsequent formation of the “consolidation zone” can be reflected by the increase in the bulk density curves illustrated in Figure 3.2 where the increase in bulk density over time indicated the increase in “consolidation zone”. The steeper rate of increase in bulk density of S5 and S4 show evidence that the higher composition of larger silt particles in the hydraulic dredged materials resulted in faster self-weight consolidation of the newly form sedimentation. The higher bulk densities achieved at the end of the column tests also indicate that the sediments form had higher shear strength.

The findings of the column tests have provided valuable information for priorities, planning and decision making for reclamation projects employing dredged seabed materials as primary fill materials. The tests had verified and concluded that the presence of higher compositions of silts will help increase the settlement rate and result in greater consolidation under the sediments own self-weight. Based on these findings, we can deduce that the presence of higher silt content in the seabed would not only will help reduce the waiting time for each cycle of hydraulic infilling but more dredged materials can also be deposited with the formation of sediments with probably higher shear strength.

3.3 Laboratory model tests on flocculant-treated soil suspensions

A typical cycle for infilling of the containment facilities can be broken down into three stages. They are (a) slurry infilling by hydraulic pumping, (b) natural sedimentation of the suspended soil particles, and (c) draining of free water from the sedimentation process and (d) self-weight consolidation (Bo, 2008). Among the three stages of a typical cycle, the natural sedimentation of the infilled slurry requires the

most time. As most reclamation projects must be completed within a stipulated timeline and budget, the presence of very high fines content and relatively low solid content coupled with its time-consuming process of the natural sedimentation of the suspended soil particles may be the deal breaker to employ dredged seabed slurry as the primary fill materials unless the settling rate of the suspended fine soil particles can be accelerated. Laboratory studies employing commercial polymers as flocculants were conducted and examined in this section. The addition of flocculants to the hydraulically dredged seabed mixture helped accelerated the aggregation of the suspended fine soils particles to bigger flocs which settle faster than the suspended fine particles. (Gregory, 1988) reported that when sufficient flocculants is added to a stable suspension, the following process will occur both sequentially as well as simultaneously as illustrated schematically in Figure 3.3. They are (a) mixing of the polymer molecules among the particles, (b) adsorption of polymer chains on the suspended particles, (c) re-arrangement of the adsorbed chains from their initial stage to an eventual equilibrium configuration, (d) collisions between particles having adsorbed polymer to form aggregates (flocs), either by bridging or by charge effects and (d) Break-up of flocs.

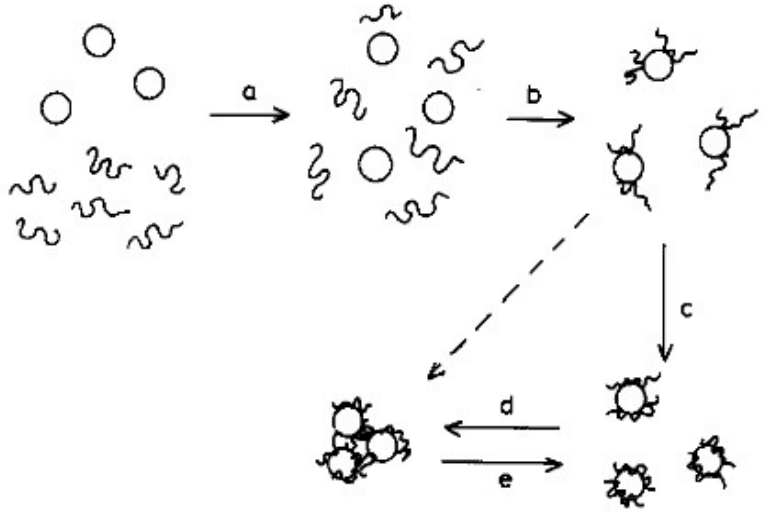

Figure 3.3 Mixing, adsorption and flocculation of suspended fined-grained particles when a polymeric flocculant is added to the soil suspension (Gregory, 1988)

The laboratory studies started with identifying the most suitable flocculant among nine selected commercial polymers. The identified polymer was then used to carry out further studies by varying the flocculant content and the water content to assess their influence on the sedimentation process. Scanning electron microscopic analyses were also carried out to examine the physical effects of flocculant-treated soil sediments at soil particles level.

3.3.1 Materials

3.3.1.1 Dredged materials

Dredged materials were used for the laboratories studies to assess the impact of using commercial flocculant to expedite the sedimentation process. The plotted distribution curves of the dredged materials illustrated in Figure 3.4 shows that the grain size was below 0.002mm. Table 3.3 lists down the basic geotechnical properties of the dredged materials. The Slurry samples were prepared by adding and mixing the dredged materials with salt water achieving a water content at 500%. The salt water was prepared with the concentration at 35 g/L NaCl.

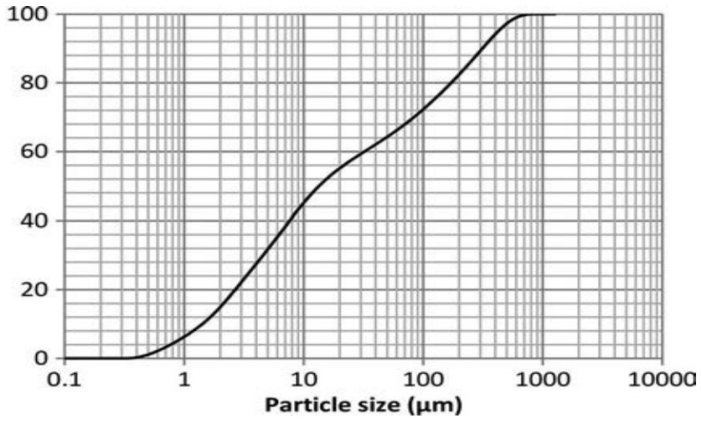

Figure 3.4 Particle size distribution curve of dredged sediments used for experiments

Table 3.3 Geotechnical properties of dredged sediments used for flocculant model tests

Geotechnical Properties	Values	Remark
Soil Classification [USCS]	CL	Inorganic clay of low to medium plasticity, gravelly clays, sandy clay, silty clays, lean clay
Water Content, W	≈ 500%	
Liquid Limit, LL [%]	36.40	
Plastic Limit, PL [%]	22.90	
Plasticity Index, Ip [%]	13.50	Ip = LL – PL
Liquidity Index, IL	13.12	IL $=\frac{W_c - PL}{I_p}$
Organic Content	9.8%	
pH	6.85	

3.3.1.2 Polyacrylamide (PAM)

Several variations of commercially polyacrylamide (PAM) flocculants were assessed to identify the most suitable flocculant to carry out subsequent laboratory model tests. PAM is a polymer formed from acrylamide subunits as illustrated in Figure 3.5. It can be synthesized as a cross-linked or simple straight-chain form. In the cross-link form, it is highly water-absorbent, forming a soft gel when hydrated. In the straight-chain form, it is used as a thickener and suspending agent. PAM forms the most common type of polymeric flocculant used in the waste treatment of kaolinite tailings in the mineral industry because of its effectiveness as flocculants to produce good settling performance for relatively low cost (Nasser and James, 2006).

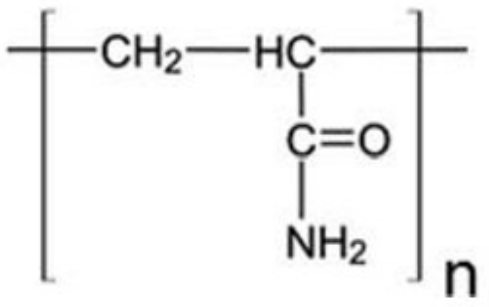

Figure 3.5 Typical acrylamide unit (He et al., 2017)

Table 3.4 PAM used to determine the most suitable flocculant for model tests

S/N	Polymer	Type	Molecular Weight	Manufacturer
1	CPAM +15	Charge Density	15 million	Longxin Co. Ltd
2	CPAM +20	Charge Density		
3	CPAM +30	Charge Density		
4	CPAM +45	Charge Density		
5	CPAM +50	Charge Density		
6	CPAM +60	Charge Density		
7	CPAM +70	Charge Density		
8	APAM	Anionic PAM	20 million	
9	NPAM	Non-ionic PAM	15 million	

Table 3.4 lists the different types of PAM polymers (cationic, anionic and non-ionic) that were evaluated to identify the most suitable flocculant for subsequent model tests. Generally, flocculation using high molecular weight cationic PAM occurs on the suspended particle surface where the cationic PAM chains are adsorbed. Thus, charge neutralisation becomes the major mechanisms in which the cationic PAM will locally reverse the particle surface charge. Pearse and Barnett (Pearse and Barnett, 1980) study reports that when high molecular weight flocculants were used, the collision with negative patches on another particles allowed bridging and then aggregation. On the other hand, when low molecular weight cationic flocculants adsorbing were used, bridging were not favoured due to the short macro-length and strong adsorption as shown in Figure 3.6

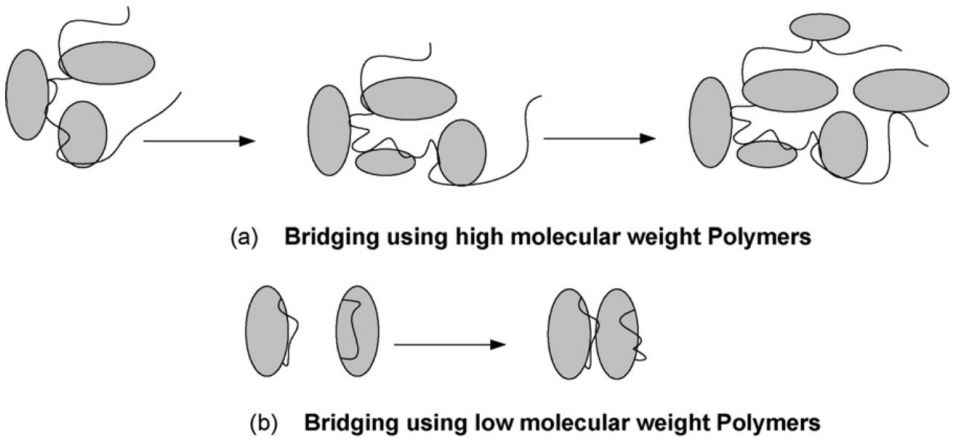

Figure 3.6 Differences in bridging mechanism for high and low molecular weight polymers (Pearse and Barnett, 1980)

For high molecular weight anionic PAM, the polymer bridging mechanism is of primary importance while its charge neutralisation will be of secondary or little importance. Anionic PAM was found to be more effective than cationic polymers in producing distinct sediment structures and highly clarified supernatants. It also may help avoid the destabilisation of clay particles by excessive polymer adsorption driven by strong electrostatic attraction (Mpofu et al., 2003).

3.3.1.3 Preparation of polyacrylamide flocculants

The PAM flocculants were introduced to the slurry mixtures in solutions form. The PAM solutions were prepared by dissolving dry PAM granules into de-ionized water at 0.2% concentration by mixing the PAM solution for 1 hour using a magnetic stirrer.

200 mL PAM solutions were introduced to 500ml of slurry samples in 5 steps of increment dosages. After each dosage, mixing was carried out manually by stirring with a rod. After the last dosage was added, the mixtures were then allowed to rest for 10 minutes and the settlement of the soil-water interface was then measured.

Table 3.5 shows the amount of equivalent flocculant added to per kg of dry dredged materials for each dosage.

Table 3.5 Dosages of flocculants added to the dredged material slurry

Flocculant Dosage	Vol. added	Equivalent flocculant added per kg of dried dredged material (g/ kg)
1	5 ml	0.11
2	20 ml	0.54
3	25 ml	1.08
4	50 ml	2.16
5	100 ml	4.32
Total	200 ml	8.21

3.3.2 PAM flocculant selection

Figure 3.7 illustrates the status of the sedimentation progress, 10 minutes after the third dosage of PAM flocculants. This is equivalent to 1.08g of flocculant added to every kg of dry dredged materials in the fine-grained soil suspension. Two more dosages will be carried out before completion of mixing. From visual inspection, the suspension in the control beaker, which contained no flocculant, remained in full suspension after 10 minutes. On the other hand, in beakers where different types of PAM were added to the suspension, distinct interfaces were observed between the settled suspensions and supernatants. In suspensions where anionic and non-ionic PAM were added, the mixtures showed clearer supernatants and thicker layers of sediments when compared with the beakers added with cationic PAM.

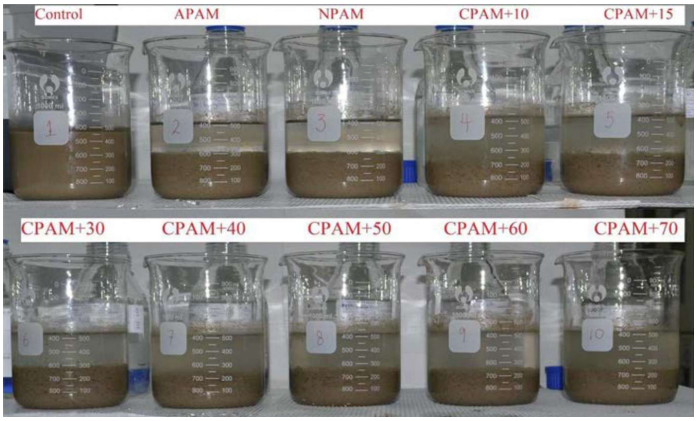

Figure 3.7 Sedimentation of dredged slurry mixtures using different PAM flocculants

Figure 3.8 presents the settlement of the water-suspension interfaces in beakers where different PAM flocculants were added at different dosage of 0.1g/kg, 0.5g/kg, 1.0g/kg, 2.0g/kg and 4.0g/kg. The mixture remained in suspension in the control beaker with no sign of settlement. Large settlements were for all types of flocculants when 0.1g/kg dosage were added to the suspensions. Sharp drops in the water-suspension interfaces were observed until the dosage reached 1.0g/kg. Drops in water-suspension interfaces continued but more gradually when the dosages increased from 2.0 to 4.0 g/kg. It is clearly noticeable that the effectiveness of PAM addition diminished for dosage above 1.0g/kg.

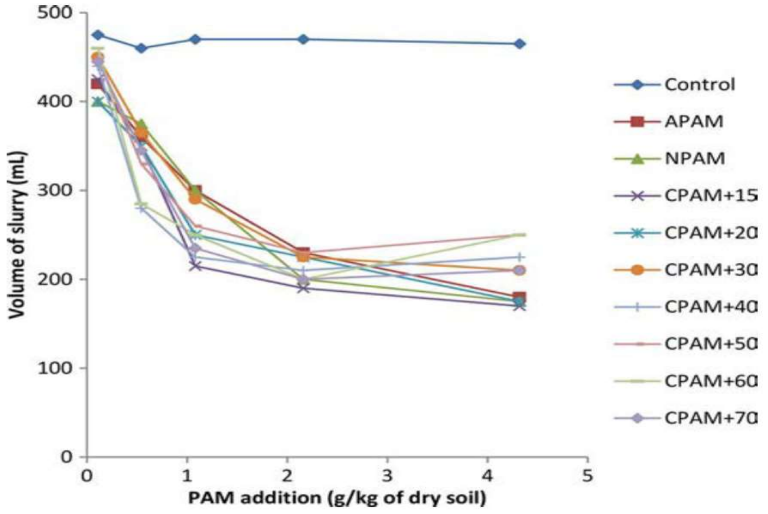

Figure 3.8 Influence of PAM dosage in the settling behaviour of clay suspensions

The effectiveness of the flocculant depends on many factors. They include the molecular weight and surface charge of the flocculant, initial conditions of the suspended mixtures, mineral contents of the suspended particles and etc. Among the 9 different types of PAM flocculant employed, CPAM +15 (cationic PAM) was noted to have the largest settlement at 60% volume of the fully suspended volume. Largest settlements were observed in every dosage (0.1 – 4.0 g/kg) using CPAM +15.

The effects to sedimentation for CPAM +15 was assessed to be most pronounced within the concentration of 0.1-1g/kg. Further increase in dosage concentration thereafter brought diminishing effects. CPAM +15 at a concentration of 1.0 g/kg was selected for subsequent experiments. This is in good agreement with the manufacturer's recommendation to apply of 1-2 g/kg of CPAM to achieve optimum sedimentation results.

3.3.3 Effects of water content and flocculant concentration

3.3.3.1 Methodology

In this group of model tests, experiments were conducted using 1-liter glass cylinders. The cylinders were 35 cm in height and 6 cm in diameter. The preparations of the suspended clay-water mixtures and the selected CPAM+15 flocculants solutions were the same as those described in section 3.3.1.3. However, the prepared flocculant solutions were added all at once instead of adding in stages. Manual mixing by stirring the slurry-flocculant mixtures for 30 rounds using a mixing rod. The slurry-flocculant mixture were rested for 60 days before measurements on the settlement were taken. Five water content ranging from 100.7 -879.5% were conducted. For each water content, 5 concentrations ranging from 0 to 3.0 of the PAM flocculent selected in experiment 1 were performed. In total, 25 experiments were carried out to understand the effects of water content and flocculant concentration to the sedimentation process.

3.3.3.2 Results and analysis of beaker model tests

The settling curves of the CPAM +15 treated clay suspension are presented in both arithmetic and logarithmic scales in Figure 3.9 (a) to (e).

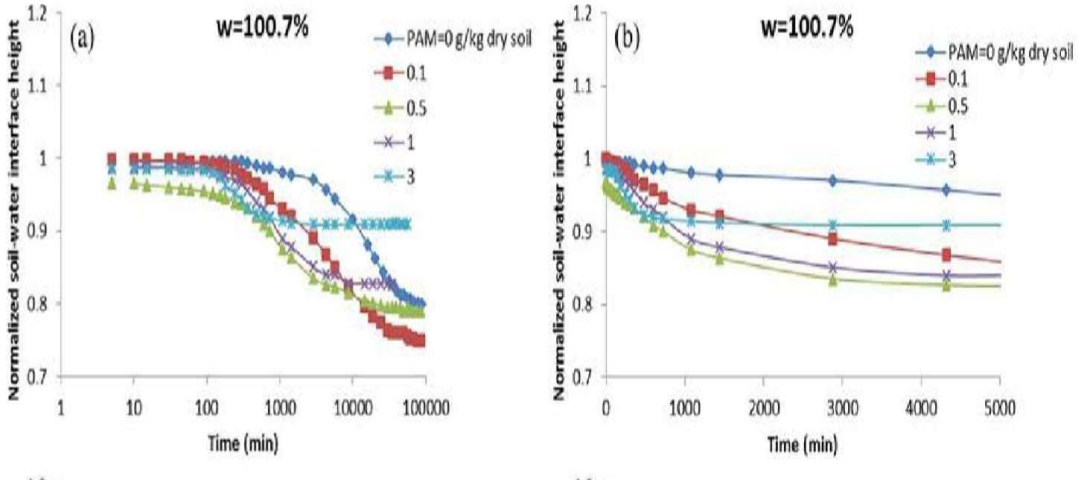

(a) Settling behaviour of CPAM +15 treated suspension at 100.7% water content

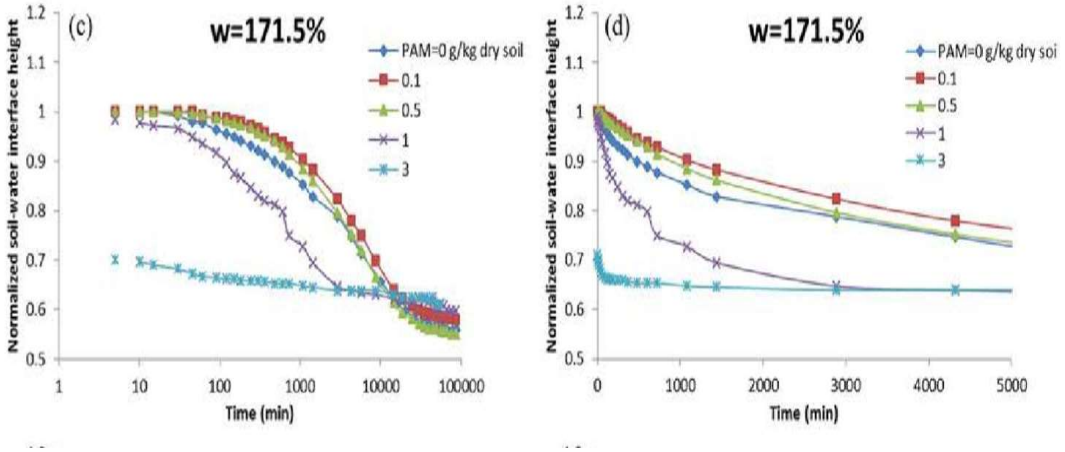

(b) Settling behaviour of CPAM +15 treated suspension at 171.5% water content

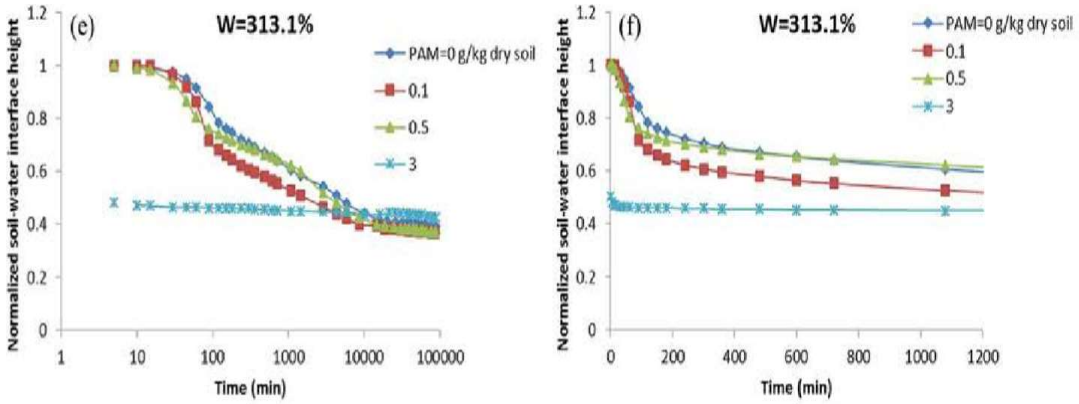

(c) Settling behaviour of CPAM +15 treated suspension at 313.1% water content

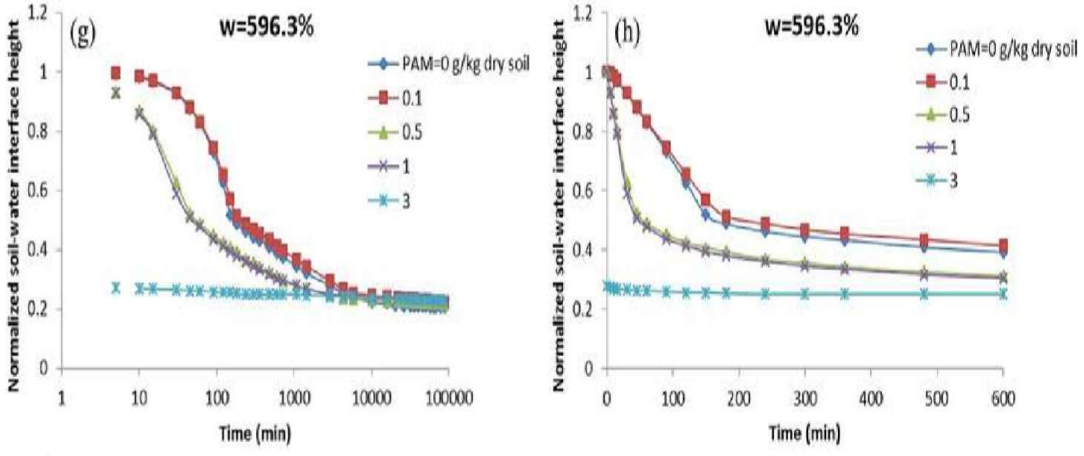

(d) Settling behaviour of CPAM +15 treated suspension at 596.3% water content

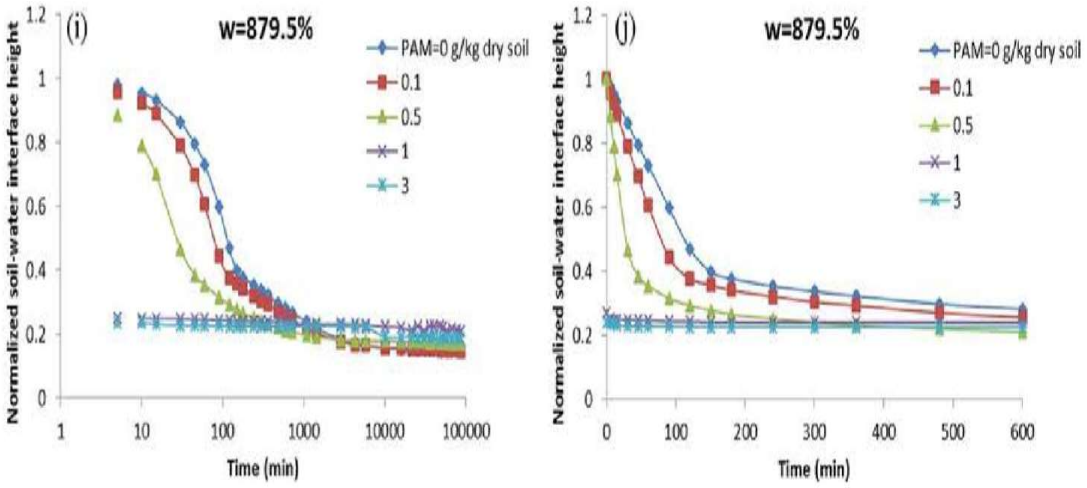

(e) Settling behaviour of CPAM +15 treated suspension at 879.5% water content

Figure 3.9 Settling behaviour of CPAM +15 treated suspension at different water content

It is notable in Figure 3.9 (a) and (b) that the flocculation stage of clay suspension with 100.75% water content took a long time. The transition from flocculation stage to settling stage took about 1000 minutes. At the end of the experiment, the settling curves show that the soil suspensions settled between 10-25% of the normalised height. At different flocculent concentrations, the settlement achieved at concentration of 1/kg and 3g/kg were 17% and 10% of the normalised height respectively. 20% settlements were observed for flocculation concentration at 0.5g/kg and when no flocculant was added. The largest settlement of 25% were observed at flocculation concentration at 0.1g/kg after 10,000 minutes. These unexpected erratic behaviours of the settling curves observed was probably due to incomplete flocculation at low water content and at the same time the formation of very small flocs from the suspended clay particles which are unable to settle as quickly.

Figure 3.9 (c) and (d) shows the settling curves at 171.5% water content. It has shorter flocculation time than the settling curves at 100.7% water content. The transition

from the flocculation stage to the settling stage took about 100 minutes. All the settling curves achieved 40-45% settlement of the normalised height. All settling curves displayed clear flocculation stage, settling stage and consolidation stage except for the settling curves with the flocculant dosage of 3g/kg which displayed an almost instantaneous drop in the clay suspension to 70% of the normalised height within 10 minutes. Similar settling behaviours were observed for all subsequent experiments with higher content with higher flocculant concentration at 3g/kg. This is probably attributed to the quick formation of large flocs which settle quickly. The clay suspension undergo natural sedimentation is observed to have a higher settling rate when compared with the settling curves with flocculant dosage of 0.1 and 0.5 g/kg.

Figure 3.9 (e) and (f) show the settling curves at 313.1 % water content. The time needed for flocculation stage was less when compared to 171.5% water content. The sedimentation procees moved from the flocculation stage to the settling stage in just 10 minutes. 50-60% settlement of the normalised height were achieved at the end of the experiment. All tests exhibited clear characteristics of the sedimentation except for the settling curves with the flocculant concentration of 3g/kg which have similar behaviour was observed at 171.5% water content. Although the settling curves of lower flocculant concentration at 0.1 and 0.5kg showed faster settling rate that control, higher settling rate of clay suspension was observed at 0.1g/kg than 0.5g/kg flocculant concentration.

Figure 3.9 (g) and (h) illustrates the settling curves at 596.3 % water content. The transition from the flocculation stage to the settling stage took only 10 minutes. 75-80% settlement of the normalised height were generally achieved at the end of the experiment. All model tests displayed clear characteristics of the sedimentation process except for model test with the flocculant concentration at 3g/kg. Model tests with the flocculant concentration at 0.5g/kg and 0.1g/kg has similar settling rate. It was observed that the settling rate at the control clay suspension is faster than the clay concentration with 0.1g/kg flocculant concentration.

Figure 3.9 (I) and (j) shows the settling curves at 879.5% water content. The transition from the flocculation stage to the settling stage also took about 10 minutes. Generally, more than 80% settlement of the normalised height were achieved for all model tests. All model tests displayed clear characteristics of the sedimentation process except for model tests with flocculant concentration at 1g/kg and 3g/kg. Both clay suspensions displayed instantaneous drop in the clay suspension interface to 80% of the normalised height in just 10 minutes. The settling curves with at lower flocculant concentrations behaved normally within expectations.

In this group of model tests, the effects of water content and flocculant concentration of CPAM+15 were examined. It was clearly demonstrated by the model tests that the water content affects the duration, rate of settling and the total amount of settlement in the clay suspensions.

The sedimentation curves behaviour of clay suspensions at water content 100.7%, 175.5% and 313.1% were erratic as the settling rate did not increase with higher flocculant concentrations. This erratic and unpredictable behaviours could probably be due to the uneven distributions of the flocculants in the clay suspension with lower water contents. Generally, it was observed that the predictability of the settling rate and the amount of clay suspension settling improved with increased flocculant concentration in samples with water content higher than 313.1%.

During the sedimentation process, the *settling rate at the settling stage* in the sedimentation curves were faster than that of the consolidation stage. They were represented as a linear function of time while in the settling rate at the consolidation stage were represented as a logarithmic function of time. As such, the settlement rate at the settling stage is defined as the slope of sedimentation curve at settling stage:

$$V_s = \frac{\Delta h_s}{\Delta t_s} \tag{3.1}$$

The *settlement rate at the consolidation stage* is defined as the slope of sedimentation curve (semi-log scale) in the consolidation stage:

$$v_c = \frac{\Delta h_c}{\log\left({}^{t_{cf}}/_{t_{co}}\right)} \tag{3.2}$$

The settlement rates at the settling stage and the consolidation stage tabulated using equations (3.1) and (3.2) are illustrated in Figure 3.11 and Figure 3.12 respectively.

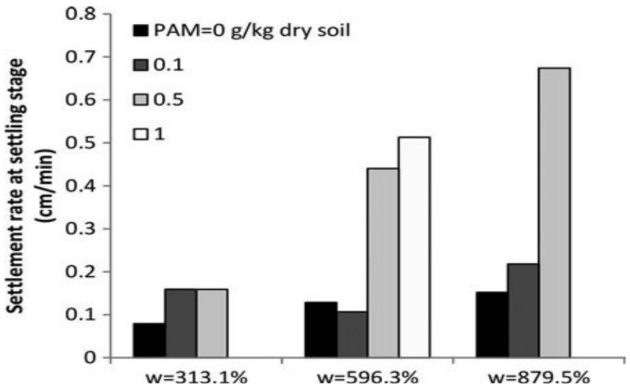

Figure 3.10 Settling rates of soil suspensions at the settling stage based on equation 3.1

Figure 3.10 illustrates that by merely rising the water content in the soil suspensions, the settling rate of the control increased without the need of flocculant. It was observed that the increase in flocculant concentrations generally improved the settling rates of the clay suspensions with higher water content. At 313.1% water content, with the additional of 0.5g/kg flocculant solutions, the settling rate doubled to that of the control. No difference was noted in the settling rates of clay suspensions with 0.1g/kg and 0.5g/kg flocculent concentrations.

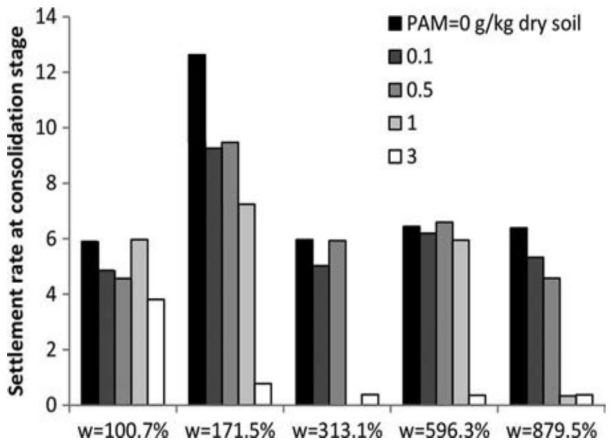

Figure 3.11 Settlement rates at consolidation stage calculated using equation 3.2

Figure 3.11 illustrates the settlement rate at the consolidation stage. The settlement rates were stable across different water content for flocculant concentrations between 0.1 to 1.0g/kg. Notable differences in settling rate were observed for clay suspensions with flocculant concentration at 3.0g/kg. Almost instantaneous liquid-solid separation of the clay suspension were observed but with considerably smaller consolidation rates when compared to clay suspension samples with lower flocculant concentration. The results demostrated that higher flocculant concentration will help acelerate the settling rate of suspended particles. However, it could also modify the sediment's fabric in such a way that the consolidation rate of sediments were inhibited. Therefore it is important to balance the benefits of expediting sedimentaion with slower sediments consolidation when flocculants are used.

Figure 3.12. illustrates the water content of the sediments at the end of the model tests. It was observed that the water content of the sediments increased with higher flocculant concentrations and the initial water content of the clay suspensions. This is because, higher flocculant concentrations and water contents could have allowed and encouraged the forming of smaller and more uniform flocs creating more micro-pore spaces , trapping more water within the sediment. Further investigations would be required to support this deduction.

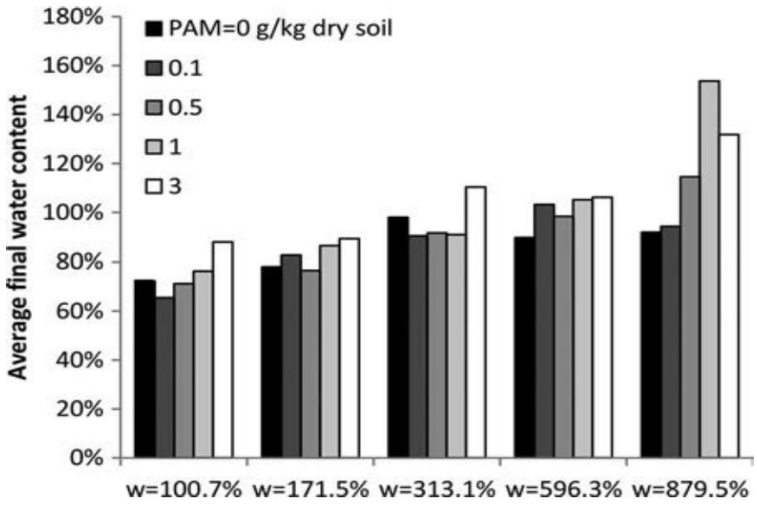

Figure 3.12 Average water content in sediments after sedimentation process

3.3.3.3 Results and analysis of 1-metre settling column

To validate the findings from the beaker model tests, 1-metre cylindrical settling columns with 15cm diameter were usedThe used of larger diameter settling columns helped reduced the influence of the wall on the settling behaviours of the flocculant treated suspensions. The 1-metre height provided greater depth for clearer and more distinct visual observations of the sedimentation process.

Four model tests were carried out. The water content for the dredged material slurry was set at 171.5% for all 4 model tests and the flocculant contents were 0, 0.5, 1, and 3 g/kg dry soil, respectively. The preparations of the clay suspensions and CPAM+15 flocculant solutions were the same as those described in Section 3.3.1.3. The prepared flocculant solutions were added all at once instead of adding in multiple steps. Mixing was performed until the clay suspensions appeared to be uniform visually.

The results of the 4 model tests are shown in Figure 3.13(a) and (b). Distinct flocculation and settling stage were observed at clay suspensions with 171.5% water content. The consolidation stage probably commenced after the settling curves show

levelling trend at 0.6 normalised soil-water interface height. Long flocculation time were taken and transition from the flocculation stage to the settling state was observed after 100 minutes. Generally, 35-40% of settlement of the normalised height were achieved at the end of the experiment. This is close to the 40-45% settlement achieved using smaller beakers at the same water content. It was noted that the control under natural sedimentation achieved more settlement in comparison. It was observed that soil suspension treated with lower flocculants concentrations achieved higher settling rate with larger settlement in the column tests. The experiment findings agrees well with the erratic behaviours observed in Figure 3.9(a) and (b).

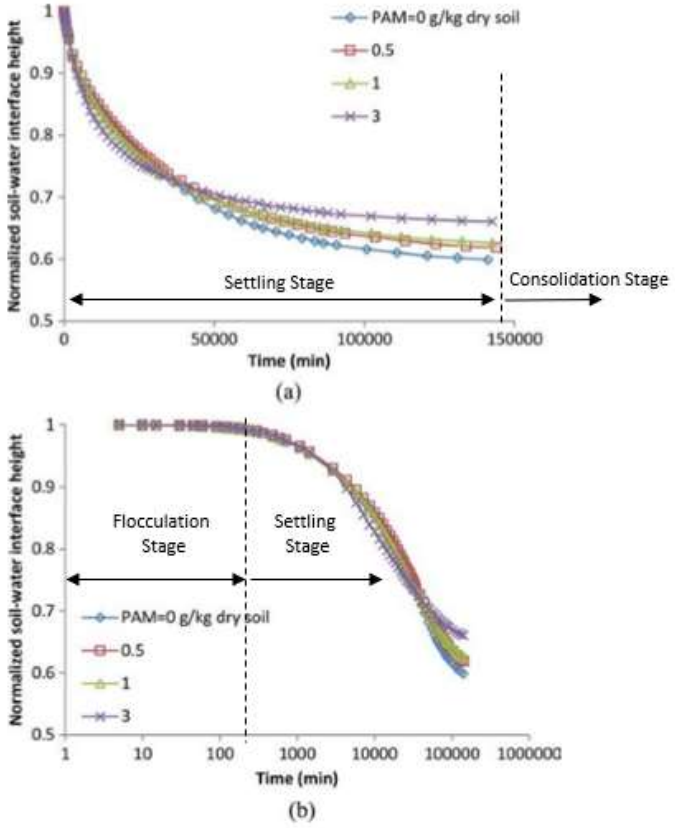

Figure 3.13 Sedimentation behaviour of CPAM+15 treated clay suspension in 1-metre columns at 171.5% water content. (a) settling curves in arithmetic scale (b) settling curves in logarithmic scale

Figure 3.14 illustrates the particle size distribution curves of the sediments at different flocculant concentrations for the 1-metre settling column tests. It is apparent that the additions of flocculant have modified the distribution of the particle sizes as the suspended particles formed bigger flocs. The floc sizes of the control show the distribution of the original clay particles spanning across a range 0.5µm to 700µm. The particle size distribution curves indicates that bigger flocs were formed at flocculant dosage of 1.0g/kg with flocs sizes spanning from 0.5µm to 1000µm when compare to control. At flocculant dosage of 0.5g/kg, the gap graded curve shows that about 34% of its flocs fall below 200µm, with minimum floc sizes between 200µm to 450µm and with 66% bigger floc between 500µm to 1000µm. At flocculant dosage of 3.0g/kg, the steep grading curve indicates the formation of uniform graded flocs sizes with 88% of the floc sizes between a narrow range of 200µm to 500µm.

From the distribution curves, it is clearly shown that the size of the focs formed does not necessary have a clear cut direct relationship with the flocculent concentrations applied which assume that bigger and heavier flocs could be formed with increased dosage of flocculant applied.

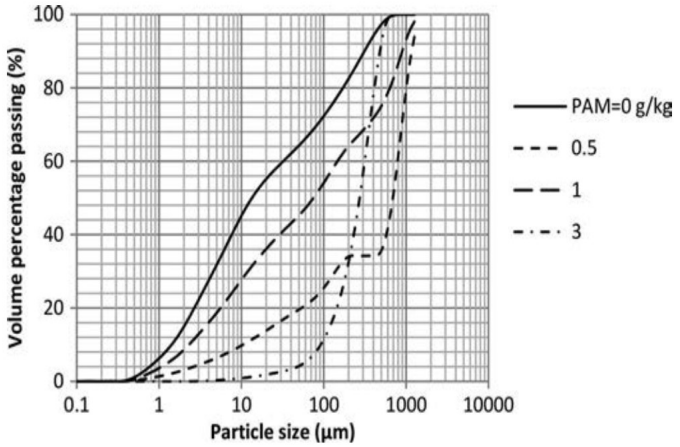

Figure 3.14 Size distribution of flocculated-treated soil slurry using hydrometer test methods

Figure 3.15(a) and (b) illustrates the Scanning Electron Microscopy (SEM) photos taken for sediments samples from the control and flocculant treated sediments at

3g/kg dosage respectively. It was observed that the clay particles at the control sediments were arranged in a parallel and compact manner with face-to-face contacts. While the clay particles in the flocculant treated sediments were randomly oriented, less compact with edge-to-edge contacts. Figure 3.16 shows the zoom out SEM image of 3.17(b) which shows how the aggregation of the clay particles through the process of flocculation formed a single unit of floc. This floc is several times larger than the size of the clay particles which therefore would settle much faster than the suspended single clay particles.

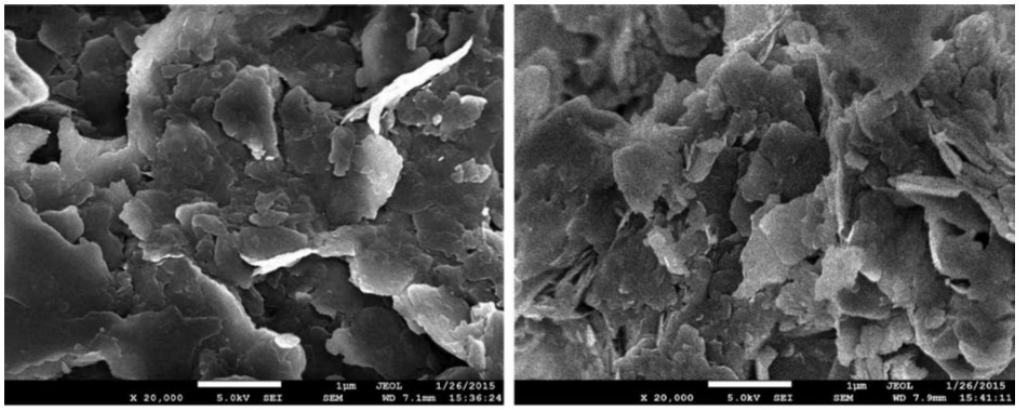

Figure 3.15 (a) SEM of sediments from Control (b) SEM image of flocculant treated sediments

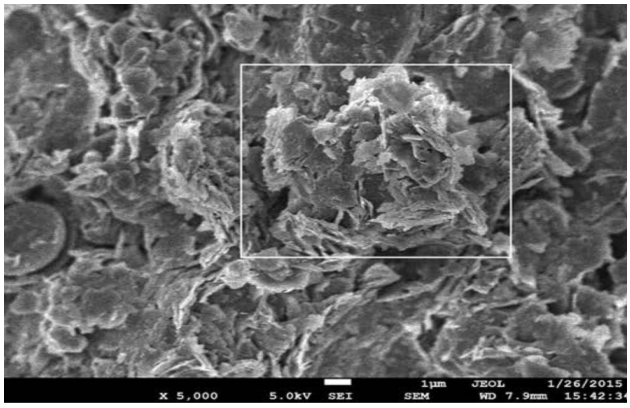

Figure 3.16 Zoom out SEM images of flocculant treated sediments

3.4 Conclusions

In this chapter, the natural sedimentation and flocculants assisted sedimentation were examined using settling columns. The studies have concluded the following findings:

i. Different soils compositions will result in different behaviours during natural sedimentation process. Soil suspensions with higher composition of silts will lead to faster settling rate and more consolidation when compare to soil suspensions with higher fines compositions.

ii. The effects to sedimentation for CPAM +15 was assessed to be most pronounced among the 9 different types of PAM polymers employed. Any further increase in flocculant concentration beyond 1g/kg at 500% water content would bring diminishing effects in the settling rates of the soil suspension.

iii. Water content of the soil suspension have tremendous impact to the sedimentation process. Erratic sedimentation behaviours were observed for soil suspensions using flocculant with water content lower than 313%. No direct relationship can be drawn from the particle size distribution curves of the flocs size form from the flocculation at these water contents. Predictability of the sedimentation behaviour improved with higher water content.

iv. Clay particles in flocculant-treated suspensions are randomly oriented with edge-to-edge contacts to form clusters of flocs. Clay particles with no flocculant added to the clay suspension were arranged in parallel face-to-face manner. The manner on how the flocs are formed from clay particles during flocculation apart from affecting the behaviour and duration of the sedimentation process and will also have direct effects to the geotechnical properties (e.g. shear strength and consolidation) and consolidation behaviours of the newly form sediments.

v. Although flocculant dosage could expedite the settling rate of suspended particles, but in the process, it had also modified the sediment's fabric in such a way that it would inhibit the consolidation rate of the sediments. As such, when considering the use of flocculant to expedite the sedimenation process, it is important to balance its positive effects in acelerating sedimentation with its negative influence on sediment consolidation.

CHAPTER 4 EFFECTS OF VACUUM CONSOLIDATION ON DREDGED SEABED MATERIALS

4.1 Introduction

Vacuum consolidation has been identified as one of the most suitable soil improvement techniques that can be applied to treat the dredged seabed sediments despite some difference in the soil skeleton structures and the stress states between the sediments and the in-situ soils.

To evaluate the effectiveness of using vacuum consolidation to improve ultra soft soils similar to dredged seabed sediments, eight laboratory model tests using a consolidation tank with a single PVD was conducted with different clay samples. The testing program, model test set up, test results and data analysis are presented in this Chapter.

4.2 Testing program

The testing program consisted of eight laboratory model tests shown in Table 4.1. The tests were grouped into four comparison studies as illustrated in Table 4.2 to examine and compare the effects of vacuum consolidation under different conditions namely:

i) Comparison study 1

The purpose is to understand the consolidation behaviors of different ultra soft soils when treated by the membrane vacuum consolidation technique. Two types of kaolin samples were used for the model tests. The lumpy kaolin samples represented the grab dredged material and the kaolin slurry sample represented the hydraulic dredged seabed materials from Cutter Suction Dredger (CSD) and Trailer Suction Hopper Dredger (TSHD). Results of Test 1, 5, 6 and 7 were examined.

ii) Comparison study 2

The purpose is to compare the effectiveness of using band drain and circular drain in the membrane vacuum consolidation technique to consolidate marine clay samples. Results of Tests 4 & 5 were studied .

iii) Comparison study 3

The purpose is to evaluate the performance between the membrane and the membraneless vacuum consolidation technique to improve dredged seabed sediments. Results of Test 1 and 3 were compared.

iv) Comparison study 4

The purpose is to study the effects of surcharge when applied together with a membrane vacuum preloading system. Results of Test 1 and 2 were studied.

Table 4.1 Details of the eight laboratory model tests

	A	B	C	D
Test	Sample	Drain	System	Surcharge
Test 1	Kaolin paste	Band	Membrane	NA
Test 2	Kaolin paste	Band	Membrane	+40 kPa
Test 3	Kaolin Slurry	Band	Non-Membrane	NA
Test 4	MC1	Circular	Membrane	NA
Test 5	MC1	Band	Membrane	NA
Test 6	Lumpy	Band	Membrane	NA
Test 7	MC2	Band	Membrane	NA

Table 4.2 Details of the comparison studies

Comparison Study 1 ***Soil samples***	**Comparison Study 2** ***Drains type***	**Comparison Study 3** ***VC technique***	**Comparison Study 4** ***Loading conditions***
Compare Kaolin, MC1 & MC2, (Test 1, 5 & 7)	Band Vs Circular Drains (Test 4 Vs Test 5)	Membrane Vs Membraneless (Test 1 Vs Test 3)	No Charge Vs + 40kPa surcharge (Test 1 Vs Test 2)
Lumpy Vs Kaolin paste (Test 1 Vs Test 6)			

4.3 Laboratory model tests materials and setup

4.3.1 Materials

Three types of cohesive soil samples with different compositions of dredged seabed sediments in different physical forms were used for the laboratory model tests. Their details of the model tests and characteristics of the soils are described in this section.

4.3.1.1 Kaolin paste

Kaolin paste is commonly used to study the engineering properties of clay. In its natural state, kaolin is a white, soft powder consisting principally of mineral kaolinite. Kaolin powder was employed in these laboratory model tests as the base material. It was mixed with water using a shear mixer to produce a consistent paste with an initial water content of 90% to mimic the dredged seabed materials high in both water and clay content shown in Figure 4.1. The kaolin paste represented hydraulic dredged materials high in clay and water content. The kaolin pastes were placed in layers by pouring the kaolin paste slowly into the consolidation tank. Time was allowed for air bubbles to escaped before the next layer of kaolin paste was poured in. The process was repeated until the consolidation tank was filled up.

4.3.1.2 Lumpy kaolin

The lumpy kaolin samples represented lumpy and stiff grab-dredged seabed sediments. The lumpy kaolin samples were prepared by consolidating kaolin paste with an initial water content of 98.2% under a pressure of 40 kPa. The water content of the kaolin sample after consolidation was 79.3%. The consolidated kaolin samples were rolled into ball-like lumpy form into two different sizes measuring 6 cm and 3 cm in diameters. The prepared lumpy kaolin balls were poured into the consolidation tank. Water was then added to the consolidation tank before testing to reproduce similar conditions where grab-dredged lumpy clay is deposited into the seabed.

4.3.1.3 Marine clay

Two sources of naturally occurring marine clay samples representing actual dredged seabed sediments with varying composition of fines, silts, sand, shell and etc. were used for the laboratory model tests. The first source of marine clay (MC1) as shown in Figure 4.2 was retrieved from the seabed at Marina South which comprised mainly of Kallang Formation which was high in clay content. The second source (MC2) was from Tuas seabed as shown in Figure 4.3. It comprised of mainly Jurong Formation which was high in silt content. In general, both marine clay samples were greyish in color with high water content.

Similar to the placement of kaolin pastes, the shear mixer was used to mix the marine clay samples into a consistent paste using its own water content. The marine clay paste were then poured directly in the consolidation tank slowly by layers. Time was allowed for the marine clay paste to "set" to ensure all bubbles were escaped from the paste before commencing with the model tests.

The grain size distributions of the marine clay samples are shown in Figure 4.4. The distributions were determined using wet and mechanical sieve analysis according to ASTM D422-03 (1998). Classifications of soils were then determined accordingly to ASTM D2487-00 (1998). MC1 has very high silt and clay compositions (80%) with a foul smell indicating the presences of organic content while MC2 gap-graded distribution curve shows higher composition of fine sand (55%).

Figure 4.1 Kaolin slurry sample that represents dredged seabed slurry with high clay content

Figure 4.2 MC1 from Marina South seabed contain mainly Kallang Formation materials

Figure 4.3 MC2 from Tuas seabed contain mainly Jurong Formation materials

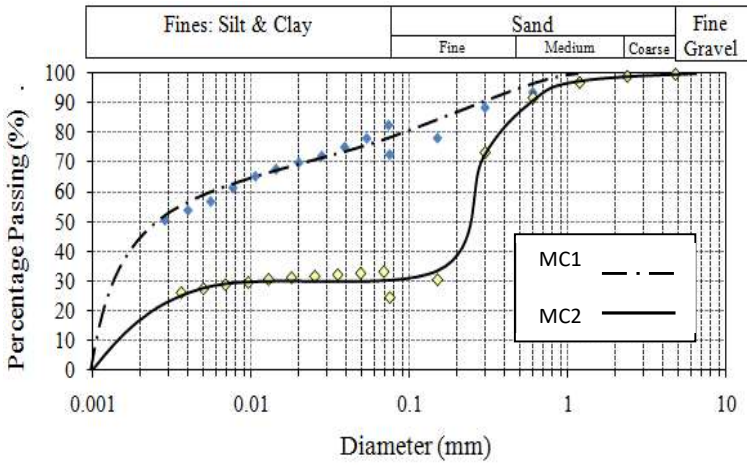

Figure 4.4 Grain size distribution of MC1 and MC2

4.3.1.4 Characteristics of materials

Table 4.3 gives a summary the physical properties of the kaolin and marine clay samples (MC1 & MC2) that were used for the laboratory model tests.

Table 4.3 Physical properties of kaolin and marine clay samples

Physical Properties	Kaolin	MC1	MC2
Specific Gravity	2.54	2.54	2.46
Liquid Limit, LL (%)	69	43.6	30.4
Plastic Limit, PL (%)	38	21.9	23.3
Plasticity Index, PI (%)	31	21.7	7.2
Fines Content (%)	100	72.34	24.28
Soil Classification	MH, Clayey Silt	OL, Organic Clay	Silty Sand

4.3.2 Model tests setup

A fully instrumented single PVD cylindrical steel consolidation tank was used for the vacuum preload model tests. The metal cylindrical tank is 30cm in diameter and 100cm in height. Figure 4.5 shows the physical setup and Figure 4.6 illustrates the overall schematic set up with its key components. The key components and their functions of the cylindrical consolidation tank are summarized in Table 4.4.

Figure 4.5 Physical set up of the cylindrical vacuum consolidation tank

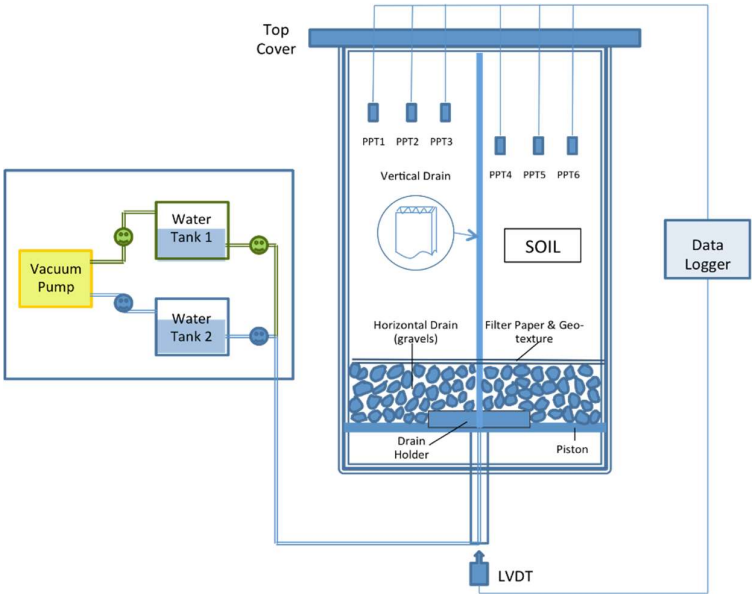

Figure 4.6 Schematic diagram of the cylindrical vacuum consolidation tank

Table 4.4 Key components and their functions in the cylindrical vacuum consolidation tank

Components	Functions	Quantities
Vacuum Pump	Creates vacuum suction in PVDs	01
Mini pore-water pressure transducer (PPT)	Measure soil consolidation response	06
(LVDT)	Electrical transformer used for measuring linear displacement (Settlement of soil)	01
Water Tanks	Store water removed from the soil samples by vacuum preloading	02
Compressed air system	Apply +40kPa of surcharge loading to soil samples (Test 2)	01
Data logger with Computer	Record PPT response during model test operations	01

4.3.2.1 Vacuum system

A system of two water tanks for water collection working in parallel was designed to ensure undisrupted continuous operations and maintenance of stable vacuum pressure within the consolidation tank. When one water tank was full, its valve was closed and the second tank valve was then opened to continue receiving the water from the soil samples under vacuum while the water in the first tank could be emptied. In all the model tests, the vacuum pressures in the PVDs were applied through the bottom. The vacuum pressure was kept consistent at -80kPa throughout every model test to simulate the optimum vacuum value that could be achieved in the field.

4.3.2.2 Pore pressure measurement

The top cover plate was used as a platform to insert six pieces of mini pore pressure transducer (Druck® PDCR81-300 kPa) at 40 mm interval to measure the pore pressure responses in the consolidation tank as illustrated in Figure 4.7. The

transducers were calibrated every time before conducting the consolidation. They were also wrapped with a layer of filter paper to prevent clogging of fine clay particles.

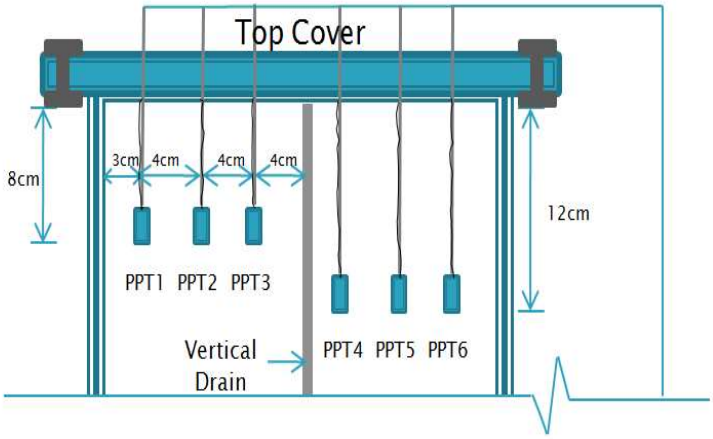

Figure 4.7 Pore pressure set up in cylindrical consolidation tank

4.3.2.3 PVD installation

Prefabricated vertical band drains (PVDs) were positioned in the center of the consolidation tank before the soil samples were placed. Colbond® CX 1000 band drain with a width of 100 mm and a thickness of 5.3 mm was used. The filter of the CX 1000 drain had a permeability of $11*10^{-4}$ m/s while the core had a discharge capacity of $70*10^{-6}$ m^3/s in a straight configuration and a $20*10^{-6}$ m^3/s in 25% buckled condition at a confining pressure of 100 kPa. The cylindrical drain used was 50 mm in diameter and wrapped with a CX 1000 filter. The filter was secured to the cylinderical drain by using staples.

4.3.2.4 Vacuum preloading set up in the consolidation tank.

Most of the model tests were conducted using the membrane vacuum consolidation technique. The set up in the consolidation tank included a 100mm thick gravel layer of about 20 mm in diameter which was used to stimulate the sand drainage blanket in the membrane system. Vacuum was transferred to the soil samples via the layer of granular drainage blanket to the PVD as shown in Figure 4.8. The granular drainage blanket was positioned at the bottom of the cylindrical consolidation tank. A layer of

geotextile was placed over the gravel layer before the consolidation tank was filled with the soil samples to segregates the two materials.

Figure 4.8 Gravel drainage layer for membrane vacuum consolidation technique

For the membraneless system, this drainage blanket layer was not included in the consolidation tank. The PVD was connected directly to the the vacuum line during the membraneless system model test.

4.3.2.5 Deformation measurement

A Linear Variable Differential Transformer (LVDT) was used to measure the settlement of the consolidated soil samples. The maximum range of the LVDT was 100 mm. It was calibrated using a manual calibrator.

4.3.2.6 Data storage

The data acquisition system consisted of Hydra® data logger, software for data collection, PC and uninterrupted power supplier. Measurements of miniature PPTs and LVDT were recorded using the data logger, and the PC served as a controller to store and transfer data recorded from data logger.

4.4 Test results and analysis

4.4.1 Water content

At the end of each model test, the vacuum improved soil samples were extruded from the cylindrical consolidation tank and were cut open along the vertical plane. Water content at the tip of each PPT was measured. As an example, the water content measured at the end of Test 3 on kaolin slurry is illustrated in Figure 4.9.

It can be observed in Figure 4.9(a) that the water content reduced from the initial 90.61% to a value around 45% at the end of the model test. The final water content varied with the positions between 44.49% and 46.11%. Generally, it was observed that the water content of the soil samples closer to the vertical drain was lower than that of soil samples collected further away from the drain. The water content curves illustrated in Figure 4.9(b) shows that zoom in water content for easy comparison. It was observed that the water content was higher at the 80-mm depth than that at the 120-mm depth. This was because the 120-mm position was closer to the source of transmitting the vacuum (gravel drain blanket) located at the bottom of the consolidation tank.

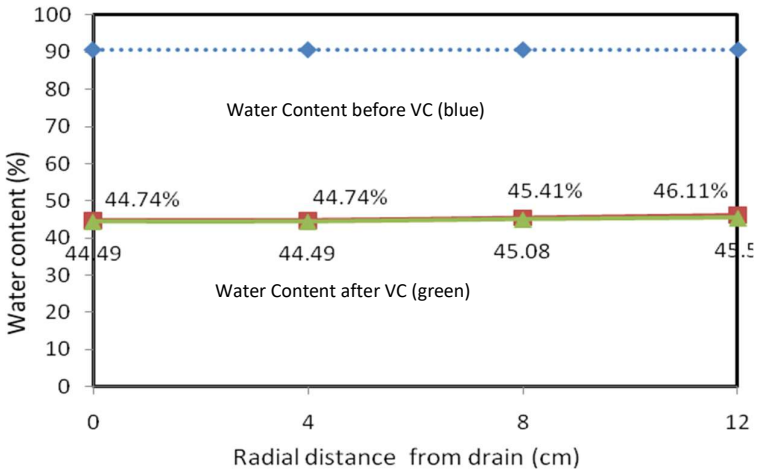

(a) Water Content of soil samples before and after model test

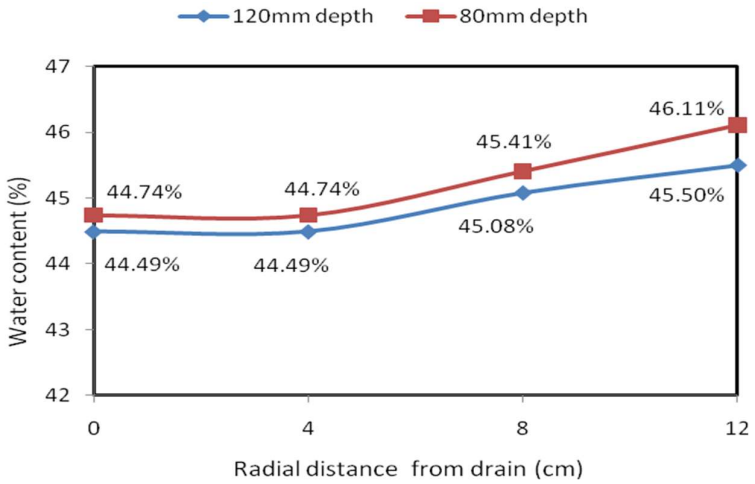

(b) Water Content of soil samples after tests at 80mm and 120mm depth

Figure 4.9 Measured water content of the soil samples extruded from Test 3

Table 4.5 tabulates the measured water contents before and after vacuum treatment for all eight model tests. Generally, it was observed that the water content in soil samples decreased after vacuum was applied. The water content in soil samples nearer to the sources where vacuum is transmitted had lower water content compared with soil samples extruded further away.

Table 4.5 Summary of water content before and after vacuum loading

	Description	W/C before VC	Ave. W/C after VC	Ave. W/C Reduction
		(%)	(%)	(%)
Test 1	Kaolin slurry	90.0	36.4	53.6
Test 2	+40 kPa	90.3	31.6	58.7
Test 3	membraneless	90.60	46.0	44.6
Test 4	Circular, MC1	87.5	34.8	52.8
Test 5	Band, MC1	89.7	37.4	52.4
Test 6	Lumpy Kaolin	98.2[1]	37.3	52.1
Test 7	MC2	72.4	33.0	39.4

[1] Average water content after water is added in

Generally, we can associate the effectiveness of the applied soil improvement method by comparing the water content reduction in the soil. The reduction of water content was examined in the four comparison studies.

4.4.1.1 Comparison study 1 (Test 1 and Test 6)

Both lumpy kaolin and kaolin paste achieved very similar final water content after the vacuum model test. Reduction of water content was observed at the end of the model tests using lumpy kaolin and kaolin slurry. However, at the end of the model tests, the observed normalized water content reduction was found higher in the kaolin paste at 59.6% when compared to lumpy kaolin at 53%. This observation verified that vacuum preloading is effective to treat both lumpy kaolin and kaolin paste. Lower normalized water content reduction in lumpy kaolin was probably due to its inter-void spaces between the lumpy kaolin samples.

4.4.1.2 Comparison study 2 (Test 4 and Test 5)

As the initial and final water content were very close between Test 4 and Test 5, average water content reduction was normalized to allow meaning performance comparison between the two drains. The normalized average water content reduction was found to be higher in circular drain at 60.3% than band drain at 58.4%. This shows that circular drain was slightly more efficient than band drain under membrane vacuum preloading.

4.4.1.3 Comparison study 3 (Test 1 and Test 3)

From the water content reduction, it was concluded that both vacuum consolidation techniques applied were effective in treating the kaolin paste. The membrane system achieved higher average water content reduction at 53.6%while the membraneless system achieved lower water content reduction at 44.6%.

4.4.1.4 Comparison study 4 (Test 1 and Test 2)

It was observed that additional surcharge was effective to further reduce water content in clay samples. Model test with surcharge had achieved 36.4% water content

reduction while similar model test with no surcharge achieved less water content reduction at 31.6%.

4.4.2 Settlements

The settlement of the soil samples in the consolidation tank were measured continuously during the vacuum preloading stage until no further settlement was observed over time.

4.4.2.1 Comparison study 1

Figure 4.10 illustrates the settlement versus time curves from Tests1, 4, 6 and 7. The rate of settlement observed for MC1 with higher organic and peat contents was much slower compared to lumpy kaolin and kaolin paste but overtime, MC1 still achieved significant amount of settlement similar to that of the kaolin samples. The slower rate of settlement could be due to the higher fines and peat content in MC1 which might have clogged the PVD filter.

MC2 (Test 7) comprised mainly of silty sand with much lower compressible soils content. At the end of the model test using MC2, less total settlement was observed. Generally, Figure 4.10 verified that vacuum preloading was effective to improve all compressible soil samples but settlement of the soil samples are with different rates and magnitude of settlement.

The largest settlement was found in the model test using kaolin lumps (Test 6). The large settlement recorded was probably attributed to the collapse of the inter-lump voids when vacuum was applied. Large and sharp settlement observed initially follow by flatten curve which indicate that not much consolidation took place within the lumpy materials.

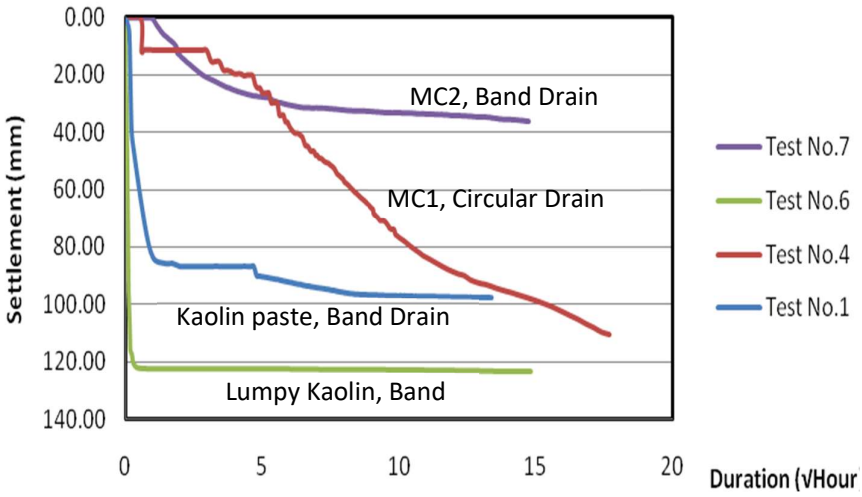

Figure 4.10 Settlement curves of different soil samples

4.4.2.2 Comparison study 2

Approximately less than 20 mm initial settlement of were registered for model tests 3,4 and 5 when vacuum was first applied. The observed settlments were due to the sealing and closing of the gaps between the marine clay samples and the consolidation tank. However for these 3 model tests, no settlement was observed for at least a few hours after the initial settlement. This were probably due to vacuum leakages in the consolidation tank which were subsequently rectified and sealed up using grease or blue tags.

Figure 4.11 illustrates the settlement curves of MC1 using circular drain (Test 4) and band drain (Test 5) where they were applied in the membrane vacuum preload system. It was observed that the circular drain brought more settlement than the band drain. This observation was consistent with the higher normalized water content reduction observed. Although this may be so, in actual field application or construction, the pushing of circular drains into the compressible soil layers using customised mandrel may resulted in less settlement due to thicker smear zones formed during the installation of the prefabricated circular drains by the customized mandrel.

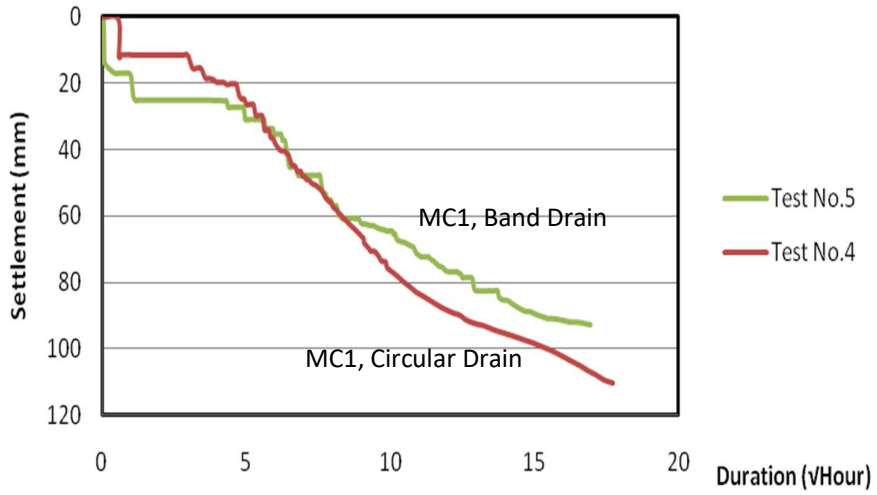

Figure 4.11 Settlement curves of MC1 using circular and band drains

4.4.2.3 Comparison study 3

Figure 4.12 illustrates the settlement curves of kaolin paste using the membrane (Test 1) and membraneless (Test 3) vacuum preloading techniques. The Y-axis was normalized by dividing the measured settlement with the initial height as the initial height for the soil samples for the two tests were different. From the settlement curves, the two vacuum preload techniques were found to be effective to consolidate the kaolin paste. The membrane vacuum system achieved more settlement and had faster settlement rate when compared to the membraneless system. Better performance of the membrane vacuum system could probably be due to addition areas exposed to the vacuum source resulting in additional consolidation. This additional areas of vacuum source exposure is at the interface of filter paper placed between the kaolin paste and the gravel layer.

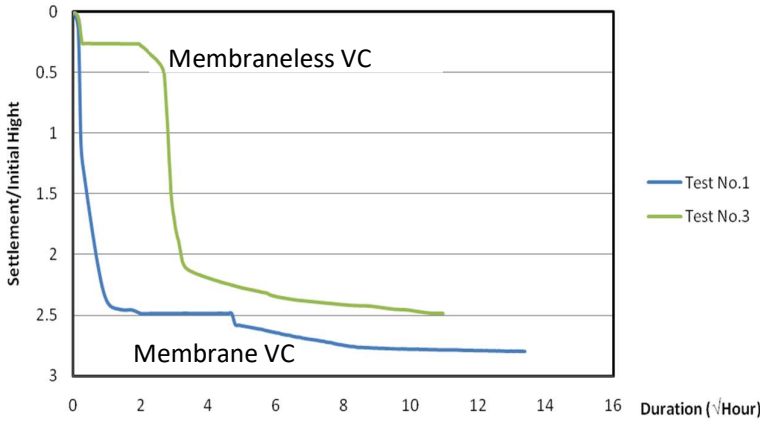

Figure 4.12 Settlement curves of kaolin paste using membrane and membraneless vacuum preloading system

4.4.2.4 Comparison study 4

Figure 4.13 illustrates the settlement versus time curves for kaolin paste using only membrane vacuum preload (Test 1) and that for combined membrane vacuum preload with additional +40kPa surcharge (Test 2). The settlement curves were similar for the two tests for the first 60mm of settlement as the kaolin paste was subjected only to vacuum loading. Surcharge was only applied to Test 2 after 60mm settlement was reached. The purpose is to account the uneven settlement due to voids found in the soil samples. By comparing the magnitude of the settlement curves, it was concluded that the additional 40kPa surcharge will bring about increased settlement.

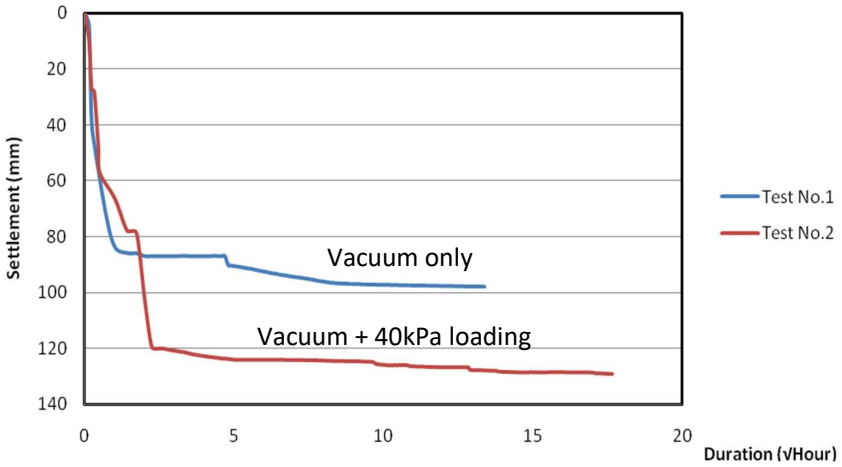

Figure 4.13 Settlement curves of kaolin paste using membrane vacuum preload only and membrane vacuum preload with 40kPa surcharge

The significant increase in settlement due to the additional surcharge loading was in good agreement with higher water content reduction at the end of the model tests. This observation indicates that the combined vacuum and embankment preloading can achieved higher degree of soil consolidation in the compressible soil layer with less volume of preload materials including their re-handling which could bring cost and time savings to the project.

4.4.2.5 Ultimate Settlement (S_{ult})

Vacuum pumping was terminated for all model tests before the ultimate settlement were reached due to time constraints. As such the final settlement for each test were obtained using the Asoka method. Figure 4.14 shows an example of how the ultimate settlement was derived for Test No. 1. The S_{ult} value predicted for all the other seven tests are summarized in Table .6.

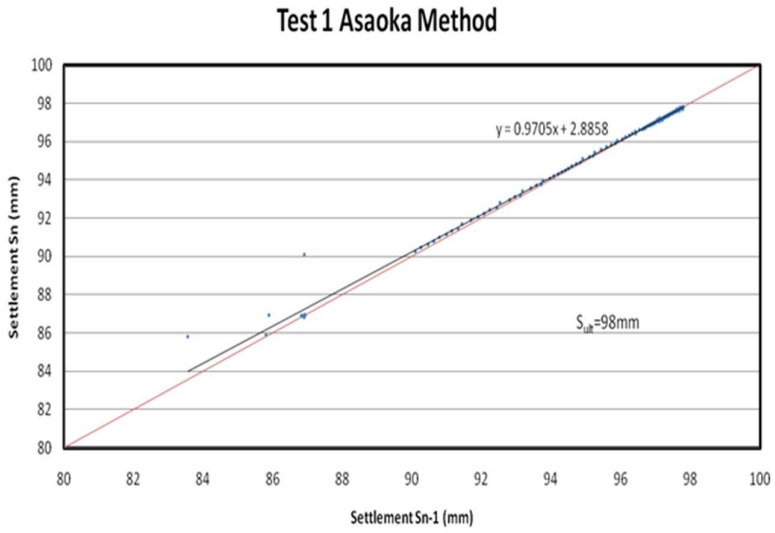

Figure 4.14 Determination of ultimate settlement using Asaoka method

Table 4.6 Summary of ultimate settlement obtained using Asaoka method

Test #	Soil tested	Type of drain	S_{ult} (mm)
Test 1	Kaolin	Band	98.0
Test 2	Kaolin	Band	130.5
Test 3	Kaolin	Band	126.0
Test 4	MC1	Band	117.3
Test 5	MC1	Circular	98.0
Test 6	Lumpy soil	Band	131.0
Test 7	MC2	Band	38.0

The average degree of consolidation using settlement, $\bar{U}s$ was computed as the percentage of S(t)/Sult, where S(t) is the settlement at any instant of time. Thus, a $\bar{U}s$ vs. time curve can be drawn for every test and the average degree of consolidation achieved at the end of each test can be calculated. Results of the degree of consolidation achieved over time derived using Asaoka method are illustrated in Figure 4.18 and discussed in Section 4.4.4 along with the degree of consolidation derived using the pore pressures measured. The changes in the measured pore pressures will be discussed first in section 4.4.3.

4.4.3 Pore water pressure changes

4.4.3.1 Monitoring of pore water pressures

Figures 4.15 (a) to (d) present the dissipation of pore water pressure (pwp) in Test 1 over time in both arithmetic and logarithmic scales. Similar observations were observed for all the model tests. Pore pressure transducers PPT1, PPT2 and PPT3 measured the pwp at 80mm below the bottom of the cover plate while PPT4, PPT5 and PPT6 measured the pwp at 120mm below the bottom of the cover plate as illustrated in Figure 4.7.

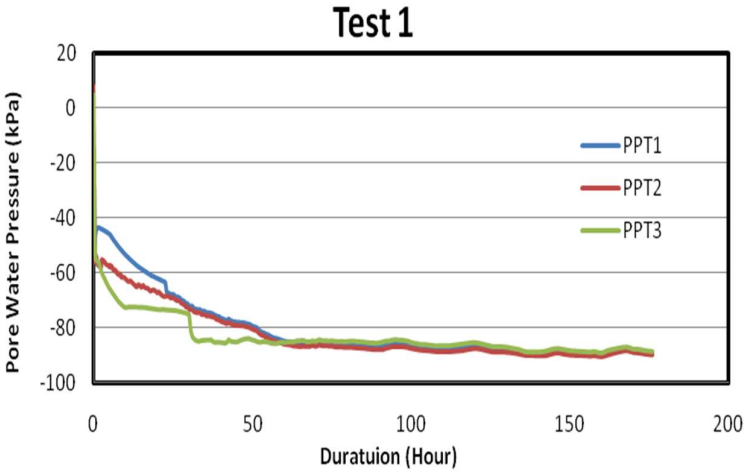

(a) Pore pressures recorded over time by PPT 1, 2 and 3 in arithmetic scale

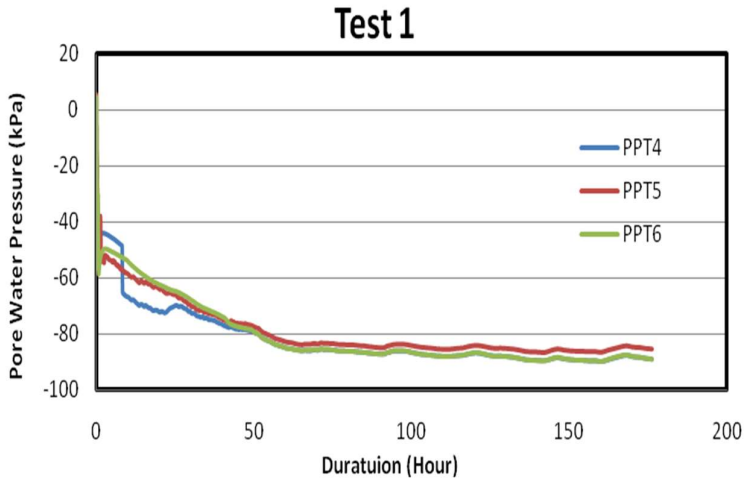

(b) Pore pressures recorded over time by PPT 4, 5 and 6 in arithmetic scale

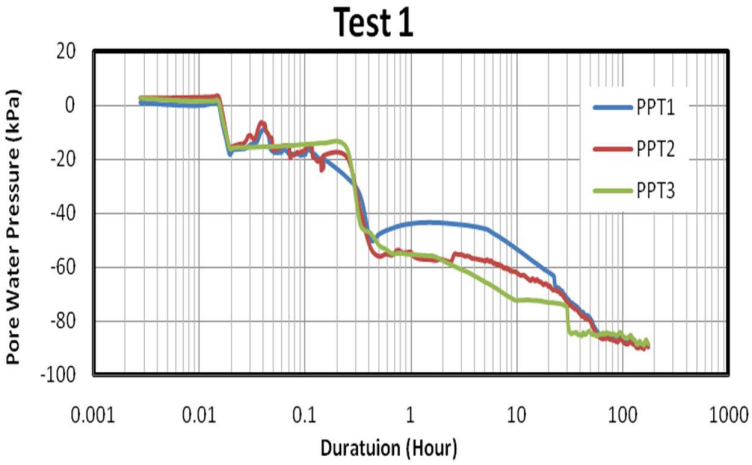

(c) Pore pressures recorded over time by PPT 1, 2 and 3 (log scale)

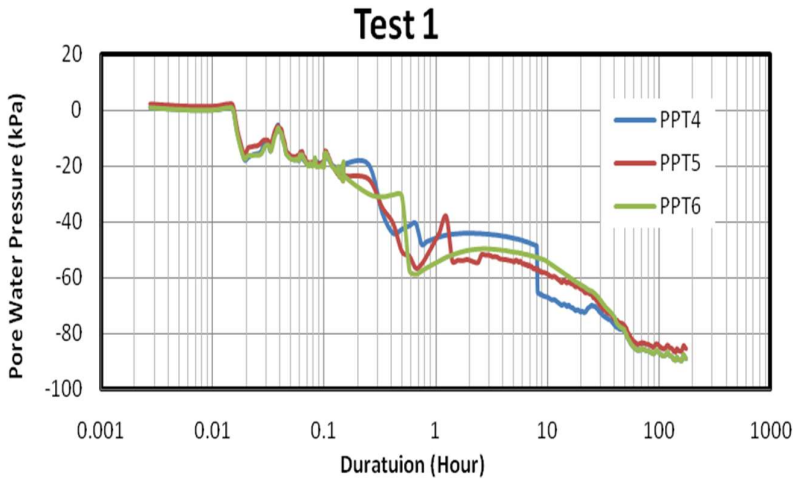

(d) Pore pressures recorded over time by PPT 4, 5 and 6 (log scale)

Figure 4.15 Pore pressures recorded over time

When vacuum was first transmitted to the soil mass via the PVD, the PPTs located furthest away from the PVD would have the highest pwp readings as the ability to transmit vacuum pressure into the soil mass will reduce with distance. However, the vacuum pressure would have been transmitted throughout the soil mass evenly over time and the pwp in the soil would eventually reached the applied vacuum pressure when consolidation was completed.

The declining and undulating of the pore water pressure curves plotted in Figure 4.15(c) and (d) reflect the dynamic changes of the measured pore water pressures throughout the duration where vacuum was applied to the kaolin paste in Test 1. The fluctuations of the measured pwp were probably due to the uneven transmittance of vacuum pressure and consolidation of the kaolin paste. During the consolidation, the soil samples nearer to the drain would have consolidated first, and the stress distribution in the soil matrix could become non-homogeneous. This could have induced the built up in pore pressure within the soil mass which could have neutralize the pore pressure dissipation or elevate the pore pressure in the soil mass (Goi, 2004).

The logarithmic time scale shows the changes in the gradient of the pwp curves indicating both slow down and sudden changes in the measured pwp during the test. These observations were common in the other model tests too. The slowdown in pwp dissipation might be partly attributed by the presence of viscous pore liquid that was bound strongly to the soil particles, and the slow release and discharge of the viscous liquid tended to slow down the pwp dissipation (Goi, 2004; Klein, 1995). It was observed that the sudden drop in the measured pwp usually follows the slowdown of the pwp dissipation. This phenomenon was probably attributed to the sudden release of pwp from the voids and then the collapsing of these voids due to consolidation.

The initial and final excess pore pressure measurements registered by various ppts in each test are tabulated in Table 4.7. The gained in effective stress of the soil samples at the various ppts locations were determined by the difference between the initial and final pore pressure readings.

It was observed that under laboratory controlled conditions the kaolin slurry treated by the membraneless vacuum system (Test 3) had smaller gain in effective stress (69 – 84 kPa) when compared to the membrane vacuum system (91 - 97kPa). This clearly indicates that the membrane vacuum system could treat the dredged seabed slurry more effectively than the membraneless vacuum system. The performance of the membraneless vacuum preload system for field applications will be further examined in Chapter 5.

Table 4.7 Summary of pore water pressure measurement in the model tests

Test	Pore Pressure Readings	PPT1	PPT2	PPT3	PPT4	PPT5	PPT6
Test 1	Initial Reading (kPa)	4.40	8.04	5.11	4.66	5.81	4.57
	Final Reading(kPa)	-88.86	-89.91	-88.43	-89.01	-85.29	-89.04
	Gain in Effective Stress (kPa)	93.26	97.85	93.54	93.68	91.10	93.61
Test 2	Initial Reading (kPa)	4.61	4.87	3.93	5.27	6.94	5.15
	Final Reading(kPa)	-84.98	-85.66	-90.49	-84.97	-84.42	-84.98
	Gain in Effective Stress (kPa)	89.59	90.52	94.42	90.24	91.36	90.13
Test 3	Initial Reading (kPa)	2.73	2.91	2.21	3.55	3.82	3.52
	Final Reading(kPa)	-66.63	-68.07	-81.51	-81.33	-79.77	-71.44
	Gain in Effective Stress (kPa)	69.35	70.98	83.72	84.88	83.59	74.96
Test 4	Initial Reading (kPa)	2.64	2.27	1.96	4.20	3.94	3.00
	Final Reading(kPa)	-76.71	-77.40	-74.34	-73.21	-74.59	-75.12
	Gain in Effective Stress (kPa)	79.35	79.67	76.30	77.42	78.53	78.11
Test 5	Initial Reading (kPa)	0.23	-0.49	-1.04	0.06	1.39	1.81
	Final Reading(kPa)	-77.43	-79.13	-71.11	-72.27	-73.29	-71.16
	Gain in Effective Stress (kPa)	77.66	78.63	70.07	72.33	75.38	72.97
Test 6	Initial Reading (kPa)	3.83	2.33	3.04	3.69	2.95	6.52
	Final Reading(kPa)	-82.97	-85.00	-84.07	-85.18	-80.05	-83.46
	Gain in Effective Stress (kPa)	86.80	87.33	87.12	88.87	83.00	89.98
Test 7	Initial Reading (kPa)	0.94	0.87	1.35	1.04	5.33	1.05
	Final Reading(kPa)	-81.36	-81.87	-78.99	-85.28	-80.21	-80.22
	Gain in Effective Stress (kPa)	82.30	82.73	80.34	86.32	85.55	81.27

The effective stress gained in Test 4 (circular drain) and Test 5 (band drain) were lower than 80kPa. This could probably attribute to the presence of high organic content such as peat in the marine clay sample, MC1, which could have reduced the performance of the vacuum preload system.

4.4.3.2 Pore water pressure distribution profiles

The isochrones in Figure 4.16 show the typical distributions of excess pwp along the radial direction of the vertical drain at different time interval for model Test 3. The initial excess pore water pressures for the left PPTs (embedded at 80mm from the top) and right PPTs (embedded 120mm from the top) were normalized to 0 kPa for easy comparison for the measured pwp.

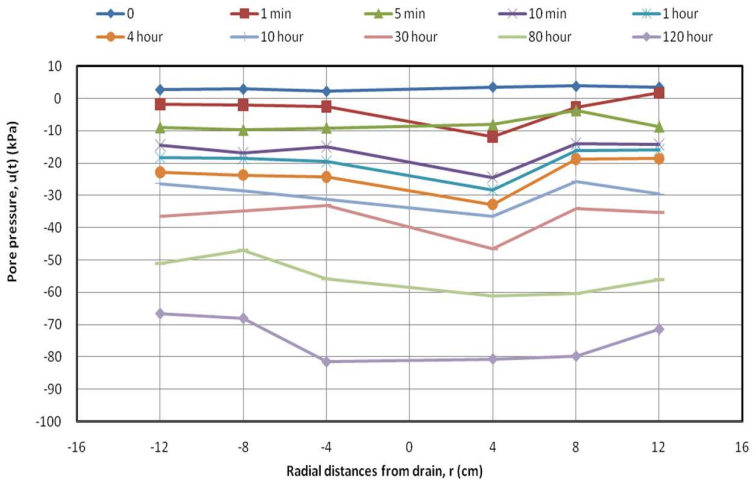

Figure 4.16 Isochrones of pore water pressure dissipation with time in Test 3

Very little physical settlement was observed in the 1st hour when vacuum was applied, however the imbedded ppts showed steady reduction in the measured pwp over the recorded time intervals. This indicated that the vacuum was transmitted to the soil matrix slowly overtime to remove the excess pwp. The isochrones at various time intervals had provided evidences that the efficiency of the transmitted vacuum reduced with increased radial distance. The pwp isochrones also suggested that the efficiency of the transmitted vacuum reduced with increase vertical distance from the gravel blanket as the ppts imbedded at 120mm showed greater reduction in pwp than the ppts imbedded at 80mm at most of the recorded intervals.

4.4.4 Degree of consolidation ($\bar{U}p$)

The excess pwp isochrones shown in Figure 4.17 can be used to determine the average degree of consolidation $\bar{U}p$, by the formula:

$$\bar{U}p = [\ 1 - \frac{\int u(t)dr}{U_i \times D}\ ] \times 100\% \qquad (4.1)$$

where,

u(t) = excess pore water pressure remaining at any time;

t = radial distance (cm);

u_i = initial excess pore pressure (0 kPa);

D = diameter of the consolidation tank (=30cm).

Applying this equation to the isochrones in Fig 4.16 using the trapezoidal method, the average degree of consolidation Ūp derived using pore water pressure at different time intervals can be calculated. Figure 4.17 (a) to (f) show the degree of consolidation calculated using settlement Ūs and the Asaoka method.

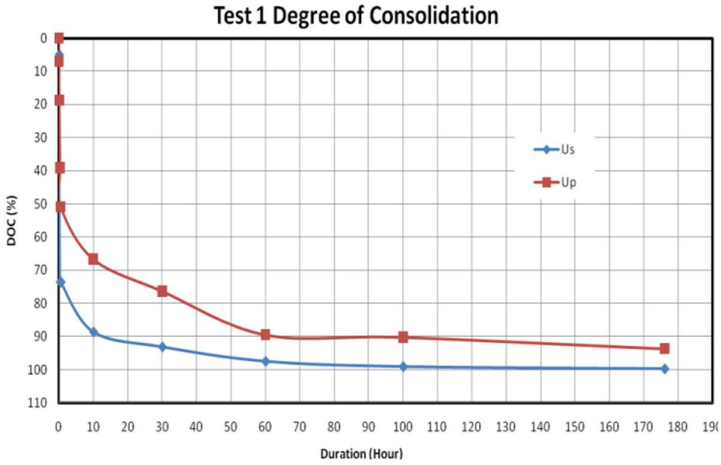

(a) Test 1 (kaolin paste, membrane vacuum preload, band drain)

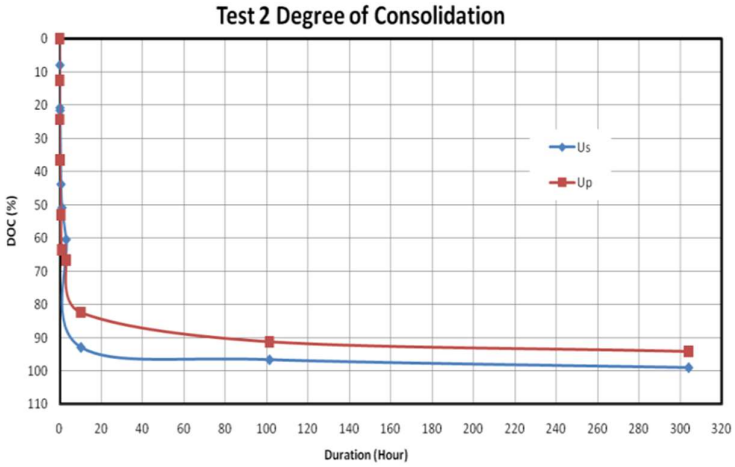

(b) Test 2 (kaolin paste, membrane vacuum preload +40kPa, band drain)

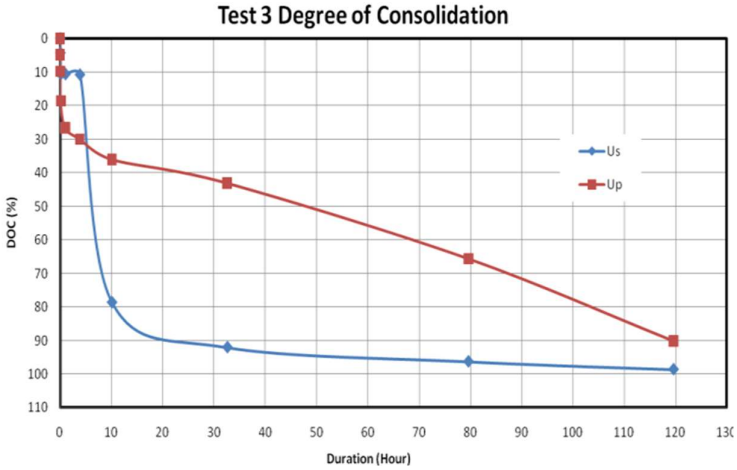

(c) Test 3 (kaolin paste, membraneless vacuum preload, band drain)

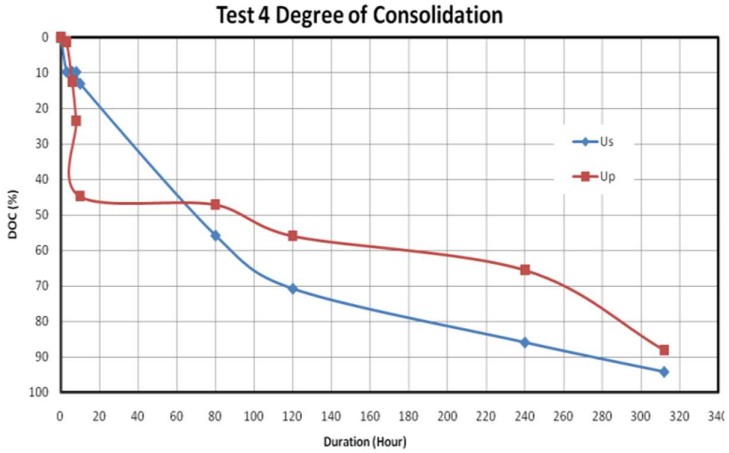

(d) Test 4 (MC1, membrane vacuum preload, circular drain)

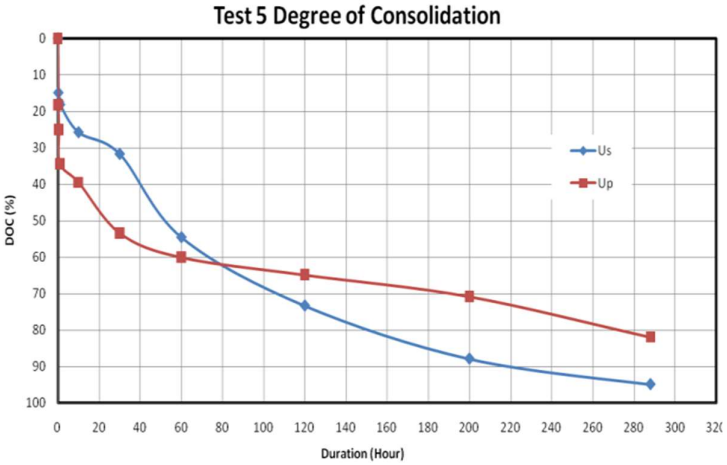

(e) Test 5 (MC1, membrane vacuum preload, band drain)

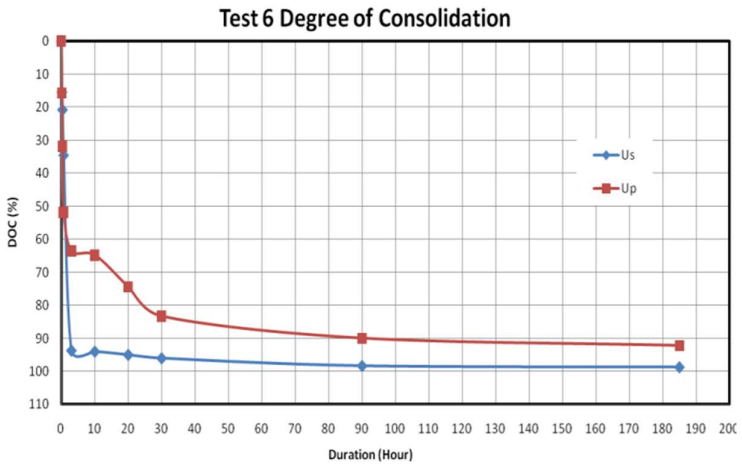

(f) Test 6 (lumpy kaolin, membrane vacuum preload, band drain)

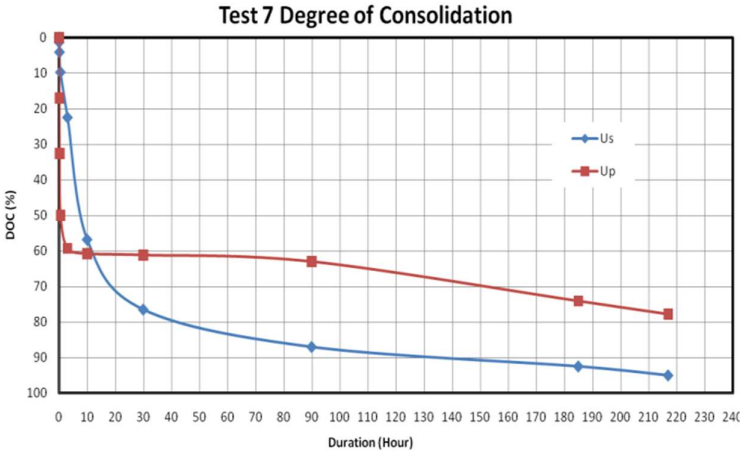

(g) Test 7 (MC2, membrane vacuum preload, band drain)

Figure 4.17 Degree of Consolidation (Test 1-7)

From the Degree of consolidation (DOC) curves for the various model tests presented in Figure 4.17 (a) to (g) which compares $\bar{U}p$ and $\bar{U}s$, it can be observed from the graphical plots that $\bar{U}p$ generally achieved higher Degree of Consolidation (DOC) at the earlier stage and then lagged $\bar{U}s$ as the consolidation continued until the end of the model tests. Similar observations were also made by Goi (2004) in his studies. Generally, the plotted graphs demonstrated that except for the initial stages, Asaoka method tends to give higher DOC value than the DOC calculated using pore water

pressure data with Equation 4.1. It shall be also noted that the difference in the derived DOC from Asaoka and Equation 4.1 are usually within a range of 10-15%.

4.4.5 One-dimension consolidation tests

Multi-staged 24-hour oedometer tests were performed on horizontally cut specimens located near the pvd drain (inner) and near to the consolidation tank wall (outer). Results of these extracted samples are presented in Table 4.8. Generally, consolidated soil samples taken near the PVD drain had lower initial void ratio, higher degree of saturation, lower water content, higher dry density, higher pre-consolidation pressure and lower compression index than the soil samples taken near the cylindrical tank wall. The tests results are predictable since more vacuum are transmitted to samples located nearer to the PVD.

Table 4.8 Summary of oedometer tests results

Oedometer Test Results	Test 1		Test 2		Test 3		Test 4	
	inner	outer	inner	outer	inner	outer	inner	outer
Initial Void Ratio, e_0	0.96	0.99	0.97	0.99	0.86	1.06	0.81	1.03
Degree of Saturation, S (%)	84.24	81.86	81.24	79.71	117.61	103.09	124.08	115.31
Water Content, w (%)	32.00	32.00	31.00	31.00	40.00	43.00	39.20	40.30
ρ_d(M g/m^3)	1.29	1.27	1.29	1.28	1.36	1.23	1.42	1.31
Preconsolidation Pressure, P_c' (kPa)	85.00	80.00	87.00	83.00	84.00	82.00	63.00	58.00
Compression Index, C_c	0.38	0.45	0.44	0.49	0.40	0.43	0.41	0.43

Oedometer Test Results (Cont'd)	Test 5		Test 6		Test 7	
	inner	outer	inner	outer	inner	outer
Initial Void Ratio, e_0	0.79	1.02	0.95	1.18	0.75	0.92
Degree of Saturation, S (%)	125.31	116.19	87.38	78.45	91.71	75.12
Water Content, w (%)	38.90	46.60	32.85	36.32	28.00	28.00
ρ_d(M g/m^3)	1.42	1.26	1.30	1.17	1.40	1.28
Preconsolidation Pressure, P_c' (kPa)	65.00	60.00	45.00	40.00	48.00	43.00
Compression Index, C_c	0.42	0.42	0.31	0.38	0.21	0.24

4.4.6 Undrained shear strength

At the end of each model tests, soil samples were extracted from the consolidation tank to perform the Unconfined Compression test to determine the undrained shear strength of these consolidated soil samples. The results of all seven model tests are tabulated in Table 4.9.

4.4.6.1 Comparison study 1

Comparison between different marine clay type

MC2 had the lowest undrained shear strength among the different types of soil samples tested

Comparison between lumpy and slurry kaolin

An important finding that contradicts common believe is that the undrained shear strengths of lumpy kaolin (Test 6) were found to be lower than kaolin paste after vacuum preloading. This observation was consistent with the average water contents measured when the kaolin paste samples (36.4%) was higher than the lumpy kaolin samples (33%) at the end of vacuum preloading. These findings suggested that the improved hydraulic dredged slurry fill by vacuum preloading could have potentially higher undrained shear strength than mechanical dredged seabed after treatment.

4.4.6.2 Comparison study 2

With reference to the membrane vacuum consolidation technique, it was observed that the soil samples consolidated using circular drain exhibited higher undrained shear (23.8%) than when they are treated with band drain (21.5%). This is in good agreement with higher settlement observed in circular drain in Section 4.4.2.2 and also the lower water content in circular drain (Test 4) at the end of the model tests.

4.4.6.3 Comparison study 3

The unconfined compression tests results show that the kaolin slurry consolidated by membrane vacuum consolidation technique exhibited higher shear strength than the kaolin slurry treated by the membraneless vacuum consolidation technique. This is

in good agreement with the other test results which indicate lower water content, higher dry density and lower void ratio in kaolin slurry treated with membrane system.

4.4.6.4 Comparison study 4

The additional 40kPa loading on the membrane vacuum method shows higher average undrained shear strength from the unconfined compression tests results which is in good agreement with the lower water content at the end of the model tests. However, no significant difference were found in the average dry density and void ratio as shown in Table 4.9

Table 4.9 Summary of UC tests results along with other parameters

Test No	Description	W/C before VC (%)	Ave. W/C after VC (%)	Ave Shear Strength, S_u (kPa)	Ave Dry Density after VC ρ_d (Mg/m^3)	Ave Void Ratio after VC e
Test 1	**Kaolin slurry**	90.0	36.4	40.3	1.24	0.99
Test 2	**+40 kPa**	90.3	31.6	45.0	1.23	1.01
Test 3	**membraneless**	90.60	46.0	28.8	1.17	1.06
Test 4	**Circular, MC1**	87.5	34.8	23.8	1.39	0.77
Test 5	**Band, MC1**	89.7	37.4	21.5	1.28	0.93
Test 6	**Lumpy Kaolin**	98.2[2]	37.3	10.3	1.26	1.02
Test 7	**MC2**	72.4	33.0	12.5	1.47	0.67

4.4.7 Back analysis for Compression Index, C_c

Besides oedometer test, the Compression Index C_c can also be derived using the results from the model tests, namely the measured void ratios and vertical stress (vacuum pressure) applied before and after the consolidation tests. The principle for deriving the back calculated Compression Index is explained in Figure 4.18. The calculation steps for arriving the Compression Index are tabulated in Table 4.10. It shall be noted that the back calculated C_c are comparable to the C_c obtained from oedometer tests presented in Table 4.10

[2] Average water content after water is added in

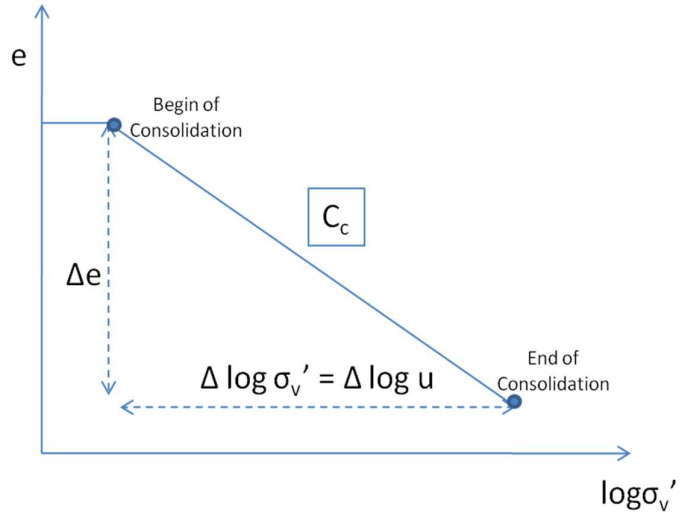

Figure 4.18 Principle for back calculations of the Compression Index, Cc

Table 4.10 Calculated compression indices (Cc)

Back Calculation of C_c	Test 1	Test 2	Test 3	Test 4	Test 5	Test 6	Test 7
$C_c = \Delta e/\log\Delta\sigma$	0.41	0.51	0.44	0.42	0.45	0.51	0.09

4.4.8 Back analysis for Consolidation Parameters, C_h and C_v

Back analysis of the model test results was carried out to estimate the consolidation parameter C_h by using the $\bar{U}$ value estimated from the settlement monitoring data and the Barron's theory. Table 4.11 describes a typical back calculation of C_h value of kaolin using data in Test 3 (non-membrane vacuum preload) as an example. Once the C_h value of kaolin has been obtained it is substituted back in Test 1 to get C_v value using the following equations:

$$\left(1-\overline{U}_{vh}\right)=\left(1-\overline{U}_{v}\right)\times\left(1-\overline{U}_{h}\right) \tag{4.2}$$

$$\overline{U}_{v}=\frac{\left(4T_{v}/\pi\right)^{0.5}}{\left[1+\left(4T_{v}/\pi\right)^{2.8}\right]^{0.179}} \tag{4.3}$$

and

$$C_v = \frac{T_v\, d_e^2}{t} \tag{4.4}$$

Table 4.11 Determination of C_h for Test 3

Equivalent diameter of drain, d_w (m) $d_w = \frac{2(a+b)}{\pi} *$	0.067
Equivalent drainage diameter, d_e (m)	0.3
Drain spacing ratio, n $n = \frac{d_e}{d_w}$	4.5
Factor F(n)≈ ln(n) - 0.75	0.75
Average degree of consolidation, $U_{average}$ (%)	92.8
Time Factor of consolidation by radial flow, T_h Based on Uaverage = 1 – exp [$\frac{-8T_h}{F(n)}$]	0.25
t (yrs)	0.034
Coefficient of horizontal consolidation, C_h (m^2/yr) $C_h = \frac{T_h\, d_e^{\,2}}{t}$	0.65

**a = 100mm, b = 5.3 mm*

The calculated C_v for Test 1 is 0.03 m^2/yr, which is almost negligible compared to C_h. Thus, horizontal drainage is neglected in the calculation of other tests, and C_h value calculated of all the seven tests is summarized in Table 4.12.

Table 4.12 Summary of the calculated Consolidation Parameter, C_h

	Test 1	Test 2	Test 3	Test 4	Test 5	Test 6	Test 7
C_h	0.65	1.86	0.65	0.54	0.75	4.25	0.64

It is observed that the calculated C_h value for Test 6 (lumpy kaolin) was much higher that the soil samples of the remaining model tests due to large number of inter lumps voids between the lumpy kaolin samples.

4.5 Conclusions

Eight laboratory model tests using a consolidation tank with a single PVD in clay were carried out to validate the suitability and effectiveness of the identified vacuum consolidation technique to improve the properties of the dredged seabed materials. The testing program, model test set up and the test results and analyses were presented in this chapter and the key findings and on the respective Comparison studies are as follows:

i. Comparison study 1 compared the consolidation behaviors of different soil samples when subjected to vacuum preloading. Vacuum preloading techniqueswere found effective in treating the different soil samples but with different settlement rate and magnitude of settlements.

ii. Comparison study 1 also confirmed that lumpy kaolin were found to be much more compressible than the kaolin slurry due to the inter-lump voids. They also yielded lower undrained shear strength and the end of vacuum consolidation. This indicates that that hydraulic dredged slurry fill would likely to have higher undrained shear strength than mechanical dredged seabed after improvement by vacuum preloading.

iii. Comparison study 2 examined the effects of using band drain and circular drain when they were incorporated into the membrane vacuum consolidation technique to consolidate marine clay samples. The test results show that circular drains could potentially further enhance the performance of the conventional membrane vacuum preload system as the kaolin paste consolidated by circular drains undergo more settlement, has lower water content and exhibited higher undrained shear strength at the end of the model tests given very close initial conditions.

iv. Comparison study 3 compared the performance between the membrane and membraneless vacuum consolidation technique to improve soil samples using MC1. The test results indicated that both vacuum consolidation techniques were

suitable and effective to improve the properties of the soil samples. However, the membrane vacuum preload system was found to be more effective producing consolidated kaolin with higher undrained shear strength with higher dry density, lower void ratio and water content at the end of the model tests.

v. Comparison study 4 concluded that the effects of the additional 40kPa loading had helped improved the undrained shear strength of the consolidated kaolin slurry samples and further reduced the water content.

vi. Finally, the test results showed that the effectiveness of the applied vacuum reduced with the increase in radial distance from the source where the vacuum was transmitted (PVD). Therefore, closer drains spacing can be considered if there is a need to accelerate the rate of consolidation given that the smear effect is not significant.

To further validate the observations made from the laboratory model tests, a field trial was carried out to examine the effectiveness and challenges of implementing membraneless vacuum preloading combine with surcharge under field conditions to expedite the soil improvement of an uneven marine clay layer underneath a newly reclaimed land. The observations of this field trial would be discussed in the next chapter.

CHAPTER 5 MEMBRANELESS VACUUM CONSOLIDATION TECHNIQUE WITH FILL SURCHARGE TO IMPROVE SOFT CLAY LAYER

5.1 Introduction

A pilot field trial was carried out at Tuas, using combined membraneless vacuum preloading with surcharge fill method to improve a soft compressible clay layer with varying thickness below a reclaimed land formed by mixed fills with permeability lower than a typical sand fill. The purpose of this field trial was to investigate the feasibility and examine the effectiveness of using this combined soil improvement solution to accelerate the soil improvement works for land reclamation projects with highly unstable foundation soil conditions. The role of the author in this field trial was the developer's project manager to carried out the planning and implementation of the reclamation works and also to facilitate the data collation and to conduct objective assessment of this field trial.

The proposed combined soil improvement solution was applied to 5000 m^2 of newly reclaimed land at Tuas as indicated in Figure 5.1. The soil improvement requirement stipulated for this trial were:

(i) Minimum 90% primary consolidation with uniform loading of 60 kPa loading.

(ii) Less than 100 mm residual settlement, cumulatively throughout the entire depth of the soil due to primary consolidation

Figure 5.1 Location of proposed field trial site in Tuas

5.2 Soil investigation program

The soil investigation program was carried out to establish the subsurface geological profile and to obtain the soil parameters and properties that were required for the design of the proposed combined membraneless vacuum preloading with surcharge. Details of the soil investigation program are summarized in Table 5.1.

Table 5.1 Soil investigation program before field trial

S/N	Methods	Qty.	Remarks
1.	Boreholes (dia 150mm)	04	To conduct the SPT and FVST and collect disturbed and undisturbed soil samples
2.	Standard Penetration Test (SPT)	NA	To determine the soil profile, get the disturbed soil samples
3.	Field Vane Shear Test (FVST)	04	To determine the shear strength of the soft soil
4.	Cone Penetration Test (CPT)	03	To classify the soil type and judge soil category
5.	Laboratory Test	NA	To determine the physical properties and mechanical properties of soil samples collected from the boreholes

The field works were carried out following the British Standard BS5930:1999 and BS1377:1990. Figure 5.2. shows the locations of the various boreholes. Soil drilling was performed to obtain soil samples for visual inspection and laboratory testing.

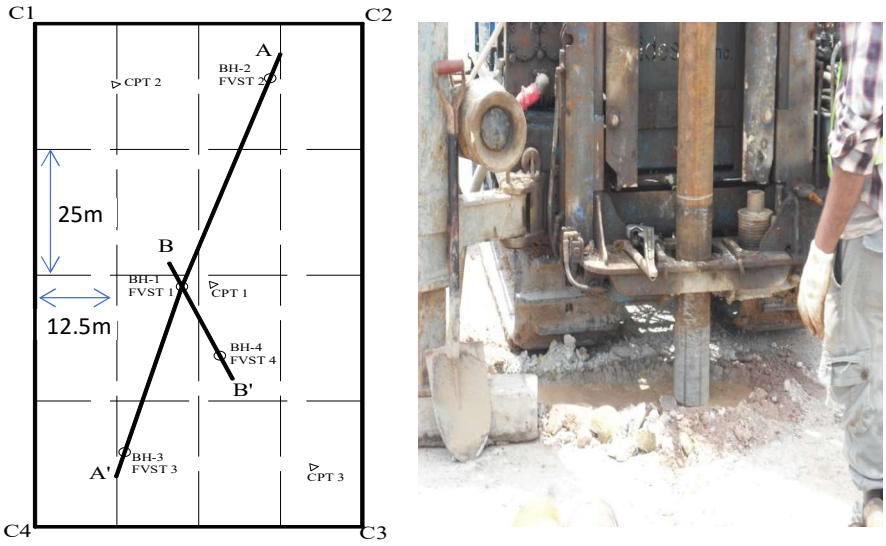

Figure 5.2 Location of boreholes at trial site

5.2.1 Standard penetration tests

Standard Penetration Test (SPT) was carried out in accordance with BS 1377. A standard split barrel sampler was penetrated by 450 mm into the soil by using 63.5 kg free falling hammer over a height of 760 mm. The number of blows required to advance the sampler for each of 150 mm increment was recorded. The N-values were reported in the borehole logs provided by the contractor. Figure 5.3 shows the field works at BH3.

Figure 5.3 Standard penetration test carried out in borehole 3

The recovered samples from SPT tests were kept in plastic bottles, labeled and sealed for identification. Undisturbed soil samples were taken using thin wall piston sampling in the clayey soil layer as shown in Figure 5.4.

Figure 5.4 Sample retrieval from SPT test

5.2.2 Field vane shear tests

Field vane shear tests (FVT) were carried out to determine the in-situ undrained shear strength of clay at the same location with borehole. The shear strengths with depth measured by FVT are presented in Figure 5.5. The summary of undisturbed and remolded FVT results are presented in Table 5.2. The results indicated that the strength of the underlying soil increased with depth. The sudden increased in shear strength beyond 20m depth denoted that the FVST had probably hit the weathered silt stone layer.

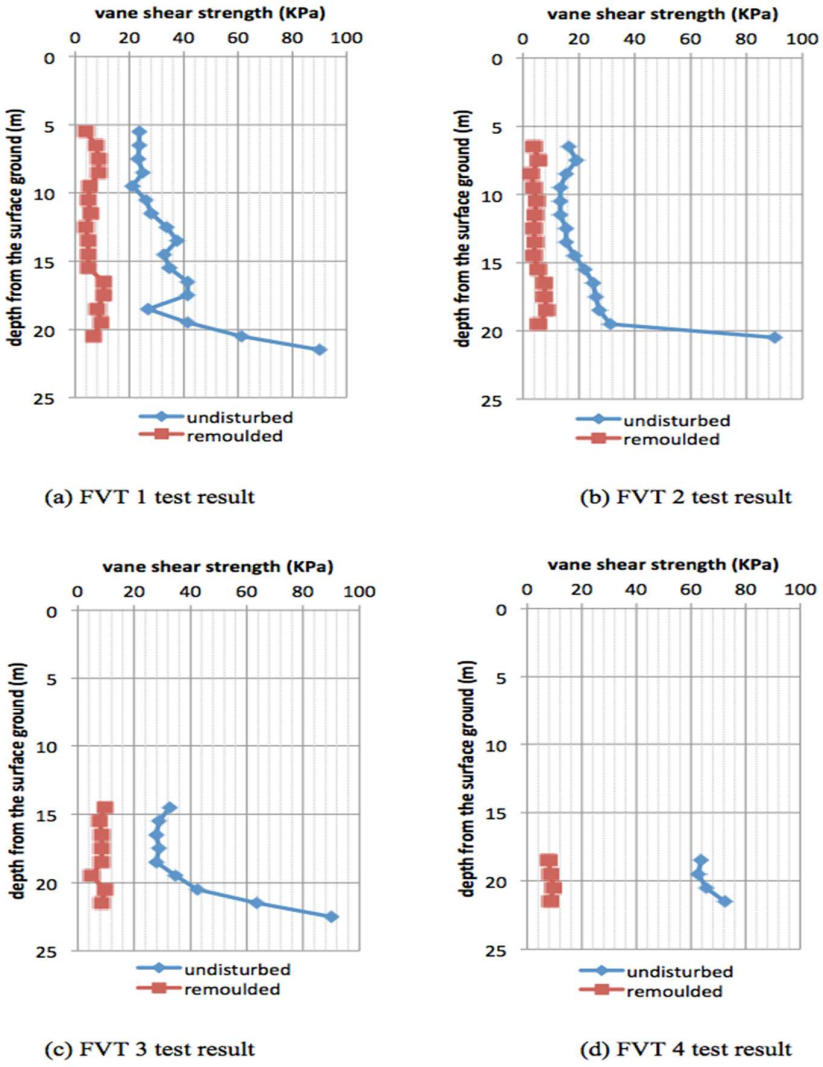

Figure 5.5 Results of FVT at different locations of the trial site

Table 5.2 Summary of undisturbed and remolded FVT results

Soil type	**Undisturbed (kPa)**		**Remolded (kPa)**		**Sensitivity**	
	Range	**Ave**	**Range**	**Ave**	**Range**	**Ave**
Marine clay	13.4~ 90	32.5	2.9~10.5	6.6	2.7~9.4	4.8
Residual soil	72.3~ 90	84.1	NA.	8.6	NA.	8.4

5.2.3 Cone penetration tests

Three numbers of Cone Penetration Tests (CPT) were carried out. The interpretations of CPT1 & CPT2 are shown in Figure 5.6. The plotted CPT profile indicated high degree of variability of the top 5 m fill as the area was reclaimed by heterogeneous mixed fills. The CPT profile also indicated that the thickness of the marine clay deposits underneath the reclaimed land varied. This undulating vertical soil layer profile coupled with highly unstable foundation soil conditions became a challenge to the implementation of conventional soil improvement using PVDs and surcharge fill. Table 5.3 tabulates the 3 CPT data from the pre-works site investigations.

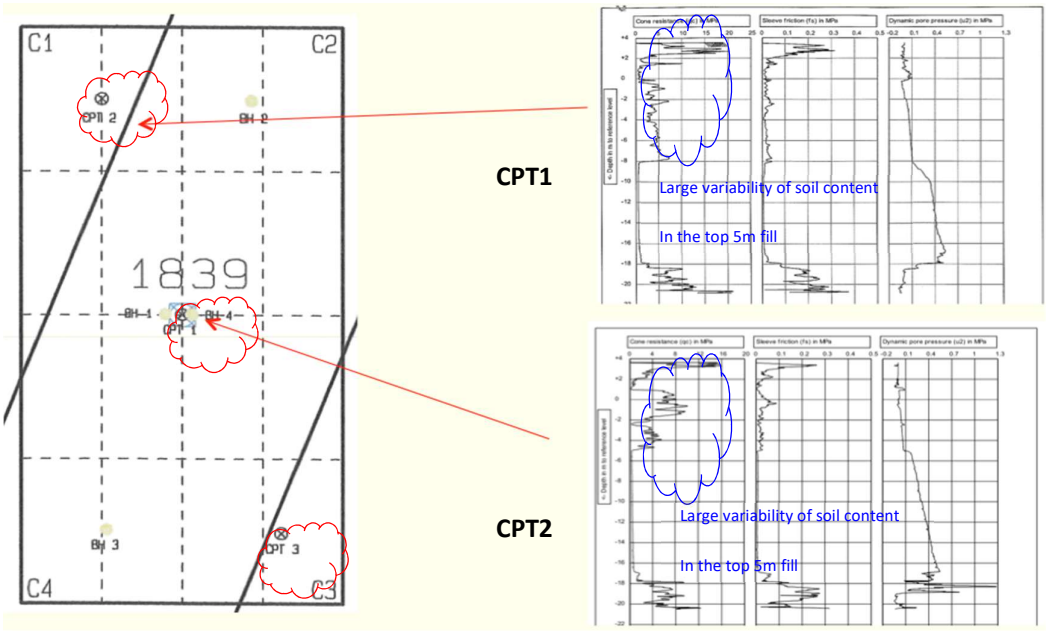

Figure 5.6 CPT profile of the existing soil layer trial site

Table 5.3 Summary of CPT results

Soil type	Cone resistance (MPa)		Sleeve friction (MPa)		Pore pressure(MPa)	
	Range	Ave	Range	Ave	Range	Ave
Fill	0.01~8.60	4.49	0.00~0.26	0.03	-0.05~0.17	0.05
Marine clay	0.28~0.50	0.56	0.00~0.06	0.01	0.07~0.63	0.40
Residual soil	0.83~20.78	6.15	0.00~0.39	0.16	-0.07~1.18	0.11

5.2.4 Laboratory tests

The types of laboratory tests performed are summarized in Table 5.4. The tests were performed in accordance with the British Standard Code of Practice BS1377: 1990, or ASTM as per terms of accreditation under SAC-SINGLAS and BCA ISO9000 scheme. Testing results of BH1 are given in Table 5.5.

Table 5.4 Types of laboratory tests and their quantities

	Index property test									Mechanical Property test	
Borehole No.	Moisture content	Bulk density	Atterberg Limits	Particle density	Grain Size Distribution	Organic content	PH value	Chloride content	Sulphate content	Triaxial test (UU)	Consolidation test
BH-1	5	5	5	5	5	2	2	2	2	5	5
BH-2	5	5	5	5	5	2	2	2	2	5	5
BH-3	4	4	4	4	4	2	2	2	2	4	4
BH-4	2	2	2	2	2	2	2	2	2	2	2
Total	16	16	16	16	16	8	8	8	8	16	16

Table 5.5 Laboratory test results for borehole 1

Borehole NO.: BH-1					
Sample NO.	**UD-1**	**UD-2**	**UD-3**	**UD-4**	**UD-5**
Depth (m)	5.00~5.80	7.00~7.60	11.00~11.85	15.00~15.85	19.00~19.80
Water Content (%)	81	84	69	84	79
Bulk Density (Mg/m3)	1.51	1.50	1.59	1.51	1.52
Liquid limit (%)	84	85	73	85	84
Plastic limit (%)	29	31	28	28	30
Particle density	2.71	2.74	2.73	2.68	2.71
Cohesion (KN/m2)	12	7.3	13	12	10
Compression index	0.94	0.67	0.62	0.77	0.71

5.2.5 Ground conditions and soil profiles

Figure 5.7 and Figure 5.8 show the simplified cross sections of the sub-soil profiles of the trial site along two axis A-A' (Figure 5.7) and B-B' (Figure 5.8). Generally, the soil profile at this trial site consisted of heterogeneous filled material, original in-situ marine clay deposits and residual soils. The two cross sections show that there were great variations of the soil layers thickness causing undulating soil profile.

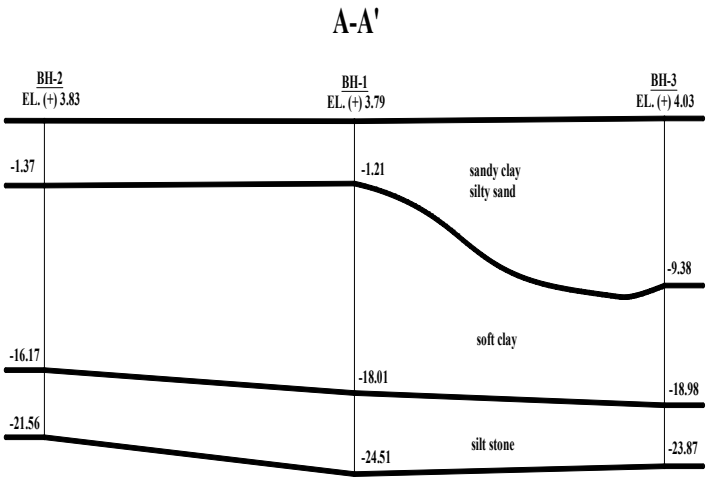

Figure 5.7 Sub-soil profiles along cross-section A-A’

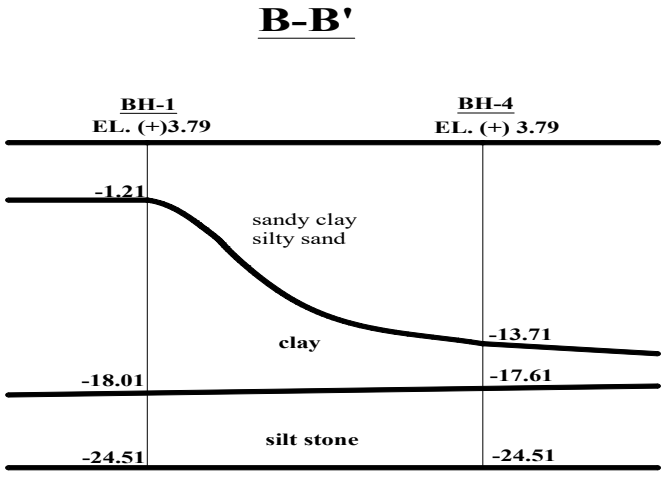

Figure 5.8 Sub-soil profiles along cross-section B-B’

Based on the soil investigation results, the filled materials were mainly consisting of sandy clay and silty sand. The SPT-N value in this layer was in the range of 2 to 17. The thickness of the fill layer ranged from 5.0 to 17.5 m.

The marine clay layer consisted of very soft to soft, light grey clay with some seashell fragments. The thickness of this soil layer ranged from 3.5 to 16.8 m. The SPT-N value was from 1 to 4. The undisturbed shear strength values measured using field vane shear tests ranged between 13.4 to 90.0 kN/m2 and 7.3 to 33.0 kPa by the laboratory UU tests.

The residual soil layer ranged from 5.39 to 7.30 m. The SPT-N value varied from 8 to 100. The undisturbed shear strength values measured using field vane shear tests were in the range of 72.3 to 90.0 kN/m2 and 67.0 to 121.0 kPa by the laboratory UU tests.

5.3 Design and installation of the membraneless vacuum preloading system

5.3.1 Detailed soil layer profiling

Due to the varying thickness of the reclaimed filled soil profile and underlying unstable soft clay layer, a combined membraneless vacuum preloading and fill surcharge method was adopted for the soil improvement works. Prior to installation of the membraneless vacuum preload system, additional investigations were required to map out a more detailed soil layer profile to allow accurate modifications of the PVDs components (tubing, cap, drains length, etc.) for optimal field performance.

The additional investigation was carried out quickly using PVD stitcher installed with penetration probes that measured the resistance of the soil as the probes was pushed into the soil layers. The soil profile thickness contours were mapped using the measured penetration forces as presented in Figure 5.9 and 5.10.

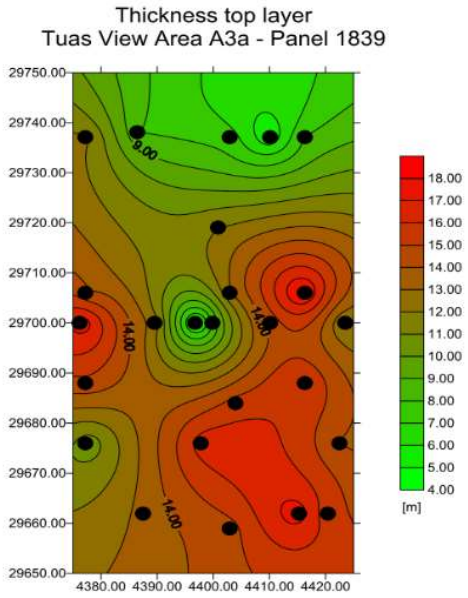

Figure 5.9 Plan view of contour lines showing soil layers profile

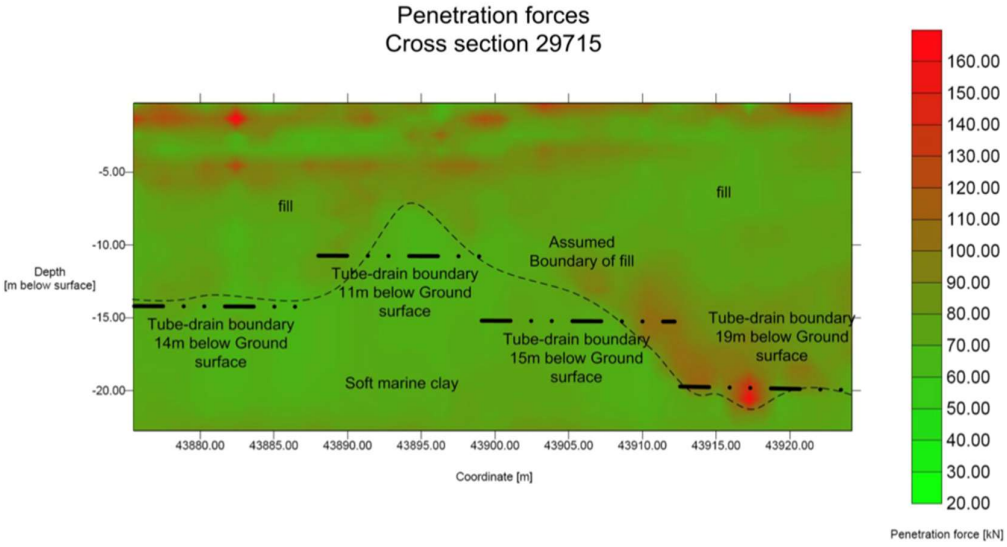

Figure 5.10 Cross section view of plotted soil profile

5.3.2 Components of the membraneless vacuum preloading system

5.3.2.1 MebraDrain MD88H

MebraDrain MD88H was chosen as the prefabricated vertical drain component for the proposed membraneless vacuum preload system. Its flexible core was made from high-quality polypropylene. Both sides of this core had groves which ran its entire length through which water could flow unhindered. This core was wrapped in a strong and durable filter made from non-woven polypropylene, which combined high water permeability with excellent filtration characteristics. MD88H has a herringbone-shaped core that was highly flexible and was therefore suited to areas where large relative settlement occured and could be used up to 65m deep. Its physical properties are shown in Figure 5.11.

PVD	MD88H, see properties below (table 1)
Tubes	HD/LDPE 16 mm
Drain fitting	PP
Plates	steel
T-coupling	PP
Manifold	steel/PP

Physical characteristics		**Standard**	**unit**	**MD88H**
Core	configuration			
	raw material			PP
	colour			white
	Channels			44
Filter	raw material			PP
	colour			grey
Weight		ASTM D3774	g/m	85
Width			mm	100
Thickness		ASTM D5199	mm	3.5

Mechanical Properties		**Standard**	**unit**	**MD88H**
Tensile strength drain	F_d	EN/ISO 10319	kN	2.2
Mobilised Force at $\square_0$ = 10%	$F_{10\%}$	EN/ISO 10319	kN/m	2
Elongation at 0,5 kN	$\square_{0,\ 0.5\ kN}$	EN/ISO 10319	%	2
Tensile strength filter MD	F_f	EN/ISO 10319	kN/m	11.7
Grab strength filter MD		ASTM D4632	N	970
Burst Strength		ASTM D3785	kN/m	1000
Tear strength filter MD		ASTM D4533	N	270

Discharge Capacity (D.C.)		**Standard**	**unit**	**MD88H**
In-Plane flow capacity 10 kPa	$q_{p(10,1)}$	EN/ISO 12958**	l/m.s	0.94
In-Plane flow capacity 100 kPa	$q_{p(10,1)}$	EN/ISO 12958**	l/m.s	0.79
In-Plane flow capacity 350 kPa	$q_{p(350,1)}$	EN/ISO 12958**	l/m.s	0.71
D.C. Straight 300 kPa (7 days)	$q_{w(300,0.1)}$	EN/ISO 12958**	10^{-6} m /s	70
D.C. Straight 500 kPa (7 days)	$q_{w(500,0.1)}$	EN/ISO 12958**	10^{-6} m /s	20
D.C. Buckled 200 kPa (7 days)	$q_{wb(200,0.1)}$	EN/ISO 12958**	10^{-6} m /s	82
Transmissivity at 10 kPa	$\square_{(10,0.1)}$	ASTM D4716***	10^{-3} m /s	0.9
Transmissivity at 200 kPa	$\square_{(200,0.1)}$	ASTM D4716***	10^{-3} m /s	0.73
D.C. Straight 200 kPa (7 days)	$q_{w(10,0.1)}$	ASTM D4716***	10^{-6} m /s	94
D.C. Straight 300 kPa (7 days)	$q_{w(10,0.1)}$	ASTM D4716***	10^{-6} m /s	73
D.C. Straight 500 kPa (7 days)	$q_{w(500,0.1)}$	ASTM D4716***	10^{-6} m /s	42
D.C. Kinked	□	ASTM D6918	%	18

Hydraulic Properties Filter		**Standard**	**unit**	**MD88H**
Velocity Index ($q_{h,50}$)	v_{h50}	EN/ISO 11058	m/s	10
Permittivity filter	□	ASTM D4491	s^{-1}	0.3
Permeability filter	k	ASTM D4491	10^{-4} m/s	1.3
Pore Size	O_{95}	ASTM D4751	µm	75

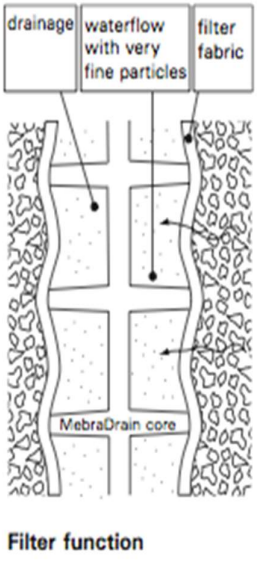

Figure 5.11 Physical properties of MebraDrain MD88H

5.3.2.2 Modified prefabricated vertical drain

In the membraneless vacuum preload system, vacuum was transmitted to each individual PVD using connected tubing which extended the connection to the surface and acted independently. These connecting components presented in Figure 5.12 were required to be assembled to form the modified PVD. Its components included (a) 16 mm HDPE tubing, (b) PVD-Tube Connector and (c) MebraDrain MD88.

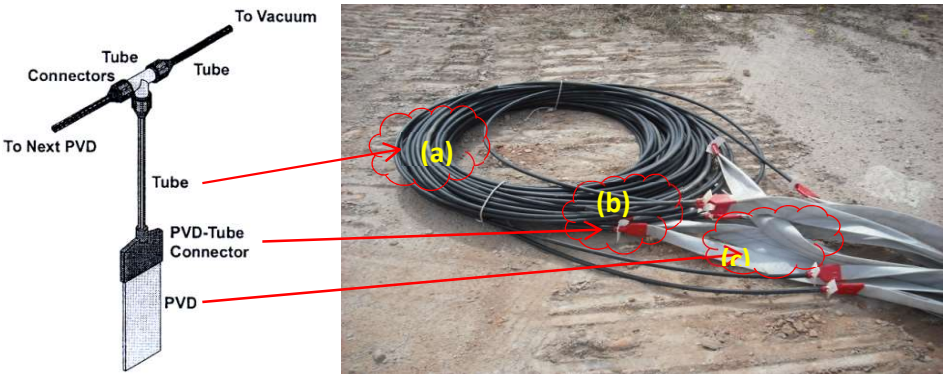

Figure 5.12 Connecting components for modified PVD

The HDPE tubing and MebraDrain MD88 were cut and their lengths adjusted to accommodate the changing soil profile as illustrated in Figure 5.13. The HDPE tubing could resist a ground pressure of 200 kPa. The PVD was connected to the HDPE tubing by means of a specially designed fittings and connectors.

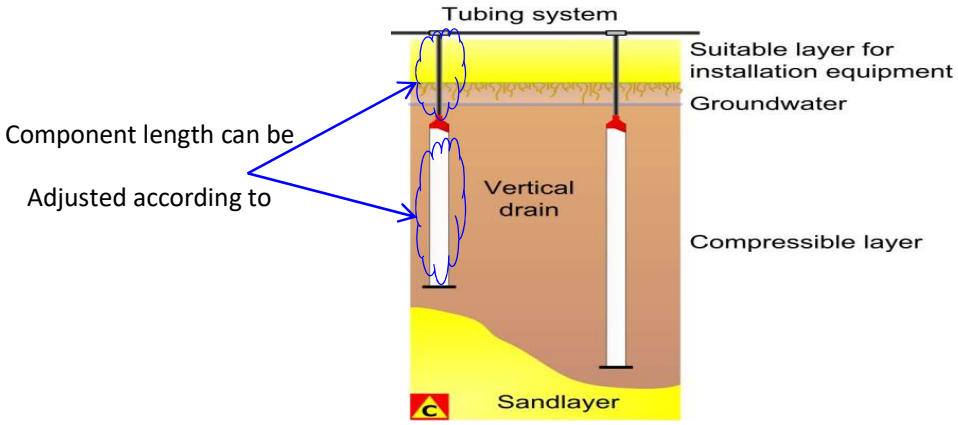

Figure 5.13 Customizable length of modified PVD

5.3.3 Membraneless vacuum preload system setup

The setup of the membraneless vacuum preload system included the driving of the modified PVD drains into the soil mass, connecting the installed drains to the horizontal transfer tubing lines on the surface via tube connectors and finally the connection of the horizontal tubing to the vacuum pump. The sequences of membraneless vacuum preload system installation are illustrated in Figure 5.14 and the actual set up the field trial site is shown in Figure 5.15

Before the installation of the modified drain, a stable load bearing working platform was prepared to level out the undulating site to allow trafficability and operations of the PVD installation rigs and other vehicles, plants and equipment on site. After the completion of the working platform, a custom built PVD installation rigs as shown in Figure 5.16 was used for the installing the modified vertical drains in triangular pattern.

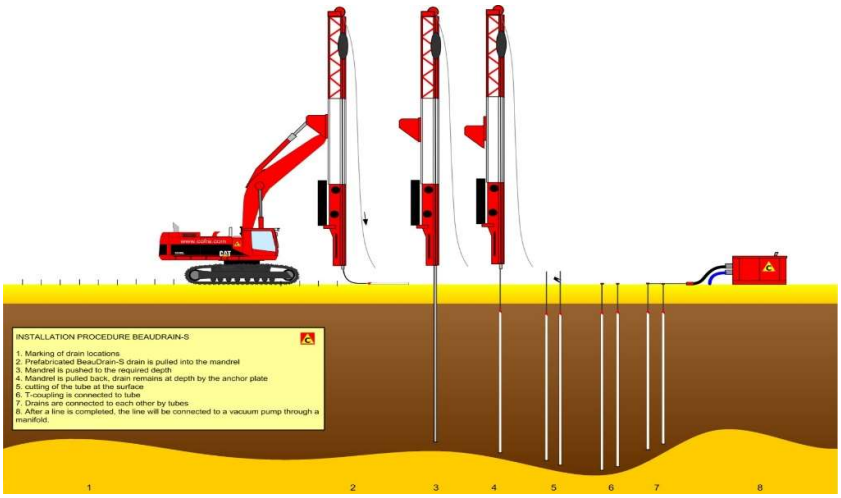

Figure 5.14 Installation sequence of the membraneless vacuum preload system

Figure 5.15 Setup of the membraneless vacuum preload system at trial site

Figure 5.16 Installation of the modified drains in triangular pattern

The assembled modified PVDs were installed in triangular pattern with a spacing of 1.0m as show in Figure 5.17. The triangular arrangement was to provide a more compact and uniform consolidation between drains than the arrangement of the square pattern. The installation points were pre-determined and marked out by the surveyor using the anchor plates before installation. The drain influence zone (D) was estimated at 1.05 times of the modified PVD spacing.

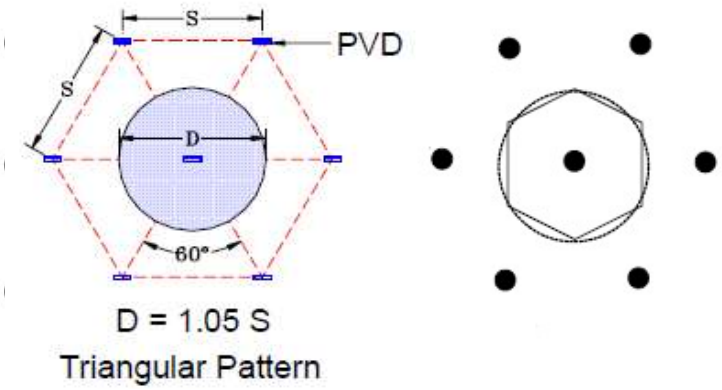

Figure 5.17 Triangular installation pattern of the modified PVDs

Before driving modified PVD drain into the soil, the PVD was wrapped around the fixture on the anchor plate. The folded end of the wrapped drain was then secured onto the base of the mandrel. Once the setup was ready, the mandrel was positioned above the drain installation point and pushed the modified PVD into the design depth. On reaching the design depth, the mandrel was withdrawn and the anchor plate secured itself at the soil mass at the driven depth fixing the modified PVD into position. Figure 5.18 (a) illustrates a schematic diagram of the anchor plate used and Figure 5.18(b) illustrates the cross section of the rectangular mandrel used.

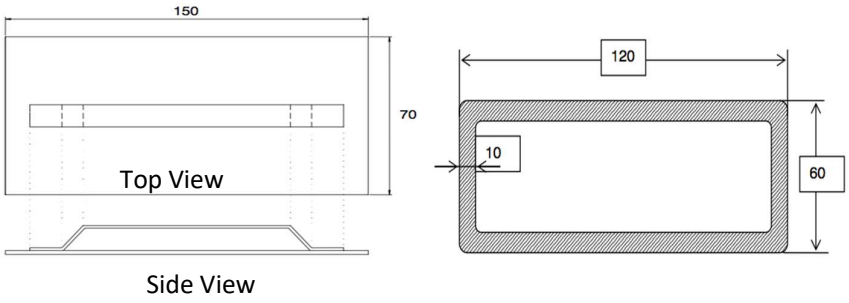

(a) Anchor plate (b) Cross Section of Mandrel

Figure 5.18 Schematic diagrams of the anchor plate and mandrel used for the installation of the modified PVDs

After the installation of the modified PVDs into the soil, the vertical tubing from the assembled drains were cut at ground level and joined to the horizontal transfer tubing with T-couples manually by workers as shown in Figure 5.19(a), (b) and (c). Each horizontal line was designed to support up to 40 modified PVDs. The connected horizontal tubing was then connected to a manifold as shown in Figure 5.19 (d) and (e). Each manifold was designed to support 10 lines of horizontal tubing. The manifolds finally were connected to a vacuum pump as shown in Figure 5.19 (f) through a larger diameter pipe. The vacuum pump used in this field trial could typically treat a land area of approximately 1500 m^2.

It was necessary to ensure that all connections of the tubing and the pipes were sealed properly to prevent any air leakage, otherwise the required vacuum pressure could be undermined. Before the placing of surcharge over the tubing and pipe network, all connections were checked from time to time.

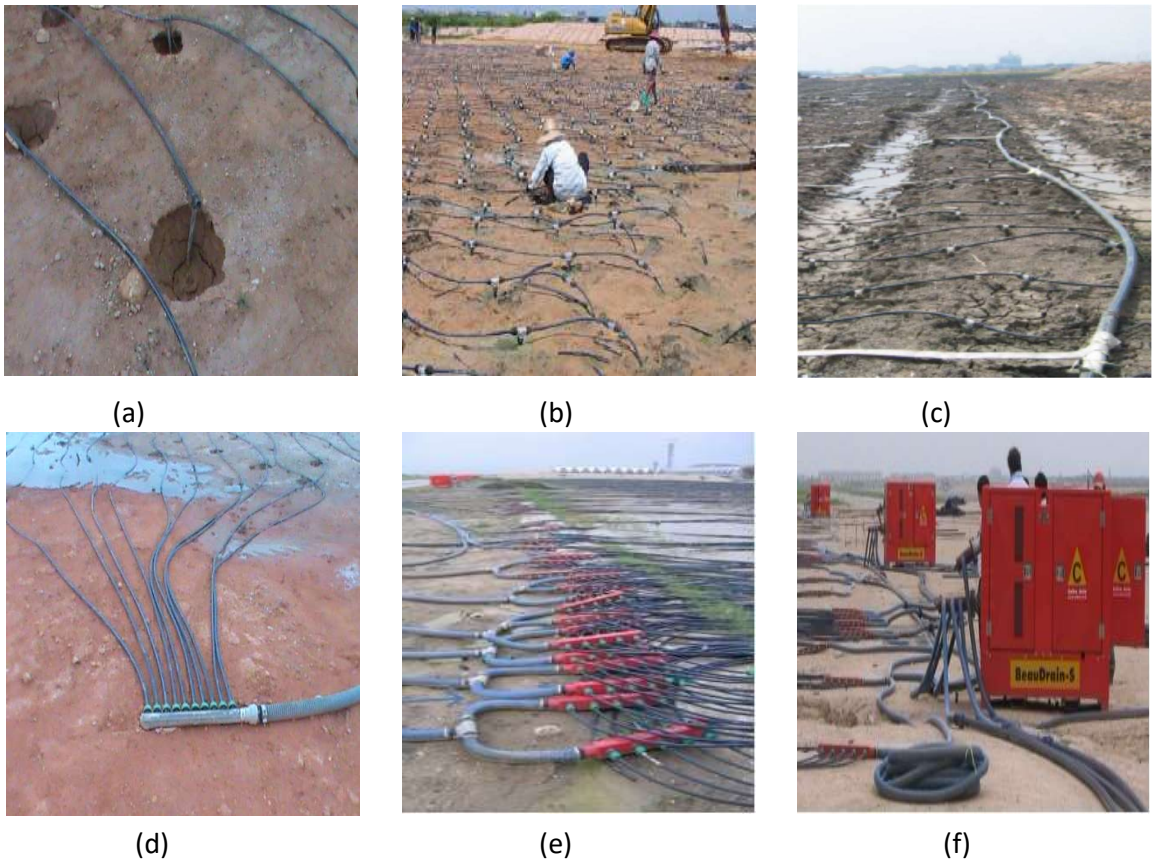

Figure 5.19 (a) to (f) Connection of the membraneless vacuum preload system from modified drains to vacuum pump

The hot climate and UV light caused the T-couples and other components of the tubing network to loosen and deteriorate overtime due to uneven expansion and contraction of materials and UV degradation made the connections more susceptible to damages. Once all the connections were made, the vacuum was applied using vacuum pumps. For this field trial, each vacuum pump treated an approximate area of 1,500 m^2. All four pumps were deployed for the field trial. The pumps were placed on sufficiently strong and dry platform with the inlet at installation level to minimize loss of vacuum. The pumps were operated continuously with maintenance on a weekly basis. Figure 5.20 shows a site photo of a typical vacuum pump used in the field trial.

Figure 5.20 Typical vacuum pump used for field trial

5.3.4 Vacuum pumping operations.

The vacuum pumping operations was divided into 4 sectors as illustrated in Figure 5.21. Each sector had an area of about 1,250 m^2 and was served by a vacuum pump. Vacuum pumping trial runs were conducted at each sector to identify and resolve teething issues such as vacuum leakages, component damages, improper installation and other potential risks before full-scaled operations and adding of fill surcharge. This was a necessary step carried out in all sectors to ensure all components and instrumentations worked well. Figure 5.22 shows the trial vacuum pumping at Sector VP2.

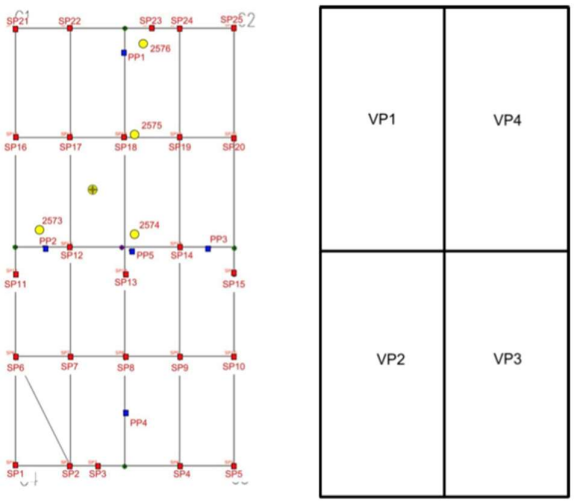

Figure 5.21 Division of vacuum pumping sectors for field trial

Figure 5.22 Worker checking for vacuum leakages during trial vacuum pumping

During one of the earlier pumping trials, it was found that the newly designed T-couples degraded under prolonged exposure to sunlight (UV degradation) and the corrosive effects of seawater. The T-couples cracked under surcharge loading resulting in vacuum leakages where the sector was unable to achieve the required design vacuum pressure. The newly designed T-couples were replaced with the original T-couples and the issue was resolved.

5.3.5 Additions of fill surcharge

After the vacuum load was applied for about one month, about 2.5 m height sand surcharge, an equivalent of 50kPa, was applied on top of the trial area to help expedite the consolidation of the underlying marine clay layer. During surcharging, the vacuum pumping operations continued without stopping. The placing and compaction of the first 50cm of the surcharge fill was done very carefully to avoid damages and disturbance to the buried tubing. No equipment was allowed to drive on top of the tubes before the placement of the first 50cm fill surcharge. Figure 5.23 illustrates the placement of surcharge during vacuum pumping and at the final surcharge elevation.

Figure 5.23 Surcharge placement during vacuum operations and final surcharge elevation

5.4 Field instrumentation program

The layout of the different field instrumentations installed at the trial site are shown in Figure 5.24. The types and quantities of the field instrumentations deployed are summarized in Table 5.6.

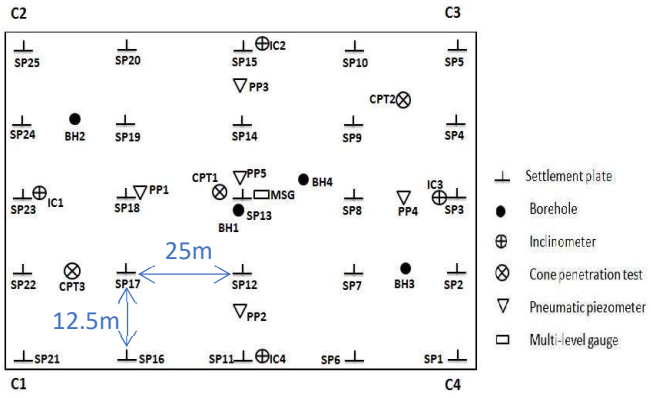

Figure 5.24 Site layout showing the locations of different field instrumentation at trial site

Table 5.6 Types and quantities of field instrumentation deployed

S/N	Monitoring Instrumentation	Quantities
1.	Surface settlement plates	25
2.	Multi-level magnetic extensometers	01
3.	Deep Settlement plate	01
4.	Water Standpipes	04
5.	Pneumatic Piezometers (group)	05
6.	Inclinometer	04

5.4.1 Surface settlement plates

A typical design of surface settlement plate is shown in Figure 5.25. A total of 25 Settlement Plates (SP) were installed in a predetermined grid arrangement as illustrated in Figure 5.26. Of the 25 SP, only 9 were installed at the top of the surcharge while the remaining 16 SP were installed on the edge of the surcharge.

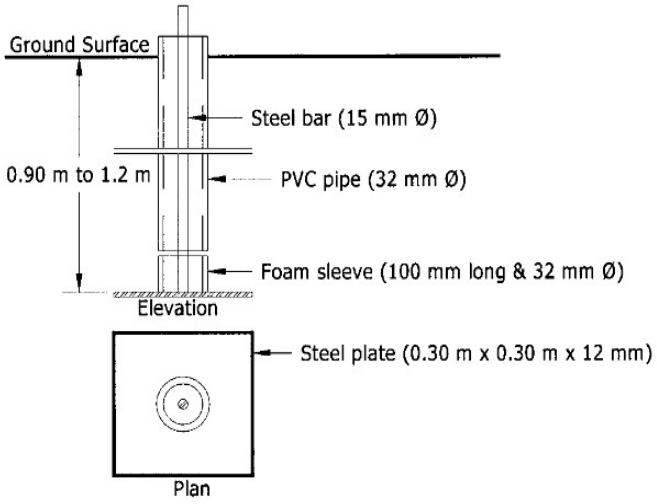

Figure 5.25 Typical setup of surface settlement plate (Atalah, 2006)

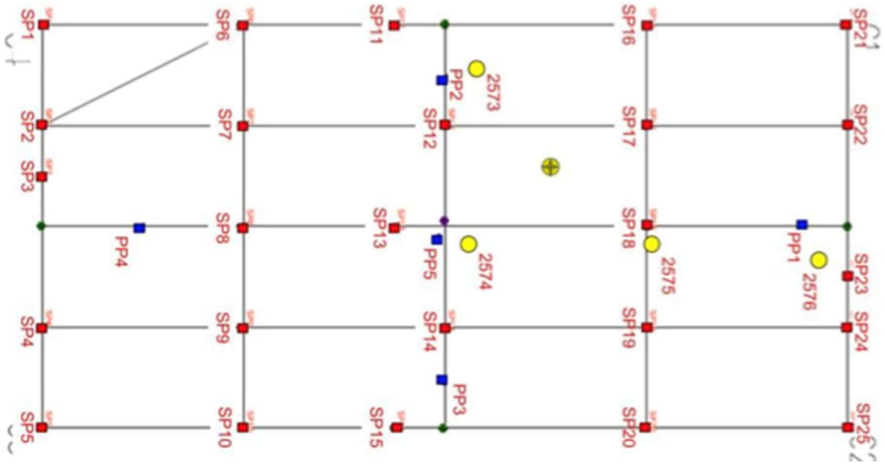

Figure 5.26 Settlement plates (SP) layout arrangement at trial site

5.4.2 Multi-level settlement gauge

Multi-level deep settlement gauges, or multi-level magnetic extensometers were used to measure the settlements at elevations below the ground surface along one borehole, which was in the center of the site indicated as MSG in Figure 5.24. They measured the settlement along the axis of a measuring tube (borehole) by means of a magnetic probe. A typical installation set up of multi-level settlement gauge is shown in Figure 5.27.

The magnetic extensometer consisted of a magnetic probe, a measuring tape, a tape reel with built in light buzzer and many measuring rings positioned at distinct intervals along the length of an access pipe. Readings were obtained by lowering the extensometer probe through the access pipe to the depth of measuring rings equipped with magnets. When the probe entered the magnetic field, a reed switch closed and the light and buzzer was activated. The actual depth of measuring ring was established from the measuring tape onto which the extensometer probe was connected and which was graduated with cm markings. The access pipe was anchored to stable ground which did not move. This depth was used as the "datum" for settlement calculations.

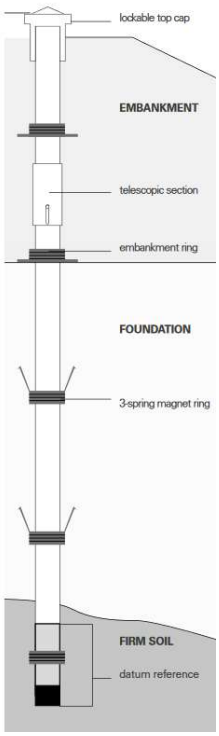

Figure 5.27 Typical setup of multi-level settlement gauge

5.4.3 Water standpipes

The standpipe piezometers were installed in borehole to monitor the groundwater levels. They typically consisted of a filter tip joined to a riser pipe as shown in Figure 5.28. Readings were obtained with a water level indicator. The water level indicator consisted of a probe, a graduated cable or tape, and a cable reel with built-in electronics. The probe was lowered down the standpipe until it contacted water. This was signaled by a light and a buzzer built into the cable reel. The depth-to-water reading was taken from the cable or tape. The water level indicator featured a sensitivity adjustment which helped the user to obtain consistent measurements and eliminated false triggering.

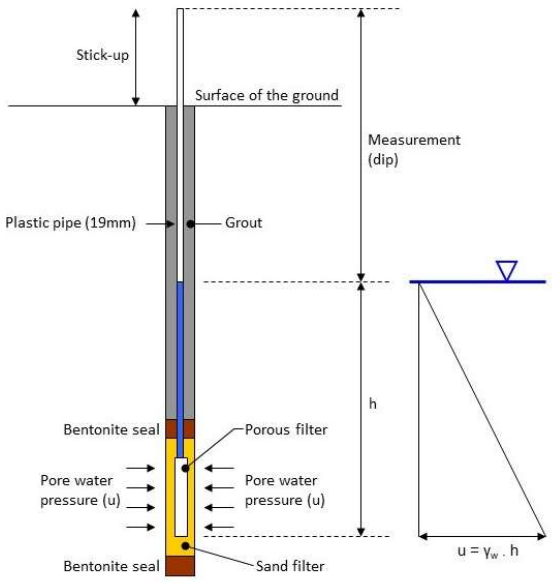

Figure 5.28 Typical setup of water standpipe (Geotechnical_Observation)

5.4.4 Pneumatic piezometers

Five groups of pneumatic piezometers were used to measure pore water pressure in the soil layer. They are indicated as PP1-PP5 and were installed at different locations. At each location, 5 piezometers were installation at different elevations in the soil. Figure 5.29(a) illustrates the typical setup of a typical pneumatic piezometer.

The pneumatic piezometer contained a flexible diaphragm. Water pressure acted on one side of diaphragm and gas pressure acted on the other. To take a reading, a pneumatic indicator was connected to the terminal. Compressed nitrogen gas from the indicator flew down the input tube to increase gas pressure on the diaphragm. When gas pressure exceeded water pressure, the diaphragm was forced away from the vent tube, allowing excess gas to escape via the vent tube. When the return flow of gas was detected at the surface, the gas supply was shut off. The gas pressure in the piezometer decreased until water pressure forced the diaphragm to its original position, preventing further escape of gas through the vent tube. At this point, the gas pressure equaled to the water pressure, and a reading was obtained from the pressure gauge on the indicator. The operating principle of the pneumatic piezometer can be seen in Figure 5.29(b).

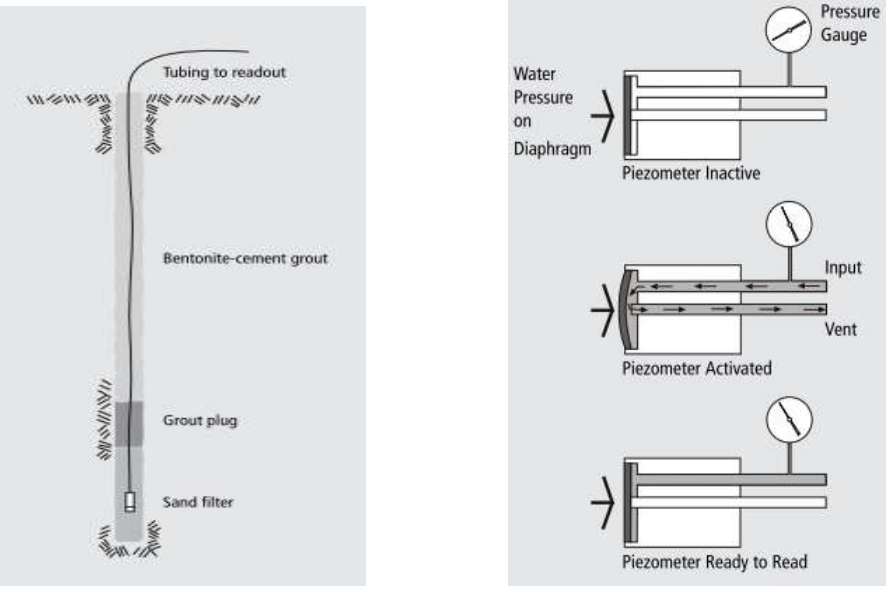

(a) Setup of single pneumatic piezometer (b) Operating principle of pneumatic piezometer

Figure 5.29 Typical setup and operating principle of pneumatic piezometer

5.4.5 Inclinometers

Inclinometer setup shown in Figure 5.30 was used to measure the horizontal/lateral movement below the ground surface at the four boundaries as shown in Figure 5.24. It consisted of a torpedo usually fitted with wheels and containing a gravity-operated tilt sensor which generated a signal and was connected to a power source and readout unit to enable the angle between the torpedo axis and the vertical to be determined. The method of measurement was using servo accelerometers located within the probe. The probe traveled in key-ways in the inclinometer tube to give measuring directions at right angles. Where two servo accelerometers were used, they could sense the inclination of the access tube in two directions at right angles to each other. This inclination was displayed in terms of angular or horizontal displacement deviation.

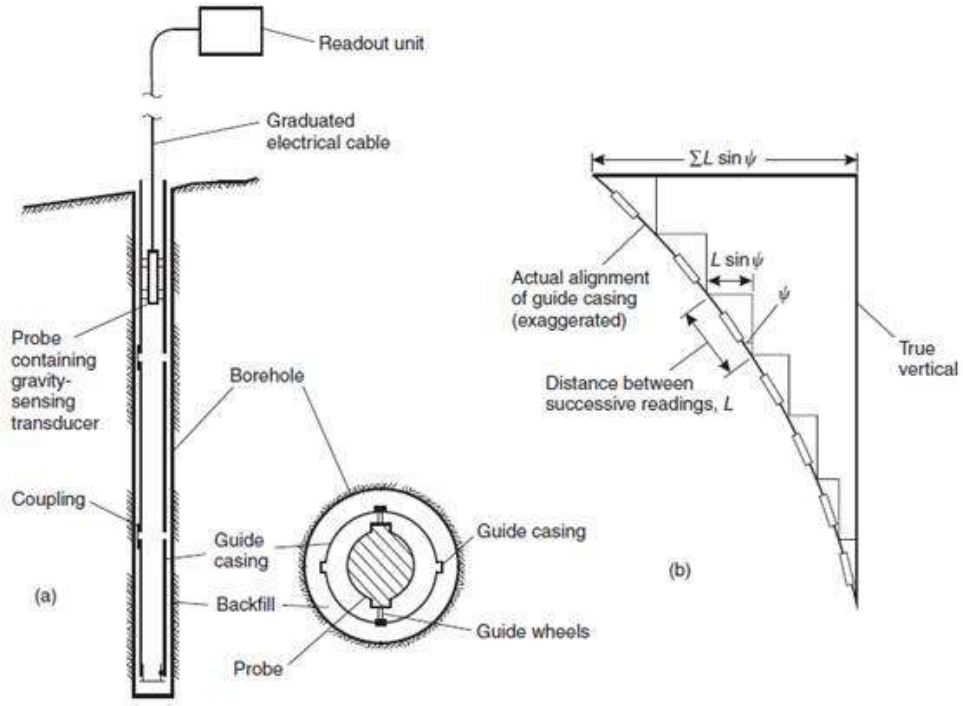

Figure 5.30 Typical setup of inclinometer

5.5 Field trial results and analysis

5.5.1 Settlement

Based on the settlement monitoring data, a 3D image of recorded settlements is illustrated in Figure 5.31. From the 3D image, we can clearly see that the amount of recorded settlements varies from locations. The difference in the settlement magnitude were largely contributed by the uneven thickness of the underlying soft clay where larger settlement were observed in locations with thicker marine clay layers. The maximum settlement recorded was 1.53 m at SP18 and the minimum settlement recorded was only 0.08 m at SP05.

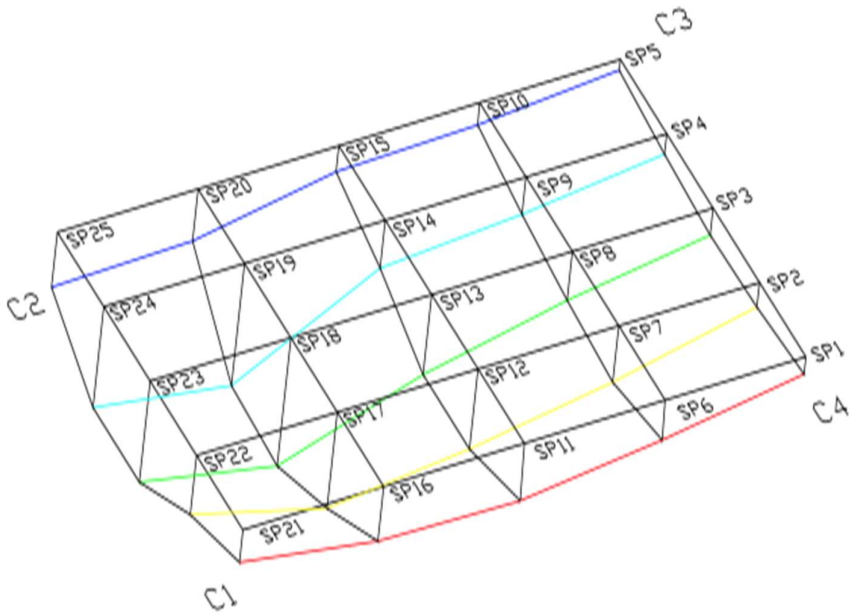

Figure 5.31 3D representation of surface settlements at trial site

Figure 5.32 shows the recorded settlement for SP05 and SP18 over time during the vacuum operations. The settlement curves of SP18 clearly demonstrate that the additional surcharge applied did accelerate the consolidation of the marine clay layers.

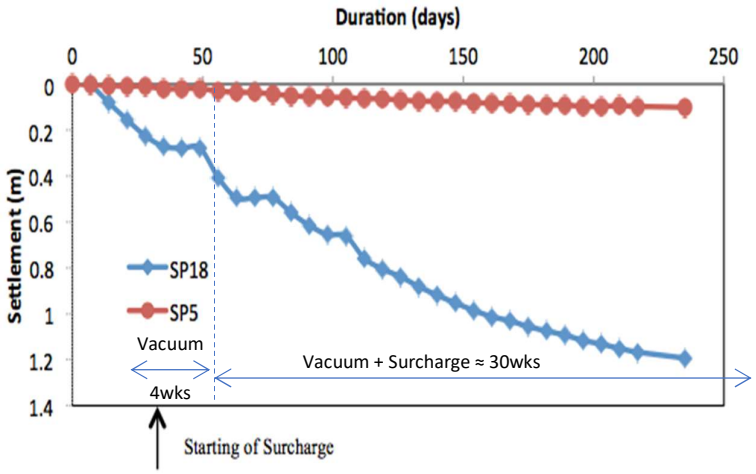

Figure 5.32 Settlements of SP05 and SP15 with time

The settlements measured by multi-level settlement gauges installed at SP13 at different depths are plotted against time in Figure 5.33. Settlement were observed over the entire depth of the marine clay layer up to a depth of 18m. It was observed that the greatest settlement occurred at the top marine clay layer and the recorded settlement for each layer reduced with depth in which the smallest settlement was observed at the most bottom layer. This phenomenon could probably be attributed to a combination of the following factors including (a) larger settlement at the top sandy clay-silty clay layer than the bottom marine clay layer due to difference in materials' property (b) the bottom clay layer had experienced a higher degree of self-weight and overburden consolidation thus leading to less settlement (c) longer drainage path for the lower clay layer to dissipate its excess pore pressure at the top pervious soil layer (d) additional drainage resistance at the lower clay layer due to buckling of the drains due to settlement as the marine clay layers consolidated.

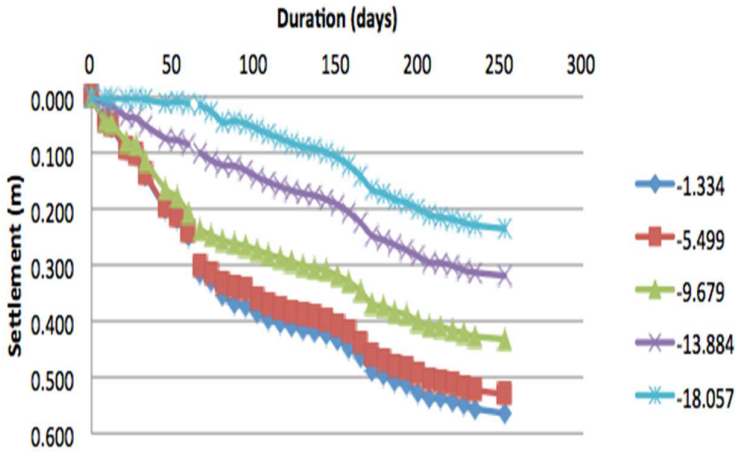

Figure 5.33 Settlements measured at different soil depths with time

It can be further observed in Fig.5.33 that each of the settlement curves at different depth had two gradients. Generally, the settlement curves for the upper soil layer (at -1.334m, -5.499m and -9.679m) were experiencing faster settlement rate before day 75 and the settlement curves gradually became less steep after day 75 showing less settlement thereafter. However opposite observations were made for the lower soil layers (at -13.884m and -18.057m) where faster settlement rate was observed after day 75. This could probably due to the delayed effect of drainage of excess pore water pressure from the soil body for the bottom clay layer that led to consolidation. Generally, the settlement curves for all the soil layers after day 75 were found to have similar gradient and trend as the combined vacuum and surcharge consolidation effect on the different soil layer stabilized.

5.5.2 Pore pressure

Pore pressures were measured by the pneumatic piezometers at five locations in the trial site. The approximate locations of these piezometers are indicated in the layout as illustrated in Figure 5.34. At each location, 5 piezometers were placed at different soil depths in between the vertical drains. The installed depth of the pneumatic piezometer sensors varied accordingly to the undulating thickness of the marine clay layer.

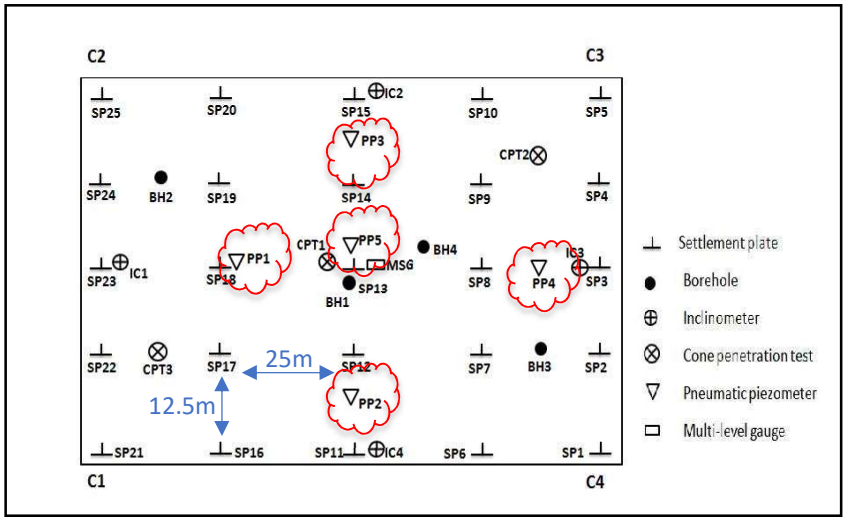

Figure 5.34 Location of piezometers at trial site.

Figure 5.35 shows the recorded pore pressures over time. Although the measured pore pressures of the 5 locations varied from less than 20kPa to more than 100kPa, they all exhibited similar trend. Generally, in the initial stage, when the trial site was only under vacuum preloading, the measured pore pressures dissipated steadily until surcharge was applied. The applied surcharge resulted the pore pressures to rise. Thereafter, the pore pressures dissipated slowly from the peak with continued vacuum pumping operations.

The monitored pore pressures difference at different soil depths against time at PP5 are presented in Figure 5.36. It was observed that the pore pressure at shallow soil depth -1.23m, -5.23m and -9.25m remained fairly stable as they were located in the permeable mixed fill layer. No built up of pore pressures due to surcharge fill nor the reduction of pore pressures overtime due to the vacuum preloading were observed. Fluctuations in the pore pressure were small, ranging between ± 5 kPa

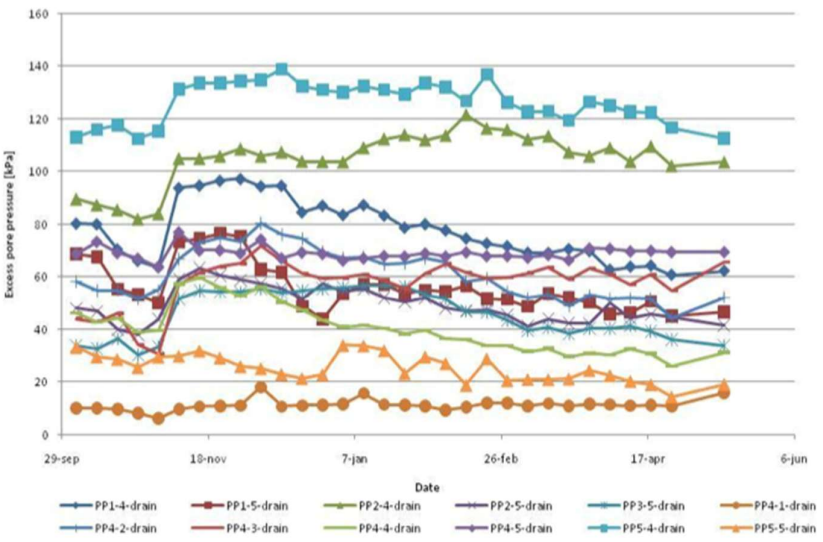

Figure 5.35 Recorded pwp with time at different piezometers

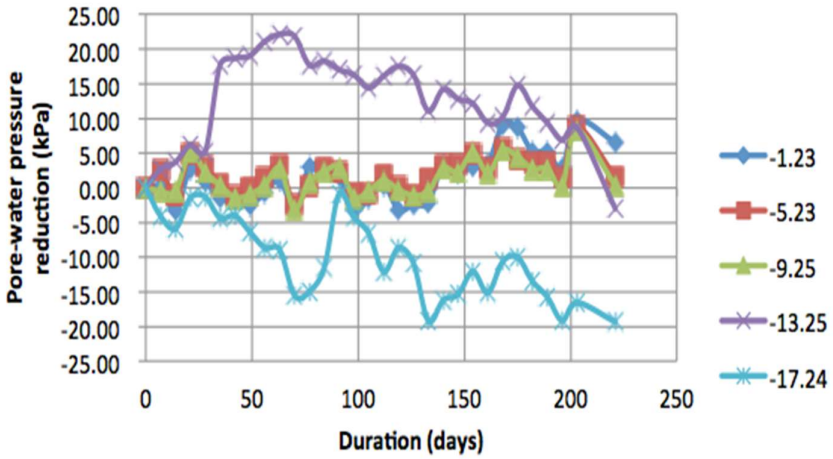

Note: the surcharge was applied from 35th day

Figure 5.36 Pore pressure reduction curves at different soil depth at PP5

However, at deeper soil depth at where the marine clay layer was found at -13.25m, increased in pore pressures were observed initially especially after the surcharge fill was applied. It is worth noting that the increased in pore pressure was contained within 25kPa instead of equivalent 50kPa surcharge applied. There could be two possible reasons to explain these observations. Firstly, the intermixed semi pervious soil-clay layer could have dissipated part of the pore pressure induced by the

surcharge. Secondly the pore pressure increment as a result of the applied surcharge load could be partially offset by the vacuum induced by the membraneless vacuum preload system.

At the depth of -17.24, the initial pore pressures measured were negative. Delayed effects of the applied surcharge was observed as the pore pressure increased after Day 70 from -15kPa to 0kPa. After 0 kPa, the pore pressures reduced again slowly until -20 kPa was reached. The reduction of the pore pressures over time demonstrated that the membraneless vacuum preloading was effective to some extended to improve the impervious marine clay layer.

A better way to examine the pore pressure development is to plot the pore pressures agaisnt depth as illustrated in Figure 5.37(a) to (e). In these figures, the initial pore pressure distributions and pore pressure distributions at 28 days, 56 days, 133 days and 221 days are plotted together with the hydrostatic pore pressures and the suction lines. These curves illustrate the changes in the pore pressure profiles with depth over time. The area bounded by the final pore pressure curves and the suction lines represent the remaining excess pore pressures that have not dissipated.

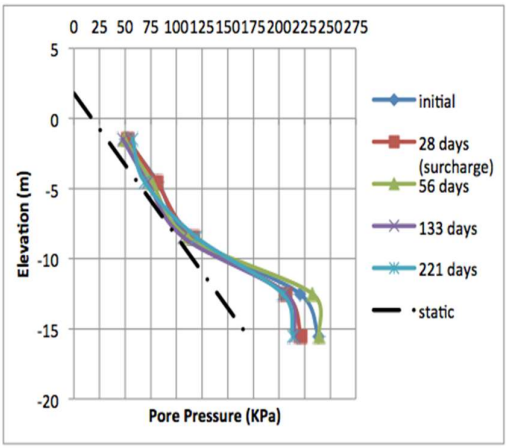

(a) PP1

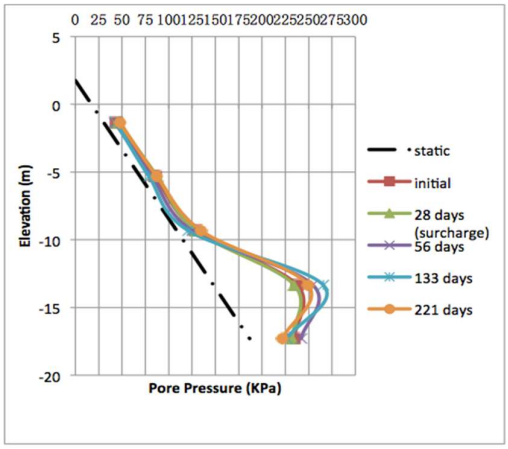

(b) PP2

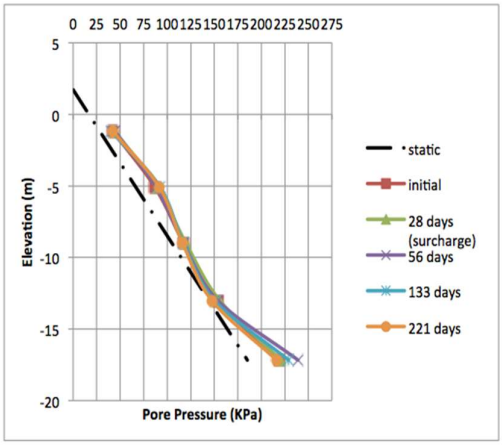

(c) PP3

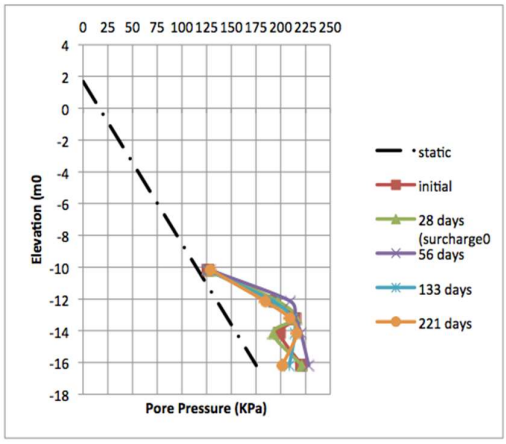

(d) PP4

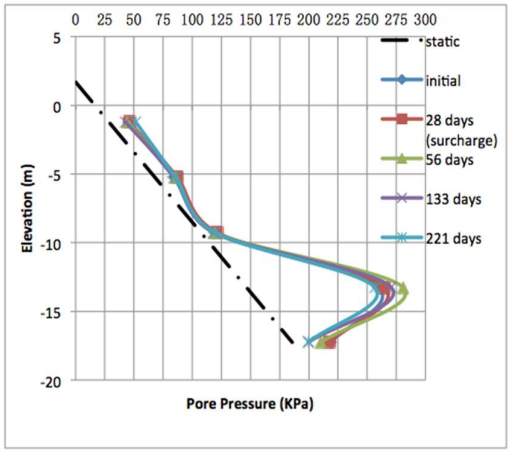

(e) PP5

Figure 5.37 (a) to (e) Pore water pressure distributions with depth at different locations in the trial site

The missing data of the vacuum pumps pressure in Figure 5.38 highlight that the membraneless vacuum preload system was not performing efficiently and effectively. The missing pump pressures were due to vacuum pumps breakdowns during the field trial period.

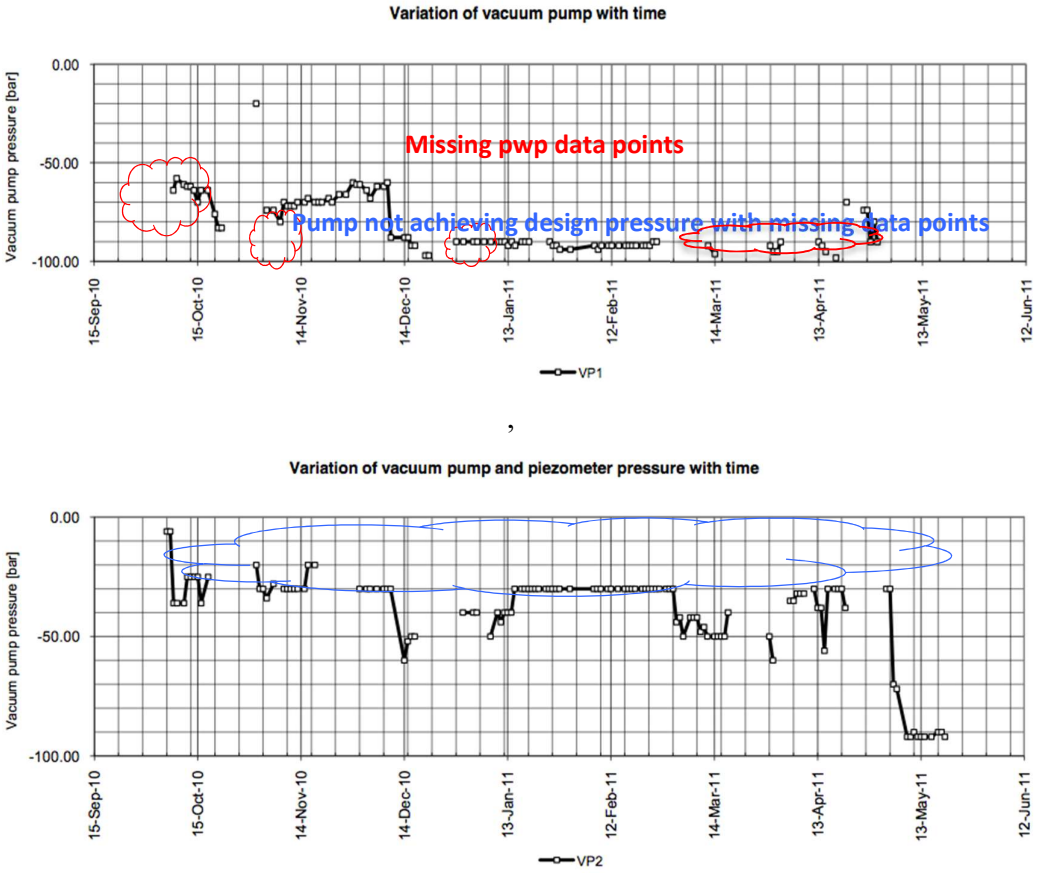

Figure 5.38 Missing vacuum pressure data for VP1 and VP2

Table 5.7 summarized the effective running time of the vacuum pump and the average vacuum pressure achieved for the field trial. It was concluded that the operational performance and reliability were far from ideal due to the frequent vacuum pumps breakdowns coupled with delayed response from contractor to provide immediate replacement. Post mortem review proposed the provision of more reliable pumps and also backup pumps to be stationed at site so that they could be deployed immediately to replace the failed pumps.

Table 5.7 Vacuum pumps reliability and average vacuum pressure achieved during operations

Pump	Operation Running Time	Average Vacuum Pressure
VP1	52%	81kPa
VP2	71%	40kPa
VP3	84%	69kPa
VP4	92%	88kPa

The vacuum pressure illustrated in Figure 5.38 were measured at the pump source. The vacuum pressures measured in the soil matrix were observed to be lower. Typically, the difference in vacuum pressure between the pump and the piezometer can be in the range of 20-40kPa as illustrated in Figure 5.39. The difference was probably due to energy loss from overcoming flow resistance and vacuum leakages in the connections.

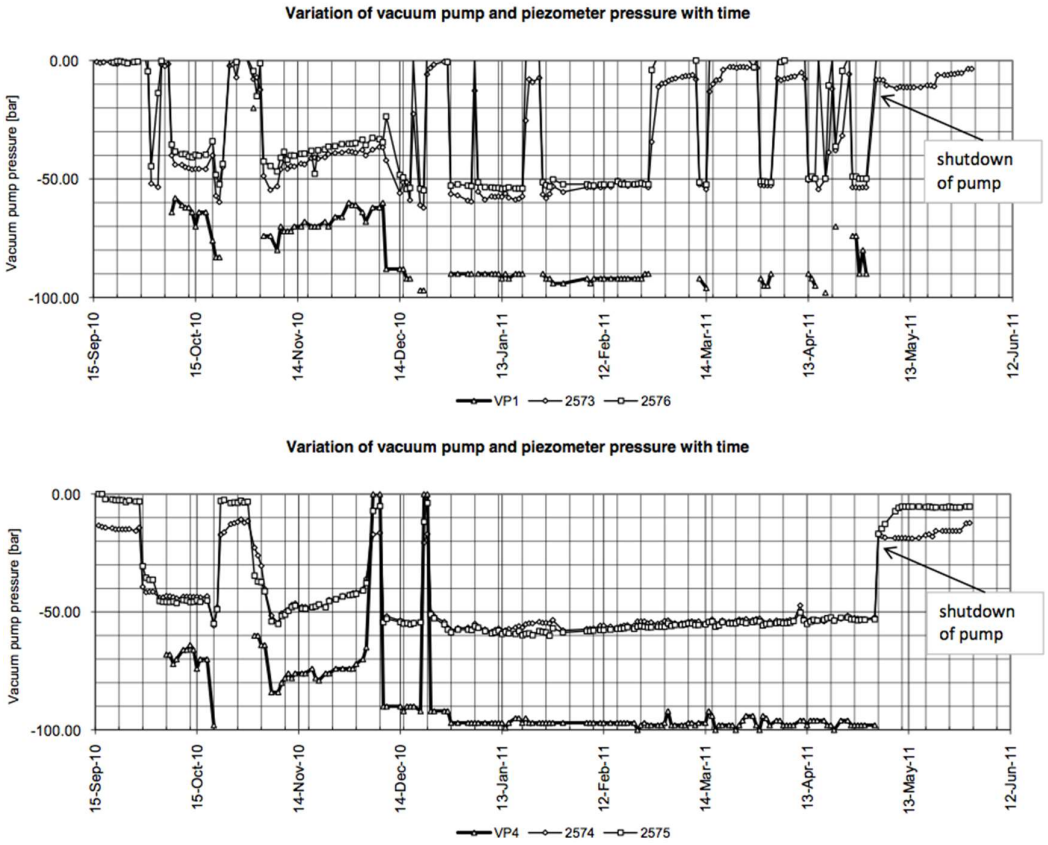

Figure 5.39 Vacuum measured at pump and soil

It should be noted that the locations where the piezometers were installed will affect the computed degree of consolidation. This can be explained using Figure 5.40. Piezometers installed in between PVDs gave higher pore pressure readings and thus lower degree of consolidations are derived. While piezometer installed nearer to PVDs will have lower pore pressure readings and thus higher degree of consolidations are computed.

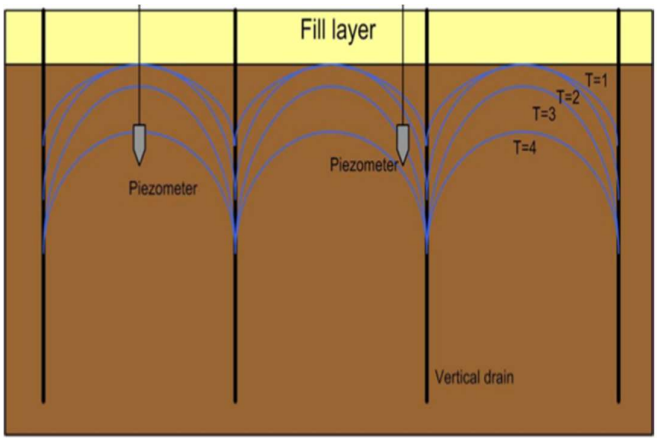

Figure 5.40 The pore pressure measurement varies with piezometer location

5.5.3 Degree of consolidation

The Degree of Consolidation (DOC) is used for assessing the effectiveness of conventional soil improvement works. It is calculated as the ratio of the current settlement to the ultimate settlement. Several methods had been proposed to estimate the DOC. Among them are the Asaoka Method (Asaoka, 1978), the Hyperbolic Method (Sridharan and Rao, 1981) and the Pore Pressure Method (Chu and Yan, 2005b). In this section, the DOC computed using Asaoka Method and Pore Pressure Method are discussed.

Asaoka method is a popular method used to estimate the ultimate primary settlement of the soil using the available settlement data. The average degree of consolidation calculated based on the settlement data using Asaoka Method in this field trial is 85%. Chu (Chu and Yan, 2005b) proposed to use the monitored pore water pressure data to estimate the degree of consolidation. Using the monitored pore water pressure data, the pore pressure distribution profiles with depth can be plotted for a combined loading case for the initial, intermediate and final states as shown schematically in Figure 5.41.

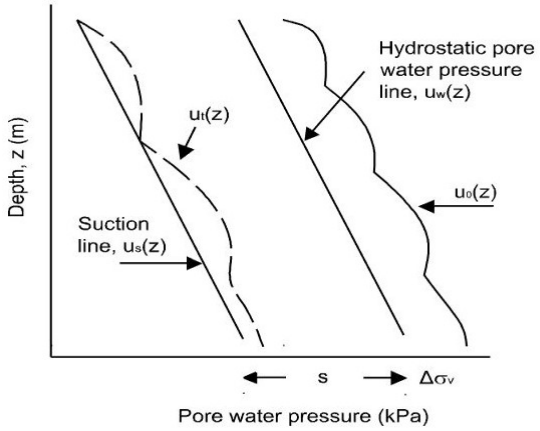

Figure 5.41 Estimation of Degree of consolidation using pore pressure distribution profile (Chu and Yan, 2005b)

Using this profile, the average degree of consolidation can be calculated as

$$U_{avg} = 1 - \frac{\int [u_t(z) - u_s(z)]dz}{\int [u_0(z) - u_s(z)]dz} \quad (1)$$

Where

$$u_s(z) = \gamma_w z - s \quad (2)$$

In Eq. (1), $u_0(z)$ is initial pore pressure + Surcharge at depth z; $u_0(z)$ is the pore pressure at depth z at time t; $u_s(z)$ is the suction line, z is the depth; γ_w is the unit weight of water and s is the suction applied. The value of s in the membraneless vacuum preload system is assumed to be 60 kPa. The integral in the numerator in Eq. (1) is the area between the curve $u_t(z)$ and the suction line $u_s(z)$, and the integral in the denominator is the area between the curve $u_0(z)$ and the suction line $u_s(z)$.

Based on the pore pressure distribution, after 221 days of membraneless vacuum preloading application, the computed average degree of consolidation was estimated to be in the range of 35% -50%. Based on the graphical presentation of the pore

pressure distribution profiles in Figure 37(a) to (e), although there were clear sign of reduction of pore pressures before and after application of surcharge, they never reduced to a value below the hydrostatic values. This was probably due to possible vacuum leakages found in the membraneless vacuum preload system where the removed water from the clay layer by vacuum was quickly replaced with the surrounding ground water. As such the excess pore pressure was unable to go below the hydrostatic pressure and moves closer towards the suction line.

The discrepancy between the degrees of consolidation estimated based on Asaoka method at 85% and Pore Pressure method at 40-50% are likely due to the following reasons:

i. In the estimation of DOC using Asaoka method, the prediction of ultimate settlement included the settlement data collected from the entire depth of the soil mass which included the upper pervious silty sand-sandy clay layer and lower impervious marine clay layer. Therefore the DOC computed by Asaoka is not reflecting the consolidation status of the marine clay layer by the DOC of the entire depth of the soil mass. In the pore water pressure method, such settlements in the pervious soil layer were not reflected in the pore pressure data and not used for computation of the DOC.

ii. The pore water distribution curves show that the marine clay layers were undergoing consolidation under the influence of surcharge and vacuum preload. However, the consolidation and rearrangement of the soil structures in the marine clay layer could probably lead to the build up of high pore water pressure being measured at day 221. This resulted a lower DOC computed using the pore water pressure data despite settlement was being observed.

iii. The Asaoka method observational settlement prediction rely on the linear ordinary differential equation gives a settlement-time relationship. The frequent vacuum pump breakdowns did not provide sufficient data points to reflect accurately the settlement-time relation of the combined vacuum and

surcharge preload. This could lead to over prediction of DOC using Asaoka method when the data were interpreted by contractor in such a way to demonstrate that the target DOC was achieved.

iv. Either the settlements or pore water pressures were measured only at a limited number of points, there were uncertainties whether the measured deformation (settlement) or pore water pressures were representative of the spatial variation of the whole site. As settlements or pore water pressures can only be measured at a limited number of points, the settlement plates were placed at where the settlements may be the largest whereas the pore pressure transducers at where the pore pressure were the highest which were typically in between the PVD drains as illustrated in Figure 5.40. As a result, the degree of consolidation estimated using settlement overestimated and that using pore water pressures would tend to be underestimated.

The accuracy of the computed DOC for both methods depend very much on the quality and quantity of field monitoring data. Any errors involved in the field settlement or pore pressure data measurement collation will inevitably affect the outcome of the computed DOC. This could lead to unreliable assessment of soil improvement result. To moderate the various uncertainties involved in the DOC computations, it is recommended to estimate the DOC using both settlement and pore pressure data Chu (Chu and Yan, 2005b) along with other available field data.

5.5.4 Post field trial soil investigations

5.5.4.1 Cone penetration tests

To verify the effectiveness of the combined membraneless vacuum preload system with surcharge fill in the field, pre and post field trial soil investigations were carried out. Figure 5.42 shows the result of pre and post CPT data carried out near BH1. Although the CPTs were not carried out at the exact same locations, their geological conditions and profile did not differ greatly. Generally, increase in the cone resistance,

sleeve friction and reduction on of the dynamic pore pressure were observed in the compressible layer treated with the membraneless vacuum preload.

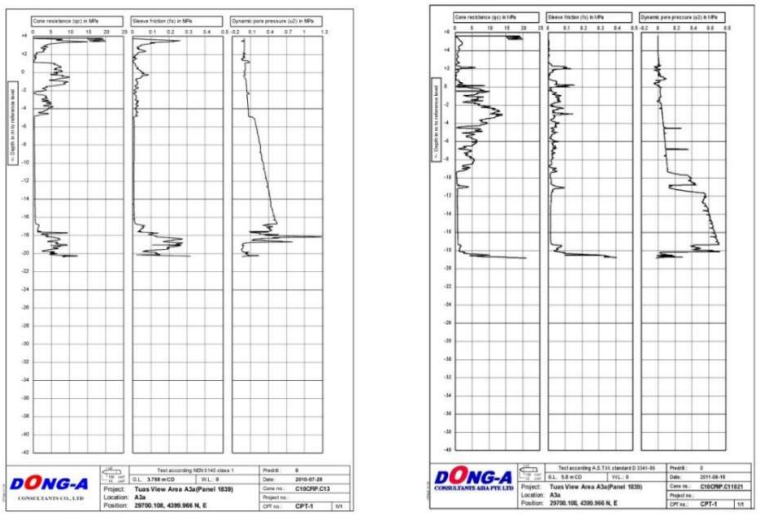

(a) Pre trial CPT data (b) Post trial CPT data

Figure 5.42 Pre & post field trial CPTu results

5.5.4.2 Field vane shear tests

Pre and post field vane shear tests (FVST) were carried for the field trial at various locations. The FVST were carried out to a depth more than 20m from the land surface elevation and the measured undrained shear strength with depth are illustrated in Figure 5.43. Generally, increase in undrained shear strength were observed over the entire depth of soil mass after combined membraneless vacuum preload with surcharge fill was applied.

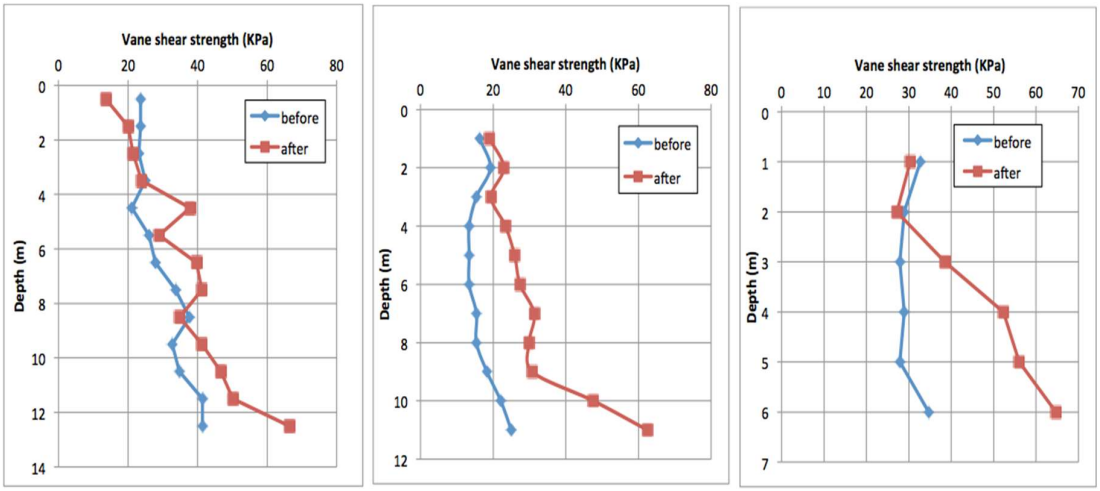

Figure 5.43 Pre & post undrained shear strength profile from field vane shear test (FVST)

5.5.4.3 Undrained shear strength computation from different post site investigations

Generally, the compressible marine clay layer was undergoing consolidation during the field trial and was classified as Normally Consolidated (NC) soil. Apart from using the FVST, the undrained shear strength can also be derived from data collated from other site data, namely cone resistance data from CPT and pore pressures data from piezometer readings.

Undrained shear strength (S_u) can be computed using the pore pressue readings from the piezometers to derive the total effective overburden and applying the information to the well established empirical relationships of undrained strength ratio (S_u/σ'_{vo}) NC = 0.22 where the subscript NC represents normally consolidated soil and σ'_{vo} represents the effective vertical overburden pressure.

Alternatively, undrained shear strenght of the compressible soil layers at the end of the field trial can also be computed using the cone resistance data (q_c) from the CPT carried out using $S_u = \frac{q_c - \sigma_{vo}}{N_k}$ where σ_{vo} represents the total overburden stress pressure and N_k is a cone bearing capacity factor having a value of around 10-15 for

normally consolidated clays and 15 to 20 for over-consolidated clays. N_k=14 is used for the computation of the undrained shear strength using the CPT data.

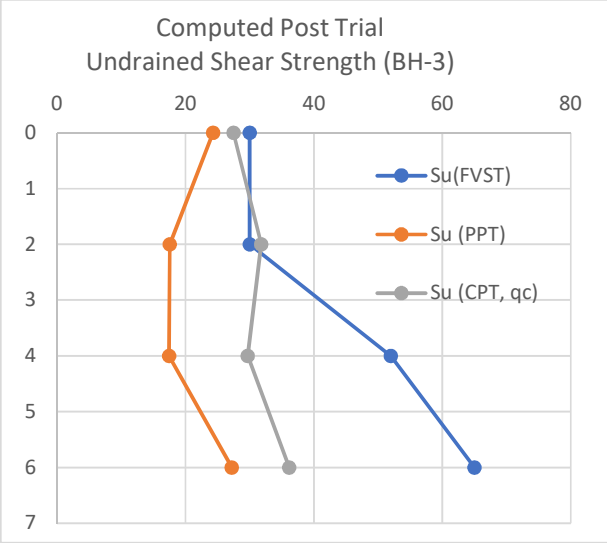

Figure 5.44 Comparison of post-trial undrained shear strength profile computed from FVST, CPT and piezometer data (PPT)

Figure 5.44 illustrated the undrained shear strength derived using three different types of field data. Generally, FVST results give the highest undrained shear strength while piezometer data provided the lowest values. The value computed using CPT cone resistance data fall in-between the two. The accurracy of the undrained shear strength computed using the the different approach would depends very much on the locations, accuracy and quality of these field data.

5.6 Conclusions

This chapter discussed the site investigation program, setup and analysis of the results of a 5000 m^2 soil improvement field trial over a newly reclaimed land using the combined membraneless vacuum preload system with surcharge. The key conclusions are:

i. The proposed combined membraneless vacuum preload system with surcharge fill is effective to a limited extend to help improve the properties of

the soft cohesive soils that was embedded several meters below permeable fill materials.

ii. Accurate profiling of the permeable layer above the marine clay layer and the frequent shutdown of the vacuum pumps resulted in the less than ideal delivery of the vacuum pressue in the membraneless preload system. A high-quality site investigation program to obtain a detailed and accurrate soil layer profile is a must while using more reliable pumps along with more frequent maintenance and backup pumps can help reduce the issue of frequent pump failures.

iii. The average degree of consolidation (DOC) derived using the Asaoka method and the pore water pressure method were compared. Generally, the DOC computed using Asaoka method was higher than that computed using the pore pressure method.

iv. Post site investigations of the field trial and computation of different sets of field data showed increased the undrained shear strength of the entire depth of the soil mass improved by the proposed combine membraneless vacuum preload system.

CHAPTER 6 FORMATION OF WORKING PLATFORM OVER DREDGED SLURRY INFILL

6.1 Introduction

Among the various dredging and reclamation methods, hydraulic dredging has been identified as one of the most efficient and cost-effective methods for the placement of a large quantity of dredged slurry as reclamation fill. To verify this, a pilot field trial was carried as part of a reclamation project in the western part of Jurong Island to study the operational feasibility and key technical and site challenges of using hydraulically dredged slurry with high fines content as fill for land reclamation projects. The following key activities were carried out as part of the pilot field trial:

a. Construction of a confinement facility for the land reclamation and the deposition of dredged materials.

b. Deposition of the dredged materials in the confinement facility in both lumpy form by direct dumping and slurry form by hydraulic infilling.

c. Construction of a load bearing working platform over the deposits to allow access, trafficability and soil improvement works.

d. Carrying out soil improvement works using suitable vacuum preloading techniques to treat the deposited soft fills underneath the working platform to the requirement of the reclamation project.

However, part (d) of the pilot field trial was deferred due to the failure of forming the working platform. Several numerical analyses were carried out to understand and identify the mechanism that could have led to the working platform failure. The findings of the analyses are presented in the following chapter.

The role of the author in this field trial was the developer's project manager to carried out the planning and implementation of the reclamation works and also the data collation and to conduct objective assessment of this field trial.

6.2 Existing seabed profile

Extensive marine soil investigations were carried out to map out existing seabed profiles of the trial site. A good understanding of the existing profile is important for the design and planning of the confinement facility as well as the subsequent soil improvement works.

Figure 6.1 shows the existing seabed profile developed from using the soils data obtained from the marine soil investigations.

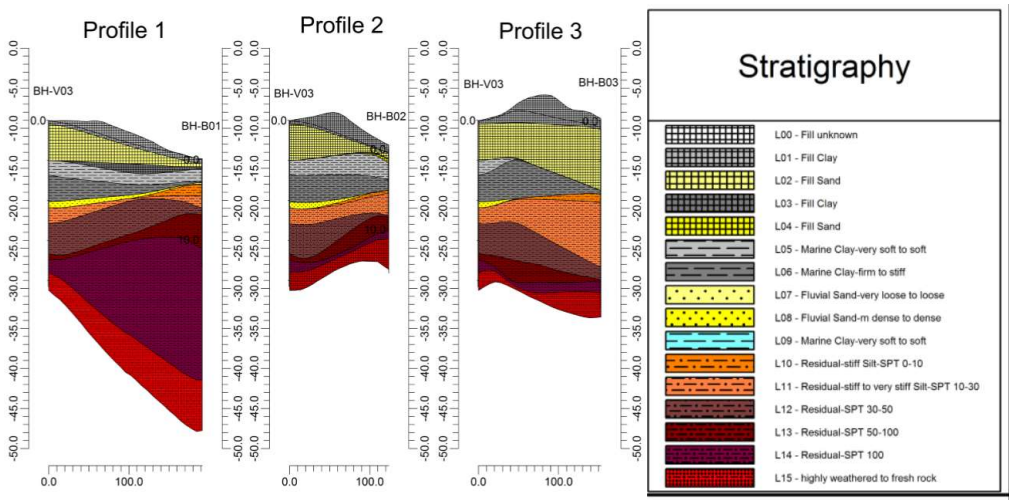

Figure 6.1 Seabed profile underneath the field trial site

The mapped seabed profile showed that there was a layer loose sand directly below the seabed. This could potentially cause vacuum leakages during vacuum preloading if the PVDs were installed into this permeable layer. To remove this risk, the loose sand layer was removed by dredging the existing seabed to the marine clay layer below. Due to its low permeability, the marine clay layer would act as impervious layer for effective sealing of the vacuum preloading.

6.3 Design and construction of confinement facility

The confinement facility measured approximately 60 m x 60 m at the bottom, at the elevation of -18 mCD (Chart Datum). The sides of the containment bund extended at a 1:3 slope from the bottom to the surface forming a pit measuring 200 m x 200 m at the crest of the containment dike, at an elevation of +8 mCD. The containment facility was formed and enclosed by the existing shoreline and the construction of a perimeter and inner bunds. The confinement facility was constructed to provide stable containment to allow deposition of dredged seabed materials up to an elevation of +6.5 mCD.

Figure 6.2 Schematic plan view of the confinement facility

6.3.1 Contracts stipulated design

In the original plan, the contractor was to construct the confinement facility in 2 stages. In stage 01, after completion of the perimeter and inner bund foundation and the removal of the loose sand layer at the bottom of the containment pit, the contractor was to raise the perimeter and inner bund using sand to - 4m as illustrated in Figure 6.2. This was to allow deposition of mechanical dredged materials by direct dumping using dump barges.

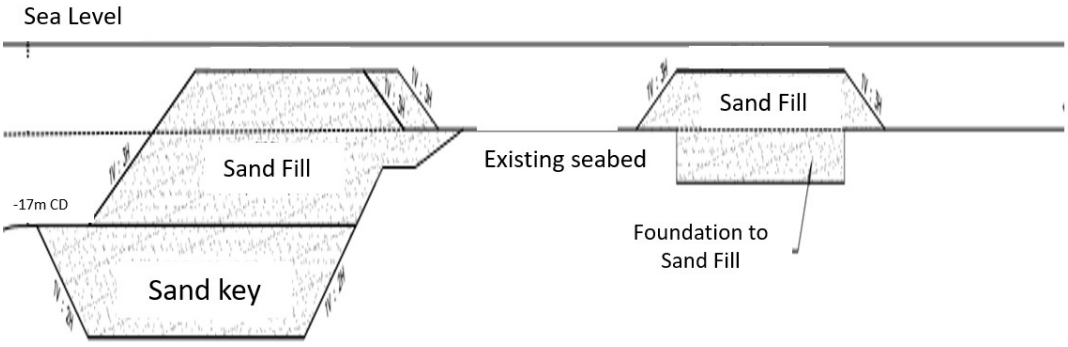

Figure 6.3 Cross section of contract stipulated stage 01 bund construction

When the deposition of the grab dredged materials had reached the design elevation, the perimeter and inner sand bunds would then be raised to +7.0 mCD in stage 02. This allowed the deposition of the dredged slurry to +6.5 mCD. A top width of 7 m and 20 m were provided at the top of the inner and perimeter bund respectively to ensure stability and to provide a decent land access to the trial area.

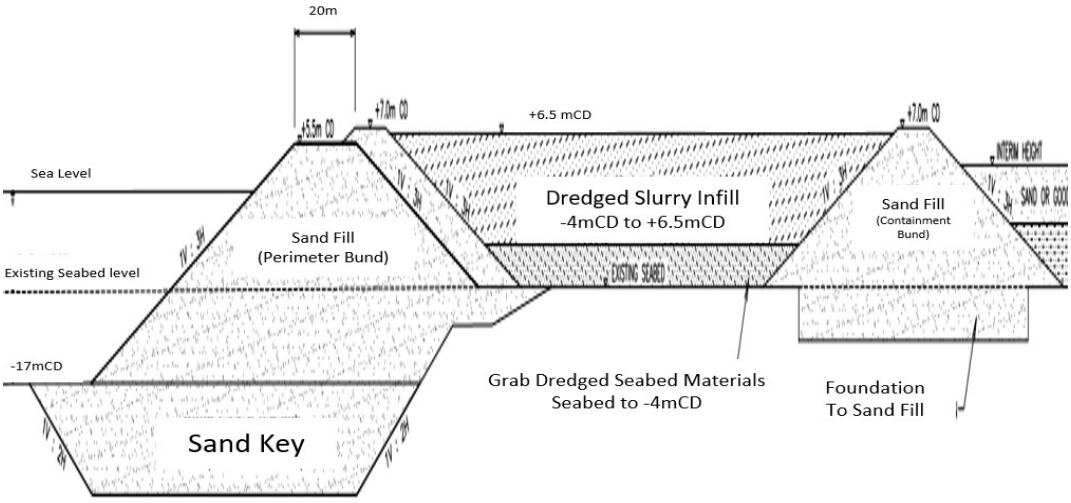

Figure 6.4 Cross section of contract stipulated stage 02 bund construction and dredged material deposition plan

6.3.2 Contractor's alternative design

An alternative design was proposed by Contractor for the confinement facility. This new design replaced approximately 200,000 m^3 of sand with dredged materials. The perimeter bund remained to be constructed in two stages but the inner containment

bunds were proposed to be constructed in 3 stages using sand and stiff dredged materials.

During the construction of the alternative inner bund in stage 01, sand was replaced with stiff dredged materials from seabed to 0 mCD as illustrated in Figure 6.4. In stage 02, sand was spread evenly and slowly over the stiff dredged materials using a sand spreader pontoon barge, forming a slope of 1:5 until the maximum placement by sea was reached. Land equipments were then deployed to continue the sand spreading fill up to +3.5 mCD. In the final stage, the bund was raised from +3.5 to +7.0 mCD with sand at a slope of 1:3 as illustrated in Figure 6.4.

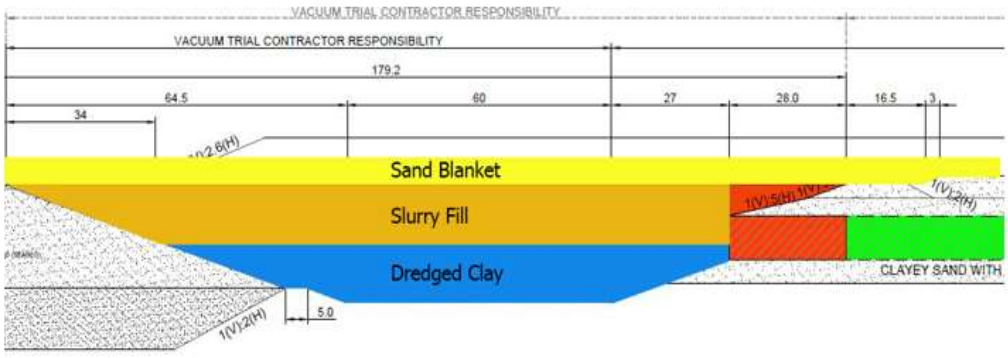

Figure 6.5 Cross section of contractor's alternative confinement facility design

The actual construction of raising the containment bunds using conveyor belt barges and land equipment are shown in Figure 6.5 and 6.6. Figure 6.7 shows the aerial view of the completed confinement facility.

Figure 6.6 Raising containment bund from seabed using conveyer belt barges

Figure 6.7 Raising and trimming containment bund to final elevation using land based equipment

Figure 6.8 Aerial view of the completed confinement facility

6.4 Dredged materials filling

6.4.1 Acceptance criteria

The approved infilling materials in the confinement facility comprised of grab-dredged seabed , cutter dredged seabed slurry and excavated fine-grained soils from construction projects.

6.4.2 Materials filling

The infilling of the confinement facilities were carried out in 2 phases. In phase 1, the confinement facility was filled with grab dredged materials. These semi-lumpy dredged materials were loaded and sent to the trial site for direct dumping using hopper and flat top barges. In phase 2, the confinement facility was filled with cutter dredged slurry from nearby seabed. The dredged slurry was transported and pumped into the confinement facility using floating steel pipes. Table 6.1 summarizes the dredged materials details deposited in the confinement facility.

Table 6.1 Actual infill profile carried out by contractor

Layers	Actual infill layers	Sources
Bearing layer	1.5 m thick sand	Contractor's Sand
Dredged Slurry	-6 to +6.5 mCD (thickness 12.5m)	Dredging of fairway adjacent to reclamation works
Grab Dredged Materials	-18 to -6 mCD (thickness 14.0m)	
Bottom of Trial	Dredged to -18mCD	Existing seabed

6.4.2.1 Phase 1 filling – direct dumping

Prior to direct dumping of the mechanical dredged materials, the loose sand layer was removed from the existing seabed to prevent vacuum leakages when vacuum preload is applied. Infilling works by direct dumping were carried out from -18 to -6 mCD by direct dumping using hopper and flat top barges. Direct dumping was limited up to an elevation of -4 mCD after taking into account the minimum draught needed for a fully loaded barge to manoeuvre and carry out the direct dumping operations over the deposited infills.

Figure 6.9 Grab dredger loading dredged materials into dump barge (left) and dump barges moving into position over the underwater containment facility for direct dumping (right)

Grab dredged materials were sent to the confinement facility and depostied as infill. Samples were collected and sent to laboratory for physical properties testing. The properties of these dredged materials are tabulated in Table 6.2 to 6.4. The tests were carried out in accordance with the testing methods stipulated in BS1377-Part 2:1990.

Table 6.2 Dredged materials' composition [Particle Size Analysis BS1377 – Sieve Analysis]

Composition (weight /%)	**Clay**	**Silt**	**Sand**	**Gravel**
Range [%]	23 - 60	19 - 59	6 - 51	0 - 13
Ave [%]	40.3	28.8	30.3	1.6

Table 6.3 Dredged materials' density, water content & void ratio

Parameters	**Range**	**Average**
Bulk Density, $\gamma_{bulk,}$ [kN/m^3]	14.7- 18.3	16.5
Dry Density, γ_{dry} [kN/m^3]	7.4 – 14.0	10.6
Water Content, *w* [%]	29 - 105	59
Void Ratio, e_0	0.90 – 2.51	1.60

Table 6.4 Dredged materials' Atterberg's limit & consistency indices

Atterberg's Limit & Consistency Indices	Range	Ave. Values
Liquid Limit, LL [%]	34.0 – 74.0	66.40
Plastic Limit, PL [%]	20.0 – 27.0	23.40
Plasticity Index, I_p [%]	14.0 – 52.0	42.90
Liquidity Index, I_L	0.11 – 1.86	0.90
Consistency [ISO 14688]	Stiff – Very Soft	Very Soft

6.4.2.2 Phase 2 filling – hydraulic infilling

In Phase 2, hydraulic infilling was implemented. This approach allowed dredged materials to be deposited above sea level. After pumping the dredged slurry into the confinement facility, the high water content dredged slurry was able to spread and level itself by the action of gravity alone due to its high workability.

The initial dredged slurry infilling were carried out using an amphibious excavator installed with Bell 200 pump to transfer the dredged slurry from the modified flat-top barge to the confinement facility as shown in Figure 6.9(a). The transfer process was slow, inefficient and not scalable to handle large quantities of dredged slurry. This method of infilling was deemed unsuitable.

A better and more efficient way was to transfer the dredged slurry directly from the cutter-suction dredger's (Ganga) dredging operations to the confinement facility for infilling through connecting floating pipes as shown in Figure 6.9 (b).

(a) Excavator installed with BELL 200 Pump (b) Cutter suction dredger (CSD)

Figure 6.10 Equipment used for dredged slurry infilling

During the CSD cutting operations, dredged seabed materials were cut, mixed and fluidised with sea water to form dredged slurry. The dredged slurry was then pumped from the CSD to connecting floating steel pipes and discharged into the confinement facility as show in Figure 6.10. After infilling, the slurry suspension will "rest" in the confinement facility for sedimentation to take place.

Figure 6.11 Dredged slurry pumped from CSD and poured into the confinement facility as fill

During the sedimentation process, the discrete solid particles in the slurry suspension separated from the seawater and settled down to the bottom of the confinement facility by the action of gravity. As this occurred, clarification of the slurry suspension was observed. The clarified water from the sedimentation process was drained out of the confinement facility via the weir box by removal of the wooden planks. The clarified water level was monitored closely and the planks removed corresponded to the elevation of the clarified water as more soil particles formed into sediments. The clarified water was guided with pipes and discharged out to the sea behind the weir box. This freed up storage capacity for the next cycle of infilling with dredged slurry. These processes were repeated over many cycles until the dredged slurry fill reached the design elevation at +6.5 mCD.

Figure 6.11 show the weir box units installed at the side of the perimeter bund to ensure only clarified water from the sedimentation process was discharged out of the confinement facility. The weir boxes were designed and installed at the most suitable elevation to allow dredged slurry to be deposited to the maximum capacity of the confinement facility for every infilling cycle.

Figure 6.12 Photo showing weir box unit before and after installation

6.4.2.3 Slurry pumping cycles

The contractor carried out 3 cycles of slurry pumping using Bell Pump and 7 cycles of infillng using CSD Ganga. It can be clearly shown in Table 6.5 that the production rate of using Bell Pump to re-handled dredged materials from flat-top barges was extremely low when compared to the CSD Ganga operations. In total, more than 1.2mil m^3 of dredged slurry were pumped into the confinement facility containing about 285,000m^3 of in-situ dredged seabed material.

Table 6.5 Production rates of the slurry pumping

Cycle	Date	Duration b/w Cycles	In-situ Vol. IS(m3)	Slurry Vol. [m^3]	Water Vol W[m^3]	W: IS Ratio	Production [m^3/hr]
Bell Pump							
1st Cycle	22 Jul 15	NA	747	935	188	0.25	209
2nd Cycle	27 Jul 15	5 days	468	935	467	1.0	178
3rd Cycle	29 Jul 15	2 days	831	935	104	0.13	208
CSD Ganga							
1st Cycle	05 Aug 15	NA	50,000	301,633	251,633	5.00	10,054
2nd Cycle	11 Sep 15	≈ 5 weeks	68,000	193,424	125,424	1.84	4,178
3rd Cycle	17 Oct 15	≈ 5 weeks	36,000	115,988	79,988	2.22	3,013
4th Cycle [3]	28 Nov 15	≈ 6 weeks	37,206	215,848	178,642	4.80	6,476
5th Cycle	08 Dec 15	≈ 2 weeks	38,151	141,655	103,504	2.71	5,977
6th Cycle	15 Dec 15	≈ 1 weeks	44,340	168,800	124,460	2.80	4,811
7th Cycle	31 Dec 15	≈ 2 weeks	9,360	66,234	56,874	6.07	8,117
		Total Volume	285,103	1,206,387	921,284	3.23	

The slurry infills were dredged directly from the seabed of Jurong Channels. In-situ seabed samples were collected and sent for testing. All tests were carried out in accordance with with the testing methods stipulated in BS1377-Part2:1990. The in-situ seabed materials properties are tabulated in Table 6.6 to 6.8.

[3] Mugbug was introduced

Table 6.6 Dredged materials' composition [Particle Size Analysis BS1377 – Sieve Analysis]

Composition (weight /%)	Clay	Silt	Sand	Gravel
Range [%]	25-51	26-47	2-48	0 – 1.25
Ave [%]	36.6	39.5	23.4	0.5

Table 6.7 Dredged materials' density, water content & void ratio

Parameters	Range	Average
Bulk Density, $\gamma_{bulk,}$ [kN/m^3]	14.5-16.5	15.35
Dry Density, γ_{dry} [kN/m^3]	6.5-7.4	8.4
Water Content, *w* [%]	58-126	86%
Void Ratio, e_0	1.59-3.12	2.27

Table 6.8 Dredged materials' Atterberg's limit & consistency indices

Atterberg's Limit & Consistency Indices	Range	Ave. Values
Liquid Limit, LL [%]	35-56	46
Plastic Limit, PL [%]	20-23	22
Plasticity Index, I_p [%]	15-33	24
Liquidity Index, I_L	2.53-3.12	2.83
Consistency [ISO 14688]	Very Soft - Soft	Soft

6.4.2.4 Settling column tests

Before each dredged slurry infill cycle began, clarified free water from the sedimentation process was drained out to allow infilling capacity for the next cycle. When more free water was drained, more dredged slurry could be deposited in each infilling cycle. A good understanding on the time needed for dredged slurry sedimentation was important to the contractor's planning and deployment of resources. Settling column tests were carried out using 2 m tall columns to understand the behaviours and the time needed for the sedimentation process of the dredged slurry suspension. The results of the settling column tests are discussed in Chapter 3.

6.4.2.5 Hydramotion mugbug

From Table 6.6, the dredged slurry composition was akin to the slurry composition used in Column S4 (MC 30%: JF 70%) in the settling column tests. 1300kg/m^3 was set as the target density for the dredged slurry before the excess free water were drained to allow the next cycle of dredged slurry infilling. The results from the settling column tests indicated that it would take approximately 120 hrs/ 5weeks for the sedimentation to achieve the target density of 1300kg/m^3 with about 30% settlement in the dredged slurry suspension interface.

The timeline interpreted from the settling column tests were followed strictly for the first 3 cycles of dredged slurry infilling by CSD. This time-consuming approach was soon deemed impractical with growing pressure to meet the reclamation programme. A new approach to determine the real-time status of the sedimentation process to shorten the waiting time between each infilling cycle time was achieved by the deployment of the "Hydramotion Mudbug" as shown in Figure 6.12.

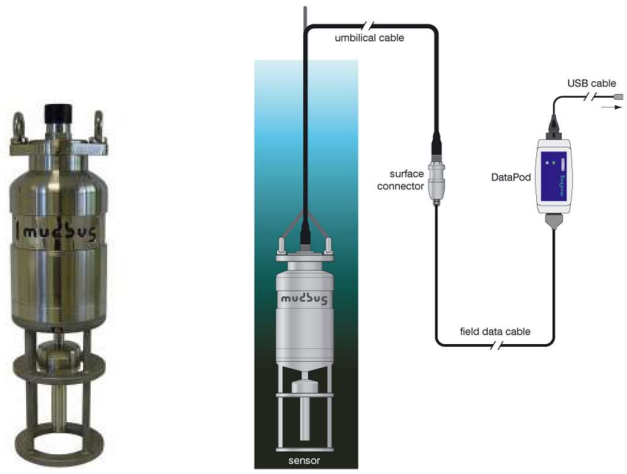

Figure 6.13 Real-time density of the slurry suspension can be determined Mugbug

The "Hydramotion Mudbug" determines the navigable depth in port and harbours by measuring the density of fluid mud. It is a "plug and play" system consisting of a rugged and towable transducer connected by an umbilical cable to DataPod connection unit to the surface. Density is measured in the range 800 to 1600 kg/m³ with an accuracy of ±1% at depths up to 100 metres. The Mudbug uses its own

pressure sensor to determine the depth of the transducer, thus allowing real-time density versus depth profiling.

The Mudbug consist a tubular structure as sensing element which can vibrate at its natural frequency. The vibration disturbs the surrounding fluids, which causes an increment in the effective mass of the tubular structure and the mass increment changes the natural frequency of the tubular structure. The changes of frequency will be converted to the density of the fluid by the built-in microprocessor.

6.5 Good earth filling

Due to the sequencing of works, the reclamation project had insufficient dredged materials to fill up the confinement facility to the design level according to the planned schedule. Good earth with high fines contents from external land sources were brought in to cover for the shortfalls in dredged seabed infill. Generally, good earth mean materials that are compactable to form a stable fill and are defined in the following two (2) categories:

(a) "Coarse-grained soil" shall include all sand and gravel that shall all pass through a 63mm BS sieve. A percentage by weight retained on the 0.063mm BS sieve shall be at least 65%. The remaining 35% passing through the 0.063mm BS sieve shall contain a liquid limit not exceeding 70% and a plasticity index not exceeding 40%. Coarse-grain soils shall exclude all forms of rock.

(b) "Fine-grain soil" shall include silt and clay that have a fraction passing a 0.063mm BS sieve of more than 35%. The fraction of particle size less than 2μm however should not be more than 80%. The liquid limit shall not exceed 60% and plasticity index not more than 30%. The moisture content of the soil shall be 40% or less.

Figure 6.13 illustrates that the location where the good earths were deposited and spread at the eastern and southern side of the confinement facility as indicated by the pink areas using land based machineries.

Figure 6.14 Good earth filling at the sides of the inner containment bund (pink)

The infilling of good earths were carried out just before the 4th cycle of dredged slurry infilling. The good earth were dumped directly by dump trucks at the side of the bund crests and re-handled by long-arm excavator and swamp excavator to spread the good earth evenly over the deposited dredged seabed surface in the confinement facility.

Figure 6.15 Filling and spreading of good earth by trucks and excavators from the sides of the inner containment bund

Table 6.9 Good earth's composition [Particle Size Analysis BS1377 – Sieve Analysis]

Composition (weight /%)	**Clay**	**Silt**	**Sand**	**Gravel**
Range [%]	25-51	26-47	2-48	0 – 1.25
Ave [%]	36.6	39.5	23.4	0.5

Table 6.10 Good earth materials' density, water content & void ratio

Parameters	**Range**	**Average**
Bulk Density, $\gamma_{bulk,}$ [kN/m^3]	14.5-16.5	15.35
Dry Density, γ_{dry} [kN/m^3]	6.5-7.4	8.4
Water Content, w [%]	58-126	86%
Void Ratio, e_0	1.59-3.12	2.27

Table 6.11 Good earth's atterberg's limit & consistency indices

Atterberg's Limit & Consistency Indices	**Range**	**Ave. Values**
Liquid Limit, LL [%]	35-56	46
Plastic Limit, PL [%]	20-23	22
Plasticity Index, I_p [%]	15-33	24
Liquidity Index, I_L	2.53-3.12	2.83
Consistency [ISO 14688]	Very Soft - Soft	Soft

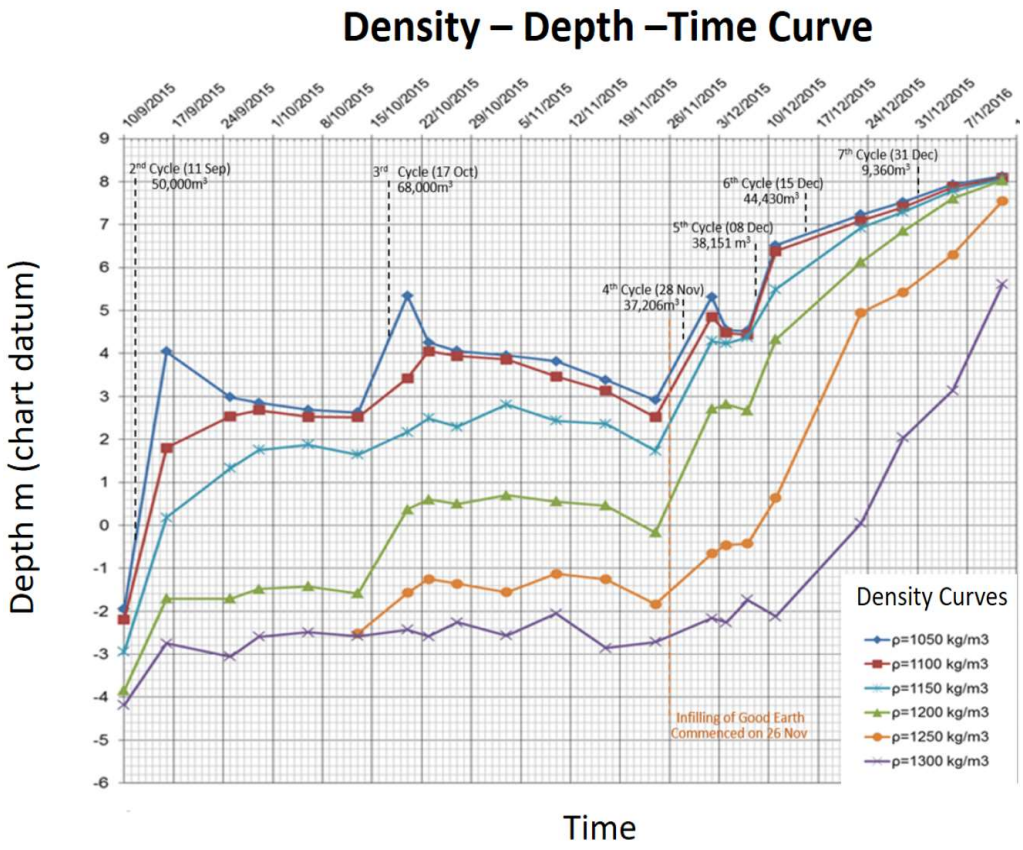

Figure 6.16 Density profiles of the slurry suspension over time

Figure 6.15. illustrates the relationship between density curves at different depths over time during the infilling operations. Prior to the good earth infilling, all the density curves raise to higher elevation after each dredged slurry infilling cycle as indicate by the sudden spikes in the density curve (1050 kg/m^3). The magnitude of rise was largest for density curve (1050kg/m^3) and smallest for density curve (1300kg/m^3). Sedimentation of the dredged slurry suspension took place after dredged slurry infilling. During this time, the density curves (1050kg/m^3) elevation would drop after a few days while the higher density curves begun to rise in elevations. This observation was attributed by the settling of the suspended soil particles from the higher elevation to the lower elevation as the water clarified.

The elevation of these higher density curves did not rise much over the 2nd and 3rd cycle of dredged slurry infilling. After the initial little rise in elevation, it was

observed that the elevations of the density curves experienced slight drops as the duration pan out longer. This was probably attributed by further settling of the suspended particles in the slurry suspension caused by the actions of gravity. From the density curve (1300 kg/m^2) it is clearly shown that it would take many cycles of dredged slurry infilling before the surface elevation could reach the designed density of 1300 kg/m^3.

The good earth infilling was continuous with no resting intervals. No drop was observed in density curves elevation after good earth infilling commenced. The density curves were slowly converging towards the surface as more good earth was deposited in the confinement facility.

After the infilling of the confinement facility was completed, the deposited slurry fill was rested for 1 month to allow the suspended solids in the dredged slurry suspension to settle and consolidate. The surface water was also drained to allow surface desiccation. Slurry samples were taken at the elevation of +6.5 mCD with a water sampler as Mudbug Survey was not possible as the slurry was too dense to allow the deployment of the pontoon to conduct the mudbug survey. Infill samples were taken at 9 locations in the trial pit as indicated in Figure 6.16. The measured density and water content of the collected samples are summarized in in Table 6.12.

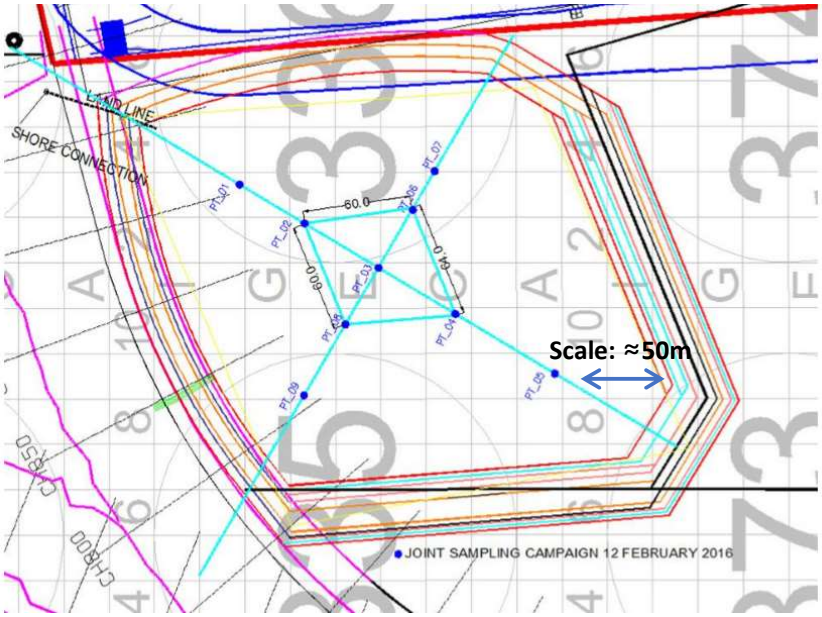

Figure 6.17 Sampling locations after infilling works were completed

Table 6.12 Soil properties of the deposited materials in the confinement facility

Soil Properties		**1**	**2**	**3**	**4**	**5**	**6**	**7**	**8**	**9**	**Average**
Bulk Density [kg/m3]		1.35	1.38	1.35	1.35	1.38	1.34	1.33	1.37	1.33	1.35
Water Content [%]		177	187	174	192	181	184	194	188	183	185
Atterberg Limit	Liquid Limit [%]	63	52	60	59	60	61	64	55	59	59
	Plastic Limit [%]	25	23	24	27	23	26	27	26	25	35
	Plasticity Index [%]	38	29	36	32	37	35	37	29	34	34

The laboratory tests show that the hydraulic dredged seabed deposits at the surface generally achieved an average bulk density of 1.35kg/m^3 and an average water content of 185%. The deposited slurry fills were generally in the liquid state with extremely low strength. Generally, the deposited infill were classified as ultra-soft cohesive soils.

6.6 Working platform design

Contractor was to construct a load bearing working platform over the soft deposits after the infilling of the confinement facility to the design level was completed. The working platform was designed to provide adequate shear strength and stability to

withstand a uniform load of 25kPa to allow access, trafficability and carry out other construction activities above the deposited infill. Figure 6.17 shows the aerial view of the confinement facility after infilling works were completed.

Figure 6.18 Aerial view of the confinement facility after infilling works were completed

6.6.1 Contract stipulated design

The contractor is to construct the load bearing working platform in 3 stages. In stage 1, contractor is to install short PVDs of approximately 8m long at interval at 1.5m spacing into the soft deposits as illustrated in Figure 6.18. This is to help the soft deposits at the top layer to gain effective shear strength by accelerating self-weight consolidation by reducing the drainage path through the installation of short PVDs for pore pressure dissipation.

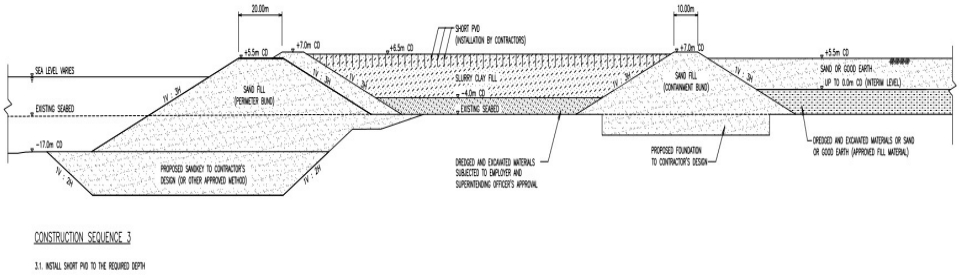

Figure 6.19 Contract stipulated design scheme for load bearing working platform

In stage 2, the surface water over the soft deposits was supposed to be drained out to allow sun drying to form a layer of desiccated crust on surface of soft deposit. Desiccation cracks were observed mainly along the sides of the inner containment bund where the surface water could be drained out (see Figure 6.19) and the infilling of dry good earth also helped in migrating the water in the slurry to the dry earth. Surface desiccation was not observed on soft deposits located at the centre of the confinement facility where water could not be drained properly due to its lower elevation as shown in Figure 6.19. Visual inspections showed that “cracks” were developed at the side over time as desiccation took place. It was also observed that the initial desiccated flat surface warped slighted turning into slightly concave plates.

Figure 6.20 Development of the surface desiccation over time at the side of the containment bund and water ponding at the centre surface of the confinement facility

The effects of desiccation were observed to be limited to the surface depths in the soft deposits. Generally, sun drying produced about 5-15 centimetres hardened crust layer. The soft deposits underneath the desiccated crust layer remained largely slurry like with little or no strength when penetrated. Shallow trenching was proposed to extend the effects of surface desiccation deeper by dragging cutting tools across the soft deposit surface as illustrated in Figure 6.20.

Figure 6.21 Forming shallow trenches across the surface of the desiccated surface layer

The purpose of the proposed shallow trenching is to extend the surface desiccation deeper into the soft deposits while allowing the mixing of the desiccated material with “wetter” deposits to induce further drying of the surface materials to achieve higher strength on the surface materials. However, after several trials, the incremental improvement to the surface materials were found to be very limited. When the shallow trenching was carried out on the wetter surface the newly dug trenches closed up almost instantly.

6.7 Construction of working platform

A layer of geofabric was used to overlay the soft deposit to serve as reinforcement before the placement of 1.5m of sand. The purpose of the geotextiles was to provide the necessary tensile strength and act as the reinforcement layer to support the placement of the sand layer in stages. The geotextiles layer was designed to be

secured at the side edges of the confinement facility as illustrated in the schematic diagram in Figure 6.21.

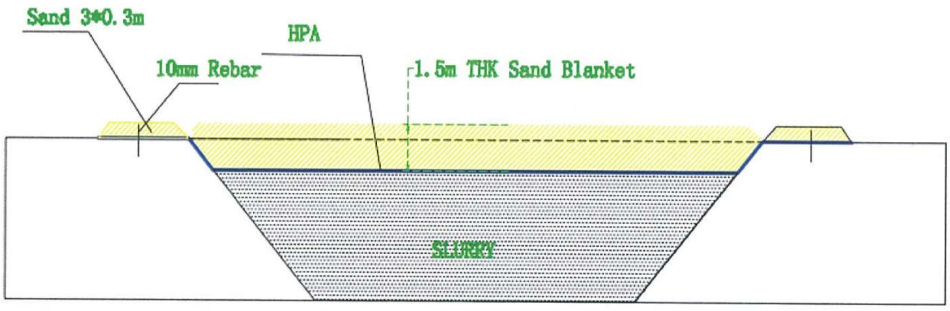

Figure 6.22 Schematic diagram of the contractor's alternative working platform design using geosynthetics

The geotextiles was designed to served multiple functions. As a reinforcing layer, the geotextiles were designed to provide the tensile strength, redistribute loads and to reduce excessive sinking and heaving of the soft deposits during placement of the sand layer. The geotextiles also functioned as a separator to segregate the soft deposits from the sand to prevent them from mixing together. The permeable geotextiles also allowed the dissipation of the pore pressure in the soft deposits during sand placement.

TenCate's Mifra Hpa 380 was selected as the reinforcement as they were woven geotextiles that combined all the critical performance functions such as separation, reinforcement, confinement and permeability. It was made of super high-tenacity polypropylene yarns formed into woven structure with high initial tensile stiffness modulus and high seaming efficiency. The super high tenacity polypropylene yarns allowed the mobilisation of tensile resistance for reinforcement benefits at low working strains of 2%. The material specification of Mirafi HPa 380 are summarized in Table 6.13.

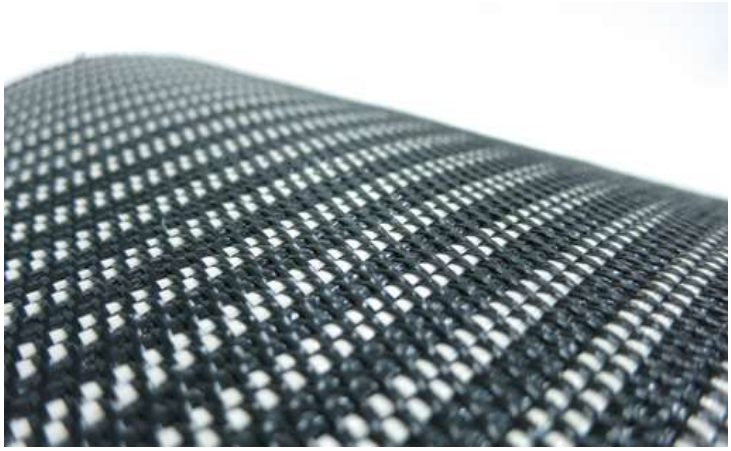

Figure 6.23 Woven fabric details of Mirafi HPa 380A

Table 6.13 Materials specifications of Mirafi HPa 380

S/N	Geotextiles properties	Direction	Value	Unit
1	Tensile modulus @ 2% strain	MD	700	kN/m
2	Tensile modulus @ 2% strain	CD	800	kN/m
3	Wide width tensile strength	MD	65	kN/m
4	Wide width tensile strength	CD	45	kN/m
5	Elongation at break	MD	12	%
6	Elongation at break	CD	10	%
7	CBR puncture strength		6	kN
8	UV resistance (at 500 hrs)		90	% retained
9	Pore size, O90		0.3	mm
10	Water Permeability, Q50		2000	$l/m^2/min$

6.7.1 Joining of geotextiles

Prior to the placing of the Mirafi HPa 380, surface water in the confinement facility was drained out to allow the soft deposits surface to be desiccated to help the laying of geotextiles. The geotextiles were hand-sewn together to cover the surface of the

soft deposits. The sewing of the geotextiles took place at the side of the confinement facility using a hand-held sewing machine with double stitches at an 150mm overlap as illustrated in Figure 6.23.

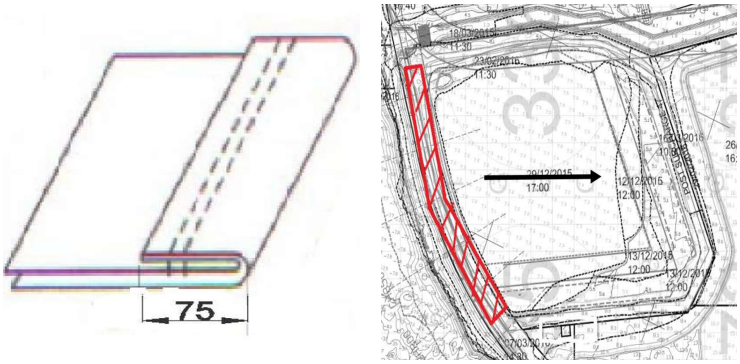

Figure 6.24 Sewing of geotextiles with double stiches at the side of the confinement facility

6.7.2 Pulling of geotextiles

The Contractor planned to pull the sewn geofabric slowly over the dredged slurry surface using 5 winches at the opposite end of the confinement facility. All 5 winches were installed onto concrete blocks and were anchored into the ground as shown in Figure 6.24. To pull the geotextiles, the pulling wire from each winch was connected to the bridle which were tied and secured onto the geotextiles. During the initial pulling attempts, the winches broke down and the bridles were dislodged several times. The unevenly distributed stresses caused by these failures resulted in damages and tearing of the geotextiles.

Figure 6.25 Typical installed winch used for the pulling of geotextiles

The contractor made three improvements to their initial methodology in laying the geotextiles. Firstly, the pulling of the geotextiles by the 5 winches were replaced with more reliable machines such as bulldozers and excavators. The pulling points were also increased from 5 points to 10 points to further re-distributed the forces applied on the geotextiles. Figure 6.25 illustrates the revised geotextiles pulling scheme. The black boxes represent the starting position of the bulldozers and excavators each approximately 25m apart. The red boxes indicate the ending position of the pulling operations for the bulldozers/excavators which was approximately 120m away from the starting position. After pulling, the machineries would return to the starting position at the black boxes to prepare for the next pulling.

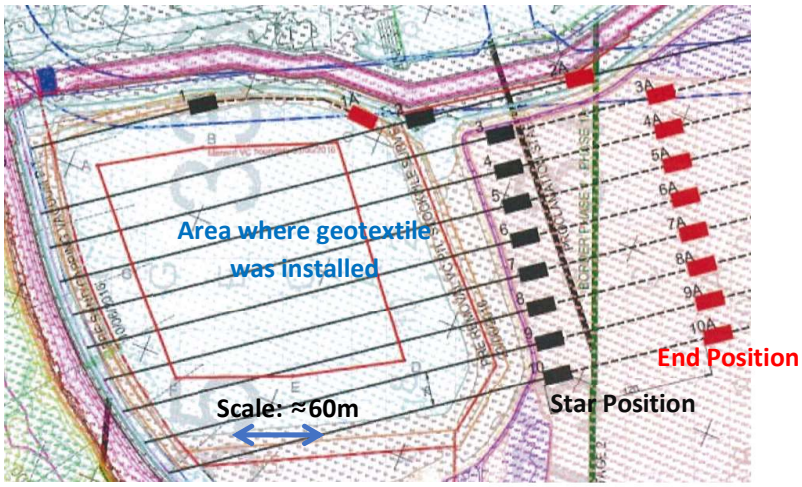

Figure 6.26 Revised geotextile pulling scheme showing starting and ending positions

The objective of the second improvement is to reduce the stress applied onto the geotextiles by the pulling wire. Steel pipes measuring 5.6m in length and 0.275m in diameter were deployed to help spread out the pulling stress along its entire length as illustrates in Figure 6.26. Two customized pad eyes were welded onto each steel pile to allow the securing of the pulling wire. The geotextiles at the edges were then cut, wrapped and then hand sewn around the steel pipes leaving a gap for the pad eyes to protrude out to allow the securing of the pulling wire onto the pad eyes as shown in Figure 6.27. Thirdly, a second line of pulling steel pipes were also installed for the purpose to distribute the increasing resistance when the geotextiles were pulled half way across the confinement facility.

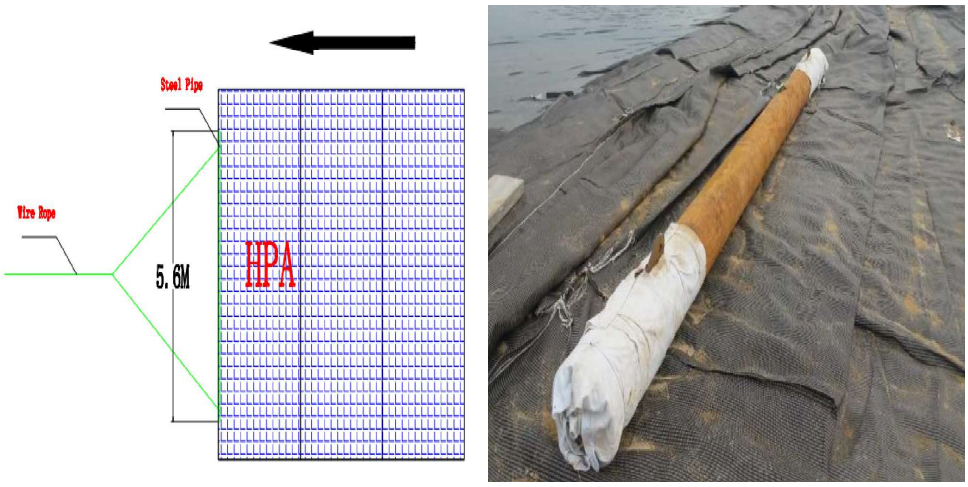

Figure 6.27 Steel pipes installation used to reduce the pulling stress acting on the geotextiles

Figure 6.28 Details of the welded eye pad onto the steel pipe

Despite the above modifications, tearing and damages on the geotextiles continued to occur at multiple areas during the pulling operations. The damages were caused by the high drag forces induced at the interface between the geotextiles and semi-desiccated deposits. The pulling operations were stopped many times to facilitate repair works on the damaged geotextiles. On the hindsight, these damages to the geotextiles can be significantly reduced if water was not drained away and maintained at an appropriate level in the confinement facility to reduce frictions of the pulling operations. The pulling of the HPA380 should also be carried out in the machine direction instead of the cross-machine direction to prevent the geotextiles at ripping apart at the joints.

The geotextiles were placed over the soft deposits eventually. The geotextiles were stretched out as far as possible mechanically and pulled up to the crest of the perimeter bund and anchored into position with 10 mm rebars at regular spacing. Thereafter a 300 mm thick sand cover was placed over the geotextiles to secured it in position as shown in Figure 6.28.

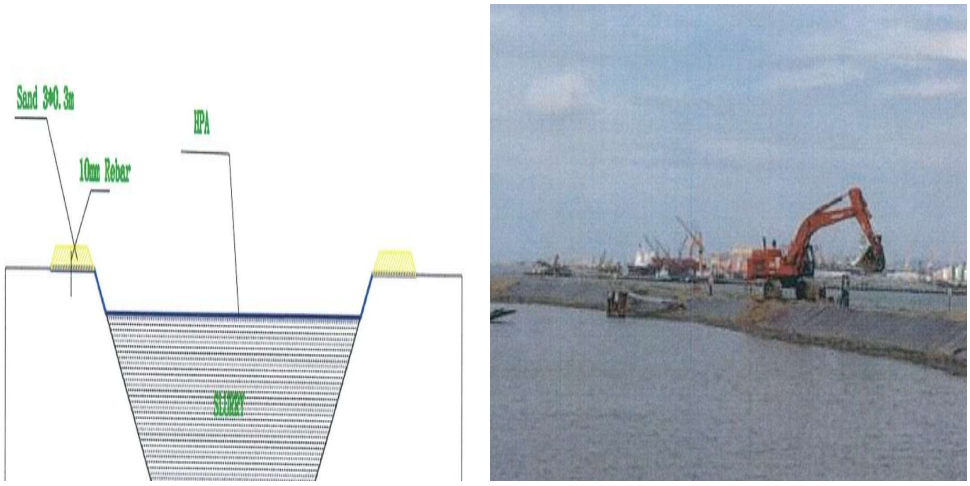

Figure 6.29 Installed geotextiles secured into position with rebars and sand berms

6.7.3 Sand placement over geotextiles

After the placement of geotextile was completed, 1.5 m the sand was placed in 3 layers over the geotextiles, at 0.5 m per layer as illustrated in Figure 6.29. The initial sand placement began at the side of the containment bund and was spread 15 m inwards using long arm excavators as shown in Figure 6.30.

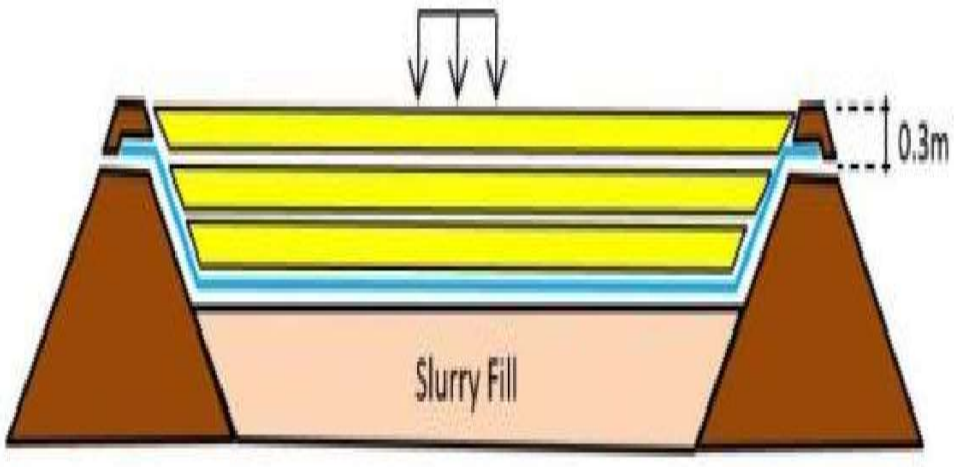

Figure 6.30 Cross section of the confinement facility with geotextiles-sand working platform

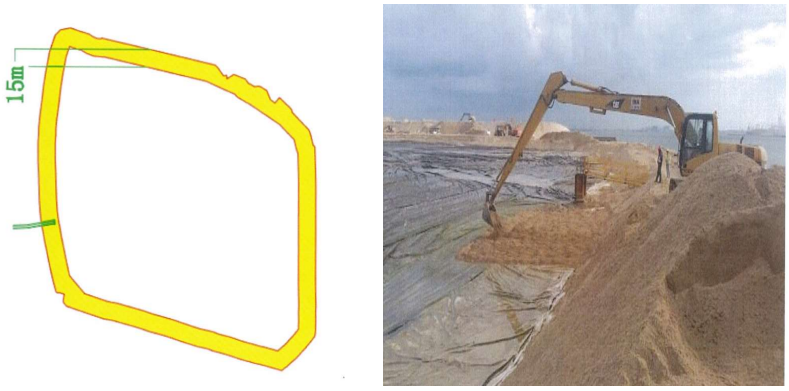

Figure 6.31 Initial sand placement from the sides of containment bund

6.7.4 Hydraulic sand placement over geotextiles

Hydraulic sand placement at 0.5m lift was adopted to limit excessive deformation of the underlying soft deposits. Figure 6.31 shows the schematic cross section of the sand re-handle pit that was constructed next to the confinement facility. Sand was fluidised with sea water in the re-handle by using jet pumps. The mixture was then pumped out of the re-handle pit using a 90kw high pressure water pump and transported hydraulically via the transmission steel pipes and into the confinement facility. In the confinement facility, the mixture was branch out to several discharge points and connected by small flexible hoses to spread and redistribute the sand mixtures over the geotextiles. The contractor will proceed to the next layer of sand placement after the current placement has reached its target height level.

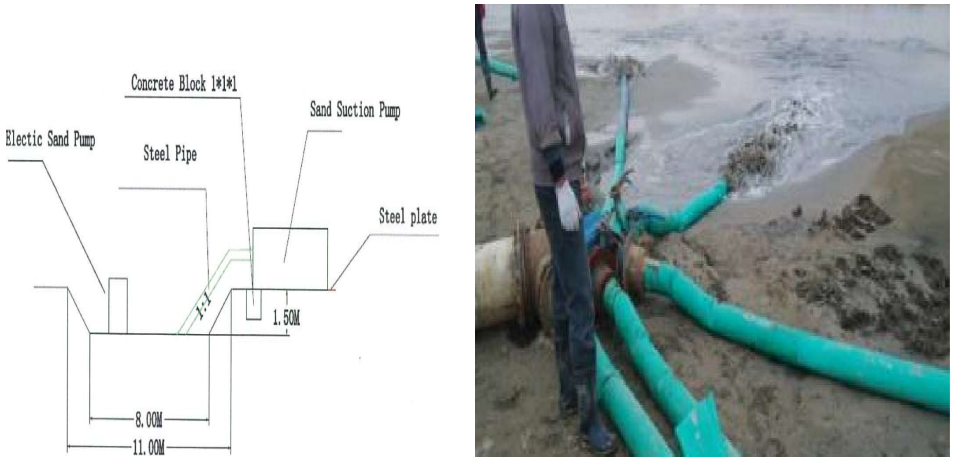

Figure 6.32 Schematic diagram of the re-handle pit and hydraulic sand discharge point

It was observed that the hydraulic placed sand was unable to spread evenly across the geotextiles surface as the installed geotextiles were not in tension. The weight of the sand coupled with the loose and relaxed geotextiles surface led to the formation of depressions on the geotextiles surface. The sand began to accumulate on these depressions through the action of gravity and water flow. The accumulated sand weighted down on the geotextiles and formed geotextiles pockets that sunk into the soft deposits. As the geotextiles pockets grew bigger, the deformation induced higher stresses on the stitched joints of the geotextiles. If the geotextiles pocket was allowed to grow, the stitched joints would be ripped apart due to increased stresses induced by the growing geotextiles pockets.

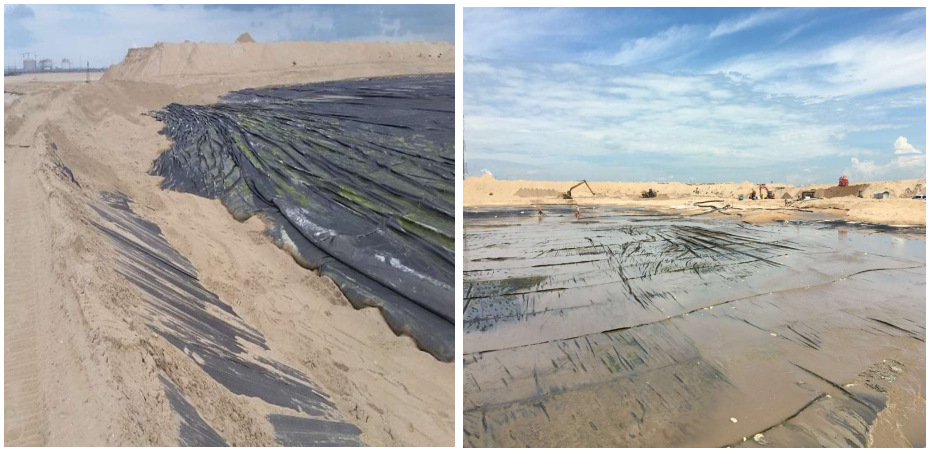

Figure 6.33 Placed geotextiles not in tension

Figure 6.34 Geotextiles pockets containing sand

The formation of geotextiles pockets continued to be observed despite multiple attempts to change the configurations of hydraulic filling to achieve more even sand spreading. The key factors that probably contributed to the formation of the geotextiles pockets are summarized:

i. Anchoring of geotextiles at the sides of the confining facility was not enough to activate the required tension of the placed geotextiles due to its large installed area.
ii. As most of soft deposits were still in slurry-paste like form, the soil-geosynthetics interface were not able to provide enough frictional resistance to prevent the formation of the geotextiles pockets
iii. Difficulty in controlling and directing the sand placement when high energy hydraulic sand placement was adopted

It was therefore concluded that the hydraulic sand placement is not suitable over the loosely installed geotextiles over the soft deposits with zero shear strength and resistance.

6.8 Use of geotubes to form working platform

6.8.1 Working principle

As proposed by Broms (1981) finger berms as illustrated in Figure 2.32 and Figure 2.33 can be placed over geotextiles to mobilise tensile stress to stretch and stabilise the reinforcing geotextiles to support the construction of the working platform. However, it was technically impossible to form the finger berms using sand as the placed sand would have collapsed from the deformation of the geotextiles. As such, geotubes were proposed to form the berms as they offered confinement for its infilled materials which made berm placement possible. The geotubes were placed at regular intervals to stretch the geotextiles sufficiently to form a firm supporting platform that allowed dry sand placement.

Figure 6.34 illustrated the placement of the geotubes on geotextiles and the subsequent placement of sand in layers to form a working platform. When the geotubes were placed, they sank and pushed the underlying geotextiles into the soft deposits displacing the materials vertically and laterally as illustrated in Figure 6.35. This led to the heaving of the geotextiles adjacent to the geotubes. When a new geotube was placed adjacently at the fixed interval, its weight will be pressed against the heaved geotextiles causing new deformations. This pattern will continue as geotubes were placed side by side at fixed distance apart. The sinking and heaving deformation of the geotextiles caused by the placement of geotubes would activated the tensions in the geotextiles. This actions provided the stabilising and reinforcement effect on the geotextiles to form a stable platform over the soft deposits for dry sand placement.

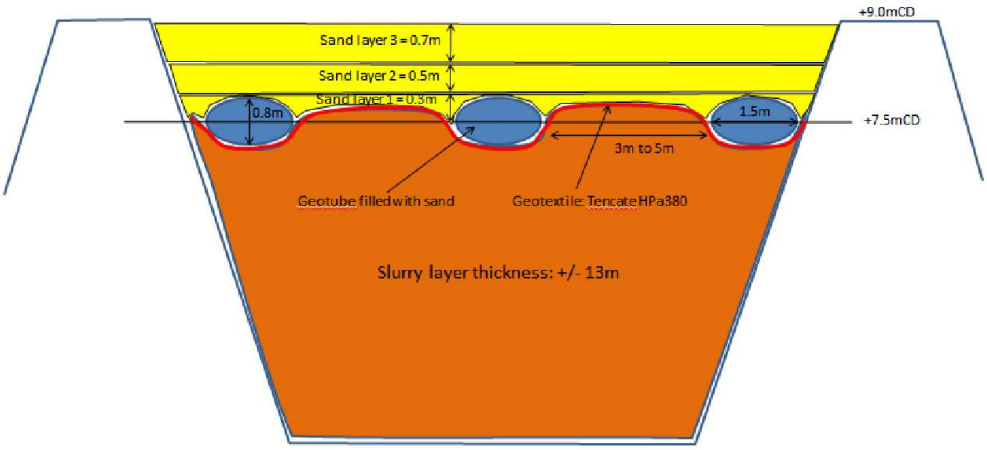

Figure 6.35 Placement of geotubes caused deformation and tension in the geotextiles

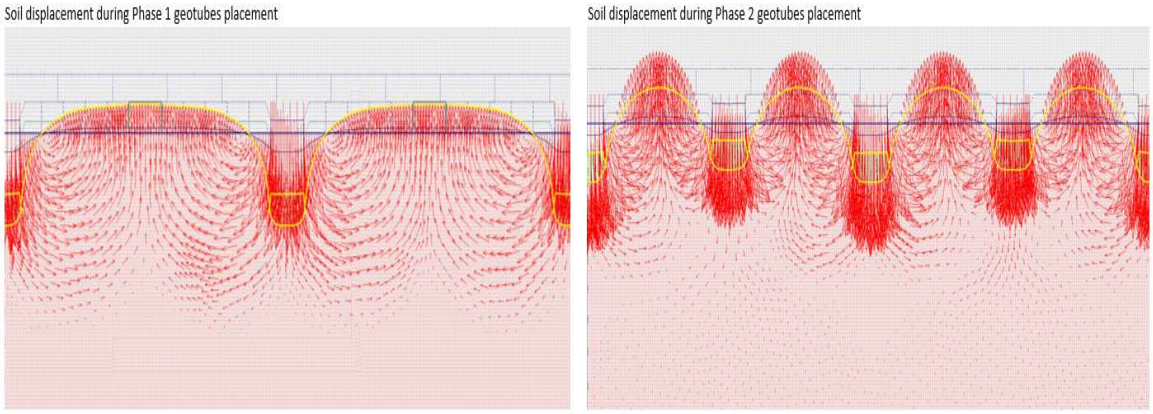

Figure 6.36 Arrows indicating directions of displaced soft soils underneath the geotextiles as a result of geotubes placement

6.8.2 Geotubes preparation

The geotubes were made from geotextiles by sewing them into long bags measuring 2.5 m in width and 15 to 30 m in length. The empty geotubes were carried by workers and placed into position in the confinement facility manually by workers as illustrated in Figure 6.36.

Figure 6.37 Geotube preparation and placement over geotextiles

The empty geotubes were laid in perpendicular direction across the underlying geotextiles joining seams. Once the geotube bags were in position, the sand discharge hose would be inserted into the geotube. Fluidised sand was then pumped into the

geotubes hydraulically. Water was filtered out from the geotubes as the hydraulic filling continued and only sand was retained in the geotubes. The sand will fill up the geotubes eventually and the sequence were repeated on other geotubes as illustrated in Figure 6.37.

Figure 6.38 Sequence of filling up geotubes using sand

6.8.3 Geotubes placement

The geotubes were placed in two stages. In stage 1, the geotubes were placed at 10m spacing. After the placement of stage 1 geotubes was completed, the contractor proceeded to stage 2 where the new geotubes were placed inbetween the previously placed geotubes. This created closer spacing between adjacent geotubes at 5m spacing as illustrated in Figure 6.38. It can be observed that after the placement of the stage 2 geotubes, the geotextiles surface was further stretched creating tighter and more stable surface for the dry placement of sand.

Figure 6.39 shows the Plaxis 2D analysis on the axial forces developed in the geotextiles for both stages of geotubes placement. The axial forces are represented in this graph are all in tensions as geotextiles cannot take compressive forces. It was observed that the tension forces caused by the geotubes self-weight were greater than the tensions caused by the heaving actions of the displaced soil. The axial forces developed on the reinforcing geotextiles by the geotubes self-weight were represented by the protruded lines of columns in the Axial forces diagrams. Figure

6.39 illustrates that the 2nd stage placement shows higher axial forces developed in the geotextiles as more geotubes were placed. Figure 6.40 shows the site photos of the tension on the geotextiles in both stages of geotextiles placement.

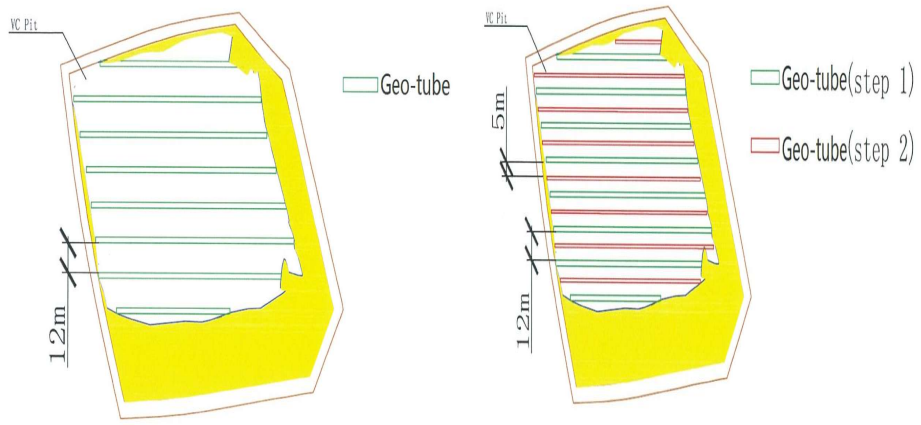

Figure 6.39 Placement sequence of geotube over the installed geotextiles

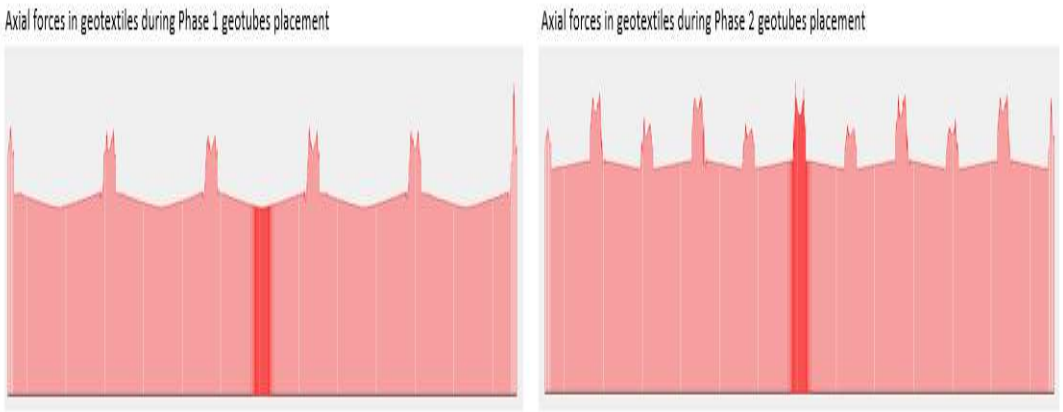

Figure 6.40 Plaxis 2D showing axial forces developed in geotextiles during geotubes placement

Figure 6.41 Two stage geotube placement at 12m and 5m spacing in stage 1 & 2 respectively

6.8.4 Sand placement by dry filling

After the geotubes were installed, 300mm thick sand were placed perpendicularly across the geotubes spacing as shown in Figure 6.41. After sand placement, two layers of plywood were placed on top of the placed sand to prevent damaging the underlying geotextiles and to allow access of heavier plants and equipment. The spacing between each temporary path formed by the placed sand were about 8m apart. After completion, the installed geotubes and the placed sand formed a rectangular grid as illustrated in Figure 6.42. Beside distributing the load evenly on the supporting geotextiles, the rectangle grid also doubled up as access for the transporting and placement of the first layer of sand. The laying of the first layer sand was smooth and successful as shown in Figure 6.43.

Figure 6.42 Photo showing dry sand placement across geotubes with light equipment

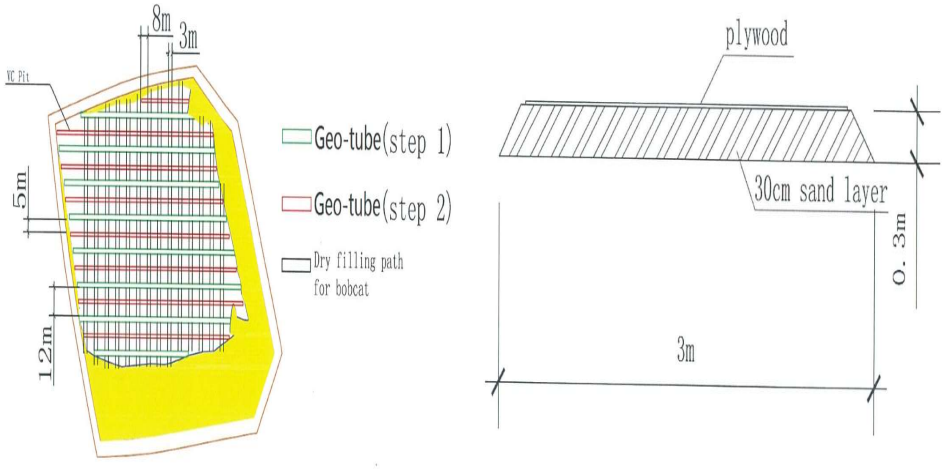

Figure 6.43 Rectangle grid over geotextiles formed by geotubes and 300mm of dry fill sand

6.8.5 Failure of the working platform

The placement of the second sand layer proceeded after the first layer was completed. Just before the completion of the second sand layer, seepage of slurry fill over the placed sand was observed. The slurry covered an area of about 964m^2 and was contained by forming a small sand containment bund as shown in Figure 6.44. Geotextiles was used to cover the area where the rupture was believed to be located to prevent further slurry outflow. On the second day, it was observed that the slurry

outflow has stopped and stabilised. The dry filling of the second sand layer continued from about 100m where the the slurry pool was located.

Figure 6.44 Photo showing completed placement for the first layer of sand

Figure 6.45 Photo showing containment of the slurry seepage from day 1 using sand bund

On the third day, it was reported that the slurry pool was enlarged by nearly four times covering a surface area of about 3622m^2. Sand placement was stopped immediately and containment bund was installed around the slurry pool to contain the slurry seepage.

Figure 6.46 Photo showing enlargement of the slurry coverage on day 2

On the fourth day, the slurry outflow appeared to be stabilised. No work was carried out to allow further monitoring of the slurry outflow. On the fifth day, the slurry area had extended its coverage significantly overnight and covered an area measuring 19,850m^2. The previously geofabric installed in day to remedy the ruptured area in day 1 was pushed out to another location in the expanded slurry pond. Sand containment bund surrounding the outflow slurry pool was raised to prevent the slurry pool from further enlarging. Air bubble was observed to escape slurry pond at several locations. No further extension of the outflow slurry was observed thereafter.

Figure 6.47 Photo showing the extend of the coverage of the slurry seepage on day 4

6.9 Investigation of the bursting of mud incident

Investigations were carried out to identify the key causes for the outflow of the slurry beneath the working platform. The development and coverage of the slurry seepage over the 5 days were plotted over the aerial map as illustrated in Figure 6.47 to assist in the investigate.

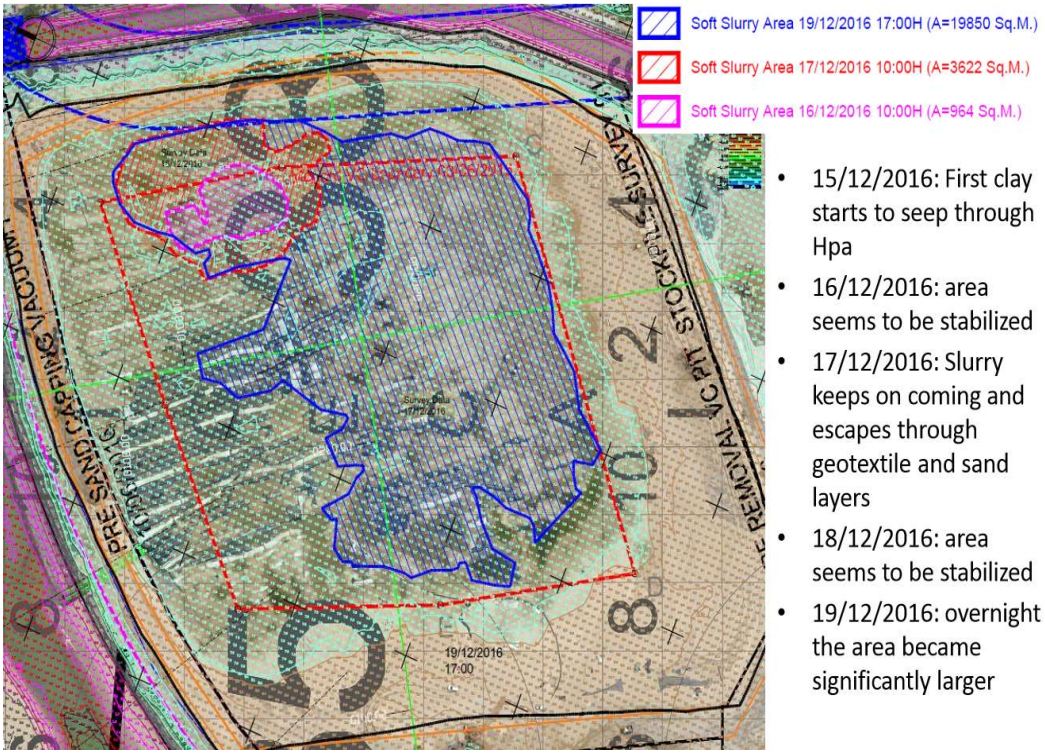

Figure 6.48 Aerial view showing the development of the slurry seepage over time

Based on the collated information, the slurry seepage was probably caused by the tearing of the underlying geotextiles joining seams as a result of the stresses built up in the geotextiles due to uneven sand placement. This caused large deformation and uneven stress distribution in the geotextiles. As illustrated in Figure 6.48, the uneven sand placement was the result of contractor fast forwarding the placement of the third sand layer before the completion of second sand layer 2.

It was believed that multiple ruptures could have occurred at the geotextiles weak spots. These weak spots include (i) the damaged geotextiles areas during its installation and were not properly repaired and remedied and (ii) failure at the joining seams after a prolong exposure to sun and (iii) multiple stressing due to earlier failed attempts to pull and place the geotextiles over the soft deposits.

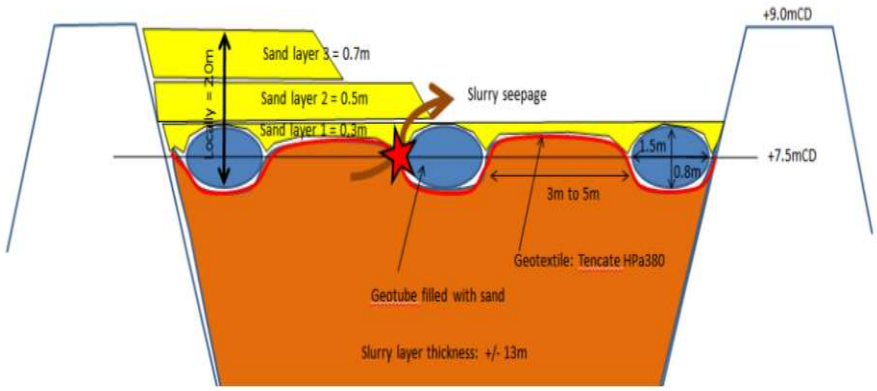

Figure 6.49 Accelerating the placement of the third layer of sand could have resulted in large deformation and stress build up in the geotextiles leading to its failure

The weight of the geotubes and the placed sand layers over the geotextiles had caused the geotextiles to sink, squeezing out the slurry previously underneath the geotextiles in the process from the ruptured and torned areas of the geotextiles. Surveys were carried out to determine the profile of the sank geotubes and geotextiles. These were carried out manually by pushing down a pole into the slurry pool until the bottom tip of the pole reached the surface of the sunk geotextiles or geotubes as indicated in Figure 6.49. When the pole could not be pushed further down by the survey assistant, the depth of the inserted pole depth will be recorded by the surveyor. Figure 6.50 shows the the cross section profile of the slurry pool where the depth of the sunken geotubes and geotextile ranges between 1.5 to 8.5 m deep from the surface of the slurry pool.

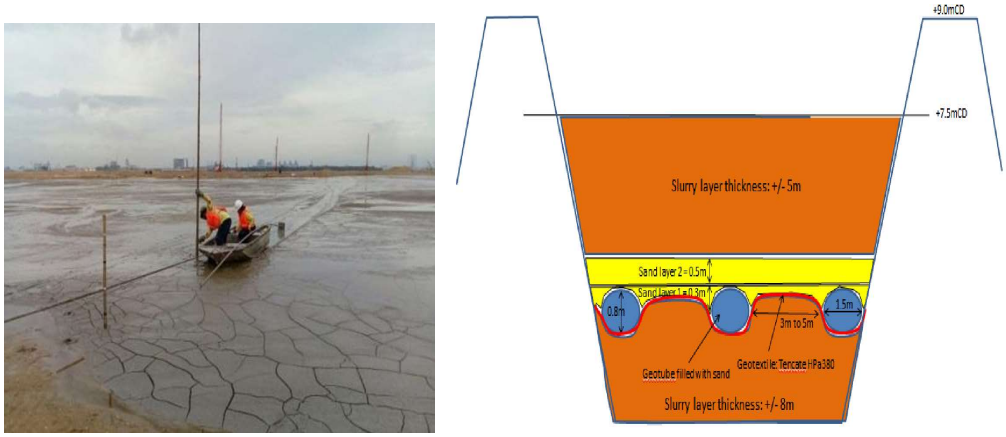

Figure 6.50 Survey to determine depth of the sunken of the geotextiles

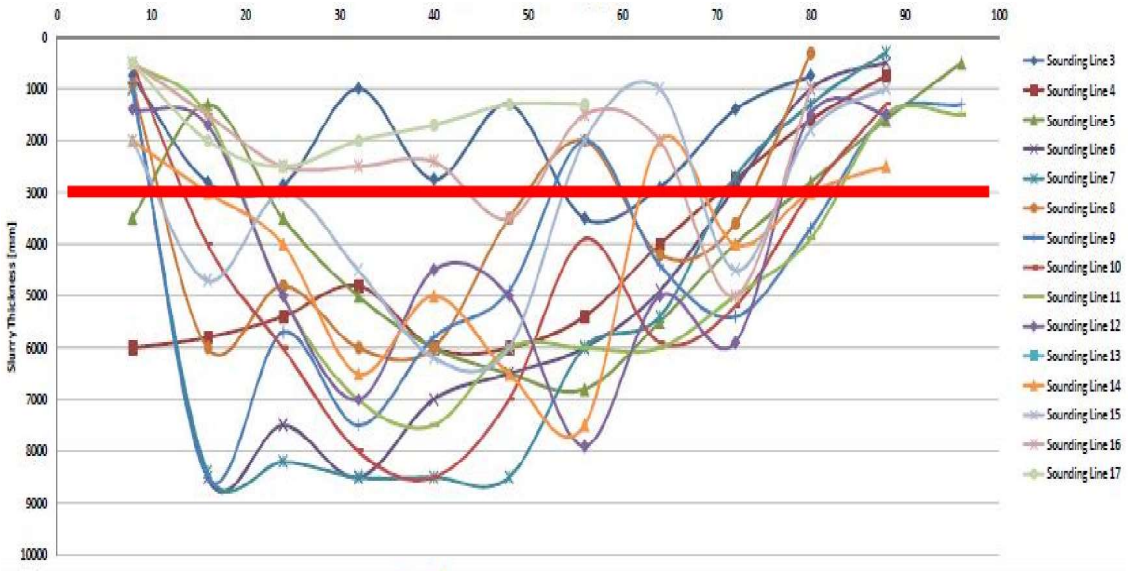

Figure 6.51 Cross sectional profiles of the sunken geotextiles-sand working platform

6.10 Conclusion

This chapter presents a pilot field trial comprising the design, construction and infilling of a confinement facility with dredged seabed material and fine-grained excavated earth materials. This chapter also elaborates the site challenges in the construction of a load bearing working platform over the soft deposits. The conclusions arrived for this pilot field are as follows:

i. Two proposals for the construction of the confinement facility were presented. The contractor's alternative design of using stiff marine clay to replace part of the sand for inner containment bund construction had resulted in huge savings in sand and the use of dredged materials was maximized in a reclamation project. However, it shall also be pointed out that longer time was taken to complete the confinement facility due to the untimely supply of stiff marine clay and slower construction process.

ii. Hydraulic dredging and infilling was more efficient and cost-effective to handle large quantities of dredged seabed materials. Hydramotion Mudbug was deployed to determine the real-time status of the sedimentation process by measuring the densities of the infilled slurry at different depths. The Hydramotion mudbug has provided important information to shorten the waiting intervals between hydraulic infilling cycles of dredged seabed. Observation on the change in the density curves of the infilled slurry over time and depth is also presented in this chapter.

iii. Formation of a desiccation layer and the use of shallow trenching to extend the depth of the desiccation layer on top of slurry deposits are found to be unproductive unless proper drainage could be provided at the areas with lower elevation

iv. Two methods were tried out to form a load bearing platform. The first method was to place sand hydraulically at 0.5 m thick per layer using pump. This method created considerable uneven distribution of the sand layer and damages to the geotextiles. The second method was to adopt a method similar to that proposed by Broms using sand filled geotubes to formed a stable platform for sand placement. This method appears to be better initially. However, a rupture of geotextile occurred as a result of contractor's actions to fast forward the sand placement resulting the bursting of the geotextiles and overflowing of slurry to the surface covering more than half the surface of the confinement facility as shown

in Figure 6.51. In other words, the proposed methods of using geotexiles to support the load working platform was assessed to be unsuitable, risky and inadequate resulting in costly remedy works. Better and more efficient methods shall be developed to form a stable load working platform to overcome these challenges.

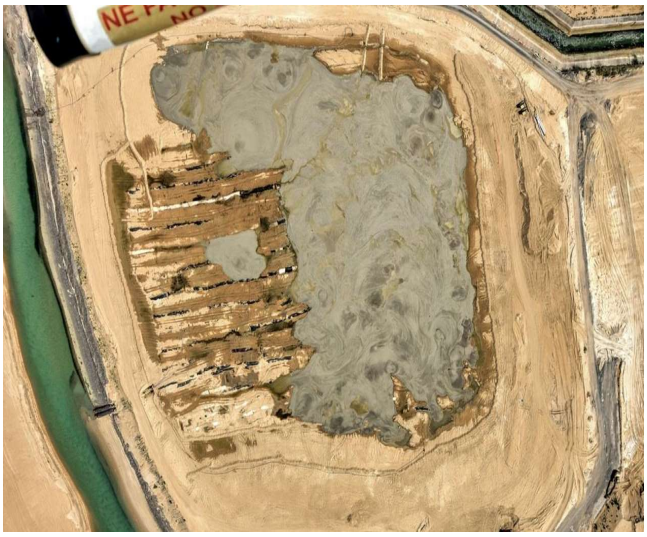

Figure 6.52 Aerial view of the coverage of the slurry from the working platform failure

CHAPTER 7 IMPROVEMENT OF SOFT DREDGED MATERIALS USING HORIZONTAL DRAINS AND VACUUM PRELOADING

7.1 Introduction

The pilot test demonstrated that it was challenging to form a working platform on top of clay slurry. To overcome the difficulties associated faced in the pilot test, an innovative soil improvement method using vacuum preloading with horizontal drains is proposed when hydraulically dredged materials is used as land reclamation infill. The proposed soil improvement method involves the placement of horizontal drains in layers after each hydraulic filling cycle to form a network of horizontal drainage paths. Vacuum can be applied to the horizontal drains when the dredged materials infilling is taking place concurrently (1) to accelerate the sedimentation process in the suspension surrounding the horizontal drains to shorten the waiting interval between infill cycles and (2) to consolidate the sediments to form denser sediments with higher undrained shear strength and (3) to allow more infill materials to be placed in the confinement facility.

To verify the effectiveness of this new proposed method, two laboratory model tests using an open rectangular consolidation tank were carried out. A single or doubled-layered prefabricated horizontal drains were used to consolidate the clay slurry placed in the open consolidation tank. Numerical analyses using Plaxis 2D were also carried out to examine the effects of treating the soft deposit in layers to form a safe working platform to support future construction activities.

7.2 Proposed innovative soil improvement methods - Vacuum preloading with prefabricated horizontal drains

7.2.1 Proposed innovative soil improvement method

The proposed innovative soil improvement method is designed to overcome the site challenges when hydraulic dredged slurry is used as reclamation fill. The method

consists of laying prefabricated drains horizontally in the dredged slurry after each hydraulic infilling cycle as illustrated Figure 7.1.

Vacuum is applied onto the horizontal drains embedded in the dredged slurry to expedite sedimentation and consolidation of sediments. The horizontal drains can be laid within the confinement facility using a customised installation pontoon or barge. Weights can be attached to the horizontal drains to help them stay submerge and in position when placed over the slurry deposits. Each horizontal drain is extended by a plastic tubing to transfer vacuum from the vacuum pump located on land. The purpose and connection between the plastic tubing is similar to the membranless vacuum preload system described in Chapter 5. Vacuum can be applied when sufficient dredged materials are placed to cover the horizontal drains,.

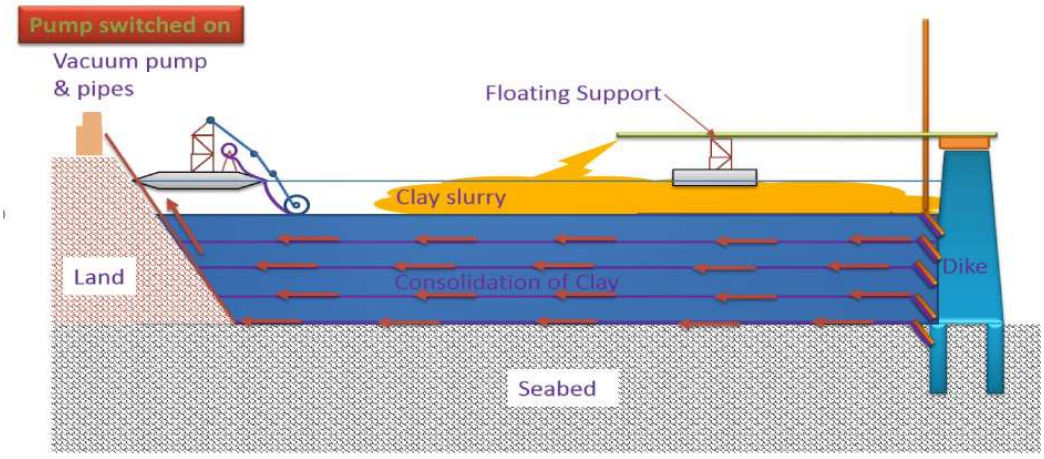

Figure 7.1 Prefabricated horizontal drains laid at different depths after each infilling to improve the deposited dredged slurry via vacuum preloading

When the vacuum suction is first applied, the vacuum transmitted to the prefabricated horizontal drains help expedited the sedimentation process as water is being drained away form the dredged slurry. Over time, the slurry suspension surrounding the horizontal drain becomes a thick paste with high solid sediments content. The sediment paste will gradually become more solid as more excess pore water is dissipated by the vacuum. As the sediment paste consolidate with time, the water

content in the sediment paste will reduce resulting gain in effective stress and undrain shear strength. As the vacuum suction continues, the consolidating sediments layer will develop sufficient undrained shear strength and bearing capacity to support load and allow works to be carried out above them.

7.2.2 Key benefits of the proposed method

The proposed vacuum preloading with horizontal drains soil improvement method has several advantage and benefits over existing methods in treating dredged slurry infill. These include:

i. Time savings

   It does not require the confinement facility to be fully filled with dredged material nor does it need a stable load bearing land platform over the slurry deposit to allow its installation and consolidation of clay. Dredged slurry infilling can be carried out immediately after the first layer of horizontal drains are installed. Vacuum preloading can start as soon as the horizontal drains are properly installed with sufficient dredged material cover. Finally, the vacuum pressure transmitted by the horizontal drains can help accelerate the sedimentation process, shortening the waiting interval between each infilling cycle.

ii. Increase storage capacity for infill cycle

   The vacuum transmitted via the horizontal drain will help to dewater the dredged slurry causing huge reduction in its infilled volume as water is being removed. This water volume reduction will free up more storage capacity for the next infilling cycle.

iii. Reduce settlement

   After dewatering, consolidation of the dredged deposits will occur as vacuum suction continue to be transmitted via the horizontal drains. This would lead to denser dredged materials being deposited in the confinement facility. As

such, less settlement is expected along with less compensation fill needed in future soil improvement works.

iv. Higher undrained shear strength

The deposited dredged materials can be pre-treated to reasonable undrained shear strength to provide better stability required to facilitate the construction of the load bearing working platform to allow works to be carried out over the deposited materials.

7.3 Laboratory model tests

Two sets of laboratory model tests using (a) Single horizontal drain and (b) double layered horizontal drains, were conducted in a consolidation tank to study the effectiveness of the proposed vacuum preloading with horizontal drains.

7.3.1 Marine clay samples

Dredged marine clay was used for the laboratory model tests. To simulate the actual dredged slurry properties that were placed in the confinement facility by hydraulic infilling, 1260kg of water is mixed with 900kg of dredged marine clay samples to achieve a water content of 140%. The properties of the marine clay sample are summarised in Table 7.1.

Table 7.1 Physical characteristics of marine clay samples used for model tests

Physical Properties	**Clay Samples**
Specific Gravity	2.63
Liquid Limit, LL (%)	76
Plastic Limit, PL (%)	2
Plasticity Index, PI (%)	44
Fines Content (%)	100
Soil Classification	MH, Clayey Silt

Grain size distribution of the marine clay samples plotted in Figure 7.2 was determined using wet sieving and hydrometer tests. Odemeter tests were conducted to determine the Compression Indices (C_c & C_r) and permeability of the clay samples as illustrated in the plotted graphes in Figure 7.3 and Figure 7.4 respectively.

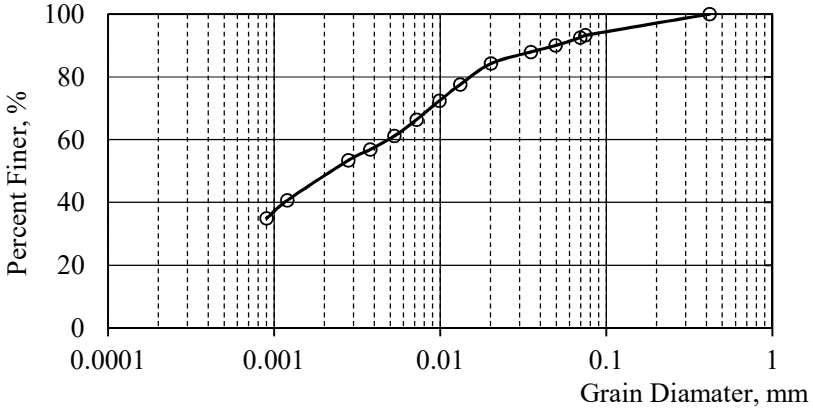

Figure 7.2 Grain size distribution of marine clay samples

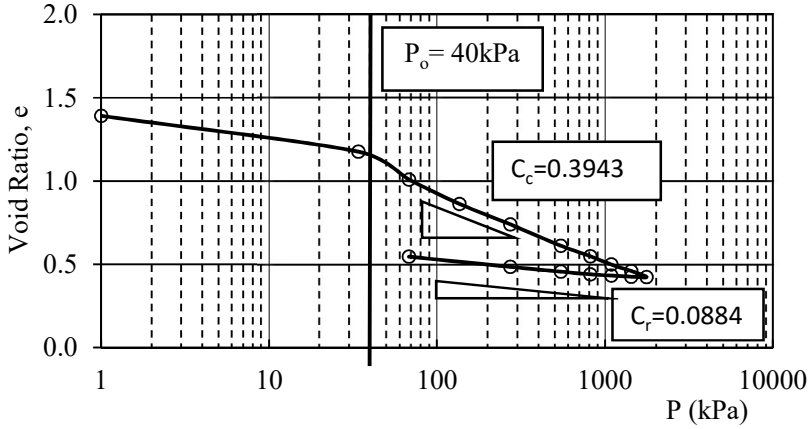

Figure 7.3 Compression indices of marine clay samples

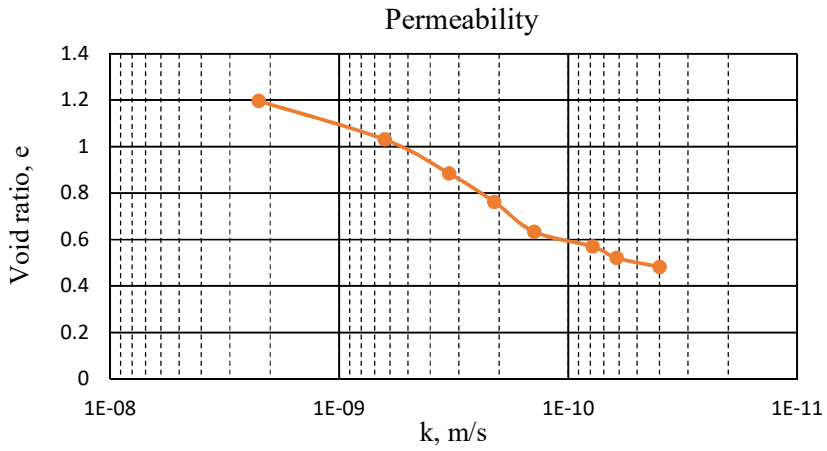

Figure 7.4 Permeability of marine clay samples

7.3.2 Prefabricated drains

The cross section of the prefabricated drains used for the laboratory model test was 100 mm in width and 2 mm in thickness. The prefabricated drains consisted of the inner core and the filter jackets as illustrated in Figure 7.5. The inner core was made from plastic and was flexible to accommodate to the deformation with the consolidating soils. The unique groove pattern of the inner core provided flow paths on both sides of the prefabricated band drain for the fluids entering the filter jackets. The filter jackets were made from geotextile which main function is to maintain the hydraulic capacity of the grooves and to prevent the intrusion of fine soil particles from clogging the prefabricated drains.

Figure 7.5 Components of prefabricated drains used for model tests

7.3.3 Model setup

Figure 7.6 shows the laboratory setup for the model tests. It consisted of a rectangular open consolidation tank with internal dimensions measuring 1.5 m (L) by 1 m (H) by 1 m (W). All boundaries of the rectangular consolidation tank were vertical and smooth to reduce friction between marine clay and the side of tank. Two sets of spanning frame were placed above the top of the consolidation tank for measurement of the surface settlement manually.

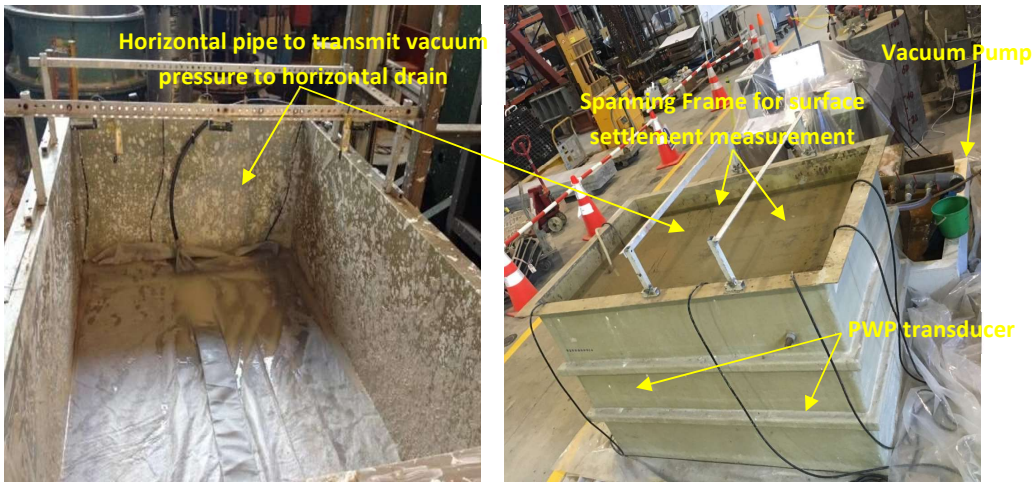

Figure 7.6 Key components of the proposed model tests

For each set of model test, 1.5 m^3 of marine clay slurry was used to fill the consolidation tank. Prefabricated band drains were placed horizontally over the clay slurry at prescribed height depending on the model test scenario for validation. After placement, the horizontal drains were covered by clay slurry to the placement height of 1 m. Figure 7.7 illustrates the setup of a single horizontal drain model test. The horizontal drain was connected to a vacuum tube which transmitted vacuum pressure from the vacuum pump to the drain.

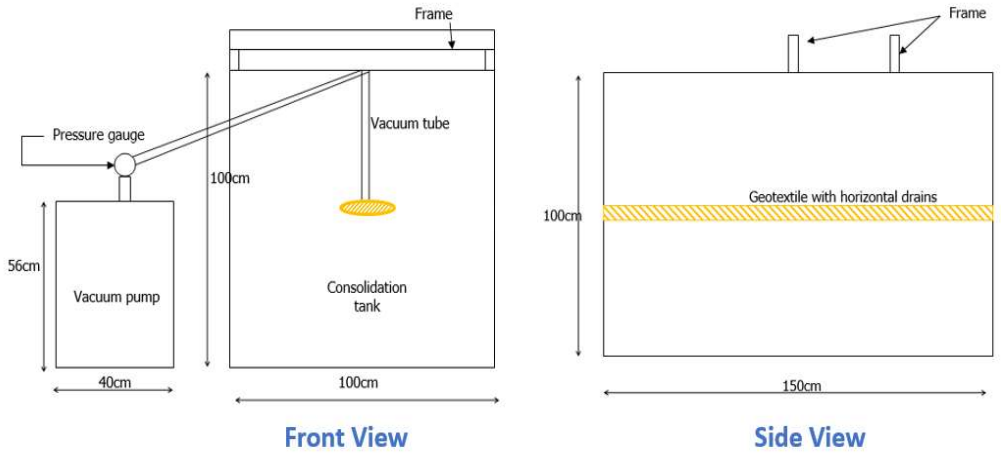

Figure 7.7 Schematic layout of a single horizontal drain model test

Water jet ejector illustrated in Figure 7.8 was used to produce vacuum for the model test. It was chosen for its reliablity in operations as it did not have any movable parts. In operation of the water jet ejector, pressurized water (i.e. Motive Fluid) entered the primary fluid inlet of the ejector and was then accelerated to a high velocity through the nozzle which discharged a high velocity jet stream of the fluid through the chamber into the convergent inlet end of the diffuser. Acceleration of the primary fluid through the nozzle into the vacuum chamber created a reduced pressure in the chamber which induces vacuum suction of 80 kPa in the clay slurry via the horizontal drains.

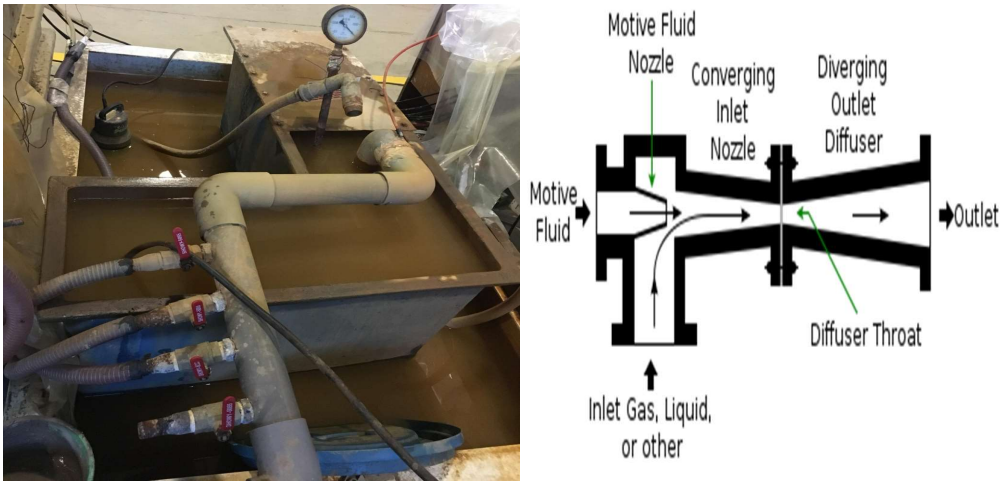

Figure 7.8 Water jet ejector used for vacuum generation

Two sets of model tests with slightly different setup of the horizontal drain placements were carried out to investigate the effectiveness of the proposed method using vacuum preloading with horizontal drain to accelerate the consolidation and improve the undrained shear strength of the marine clay samples.

In the first model test, only a single horizontal drain was placed horizontally in the middle of the consolidation tank as shown in Figure 7.9(a). The purpose is to study the effective range of a single horizontal placed prefabricated band drain in consolidating the marine clay slurry. In the second model test, two layers of horizontal drains were placed in the consolidation tank. The purpose is to study the improvement made to the marine clay samples found between the placed horizontal drains as illustrated in Figure 7.9(b). The prefabricated drains were spaced at 35cm apart laterally and 70cm apart vertically.

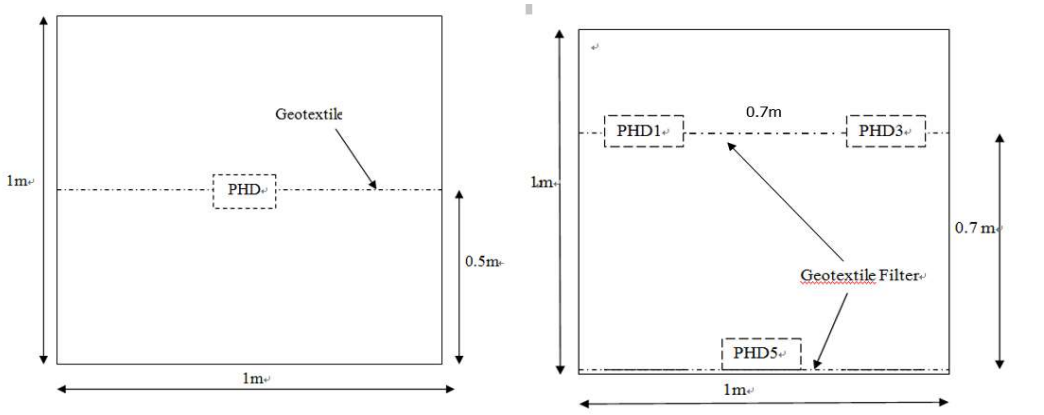

(a) Location of prefabricated drains in model test 1 (b) Location of prefabricated drains (two layers) in model test 2

Figure 7.9 Schematic cross section layout of horizontal drains for Model test 1 and 2

TDS-530 data logger was used to monitor and record the readings of the Pore Water Pressure Transducers (PPT) sensors at suitable prescribed intervals. KDP-200kPa (PPT) were used to measure and monitor the pore pressure response during the consolidation of the clay slurry in the laboratory trial. Prior to usage, the sensors of the PPT were soaked in water for more than 24 hours to get rid of the trapped air

bubbles. They were then wrapped in geotextile to prevent soil particles from entering the PPT sensors. Figure 7.10 shows the PPT sensors and Data Logger used in the laboratory model tests.

Figure 7.10 Pore water transducers and data logger used for model tests

Figure 7.11 shows the locations of the monitoring instruments for model test 1. PPTs E10、E14 and E13 were installed at bottom of ; PPTs E15 and E16 were placed at the same level on the left side of the horizontal drain; E12 was placed at the same elevation at the right side of the horizontal drains. The purpose to place the PPT at different radial distance from the horizontal drain was to establish the effective influence zone of the horizontal drain by measuring the changes in the pore pressures of the marine clay surrounding the drain.

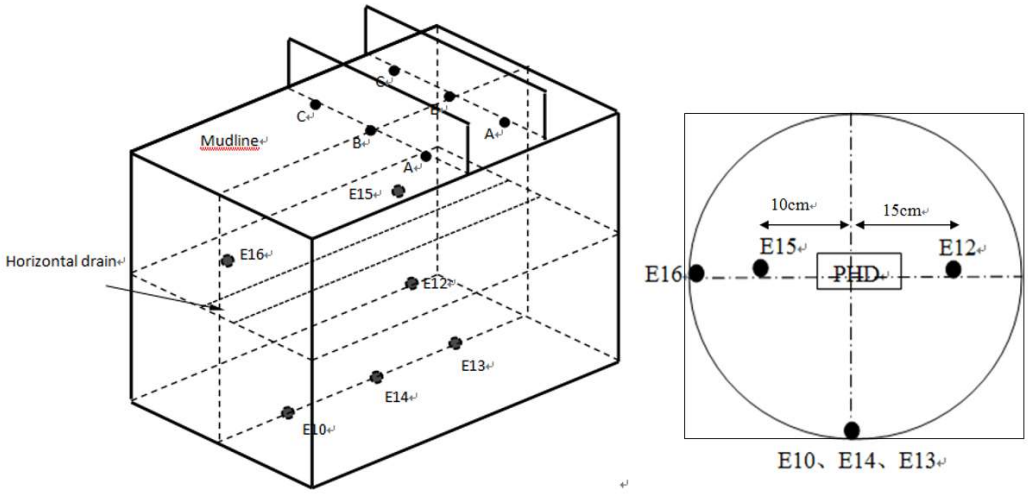

Figure 7.11 Locations of the monitoring instruments for model test 1

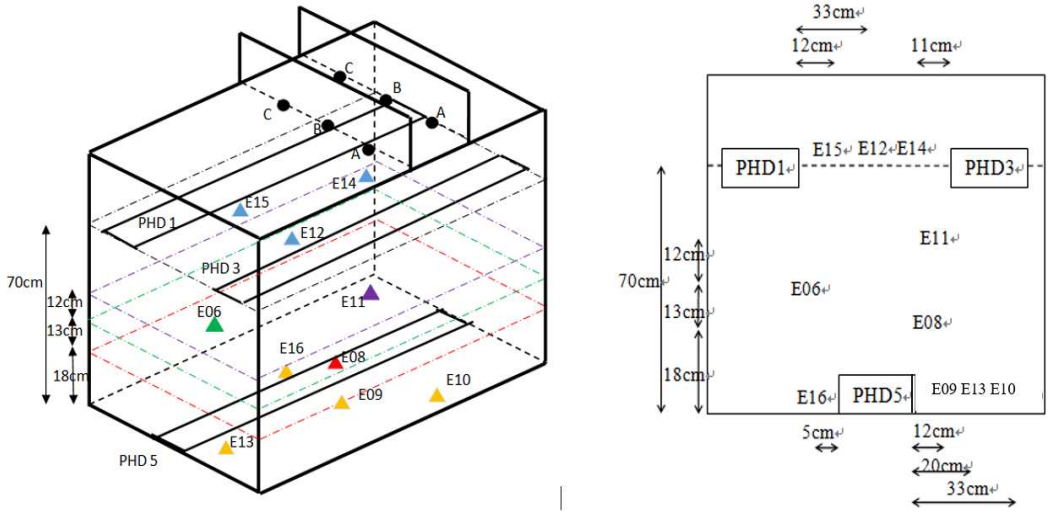

Figure 7.12 Locations of the monitoring instruments for model test 2

7.4 Results and analysis for the single horizontal drain model test

7.4.1 Surface settlement

The single horizontal model test was carried out for 3 months where vacuum was applied continuously. The measurement of the settlements induced by the consolidation of the marine clay were carried out manually with steel ruler which took reference from the two plastic spanning frames, herein refer as Bars. The bars were installed at the brim of the open consolidation tank as illustrated in Figure 7.6. 3 sets of readings were taken for each Bar. The measured surface settlement were taken at regular intervals and the recorded readings is plotted against time as illustrated in Figure 7.13 for Bar 1 and Figure 7.14 for Bar 2.

The surface settlement curves of Bar 1 and Bar 2 registered settlements of approximately 29cm by the end of 91 days of vacuum pumping operation giving about a 30% vertical strain reduction (95cm thickness). Due to the limitation on the model test set up, lateral strains cannot be measured, and were assumed to be the same as the initial conditions. As such, volume changes were assumed to be equivalent to the measure vertical strains. The volume reduction was estimated to be approximately 30% of the initial volume after vacuum pumping.

The reduction in volume of the soil samples was mainly attributed by the water loss in the marine clay matrix. As illustrated in the water content vs depth plot in Figure 7.21, there was significant drop in the water content from the initial 140% to around 50%. Water loss by surface evaporation were assumed to be negligible.

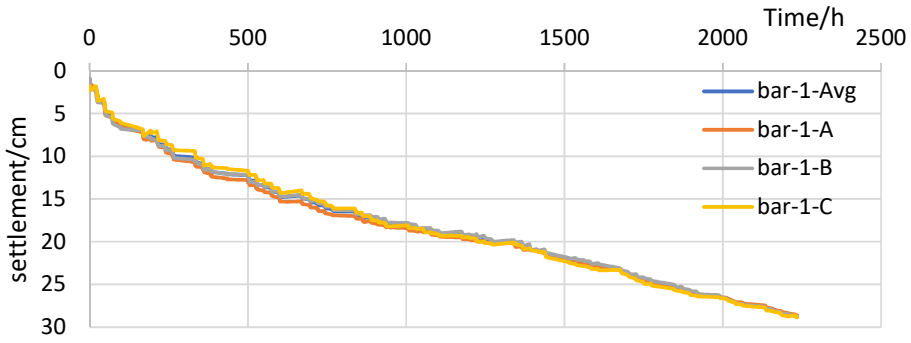

Figure 7.13 Surface settlement over time measured at Bar 1

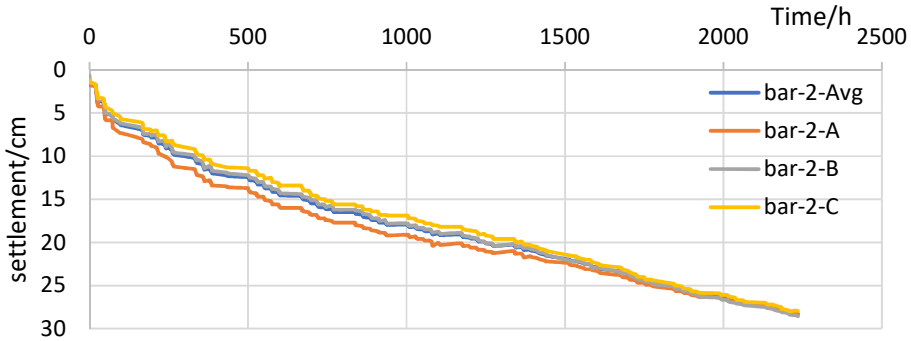

Figure 7.14 Surface settlement over time measured at Bar 1

Both curves exhibit akin trend where the slopes of the settlement curves (settlement rate) are steeper initially and become more gradual as the model test continued. Generally, the consistency and similarity in the observed settlement curves at both bars show that the distribution of the vacuum pressure was evenly spread by the horizontal drains. From the slopes of the settlement curves, we can deduce that the settlement will continue when vacuum pumping continues beyond the third month.

7.4.2 Degree of consolidation

The ultimate settlement (S_{ult}) at Bar 1 and Bar 2 can be predicted graphically from the settlement monitoring data using the Asaoka method shown in Figure 7.15 and Figure 7.16 respectively. The ultimate settlement for Bar1 and Bar 2 can be computed using Equation 7.1 and Equation 7.2.

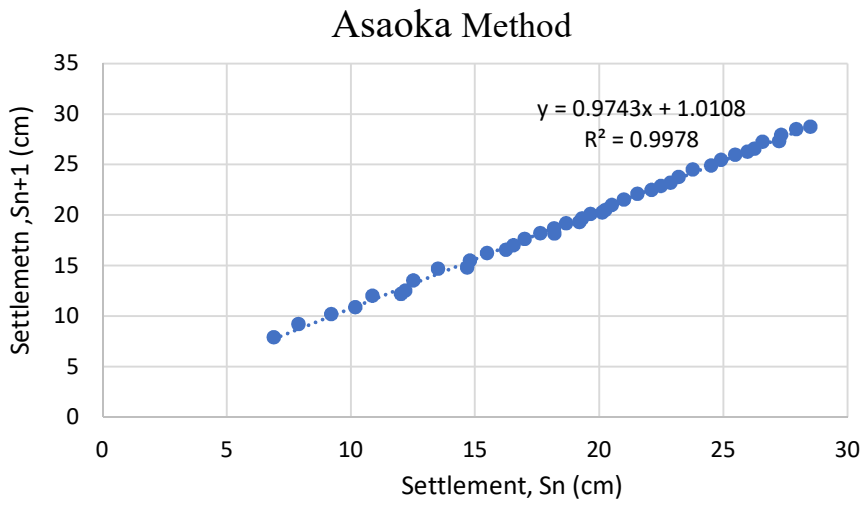

Figure 7.15 Ultimate settlement computed for Bar 1 using Asaoka method

$$\text{Ultimate Settlement, } \delta_{ult1} = \frac{\beta_1}{1-\alpha_1} = \frac{1.0108}{1-0.9743} = 39.33cm \quad (7.1)$$

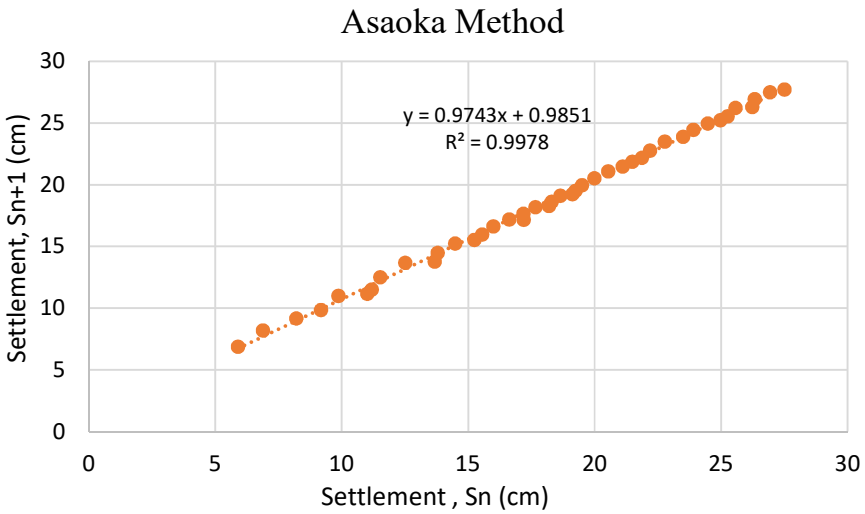

Figure 7.16 Ultimate settlement computed for Bar 2 using the Asaoka method

$$\text{Ultimate Settlement, } \delta_{ult2} = \frac{\beta_2}{1-\alpha_2} = \frac{0.9851}{1-0.9743} = 38.33cm \quad (7.2)$$

The predicted ultimate settlement using the Asaoka method was used to compute the Degree of Consolidation achieved for the marine clay at the end of the 91 days single prefabricated horizontal drain. The Degree of Consolidation are computed by using Equation (7.3) for Bar 1 and Equation (7.4) for Bar 2. The average Degree of Consolidation of 74% was achieved by the single horizontal drain model test is computed using equation (7.5).

$$U_{v1} = \frac{S_c(t)}{(S_c)_{ult}} 100\% = \frac{28.73}{38.33} \times 100\% = 75\% \quad (7.3)$$

$$U_{v2} = \frac{S_c(t)}{(S_c)_{ult}} 100\% = \frac{28.28}{39.33} \times 100\% = 72\% \quad (7.4)$$

$$U_{avg} = \frac{U_{v1}+U_{v2}}{2} = \frac{75\%+72\%}{2} = 74\% \quad (7.5)$$

7.4.3 Pore pressures

Figure 7.17 shows the pore pressure measured at PPT E12 and E15 over 91 days during the model test. PPT E12 and E15 were installed at a horizontal distance of 15cm and 10cm from horizontal drain respectively. It should be noted that the applied vacuum pressure had to be terminated in the night due to lab safety requirement. Pore Pressure of -10kPa were measured at E12 and E15 at the beginning of the model test 1 shows that vacuum pressure was transmitted rather quickly through the short radial distance. The measured pore pressure at E12 and E15 increased gradually over time at decreasing rate with the highest pore pressured measured at -70kPa and -60kPa respectively. It is interesting to note that E12 (15cm) which was installed at a further distance than E15 (10cm) has developed higher negative pore pressure throughout the duration of model test 1. This could be attributed by the different consolidation mechanism of the marine clay samples due to uneven mixing of the marine clay slurry. Nevertheless, the results show that vacuum pressure was effectively transmitted over a short radial distance from the horizontal drains.

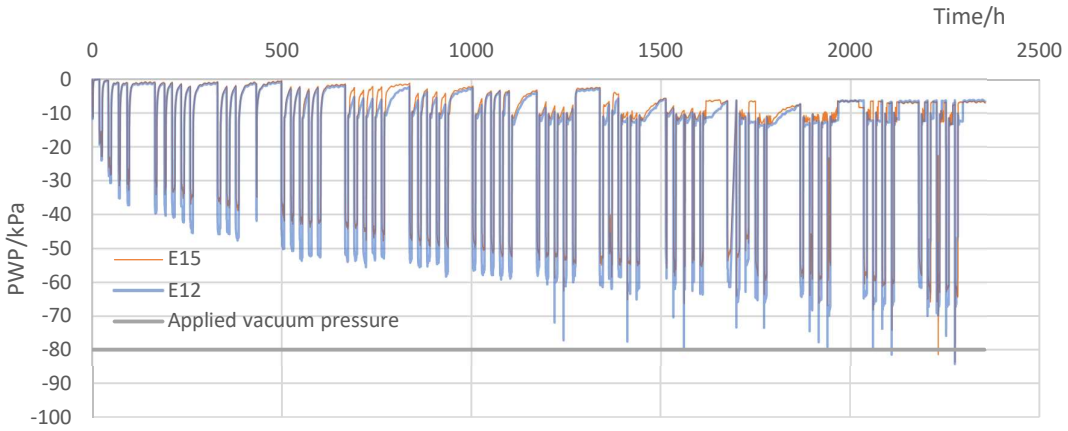

Figure 7.17 Measured pore pressure at E15 and E12

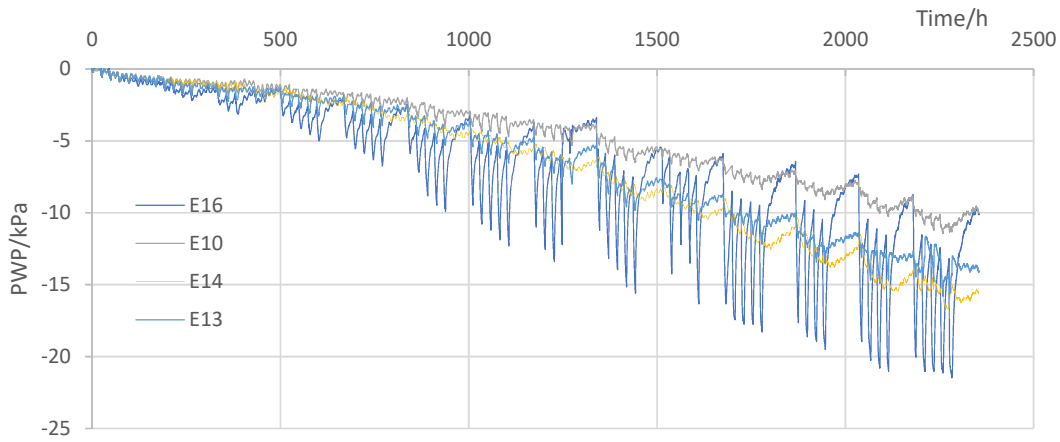

Figure 7.18 Measured pore pressure at E10, E13, E14 and E16

Figure 7.18 shows the pore pressures developed at PPT E10, E13, E14 and E16 over the 91 days model test. These PPTs were located at 0.5m from the horizontal drain. Unlike the trend observed in Figure 7.17, although the measured pore pressures increased gradually from -2kPa at the beginning to -22kPa at the end of the model test, the magnitude of the negative pore pressures were smaller. It took more than 1000 hours for the PWP to reached -5kPa. This observations confirm that the transmittance of vacuum pressure decrease with distance. It was also observed that E16, located above the prefabricated drainsdeveloped higher negative pore pressure than E10, E13 and E14 which were located at the bottom of the open consolidation tank. This could be attributed by the different consolidation mechanism of the uneven

mixed clay samples at the different locations and also the influence of gravity could come to play, in this case the gravity could have enhanced the transmittance of the vacuum pressure.

7.4.4 Undrained shear strength

At the end of the model test, Laboratory Vane Shear (LVS) tests and Unconfined Compression (UC) tests were carried out to determine the undrained shear strength (S_u) of the consolidated marine clay. LVS tests were carried out directly on the consolidated marine clay in the open consolidation tank and UC tests were carried out using extruded samples from the open consolidation tank. The undrained shear strength (S_u) and water content of the consolidated marine clay in the single horizontal drain model test were separated to two layers namely the "top layer" which refers to marine clay sample above the horizontal drain while the "bottom layer" refers to the marine clay below the horizontal drain.

7.4.4.1 Lab vane shear tests

After the model tests, Pilocon Hand Vane Tester SL815 was used to determine the undrained shear strength of the consolidated marine clay directly from the open consolidation tank. The instrument comprises of a torque head with direct reading scale which was turned by hand as shown in Figure 7.19. When calibrated and conducted properly, the Pilocon Hand Vane Tester would give reasonable and consistent results. This instruments works on the principle that the undrained shear strength of the saturated soil is proportional to the applied torque and the dimension of the vane. The undrained shear strength is calculated by equating the torque to the moment corresponding to the total shear strength over the sides and ends of the cylinder shear failure surface:

$$Torque = Ts + Te \qquad (7.6)$$

$Ts = \ moment\ of\ shear\ resistance\ force\ on\ th\ side\ of\ the\ cylinderical\ failure\ surface$

Te

$= moment\ of\ shear\ resistance\ force\ at\ the\ two\ ends\ of\ the\ cylindrical\ failure\ surface$

Replacing the above equation with test parameters, and solving the undrained shear strength, we obtained:

$$S_u = \frac{T}{\pi D^2 \left[\frac{H}{2} + \frac{D}{6}\right]}$$

Where

S_u = undrained shear strength of the soil sample

T = Torque

D = Overall diameter of vane

H = Vane Length

Figure 7.19 Pilocon hand vane tester used for undrained shear strength measurement

The laboratory vane shear test commenced by pushing the vane and the rod vertically directly into the consolidated marine clay in the open consolidation tank. The vane was then rotated slowly at about 6° to 12° per minute. The maximum torque reading was indicated by the non-return pointer when the marine clay failed in shear on a cylindrical surface around the vane. The rotation was usually continued after shearing and the torque was measured to estimate the remoulded shear strength. Figure 7.20 shows the locations where the vane shear tests were carried out at the end of the model test.

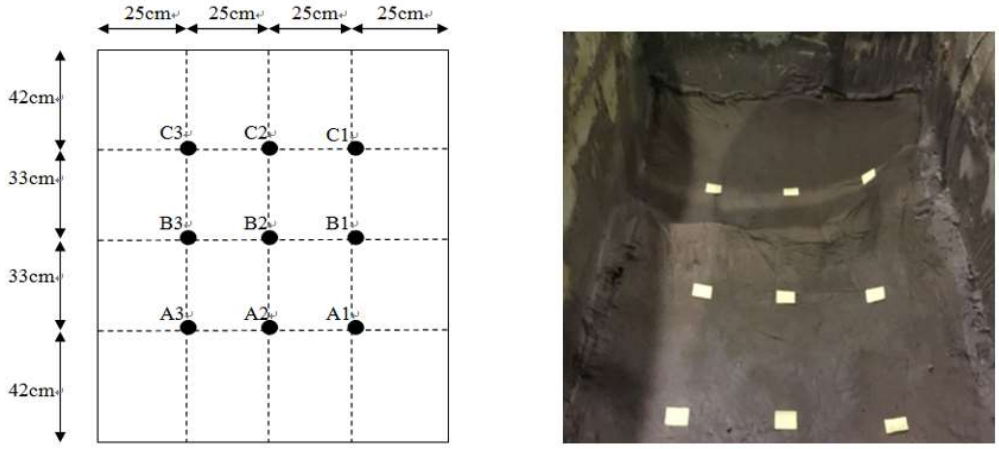

Figure 7.20 Locations of vane shear tests were carried out in the consolidation tank

With reference to the location of the prefabricated horizontal drain, Figure 7.21 illustrates the measured undrained shear strengths and water contents distributions of the consolidated marine clay at the end of model test. The results show that the marine clay was improved from a slurry with no apparent shear strength to a stiffer consolidated clay layer with varying shear strengths at different depth. The undrained shear strength were highest nearest to the horizontal drain and decrease with distance from the horizontal drain. The highest undrained shear strength was 47kPa. It decreaseb abruptly with distance from the drain. The undrained shear strength dropped to 17.6kPa at 10cm above the horizontal drain and reduced to 24kPa at 10cm below the drain. It was observed that the consolidated marine clay layer at the bottom layer had higher shear strength than the top layer. This could be attributed to the higher overburden stress acting on the bottom consolidated clay layer. Generally, the undrained shear strength continued to decrease sharply with increased vertical distance from the horizontal drain.

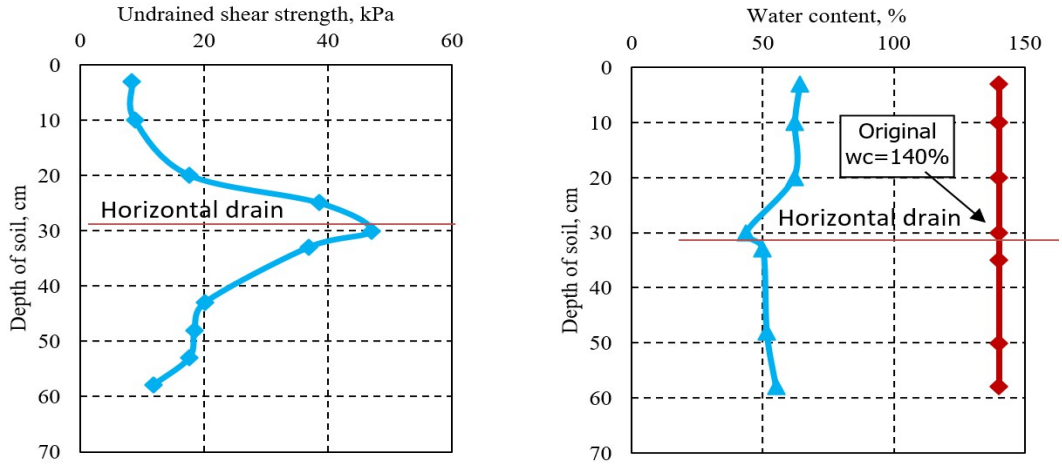

Figure 7.21 Undrained shear strength and water content distribution with depth

It was observed that the average water content reduced by more than 90% from the initial 140%. Figure 7.19 shows that the average water content at the end of the model test was around 50%. Lowest water content was measured just next to the horizontal drain at 43%. The reduction of water content was observed to be lesser for the consolidated marine clay above the horizontal drain especially for samples extruded further away.

Figure 7.22 illustrates the correlations of the measured undrained shear strength with the measured water content. The plotted curve shows that undrained shear strength has an inverse relationship with water content i.e. a reduction in water content in the consolidated marine clay will result in the increase in undrained shear strength.

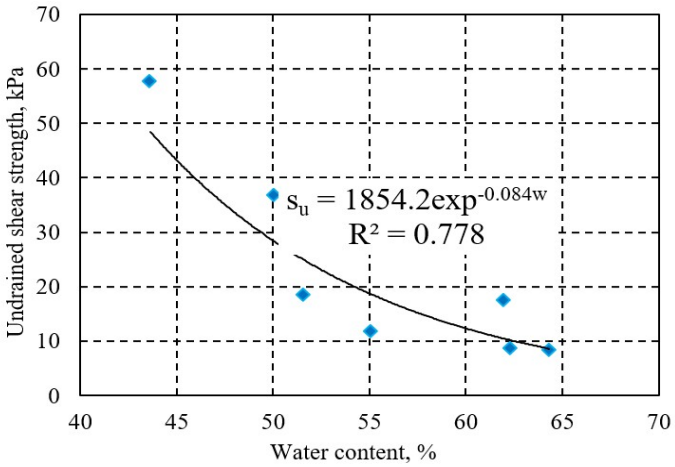

Figure 7.22 Correlations between undrained shear strength and water content

7.4.4.2 Unconfined compression tests

Unconfined compression test (UC Test) is an unconsolidated undrain test where the lateral confining pressure is equal to zero (atmospheric pressure). It is commonly adopted for the measurement of shear strength of saturated cohesive soil samples as it is fast and cheap to carry out. Cylindrical marine clay samples were extracted from the open consolidation tank at the end of the model test and trimmed such that the ends were reasonably smooth and the length-to-diameter ratio was on the order of 2:1 as shown in Figure 7.23. The trimmed marine clay samples were then placed in the UC Test apparatus where axial forces were applied a constant strain rate. The axial loads were gradually increased on the sample until an obvious shear plan was developed on the marine clay sample or deformation becomes excessive. At the end of the UC Test, the marine clay samples were oven dried to determine its water content. The maximum load per unit are is defined as the unconfined compressive strength,

$$q_u = \frac{F}{A} \qquad (9.6)$$

where qu = *unconfined compressive strength of the soil sample*

F = *axial load at failure*

$A = \frac{A_0}{1-\varepsilon}$, *Cross section area of sample*

$A_0 = inital\ area$

$\varepsilon = axial\ strain$

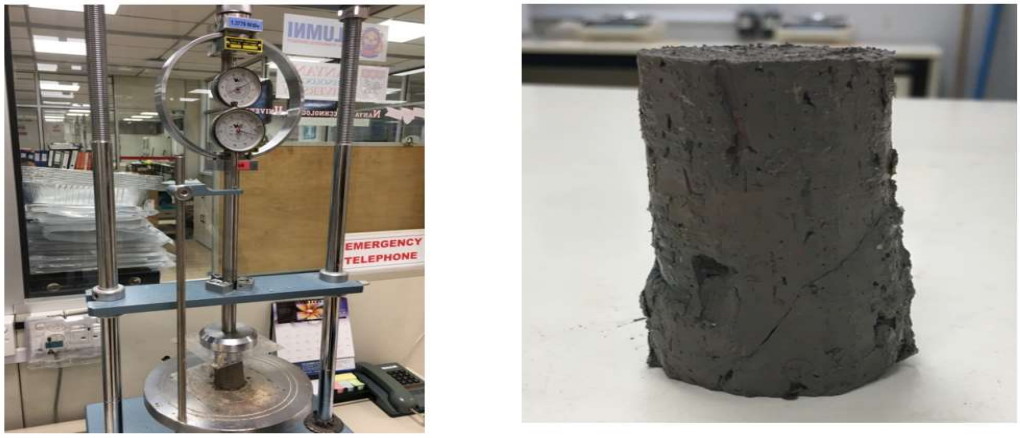

Figure 7.23 Unconfined compression test apparatus and a typical failed soil sample

The undrained shear strength of the marine clay is half the value of the unconfined compressive strength computed from the UC Test as illustrated in Equation 7.7.

$$S_u = \frac{1}{2} q_u \qquad (7.7)$$

Figure 7.24 shows the comparison of the undrained shear strength computed from Pilocon Hand Vane Tester. The tabulated lines show trends that undrained shear strength decreased with increased water content. Despite the similar trends, we can see that the vane shear test yielded much higher undrained shear strength than the UC test method.

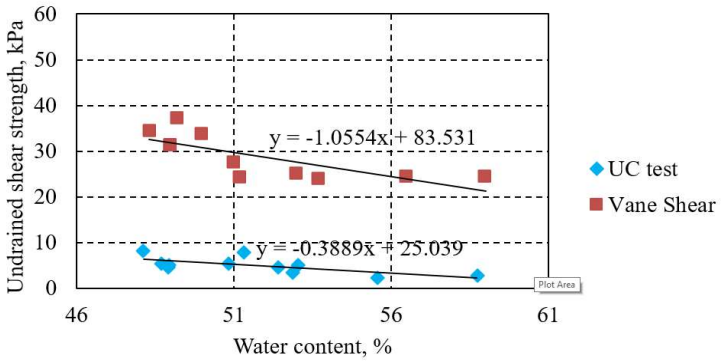

Figure 7.24 Comparison between undrained shear strength from UC and vane shear tests

7.5 Results and analysis for the double-layer horizontal drains model test

The results of the first model using a single horizontal drain have shown evidences that it was effective to consolidate marine clay slurry and increase its undrained shear strength. However, the improvement was limited. The improved strength will decrease with distance from the horizontal drain. The purpose of the second model test is to simulate a typical section of the proposed soil improvement method in actual field installation where the horizontal drains were placed in layers at regular distance apart, to provide a network of horizontal drainage paths to improve in hydraulic dredged slurry infill.

The layouts of the double layered horizontal drains model test is shown in Figure 7.12. The first layer consisted of a single horizontal drain laid directly at the bottom of the open consolidation tank. After the single drain was placed, it was covered with 0.7 m of marine clay slurry before the second layer consisting of two horizontal drains were placed. The second layer of horizontal drains were then covered with 0.3 m of marine clay slurry. The intial water content of the marine clay slurry for this model test was 146%.

7.5.1 Surface settlement

In the double layered horizontal drains model test, vacuum pumping was carried out for 42 days. The settlement measurements were carried out in the same way as the first model test. The recorded settlements over time at Bar 1 and Bar 2 are displayed in Figure 7.25 and Figure 7.26 respectively.

By the end of this model test, the average surface settlement measured at the two bars ranged between 28cm to 30 cm, giving about 30% vertical strain. Similar to model test 1, due to the limitation on the model test setup, lateral strains cannot be measured

and were assumed to be similar to the vertical strains. It was concluded that the reduction of 30% volume was attributed to the consolidation of the marine clay slurry where excess water was removed from the marine clay samples via the vacuum transmitted by the horizontal drains.

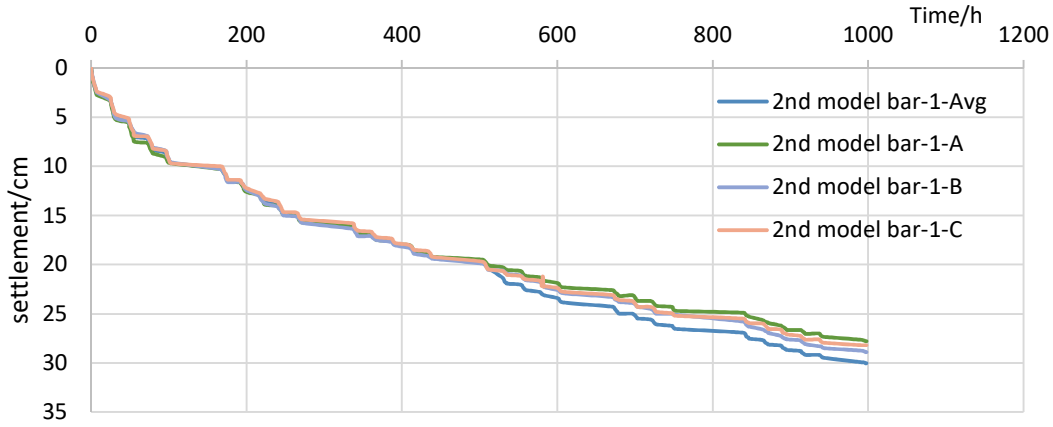

Figure 7.25 Surface settlement over time at Bar 1

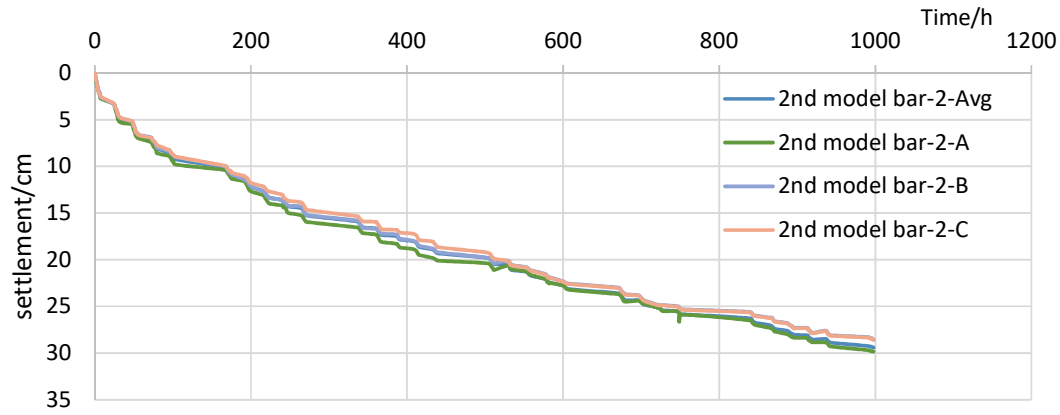

Figure 7.26 Surface settlement over time at Bar 2

7.5.2 Degree of consolidation

Akin to the first model test, the ultimate settlement (S_{ult}) are predicted graphically from the settlement monitoring data using the Asaoka method. The linear Asaoka plots for the 2 average settlement points from Bar 1 and Bar 2 are illustrated in Figure 7.27 and Figure 7.28 respectively. The ultimate settlement for Bar1 and Bar 2 can be computed using Equation 7.1 and Equation 7.2

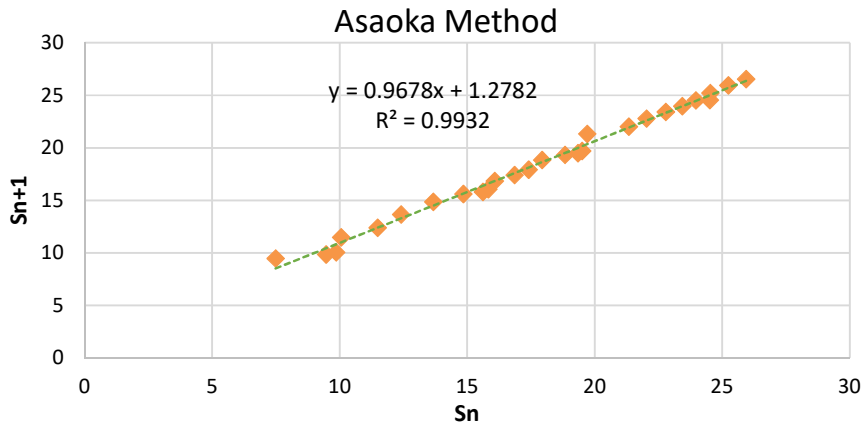

Figure 7.27 Ultimate settlement computed for Bar 1 using Asaoka method

$$\text{Ultimate Settlement, } \delta_{ult1} = \frac{\beta_2}{1-\alpha_2} = \frac{1.2782}{1-0.9678} = 39.7cm \quad (7.7)$$

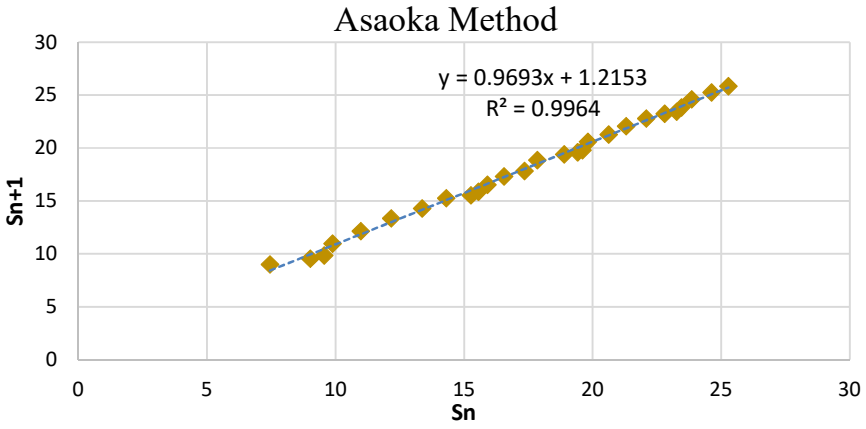

Figure 7.28 Ultimate settlement computed for Bar 2 using Asaoka method

$$\text{Ultimate Settlement, } \delta_{ult1} = \frac{\beta_2}{1-\alpha_2} = \frac{1.2153}{1-0.9693} = 39.59cm \quad (7.9)$$

The predicted ultimate settlement from the Asaoka method was used to compute the Degree of Consolidation achieved for the marine clay at the end of the 2nd model test. The Degree of Consolidation are computed by using Equation (7.10) for Bar 1 and Equation (7.11) for Bar 2. The average Degree of Consolidation for 76% was

achieved from the double layered horizontal drains model test can be computed using equation (7.12)

$$U_{v1} = \frac{S_c(t)}{(S_c)_{ult}} 100\% = \frac{30.03}{39.7} \times 100\% = 76\% \quad (7.10)$$

$$U_{v2} = \frac{S_c(t)}{(S_c)_{ult}} 100\% = \frac{29.42}{39.59} \times 100\% = 74\% \quad (7.11)$$

$$U_{avg} = \frac{U_{v1}+U_{v2}}{2} = \frac{76\%+74\%}{2} = 75\% \quad (7.12)$$

7.5.3 Pore pressure

Pore pressure transducers were installed at different depths within the open consolidation tanks. Table 7.2 shows the pore pressure transducers and their corresponding depths measuring from the bottom of the consolidation tank.

Table 7.2 Pore pressure transducers installed at different depths

Depth	Pore Pressure transducers
0 cm	E09, E10, E13, E16
18cm	E08
31cm	E06
43cm	E11
70cm	E12, E14, E15

Figure 7.29 shows the recorded pore pressures developed over time at the same levels as the horizontal drains. At the top layers which is 0.7 m from the bottom of the tank, two horizontal drains were placed at 0.7 m apart horizontally, the pore pressure transducer readings show that the marine clay between the horizontal drains at this elevation experienced high level of vacuum pressures ranging from 83kPa to 98kPa. While at the bottom layer, where only a single horizontal drain was placed at the bottom of the consolidation tank, the vacuum pressure experienced by the pore

pressure transducers ranged from 84kPa to 100kPa. Highest vacuum was measured nearest to the horizontal drains (E16, 5cm away) and decrease with distance from the vacuum transmitting horizontal drains.

The pore pressure transducer readings show that the marine clay at this elevation experienced high level of vacuum pressures of at least -80kPa when they were not placed more than 20cm away from the horizontal drains. After 800hrs into the model test, the vacuum pressure in the marine clay continued to increase incrementally as consolidation continued.

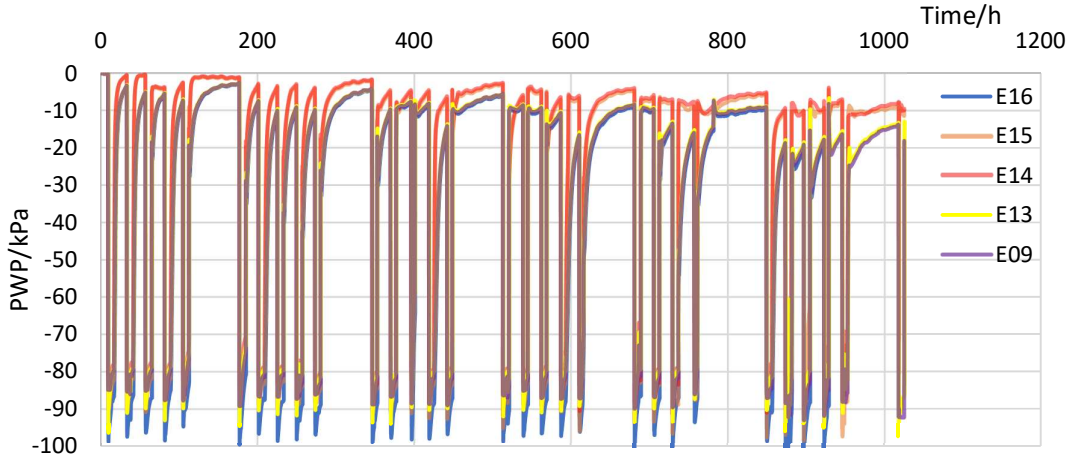

Figure 7.29 Measured pore pressures at E09, E13, E14, E15, E16

Figure 7.30 compares the pore pressure measured at E10 which was placed 33cm away from the PHD 5 located at the bottom of the consolidation tank and the pore pressures measured at E12 which was placed 33cm away from PHD1 and 37cm from PHD3 as illustrated in Figure 7.12. The E10 curves show that the pore pressure increased from the initial -20kPa to -89kPa at the end of the model test. The E12 curves show that a high degree of vacuum pressure at -80kPa was experienced by the marine clay initially and increment in vacuum experienced was small at about -90kPa at the end of the model test. The results indicate that despite the same distance from the horizontal drains, the marine clay sample found between two horizontal drains will experience higher intial vacuum pressure leading to faster and higher consolidation. However, if time is not a factor, the marine clay in the a single

horizontal drain model test can also experience vacuum of -90kPa after a long period of vacuum pumping.

Based on the observations made in the model tests, it was deduced that higher consolidation rate can be achieved by vacuum preloading with closer spaced horizontal drains. However, the magnitude of consolidation, assumming that there is no vacuum loss, is limited by the maximum vacuum pressure of -100kPa.

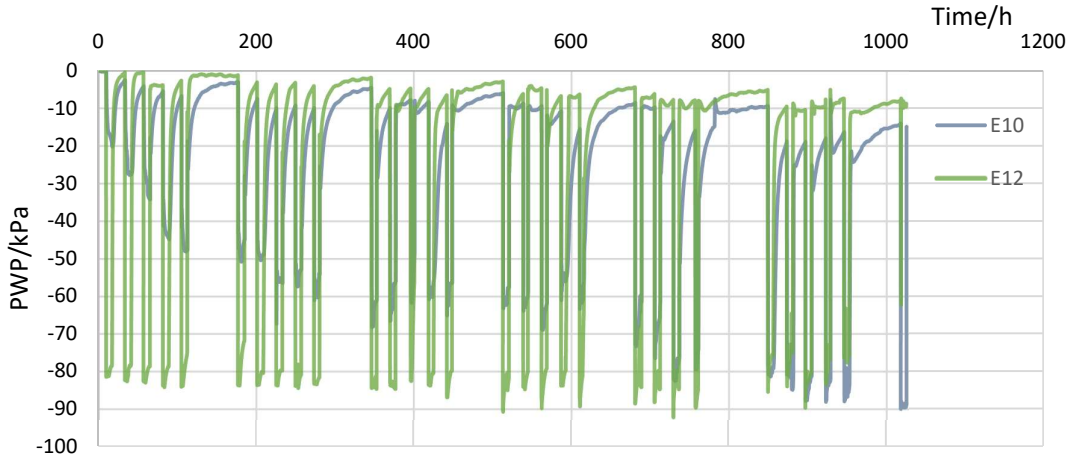

Figure 7.30 Measured pore pressure over time at E10 and E12

Figure 7.31 compares the measured pwp between E06, E08 and E11. Generally, the measured pore pressures for all three pore pressure transducers shows similar trend of increasing negative pressure over time from 0 to -10kPa for E06, 0 to -12.9 for E08 and 0 to -15.1 for E11.

E08 being the furthest away from the two upper horizontal drains and nearest to the single horizontal drain at the bottom of the consolidation tank experienced steady increase in vacuum over time when compared to E06 an E11 where intermittence peaks of large increments of the vacuum pressure were observed. The intermittence vacuum pressure peaks at E06 and E11 occurred temporarily and dropped to lower level but with increasing negative pore pressure trend over time. These intermittence peaks registered in E06 and E11 was likely influenced by the vacuum pressured induced by the horizontal drains at the upper layer which was placed further away.

The intermittence peaks were not observed in the pore pressure reading of E08 as they may be located too far away from the upper horizontal drains.

A detailed comparison between the pore pressures of E06 and E08 over the entire timeline of the model tests where the registered spikes in vacuum in E06 were excluded from the analysis. E08 experienced a higher average vacuum pressure trend than E06. This could be due to the closer proximity of E08 to the bottom horizontal drain at 18 cm vertical distance when compared to E06 which was located at vertical distance of 31 cm from the bottom horizontal drain and a vertical distance of 39 cm from the top horizontal drains.

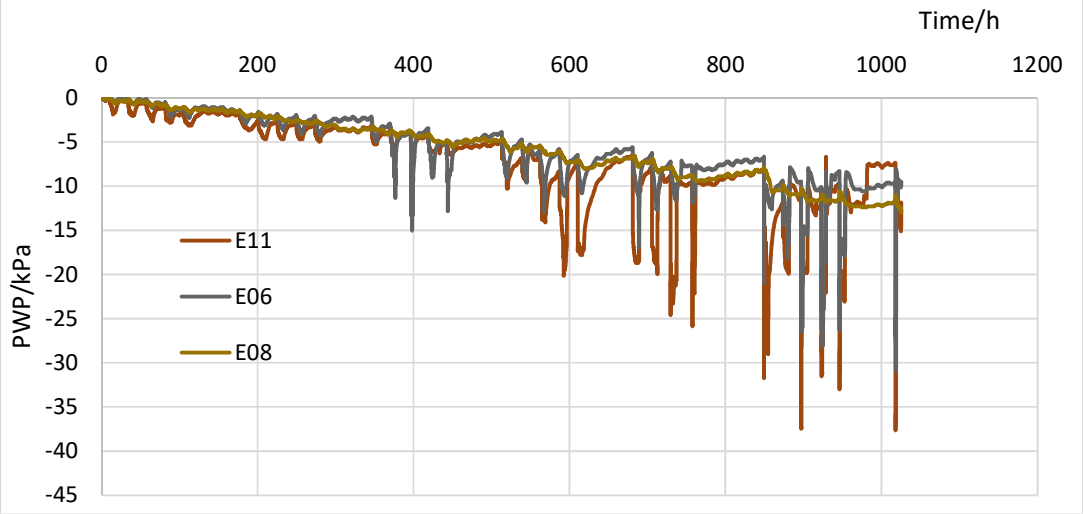

Figure 7.31 Measured pore pressures over time at E06, E08, E11

When the measured pore pressures were compared between E06 and E11, E11 being closer to the top horizontal drains at a vertical distance of 27cm experienced higher vacuum pressure when compared to E06 which the closest to horizontal drains at the bottom of the consolidation tank is located 31cm away vertically. Generally, the measured peaks in vacuum pressures in E11 in the model test were higher than the peaks recorded in E06.

From the analysis of Figure 7.29 to 7.31, it was deduced that the magnitude of the vacuum pressure experienced by the marine clay or soils depend greatly on its

proximity to the source transmitting the vacuum. With this understanding, the general observations where the negative pressure increased over time as the laboratory test continues can also be attributed to the fact that the proximity of the pore pressure transducers to the vacuum transmitting horizontal drains increased (reduced distance) over time as the marine clay consolidate and reduced in volume.

7.5.4 Undrained shear strength

Figure 7.32 shows the measured undrained shear strengths and water contents at different depths of the consolidated marine clay at the end of the double layered horizontal drains model test. The undrained shear strength were obtained by using the pilocon hand vane tester. Generally, the undrained shear strengths increased from surface of marine clay until it reached the depth where the upper horizontal drains were installed. The measured undrained shear strength at the upper horizontal drains elevation measured at 44.4 kPa. Beyond this elevation, the undrained shear strength reduces as the depth increases.

The reduction in the undrained shear strength continues until the elevation of about 40cm from the top of the consolidated marine clay layer. This is about the mid-point between the top horizontal drain and the bottom horizontal drain where the lowest undrained shear strength was recorded at 9.2kPa between the horizontal drain layers.

Thereafter the undrained shear strength picks up with increasing depth until it reaches the highest undrained shear strength at 47.7kPa which is located slightly above the bottom horizontal drains at 62cm from the top of the consolidated clay. Higher measured shear strength at the bottom horizontal drains was probably attributed to the additional overburden stress acting over the consolidated marine clay layer.

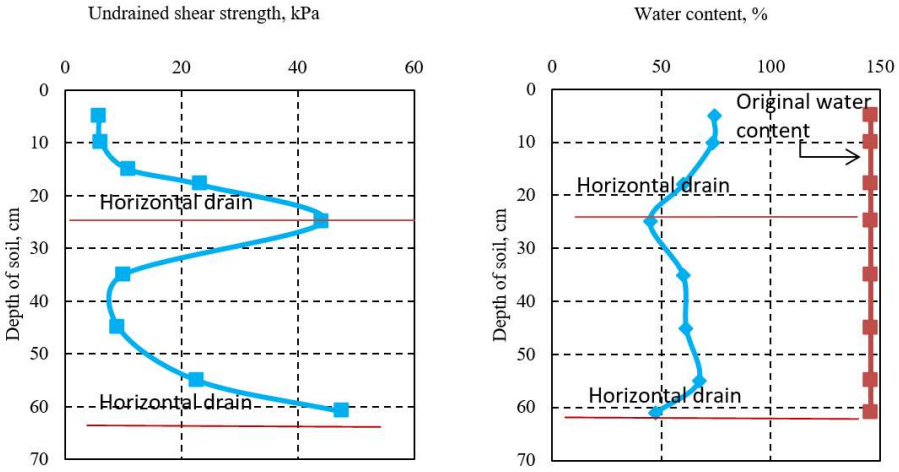

Figure 7.32 Undrained shear strength and water content distribution with depth

The initial water content of mixed marine clay slurry was 146% and water content reduced approximately 86% at the end of the model test. Generally, the water content was lowest at the horizontal drain layers and highest at distance furtherst from the horizontal drains. The lowest water content found at the top drain layer was at 44.6% and 42.7% at the bottom drain layer. Figure 7.33 plots of measured undrained shear strength against measured water content. The results show similar inverse relationship of water content with undrained shear strength where undrained shear strength increase with lower water content.

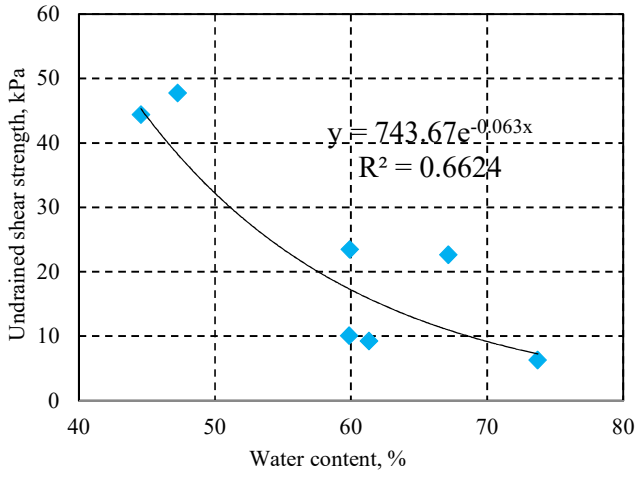

Figure 7.33 Correlations between undrained shear strength and water content

7.5.5 Comparisons between model tests with single and double-layer horizontal drains

7.5.5.1 Settlement

The single horizontal model test achieved an average settlement of 28.5cm after 2,230 hours of vacuum pumping while the double layered horizontal drain model test achieved an equivalent settlement with only 1,000 hours. This demonstrated that the consolidation rate of the marine clay can be significantly improved with installation of more horizontal drains as the drainage path for pore water dissipation were decreased and the proximity of the source transmitting the vacuum to the soil mass were increased.

7.5.5.2 Pore Pressure

The single horizontal drain model test demonstrated that the vacuum experienced by the marine clay sample was very low initially and was built up over time. Lower initial vacuum was measured by pore pressure transducer placed further away from the horizontal drain transmitting the vacuum. The double layered horizontal drains model test demonstrated that with more placement of horizontal drains, vacuum was transmitted more effectively within the marine clay sample. The pore pressure readings showed that the marine clay experienced higher vacuum at the very beginning. This high initial vacuum transmitted by more horizontal drains were the key factors leading to higher consolidation rate and faster settlement experienced by the marine clay.

7.5.5.3 Undrained shear strength and water content

The vacuum pressure transmitted from the horizontal extracted the excess pore water from the marine clay matrix led to the reduction of water content as the marine clay consolidate. The consolidation led to increase in effective stress and increase in the undrained shear strength of the marine clay. Both model tests showed that about 5cm of marine clay surrounding the horizontal drains had achieved undrained shear strength above 40kPa. However, the undrained shear strength of the marine clay

dropped very drastically measuring less than 20kPa at 10cm away from the horizontal drain. The results from the two-model tests suggest that the desired undrained shear strength in the marine clay matrix can be achieved using the proposed soil improvement methods by manipulating the quantities and the spacing of the horizontal drains.

7.6 Numerical analyses of alternative methods for formation of working platform

The laboratory model tests presented in earlier sections in this chapter had verified that marine clay slurry can be improved effectively by the application of vacuum preloading with horizontal drains. This section presents the numerical analyses using Plaxis 2D to examine other different schemes that could be adopted to form a working platform. The first is the use of a geotextile layer, 1.5 m of sand capping, plus to improve the top clay slurry layer up to depths of 1, 2, 3, 4, or 5 m respectively. The improved clay layer is also assumed to have an undrained shear strength of 1, 5, 10, 17.5 and 25 kPa respectively. The method of improvement could be vacuum preloading with either horizontal drains or vertical drains. The second is to improve the top few meters of soft clay slurry only without the use of geotextile layer and sand capping.

7.6.1 Working platform formed by shallow soil improvement, geotextile, and sand capping

7.6.1.1 Geometry model

The base geometry model of 65 m width and 26.5 m depth are presented in Figure 7.34. The phreatic water level was set at 0.00 m. The compressible soil layer was considered as clay slurry with an undrained shear strength of 0.1 kPa. The top 5 m of

the clay slurry layers were assummed to been improved using vacuum preloading together with horizontal drains to a soil with an undrained shear strength of 1, 5, 10, 17.5 and 25 kPa respectively. The thickness of the improved clay layer was assumed to be 1, 2, 3, 4 and 5 m respectively. Woven geotextile, HPA 380, was placed at the same level as the phreatic water level which acts as the reinforcing geotextile. 1.5m of sand was placed above HPA380. The design working load of 25kN/m spanning 4m was applied directly at the surface of the improved soil layer in the middle of the geometry model.

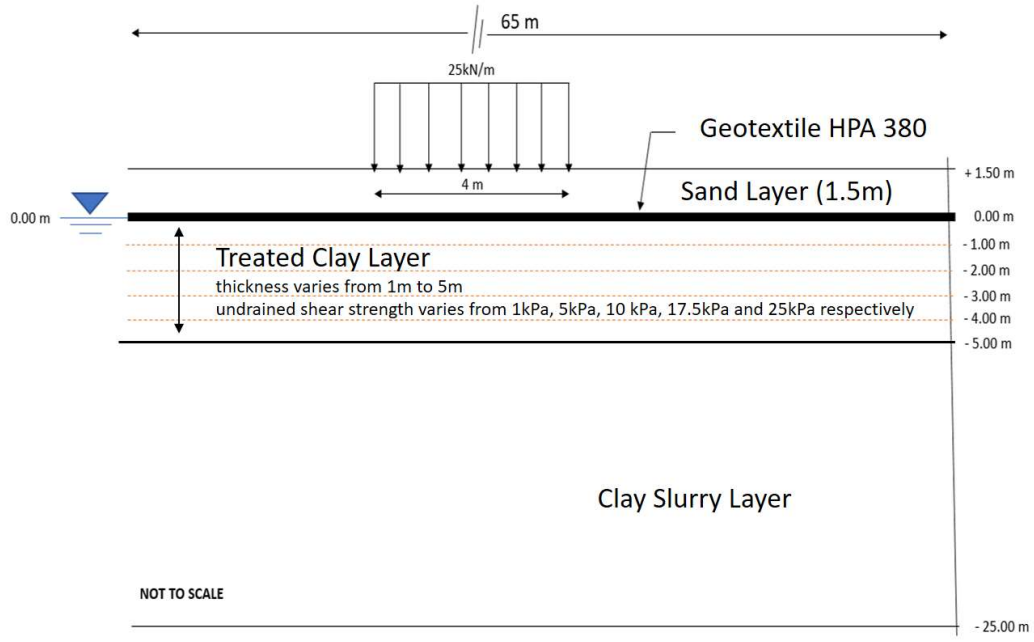

Figure 7.34 Geometry model to examine the geotextile-sand working's stability when the soft soils below the geotextile are improved by vacuum preloading with horizontal drains

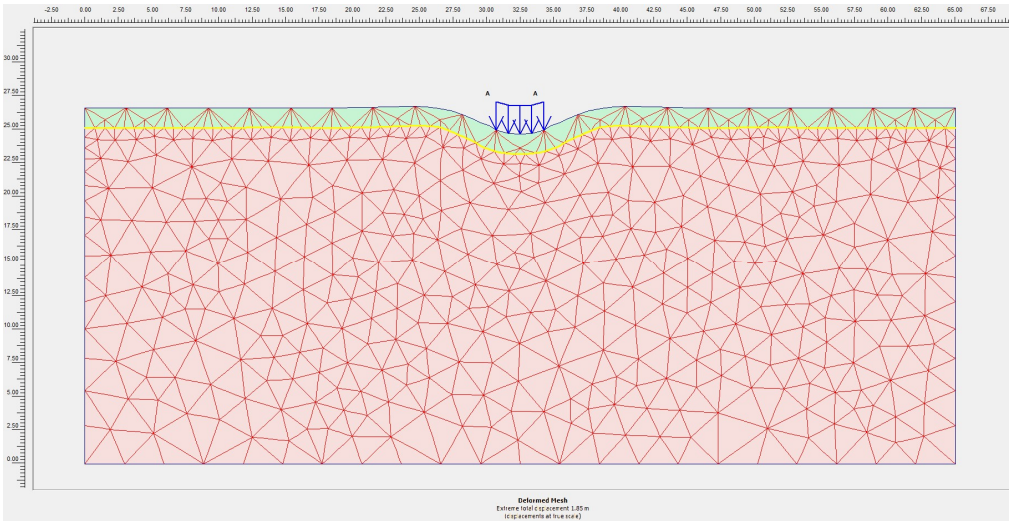

Figure 7.35 A typical finite element mesh showing the deformation of the geotextile-sand working platform

7.6.1.2 Model set up and materials

Mohr Coulomb material model was used to simulate the behaviour of sand and compressible soils as a simple first analysis of the problem considered. The materials properties are summarised in Table 7.3 & Table 7.4 Sand placed over HPA 380 was modelled as drained condition while the vacuum preload treated clay layers and the deposited clay slurry were modelled as undrained condition.

Table 7.3 Soil parameters in geometry models

Materials in each layer	**Material Type**	$\gamma_{unsat.}$ **(kN/m^3)**	$\gamma_{sat.}$ **(kN/m^3)**	E_{ref} **(kN/m^2)**	C_u **(kN/m^2)**	ϕ **(°)**	Ψ **(°)**
SAND	Drained	16.00	20.00	3000	0.00	32.00	0.00
CLAY SLURRY	Undrained	13.00	13.00	350	0.10	0.00	0.00
TREATED CLAY	Undrained	15.00	18.00	500	5[1]	0.00	0.00

[1] C_u - range from 1, 5, 10, 17.5 and 25kPa

Table 7.4 Geotextile parameters in geometry models

Materials	Material Type	EA (kN/m)
HPA 380	Elastoplastic	700

7.6.1.3 Results & analysis

A minimum Factor of Safety of 1.5 was set to ensure sufficient stability was provided for the site operations that will be carried out over the working platform. Figure 7.36 shows the Safety Factor for 5m of treated clay layer at different shear strength computed from using Plaxis 2D. The shear strength of the treated clay layer ranged from 5 kPa to 25 kPa. Generally, the Factor of Safety improved with increased shear strength for 5m of treated clayer layer.

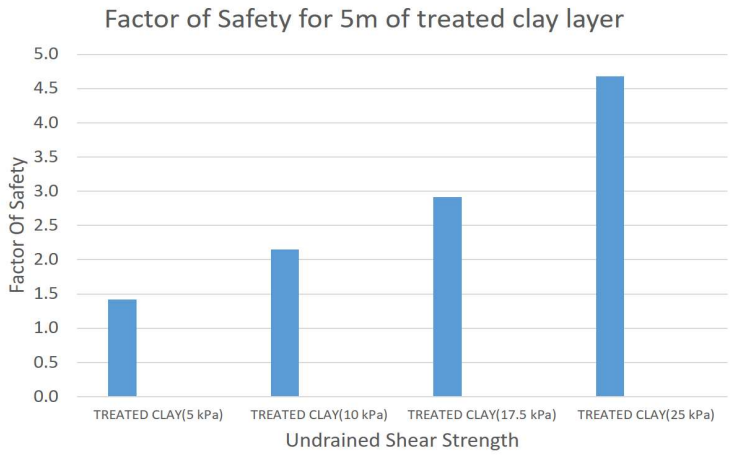

Figure 7.36 Factor of Safety for 5m of treated clay layer at different shear strength

Figure 7.37 shows the Safety Factor for clay layers treated to 25kPa at different thickness computed from using Plaxis 2D. The thickness of the treated clay layer ranged from 1m to 5m. Generally, the Factor of Safety improve with increased thickness.

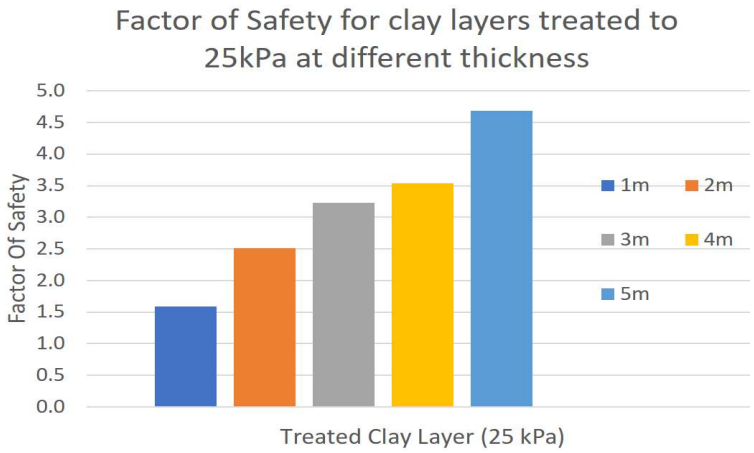

Figure 7.37 Factor of Safety for clay layers treated to 25kPa at different thickness

Figure 7.38 shows the Factor of Safety computed from Plaxis 2D. It shows the relationships between undrained shear strength of the treated clay layer with different treated clay thickness. Generally, the Factor of Safety improve with increased shear strength and increased treated soil thickness.

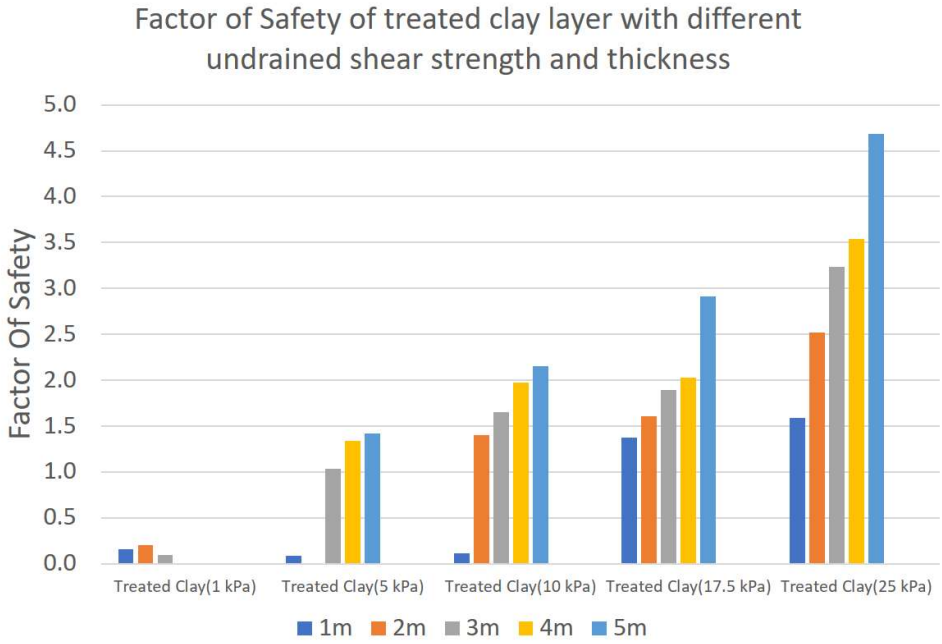

Figure 7.38 Factor of safety of treated clay layer with different shear strength and thickness

At shear strength of 1 kPa, the analysis shows very low Factor of Safety regardless of the thickness of its improved layers. When shear strength of the soft soils was increased to 5 kPa, Factor of Safety above 1.0 was attained when the improved soft soils layer was 3m thick. When 5m of the soft soils were improved to 5kPa the computed Factor of Safety was still below 1.5.

High Factor of Safety were observed for soil layers with high shear strength. The requirement to achieved a Factor of Safety above 1.5 for stability was achieved at 3m thickness when shear strength of the soft soil layer was 10kPa, 2m thickness when shear strength is 17.5 kPa and only 1m thickness was required where the improved layer shear strength equal to 25kPa. From the operational perspective, it will be more practical to choose to improve the highly compressible soils to 10kPa for 3m depth rather than improving it to a higher shear strength with lower thickness.

Figure 7.39 shows the plot of maximum soil displacement computed from Plaxis 2D with respect to varying undrained shear strength and thickness of the treated clay layer. Generally, the displacement of the soils reduced with increased shear strength and thickness of the improved clay layers. Generally, for practical site applications, the treated soil displacement should be kept within 0.6m of displacement. This can be achieved by improving the clay slurry to 10kPa and above for 4m. Further reduction in displacement below 0.4m will not be practical as the trend line shows that it may require extensive improvement which could be both costly and time-consuming.

Figure 7.40 illustrates the soil deformation profile of the soft soils improved to 5m thickness with different sheared strength. From the comparisons of the deformation profiles, we can see that despite the reduction in the computed displacement, its displacement envelope has enlarged with increased shear strength. This observation was also observed in earlier Plaxis 2D models and was probably attributed to better distribution of the working load due to the increase in shear strength.

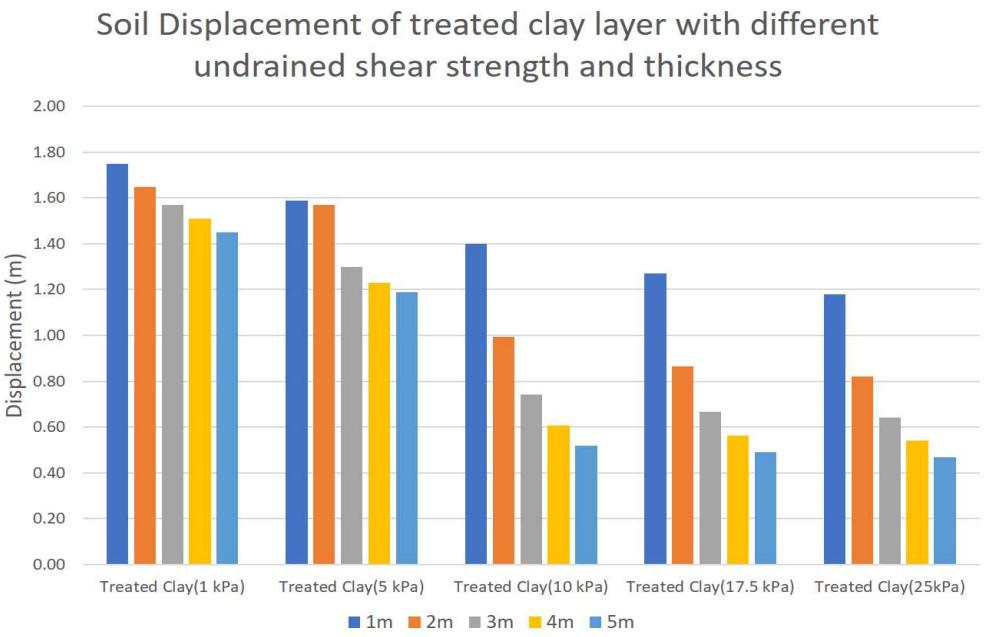

Figure 7.39 Soil displacements of treated clay layer at different shear strength and thickness

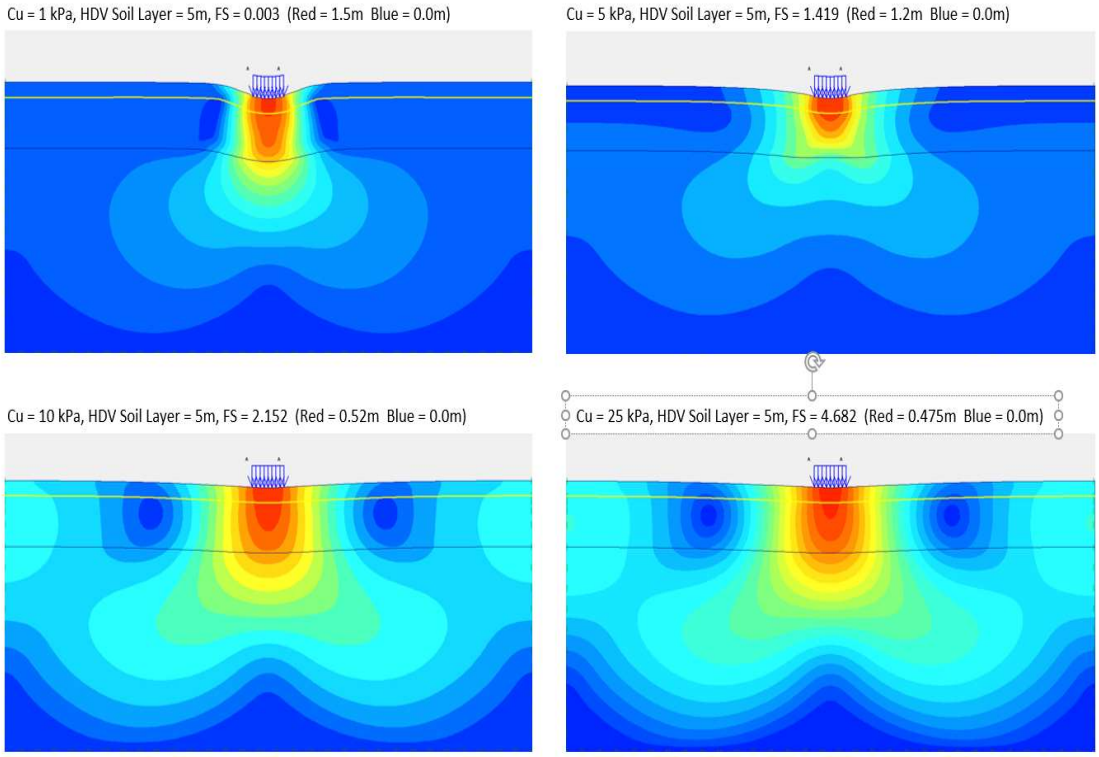

Figure 7.40 Displacement envelopes at different shear strength at 5m of treated clay

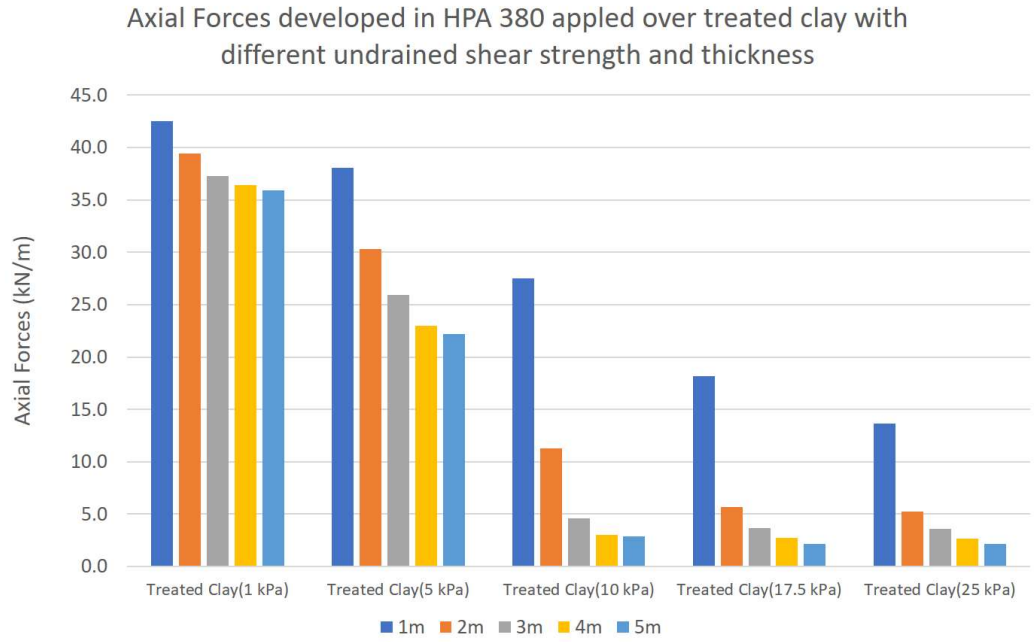

Figure 7.41 Axial forces developed at different shear strength and thickness

Figure 7.41 shows the axial forces developed in the HPA 380 at various shear strengths and soil thickness. Generally, axial forces developed in the geotextile decrease with increasing shear strength and thickness of the improved clay layer. The axial forces developed in the geotextile was highest when the shear strength of the improved soils was at 1 kPa, that is, on original soil without improvement. The high tensile forces of over 35 kN/m developed in the geotextile could rupture the geotextile and caused failure to the working platform when the working load was applied. When the shear strength of the soil layer was at 5 kPa, axial forces developed on the geotextile were mostly maintained at 20kN/m or slight above. Such forces may not have ruptured an integrated piece of geotextile but may find its way to cause failure at the joints where the geotextiles were sewed together by stiches and the locations where localised damaged would resulted in a reduction of the geotextile strength.

The axial forces decreased tremendously when the undrained shear strength of the soil layer reached 10 kPa. The significant difference in the axial forces developed between soil layer with 1m and 2m thickness would have greatly reduce the axial

forces developed in the geotextile and reduce the risks of rupture. From the operational perspective, adopting the proposed method of vacuum preloading with horizontal drains to improve merely 1m of the highly compressible soils should not be even be considered as it would not be practical and cost effective to put in the required resources, manpower and time.

7.6.2 Working platform formed by improving the top soft soil layer

7.6.2.1 Geometry model

This proposed alternative method used the same base geometry model of 65 m width and 26.5 m depth as presented in Figure 7.42. The phreatic water level was set at 0.00 m. The compressible soil layer was considered as clay slurry with an undrained shear strength of 0.1 kPa. It was assummed that the top 5 m of slurry to be improved by vacuum preload with horizontal drains to a soil with an undrained shear strength of 1, 5, 10, 17.5 and 25 kPa respectively. The thickness of the improved clay layer was assumed to be 1, 2, 3, 4 and 5 m respectively. The design working load of 25kN/m spanning 4m was applied directly at the surface of the improved soil layer in the middle of the geometry model.

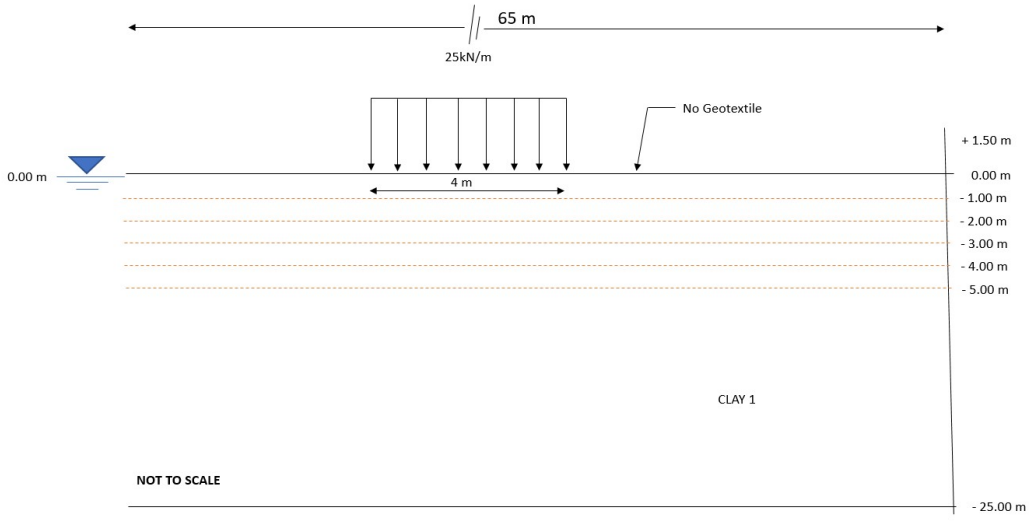

Figure 7.42 Geometry model on forming working platform directly from soft clay improved by vacuum preloading with horizontal/vertical drains

7.6.2.2 Model set up and materials

Mohr Coulomb material model was used to simulate the behaviour of the improved soil layers and the highly compressible soils underneath as a simple first analysis of the problem considered. The improved soil layers and the deposited highly compressible dredged materials were modelled as undrained condition. The soil properties are summarised in Table 7.3. The stability analysis of the working platform has been carried out using Plaxis 2D.

7.6.2.3 Results & analysis

Figure 7.43 shows the Factor of Safety computed by Plaxis 2D. The range of shear strength and thickness of the improved soil layers investigated were only meaningful from 10 kPa and above and between 3-5 m respectively. Based on the output of the Plaxis 2D models, anything lower than the prescribed ranges did not generate useful data points to carry out the investigation. It was observed in Figure 7.44 that the Plaxis 2D model adopted were not able to compute the Factor of Safety for improved soil layers with shear strength of 1 kPa and 5 kPa. This was attributed to the fact that the soils were too weak to provide any form of bearing capacity for the design working load at 25 kN/m. The application of the design working load on the improved soil layers (Cu at 1kPa and 5 kPa) would have resulted in direct shearing through them as revealed in Figure 7.44 by the displacement arrows and the vertically elongated deformation profile.

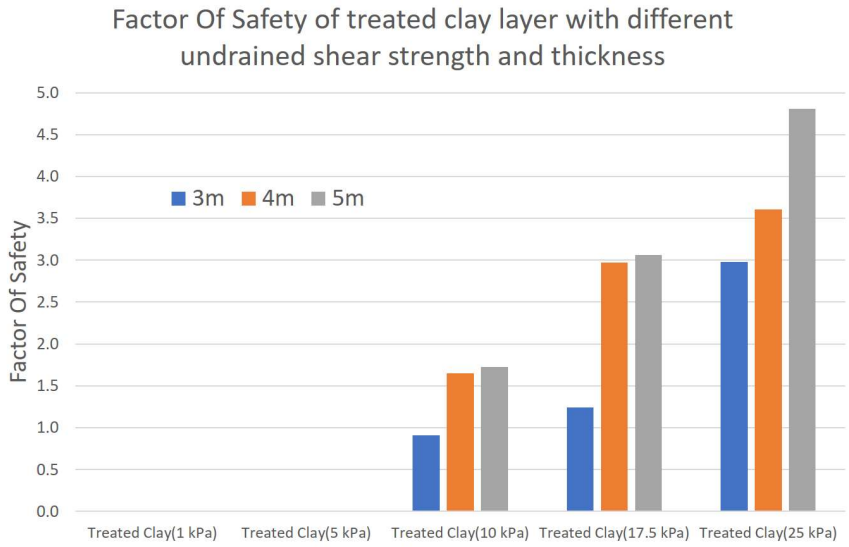

Figure 7.43 Factor of safety at different undrained shear strength and thickness

Within the clusters with shear strength of 10 kPa and 17.5 kPa, the computed increment in the Factor of Safety between improved soil layer thickness at 3m and 4m were found to be high relative to the treated clay layer with thickness between 4m and 5m. Within these two clusters, the computed Factor of Safety for the improved soil layer with 3m thickness were below the design requirement of providing a Factor of Safety of at least 1.5. Based on visual inspections of the generated bar chart in Figure 7.45, the increment of the Factor of Safety within the cluster with shear strength of 25 kN/m were found to be more progressive and more evenly spaced out. From this observation, we can say that the development of Factor of Safety - Stability in the improved soil layers with higher shear strength and thickness were more predictable exhibiting linearly increasing characteristics while soil layers with lower shear strength and thickness are less predictable.

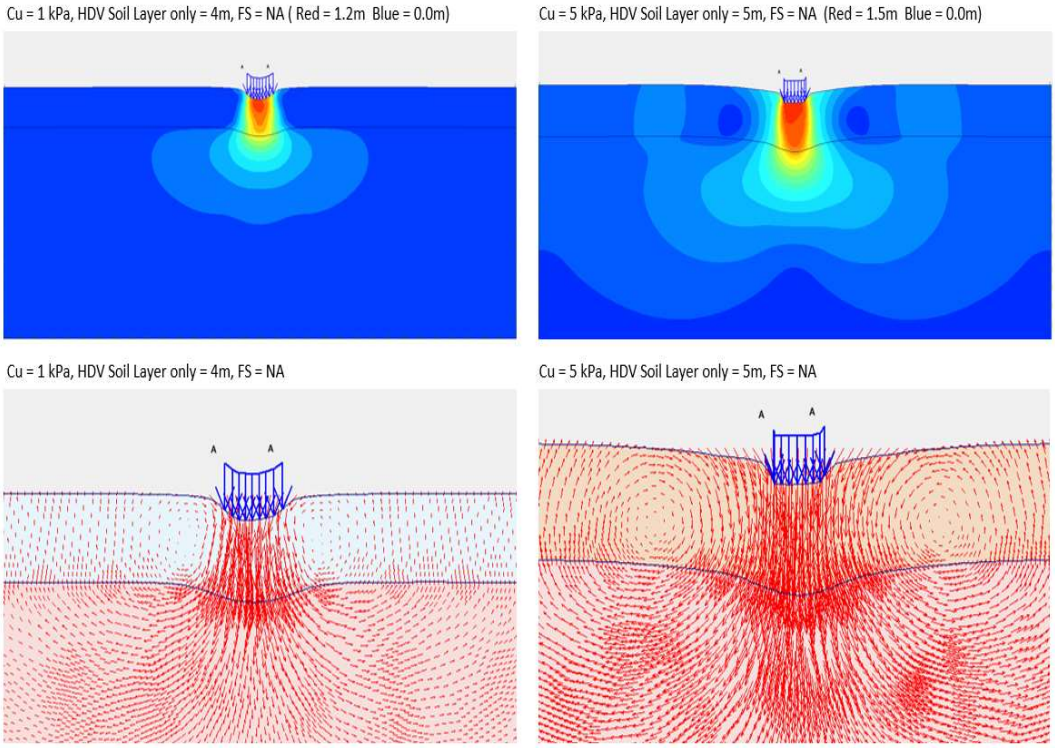

Figure 7.44 Displacement envelopes and arrows at 1 and 5 kPa shear strength at 4m and 5m treated clay thickness respectively

The Factor of Safety between the geotextile reinforced working platform and the proposed alternative method of forming the working platform with improved soil layers by vacuum preloading with horizontal drains are presented in Figure. 7.45.

Figure 7.45 Safety factor comparison between different working platforms design

From the observations made in the improved soil layer with Cu = 10 kPa, when the shear strength of soil was low, the computed safety factors in the geotextile-sand working platform regardless of soil thickness were higher than the proposed alternative working platform. For improved soil layers with higher shear strength (Cu = 17.5 and 25 kPa), the safety factor for the working platform design with no geotextiles and sand at with thicker layers (4m and 5m) of treated clay turns out to be slightly higher. Such phenomenon was not fully understood and is recommended for further investigations in future studies. The difference in deformation profiles are

presented in Figure 7.46. It should be noted that such observations with extended displacement envelope were not found with thinner improved soil layer (3m).

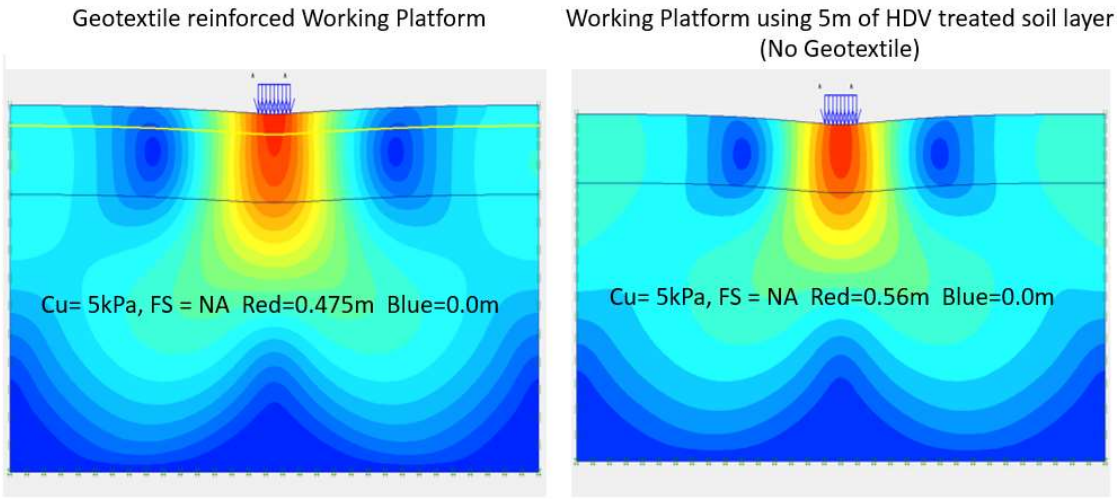

Figure 7.46 Displacement envelopes of working platforms with/without reinforcing geotextile

The Plaxis 2D analyses had provided further evidence that when the highly compressible soil layer was improved to a reasonable undrained shear strength with the improved layer to be sufficiently thick, the proposed alternative platform could provide the required stability and safety factor to allow construction works with a design working load of 25 kN/m to be carried out above the improved soil layers. The recommended shear strength and improved thickness shall be at least 10 kPa with a recommended thickness of 5m which could be achieved on site reasonably with low risks. This proposed alternative method of using only vacuum preloading with horizontal drains to improve soft soil layer if executed and coordinated properly at site has tremendous potential to bring about time, materials and overall cost savings.

7.8 Conclusions

In this chapter, a new innovative soil improvement method using vacuum preloading and horizontal drains was proposed. Two laboratory model tests using horizontal drains in clay slurry to verify the effectiveness of the proposed method was carried out presented. Other methods for the formation of working platform were also studied

using Plaxis 2D numerical analyses. Based on the observed outcome of the studies, the follow key observations and conclusions are made:

i. The model tests have demonstrated that the proposed vacuum preloading with horizontal drain were effective in consolidating the marine slurry samples. The marine clay samples in both model tests achieved approximately 30% reduction in volume. The water content of the marine clay samples reduced from the initial water content of 140% to 50-60%. The average Degree of Consolidation achieved was approximately 75% of consolidation after 2,230 hrs for single horizontal drain model test and 1,000 hrs for double layered horizontal drains model test.

ii. The pore pressures measurement verified that the vacuum experienced in the clay slurry reduced with distance from the horizontal drains. Undrained shear strength measurement of the consolidated marine clay was found highest nearest to the horizontal drains and dropped drastically with distance from the horizontal drains.

iii. The single horizontal drain model test was carried out for 2,230 hours of while the double layered horizontal drains model test took about 1,000 hours to achieved similar soil improvement outcomes for the marine clay samples. The observations conclude that the performance of the proposed method of vacuum preloading with horizontal drains can be significantly affected by the quantities and spacing of the horizontal drains.

iv. The numerical study using the Plaxis 2D demonstrated that the geotextile reinforced-sand capped working platform can achieve a high Factor of Safety and controlled displacement with the improvement of only the top few meters of the clay slurry underneath the geotextiles.

v. The numerical analyses using Plaxis 2D has also demonstrated that it is possible to form a working platform by treating the top few meters of slurry soil without the use of geotextile and sand capping layer.

vi. The proposed method of using vacuum preloading with horizontal drains can help to overcome many site constraints and operation challenges described in chapter 6 to pre-improve the hydraulic dredged slurry deposits with the benefits of time savings, increasing storage and reduced settlement.

CHAPTER 8 CONCLUSIONS & RECOMMENDATIONS

8.1 Conclusions

In view of the rising demand and shortage of sand fill, dredged seabed materials are proposed as an alternative fill for land reclamation. However, to optimize the use of dredged materials and to account for their large reduction of volume during soil improvement, dredged materials are proposed to be placed beyond existing reclamation platform level. This can be done by hydraulic dredging and infilling of seabed material into containment bund by cutter suction dredgers.

During hydraulic infilling, the soil fabrics of the dredged material are destroyed when the dredged soil are mixed and fluidized with large amount of seawater to form slurry. The dredged slurry can be conveyed quickly from the dredging site to the infill sites via connected floating pipes. Although such a hydraulic approach is efficient and economical to handle large quantities of dredged materials, it also brings about different sets of technical and site operations challenges.

Two key challenges that could impede the adoption of the hydraulically placed slurry soil dredged from the sea for land reclamation purpose are identified. Firstly, the natural sedimentation process of the suspended solid particles in the dredged slurry suspension is time-consuming. The time needed for sedimentation would have easily exceeded the timeframe given for typical reclamation project. Secondly, the remolded sediments from the hydraulic infilling have no strength and bearing capacity to support any form of land-based construction. The aim of this thesis is to investigate further into the two identified challenges through laboratory model tests, field trials and numerical analyses to develop suitable solutions to overcome the implementation and construction challenges associated with the use of clay slurry for land reclamation. The main conclusions that can be derived from this study are given as follows.

1. Chapter Three examined natural and flocculant assisted sedimentation process of dredged slurry. Multiple natural settling column tests using different

compositions of natural marine clay-silt suspensions were carried out. The experiments concluded that soil suspensions with higher composition of silts and lower composition of clay had faster settling rate and experience greater self-weight consolidation. Among the 9 different types of PAM polymers employed to expedite the sedimentation process, CPAM +15 was assessed to be most the effective. It was noted in the model tests that low water content in flocculant treated soil suspensions would lead to erratic sedimentation behaviors, while higher water content would lead to more settlement and increase settling rate for the suspended particles. SEM images revealed that clay particles in flocculant-treated soil suspensions would lead to formation of randomly oriented clay particles clusters with edge-to-edge contacts. Although the use of flocculant did expedite the sedimentation process, but it had also modified the sediment's fabric in such a way that it could cause larger consolidation in sediments with slower consolidation rate. As such, when considering the use of flocculant to expedite the sedimentation process, it is important to balance the flocculant's positive effects in sedimentation and its negative influence on the sediment's consolidation.

2. Vacuum preloading has been identified as the most suitable treatment method to improve the ultra-soft cohesive sediments from hydraulic dredging. In Chapter Four, 4 comparison studies were carried out to investigate the design variables that could affect the performance of vacuum preload systems via laboratory model tests carried out using a highly instrumented single PVD cylindrical consolidation tank. Generally, all model tests showed the effects of vacuum decreased with increasing distance from the source of vacuum (PVD). Comparison study 1 concluded that the vacuum preloading technique was effective to treat different clay samples, but at different consolidation rates and with different magnitude of settlement. In comparison study 2, for a given PVD length in the consolidation tank, the circular drain gave higher settlement rate than the band drain. Experiment results in Comparison study 3 showed that the horizontal gravel layer in the membrane vacuum preloading system was more effective and faster in consolidating the soil samples when compared to the

membraneless vacuum preload system. In Comparison study 4, the additional 40kPa loading was effective to further increase the undrained shear strength and improved other soil parameters of the clay sample in the model test.

3. Chapter Five presented a pilot trial using combined membraneless vacuum and surcharge preload to treat the marine clay layer of a newly reclaimed land. Site conditions, challenges encountered, field observations and performance of the proposed method were examined. The membraneless vacuum preload system would require accurate information of the underlying soil layer profiles to reduce vacuum leakages. High variations in performance were observed in the field trial were mainly attributed to the frequent pumps shut downs and delay in rectification of these shut downs. Nevertheless, the field trial results still showed strong evidence that membraneless vacuum preloading system was effective to some extend to improve the properties of the in-situ marine clay layer.

4. Chapter Six presented a large scaled pilot field trial within an on-going reclamation project. In this field trial, a confinement facility was constructed to allow the infilling of dredged seabed slurry above the elevation of the final reclaimed land platform. The infilling of the confinement facility with dredged slurry using Cutter-Suction Dredger and good earth dumping by trucks took about 5 months due to the time-consuming sedimentation process of the soil suspensions. Hydramotion Mudbug was deployed to determine the real-time density status of the slurry suspensions. This information provided by the Mudbug helped to shorten the infilling cycle's intervals. About 600,000m^3 of materials were deposited into the confinement facility with an average bulk density of 1.35kg/m^3 and average water content of 185%. The top layer improvement of the deposited slurry with desiccation and shallow trenching methods were assessed to be unproductive and ineffective.

5. A method to install a load bearing working platform consisting of woven geotextile and 1.5m of sand over the ultra-soft sediments was tried out. However, the geotextile installation was hindered and stopped multiple times to facilitate

repair works on the damaged geotextiles. The placement of the 1.5 m sand capping was proven difficult as the hydraulically placed sand would form deep sand pockets in the geotextiles. To mobilize the tension in the geotextiles to support future construction loads, geotubes were placed over the geotextiles to create controlled deformations. The sinking and heaving deformations provided the stabilizing effects to allow dry sand placement over the geotextiles. Unfortunately, the working platform failed and resulted in the squeezing out of the dredged slurry placed underneath the geotextiles. The failure of the working platform was due to the contractor's decision to accelerate the placement on the third sand layer before completion of the second layer. This resulted in uneven stresses acting on the geotextiles causing the weakest part to fail and rupture. Post investigation showed that part of the installed geotextile-geotubes platform had sunk several meters into the confinement facility.

6. Chapter Seven proposed an innovative soil improvement method using vacuum preloading with modified prefabricated horizontal drains to overcome the site challenges and constraints encountered in the construction of the geotextile reinforced working platform discussed in Chapter 6. The proposed technique involves the placement of the modified prefabricated horizontal drains in the seabed before and during dredged slurry infilling. Once there are sufficient materials cover to seal the horizontal drains, vacuum pressure can be applied to consolidate the dredged slurry. Two laboratory model tests were carried out to verify the new proposed method. The model tests confirmed that the proposed method was effective in improving the engineering properties of the dredged slurry. Generally, the volume of the dredged slurry fill was reduced by 30% and the water content was reduced from 140% or above to 50-60%. The average Degree of Consolidation achieved was approximately 75% for both model tests.

7. Numerical analyses using Plaxis 2D were adopted to study the deformation and stress distribution of the load bearing working platform. The study showed that with the slight improvement to the undrained shear strength of only the top few meters of the slurry together with the use of geotextile and 1.5 m thick sand

capping, a working platform with high Factor of Safety and controlled displacement could be achieved. The numerical analyses also showed that it was possible to form a working platform without the use of geotextile and sand capping layer by improving the undrained shear strength of the top 4 m of slurry soil to above 17.5 kPa.

8.2 Recommendations

8.2.1 Study of salt concentration effects on sedimentation process

Polyacrylamide (PAM) is a water-soluble high molecular weight synthetic organic polymer that primarily interacts with the clay fraction of the soil suspension. Although PAM has been shown to be non-toxic to humans, animals, fishes, and plants; the only concern has been the toxicity of its residual monomers (acrylamide) content, which is a known neurotoxin to human (Seybold, 1994). Since the residual acrylamide monomer content in PAM product has potential risks, it is not encouraged to use PAM as flocculant to expedite in sedimentation process of the dredged slurry infill for reclamation works. Imai (Imai, 1980) studies of the settling behavior of clay suspensions have pointed out that the concentration of salt in the soil suspensions can affect the degree of flocculation in the soil suspension. The manipulation of the salt concentrations in the dredged slurry suspension is considered less risky with less adverse health and environmental impacts. As such, laboratory model tests and larger scaled field trials are proposed to further investigate the mechanism and effectiveness of using salt to expedite the sedimentation process of dredged slurries.

8.2.2 Investigate the mechanism of the applied vacuum in the band and circular drains

The results of the single PVD cylindrical consolidation tank model tests in chapter 4 demonstrated that under the membrane vacuum preload conditions, the circular drain was more effective than the normal band drain in delivering vacuum to the soil matrix resulting in faster and larger soil consolidation. It is proposed to carry out laboratory model tests to further investigate the difference in the mechanism of the applied

vacuum in the band drains and circular drains to improve compressible soils and dredged slurry.

8.2.3 Development of user defined soil model for newly formed sediment-soils

Mohr-Coulomb soil model was used as a simple first approximation of the possible elastoplastic soil behaviors considered in this thesis. Although the Mohr-Coulomb model is based on soil parameters namely Young's modulus, Poisson Ratio, Cohesion, Friction Angle and Dilatancy Angle which are well-known in engineering practice, they do not accurately reflect all features and the complex behavior of newly formed sediment-soil which is high in water content, undergoing self-weight consolidation and will induced large deformation when subjected to loading. To better model the behavior of the newly formed sediment-soils, it is proposed to develop more advanced user-defined soil models with new additional parameters and verified the predicted sediment-soil behaviors and response with corresponding laboratory model tests.

8.2.4 Scaled model tests to verify the performance of the proposed innovative soil improvement method

It is proposed to carry out a scaled model tests using a large open consolidation tank to mimic the plaxis models described in Chapter 8.6 and 8.7. The purpose is to examine, verify and compare the response and performance between the numerical analyses and the laboratory model tests. This will provide important information for further development of the proposed innovative soil improvement method.

8.2.5 Proposed pilot field trial using proposed innovative soil improvement method

Both laboratory model tests and plaxis analyses using Mohr-Coulomb soil model have shown positive outcomes on the applications of the proposed innovative soil improvement method to pre-treat the top layers of the newly formed sediment-soils. A pilot field trial is thus proposed to further assess the technical and operational feasibilities and economical viability of the proposed innovative soil improvement method for future implementation.

REFERENCES

ABU-HEJLEH, A. N. & ZNIDARČIĆ, D. 1995. Desiccation theory for soft cohesive soils. *Journal of Geotechnical Engineering,* 121**,** 493-502.

ADAMS, M. T. & COLLIN, J. G. 1997. Large model spread footing load tests on geosynthetic reinforced soil foundations. *Journal of Geotechnical and Geoenvironmental Engineering,* 123**,** 66-72.

ASAOKA, A. 1978. Observational procedure of settlement prediction. *Soils and foundations,* 18**,** 87-101.

ATALAH, A. 2006. Safe distance between large-diameter rock pipe bursting and nearby buildings and buried structures. *Journal of transportation engineering,* 132**,** 350-356.

BARRON, R. A. 1948. Consolidation of fine-grained soils by drain wells. *ACSE,* 74**,** 875.

BARTHOLOMEEUSEN, G., SILLS, G., ZNIDARCIC, D., VAN KESTEREN, W., MERCKELBACH, L., PYKE, R., CARRIER, W., LIN, H., PENUMADU, D. & WINTERWERP, H. 2002. Sidere: numerical prediction of large-strain consolidation.

BEEN, K. & SILLS, G. 1981. Self-weight consolidation of soft soils: an experimental and theoretical study. *Geotechnique,* 31**,** 519-535.

BERGADO, D., ANDERSON, L., MIURA, N. & BALASUBRAMANIAM, A. Soft Ground Improvement in Lowland and Other Environments. 1996. ASCE.

BERGADO, D., CHAI, J., MIURA, N. & BALASUBRAMANIAM, A. 1998. PVD improvement of soft Bangkok clay with combined vacuum and reduced sand embankment preloading. *Geotechnical Engineering,* 29.

BERGADO, D., SAOWAPAKPIBOON, J., KOVITTAYANON, N. & DE ZWART, T. BeauDrain-S PVD Vacuum System in Soft Bangkok Clay: A Case Study of the Suvarnabhumi Airport Project. The 6th Symposium on Soil/Ground Improvement and Geosynthetics, Bangkok, 2006.

BLIGHT, G. E. Some less familiar aspects of hydraulic fill structures. Hydraulic Fill Structures, 1988. ASCE, 1000-1027.

BO, M., NA, Y., ARULRAJAH, A. & CHANG, M. 2009. Densification of granular soil by dynamic compaction. *Proceedings of the ICE-Ground Improvement,* 162**,** 121-132.

BO, M. W. 2008. *Compressibility of ultra-soft soil*, World Scientific Publishing Co Inc.

BO, M. W. & CHOA, V. 2004. *Reclamation and ground improvement*, Thomson Learning Asia.

BOER, R. D., SCHIFFMAN, R. & GIBSON, R. E. 1996. The origins of the theory of consolidation: the Terzaghi—Fillunger dispute. *Geotechnique,* 46**,** 175-186.

BOSKALIS. 2017. *Floating Grab Cranes Equipment Sheet* [Online]. Boskalis. Available: https://boskalis.com/about-us/fleet-and-equipment/dredgers/floating-grab-cranes.html [Accessed].

BOURDEAU, P. L., HARR, M. E. & HOLTZ, R. D. 1982. *Soil fabric interaction: an analytical model*, Ecole Polytechnique Fédérale de Lausanne, Laboratoires de Mécanique des Sols et des Roches.

BRONS, B. B. 1987. Stabilization of very soft clay using geofabric. *Geotextiles and Geomembranes,* 5**,** 17-28.

CARRIER, W. & BROMWELL, L. Disposal and reclamation of mining and dredging wastes. Proceedings of the Seventh Panamerican Conference on Soil Mechanics and Foundation Engineering, Vancouver, Canada, 1983.

CHAI, J., CARTER, J. & HAYASHI, S. 2005. Ground deformation induced by vacuum consolidation. *Journal of geotechnical and geoenvironmental engineering,* 131**,** 1552-1561.

CHAI, J., MIURA, N. & BERGADO, D. 2008. Preloading clayey deposit by vacuum pressure with cap-drain: analyses versus performance. *Geotextiles and Geomembranes,* 26**,** 220-230.

CHANG, M.-F., YU, G., NA, Y.-M. & CHOA, V. 2006. Evaluation of relative density profiles of sand fill at a reclaimed site. *Canadian geotechnical journal,* 43**,** 903-914.

CHOA, V. Drains and vacuum preloading pilot test. PROC INT CONF SOIL MECH FOUND ENG, A. A. BALKEMA, ROTTERDAM,(NETH), 1989, 1989. 1347-1350.

CHU, J., BO, M. & CHOA, V. 2004. Practical considerations for using vertical drains in soil improvement projects. *Geotextiles and Geomembranes,* 22**,** 101-117.

CHU, J. & YAN, S. 2005a. Application of the vacuum preloading method in soil improvement projects. *Elsevier Geo-Engineering Book Series,* 3**,** 91-117.

CHU, J. & YAN, S. 2005b. Estimation of degree of consolidation for vacuum preloading projects. *International Journal of Geomechanics,* 5**,** 158-165.

CHU, J., YAN, S. & LAM, K. P. 2012. Methods for improvement of clay slurry or sewage sludge. *Proceedings of the Institution of Civil Engineers-Ground Improvement,* 165**,** 187-199.

CHU, J., YAN, S. & YANG, H. 2000. Soil improvement by the vacuum preloading method for an oil storage station. *Geotechnique,* 50**,** 625-632.

COVO-TORRES, Á., ELJAIEK-URZOLA, M. & VIVAS-REYES, R. 2015. Radial Consolidation for equal strain with resistance in the vertical drain. *Soil and Tillage Research,* 145**,** 87-92.

ESPINOZA, R. D. 1994. Soil-geotextile interaction: evaluation of membrane support. *Geotextiles and Geomembranes,* 13**,** 281-293.

ESPINOZA, R. D. & BRAY, J. 1995. An integrated approach to evaluating single-layer reinforced soils. *Geosynthetics International,* 2**,** 723-739.

FITCH, B. 1966. Mechanism of sedimentation. *Industrial & Engineering Chemistry Fundamentals,* 5**,** 129-134.

FITCH, B. 1979. Sedimentation of flocculent suspensions: state of the art. *AIChE Journal,* 25**,** 913-930.

FITZSIMONS, M. 2017. Development of mega cutter suction and trailer suction hoper dredgers and related projects in Canada. DREDGING SUMMIT & EXPO '17 2017 Vancouver.

FREDLUND, D. G. & RAHARDJO, H. 1993. *Soil mechanics for unsaturated soils*, John Wiley & Sons.

GEOTECHNICAL_OBSERVATION. *Piezometers* [Online]. Available: http://www.geo-observations.com/piezometers/ [Accessed].

GIBSON, R., ENGLAND, G. & HUSSEY, M. 1967. The Theory of One-Dimensional Consolidation of Saturated Clays: 1. Finite Non-Linear Consildation of Thin Homogeneous Layers. *Geotechnique,* 17**,** 261-273.

GIROUD, J.-P. & NOIRAY, L. 1981. Geotextile-Reinforced Unpaved Road Design. *Journal of the Geotechnical Engineering Division,* 107**,** 1233-1254.

GIROUD, J., AH-LINE, C. & BONAPARTE, R. 1984. Design of unpaved roads and trafficked areas with geogrids. *Polymer grid reinforcement.* Thomas Telford Publishing.

GORDON, R. B. & MITCHELL, J. K. 1976. Fundamentals of Soil Behavior. JSTOR.

GREGORY, J. 1988. Polymer adsorption and flocculation in sheared suspensions. *Colloids and Surfaces,* 31**,** 231-253.

GRIFFIN, H. & O'KELLY, B. C. 2014. Ground improvement by vacuum consolidation–a review. *Proceedings of the Institution of Civil Engineers-Ground Improvement,* 167**,** 274-290.

GRIM, R. 1959. Physico-chemical properties of soils: Clay minerals. *Journal of the Soil Mechanics and Foundations Division, ASCE,* 85**,** 1-17.

GUIDO, A., BIESIADECKI, G. & MJ, S. 1985. Bearing capacity of a geotextile-reinforced foundation.

HANSBO, S. 1976. Consolidation ofclay by band-shaped prefabricated drains. *Ground Engineering,* 12**,** 21.

HANSBO, S. 1981. Consolidation of fine-grained soils by prefabricated drains. *Proc. 10th ICSMFE, 1981,* 3**,** 677-682.

HANSBO, S. 1994. *Foundation engineering,* Amsterdam, Elsevier Science.

HAUSMANN, M. R. 1990. *Engineering principles of ground modification*, McGraw-Hill.

HE, J., CHU, J., TAN, S. K., VU, T. T. & LAM, K. P. 2017. Sedimentation behavior of flocculant-treated soil slurry. *Marine Georesources & Geotechnology,* 35**,** 593-602.

HIGLEY, D. K., PANTEA, M. P. & SLATT, R. M. 1997. *3-D Reservior Characterisation of the House Creek Pil Field River Basin, Wyoming* [Online]. US: United State Department of the Interior, U.S Geological Survey. Available: https://pubs.usgs.gov/dds/dds-033/USGS_3D/ssx_txt/3dstart.htm [Accessed].

HOLTZ, R. D., JAMIOLKOWSKI, M., LANCELLOTTA, R. & PEDRONI, R. 1991. *Prefabricated vertical drains: design and performance,* Oxford, Butterworth -Heinemann Ltd.

HOLTZ, R. D. & KOVACS, W. D. 1981. *An introduction to geotechnical engineering*.

HOLTZ, R. D. & WAGER, O. 1975. Preloading by vacuum: current prospects. *Transportation Research Record*.

IMAI, G. 1980. Settling behavior of clay suspension. *Soils and Foundations,* 20**,** 61-77.

IMAI, G. 1981. Experimental studies on sedimentation mechanism and sediment formation of clay materials. *Soils and Foundations,* 21**,** 7-20.

INDRARATNA, B. & REDANA, I. 1998. Laboratory determination of smear zone due to vertical drain installation. *Journal of geotechnical and geoenvironmental engineering,* 124**,** 180-184.

INDRARATNA, B. & RUJIKIATKAMJORN, C. 2008. Effects of partially penetrating prefabricated vertical drains and loading patterns on vacuum consolidation. *GeoCongress 2008: Geosustainability and Geohazard Mitigation.*

INDRARATNA, B., RUJIKIATKAMJORN, C., AMERATUNGA, J. & BOYLE, P. 2011. Performance and prediction of vacuum combined surcharge consolidation at Port of Brisbane. *Journal of Geotechnical and Geoenvironmental Engineering,* 137**,** 1009-1018.

INGOLD, T. S. 2013. *Geotextiles and geomembranes handbook*, Elsevier.

JAMIOLKOWSKI, M. Precompression and speeding up consolidation. Proceedings, Eighth European Conference on Soil Mechanics and Foundation Engineering, 1983 Helsinki. AA Balkema, 1201-1226.

JEWELL, R. 1996. *Soil reinforcement with geotextiles*, Construction Industry Research and Information Association.

JEWELL, R. & WROTH, C. 1987. Direct shear tests on reinforced sand. *Geotechnique,* 37**,** 53-68.

JOHN, N. W. 1987. *Geotextiles*, Blackie. Chapman and Hall.

JOHNSON, S. J., CUNNY, R. W., PERRY, E. B. & DEVAY, L. 1977. State-of-the-art applicability of conventional densification techniques to increase disposal area storage capacity. ARMY ENGINEER WATERWAYS EXPERIMENT STATION VICKSBURG MS.

KANMON. 2017. *Kanmon Company's Webpage* [Online]. Available: http://www.kanmon-const.co.jp/English/youdo/youdo-index.html [Accessed].

KJELLMAN, W. 1952. Consolidation of Clay by Mean of Atmosperence on Soil Stabilization. *M IT*.

KWT, S. 2015. *Reclamation by Pelican Barge- Bay island north* [Online]. Available: https://www.youtube.com/watch?v=KXaRfqnRdqw [Accessed].

KYNCH, G. J. 1952. A theory of sedimentation. *Transactions of the Faraday society,* 48**,** 166-176.

LAMBE, T. W. 1958. The Structure of Compacted Clay. *Journal of the Soil Mechanics and Foundations Division,* 84**,** 1-34.

LEE, K. M., SHEN, C., LEUNG, D. & MITCHELL, J. 1999. Effects of placement method on geotechnical behavior of hydraulic fill sands. *Journal of Geotechnical and Geoenvironmental Engineering,* 125**,** 832-846.

LEE, S., KARUNARATNE, G., YONG, K. & GANESHAN, V. 1987. Layered clay-sand scheme of land reclamation. *Journal of geotechnical engineering,* 113**,** 984-995.

LOVE, J., BURD, H., MILLIGAN, G. & HOULSBY, G. 1987. Analytical and model studies of reinforcement of a layer of granular fill on a soft clay subgrade. *Canadian Geotechnical Journal,* 24**,** 611-622.

LUTENEGGER, A. 1995. Geotechnical behavior of overconsolidated surficial clay crusts. *Transportation research record,* 1479**,** 61.

MADHAV, M. & POOROOSHASB, H. 1989. Modified Pasternak model for reinforced soil. *Mathematical and Computer Modelling,* 12**,** 1505-1509.

MADHAV, M. R. & POOROOSHASB, H. B. 1988. A new model for geosynthetic reinforced soil. *Computers and Geotechnics,* 6**,** 277-290.

MASSE, F., SPAULDING, C. A., WONG, I. C. & VARAKSIN, S. Vacuum consolidation: A review of 12 years of successful development. Proceedings of the GeoOdyssey 2001 Conference, 9th–13th June, 2001.

MCGOWN, A., ANDRAWES, K. & AL-HASANI, M. 1978. Effect of inclusion properties on the behaviour of sand. *Geotechnique,* 28**,** 327-346.

MCROBERTS, E. & NIXON, J. 1976. A theory of soil sedimentation. *Canadian Geotechnical Journal,* 13**,** 294-310.

MND Land Use Plan, 2013. Land Use Plan to Support Singapore's Future Population: A High Quality Living Environment For All Singaporeans.

MND Population White Paper, 2013. Population White Paper: A Sustainable Population For A Dynamic Singapore. *In:* DIVISON, N. P. A. T. (ed.).

MORRIS, P. H., GRAHAM, J. & WILLIAMS, D. J. 1992. Cracking in drying soils. *Canadian Geotechnical Journal,* 29**,** 263-277.

MPOFU, P., ADDAI-MENSAH, J. & RALSTON, J. 2003. Investigation of the effect of polymer structure type on flocculation, rheology and dewatering behaviour of kaolinite dispersions. *International Journal of Mineral Processing,* 71**,** 247-268.

NASSER, M. & JAMES, A. 2006. The effect of polyacrylamide charge density and molecular weight on the flocculation and sedimentation behaviour of kaolinite suspensions. *Separation and purification technology,* 52**,** 241-252.

PARK, H., LEE, S.-R. & JEE, S.-H. 2014. Cover Placement on Dredged Marine Clay Reclaimed Deposit. *Marine Georesources & Geotechnology,* 32**,** 38-61.

PEARSE, M. & BARNETT, J. 1980. Chemical treatments for thickening and filtration. *Filtration and Separation,* 17**,** 465-468.

QIAN, J., ZHAO, W. B., CHEUNG, Y. & LEE, P. 1992. The theory and practice of vacuum preloading. *Computers and Geotechnics,* 13**,** 103-118.

SCHIFFMAN, R. L., PANE, V. & GIBSON, R. E. The theory of one-dimensional consolidation of saturated clays: IV. An overview of nonlinear finite strain sedimentation and consolidation. Sedimentation and Consolidation Models: American Society of Civil Engineers Geotechnical Engineering Division Symposium, San Francisco, California, Proceedings, 1984. 1-29.

SEAFCO Prefabricated Vertical Drains Ground Improvement Technique. *In:* IMPROVEMENT, S. G. (ed.). Seafco Construction Engineering Company.

SEAH, T. H. 2006. Design and construction of ground improvement works at Suvarnabhumi Airport. *Geotechnical Engineering,* 37**,** 171.

SELLMEIJER, J. Design of geotextile reinforced paved roads and parking areas. Proceedings of the Fourth International Conference on Geotextiles, Geomembranes and Related Products, 1990. 177-182.

SELLMEIJER, J., KENTER, C. & VAN DEN BERG, C. Calculation method for a fabric reinforced road. Proceedings of the second international conference on geotextiles, 1982. 393-398.

SEYBOLD, C. 1994. Polyacrylamide review: Soil conditioning and environmental fate. *Communications in Soil Science & Plant Analysis,* 25**,** 2171-2185.

SHIN, H. & SANTAMARINA, J. 2011. Desiccation cracks in saturated fine-grained soils: particle-level phenomena and effective-stress analysis. *Géotechnique,* 61**,** 961-972.

SHUKLA, S. K. 2011. *Handbook of geosynthetic engineering*, ICE Publishing.

SHUKLA, S. K. & CHANDRA, S. 1994. A generalized mechanical model for geosynthetic-reinforced foundation soil. *Geotextiles and Geomembranes,* 13**,** 813-825.

SILLS, G. 1998. Development of structure in sedimenting soils.

SRIDHARAN, A. & RAO, A. S. 1981. Rectangular hyperbola fitting method for one dimensional consolidation.

STAPELFELDT, T. 2006. Preloading and vertical drains. *Electronic publication, http://www. tkk. fi/Yksikot/Rakennus/Pohja/Preloading_and_vertical_drains. pdf*.

SYSTEMINDO, G. Prefabricated Vertical Drains. Geotechnical Systemindo.

TAN, S.-A., LIANG, K.-M., YONG, K.-Y. & LEE, S.-L. 1992. Drainage efficiency of sand layer in layered clay-sand reclamation. *Journal of geotechnical engineering,* 118**,** 209-228.

TAN, T., YONG, K., LEONG, E. & LEE, S. 1990. Behaviour of clay slurry. *Soils and Foundations,* 30**,** 105-118.

TANG, C.-S., CUI, Y.-J., SHI, B., TANG, A.-M. & LIU, C. 2011. Desiccation and cracking behaviour of clay layer from slurry state under wetting–drying cycles. *Geoderma,* 166**,** 111-118.

TOORMAN, E. 1999. Sedimentation and self-weight consolidation: constitutive equations and numerical modelling. *Géotechnique,* 49**,** 709-726.

TORY, E., BÜRGER, R., CONCHA, F. & BUSTOS, M. 2013. *Sedimentation and thickening: Phenomenological foundation and mathematical theory*, Springer Science & Business Media.

TOWNSEND, F. & MCVAY, M. 1990. SOA: Large strain consolidation predictions. *Journal of geotechnical engineering,* 116**,** 222-243.

US 2015. Dredging and Dredged Material Management Manual. USA: US Army Corps.

VAN'T HOFF, J. & VAN DER KOLFF, A. N. 2012. *Hydraulic Fill Manual: For Dredging and Reclamation Works*, CRC press.

VAN IMPE, P., VAN IMPE, W., MANZOTTI, A., MENGÉ, P., VAN DEN BROECK, M. & VINCK, K. 2015. Compaction control and related stress–strain behaviour of off-shore land reclamations with calcareous sands. *Soils and Foundations,* 55**,** 1474-1486.

WANG, L., ZHU, W., XIE, J., LI, L. & ZHANG, C. 2015. Study of the Shear Strength of Sediments in Main Sedimentation Stages. *Marine Georesources & Geotechnology,* 33**,** 556-566.

WATARI, Y. Reclamation with clayey soils and method of earth spreading on the surface. Proc., Seminar on Soil Improvement and Construction Techniques in Soft Ground, 1984. 103-119.

WELP, T. 2006. *Dredging and Dredged Materials Overview* [Online]. Available: https://www.engr.colostate.edu/~pierre/ce_old/classes/ce717/2_OverviewofDredgingandDMD_Welp.pdf [Accessed].

WESTERGAARD, H. M. 1939. *A Problem of Elasticity Suggested by a Problem in Soil Mechanics: Soft Material Reinforced by Numerous Strong Horizontal Sheets*, Harvard University.

YAMAUCHI, H. & KITAMORI, I. 1985. Improvement of soft ground bearing capacity using synthetic meshes. *Geotextiles and Geomembranes,* 2**,** 3-22.

YAN, S. & CHU, J. 2005. Soil improvement for a storage yard using the combined vacuum and fill preloading method. *Canadian Geotechnical Journal,* 42**,** 1094.

YEUNG, A. T. 1997. Design curves for prefabricated vertical drains. *Journal of geotechnical and geoenvironmental engineering,* 123**,** 755-759.

YONG, K. 1989. Coastal Reclamation in Singapore: A Review. *1D. e Experience of Singapore***,** 59.

ZEMENU, G., MARTINE, A. & ROGER, C. 2009. Analysis of the behaviour of a natural expansive soil under cyclic drying and wetting. *Bulletin of engineering geology and the environment*.

ZNIDARCIC, D., CROCE, P., PANE, V., KO, H.-Y., OLSEN, H. W. & SCHIFFMAN, R. 1984. The theory of one-dimensional consolidation of saturated clays: III. existing testing procedures and analyses.

APPENDIX

ASTM D2166 (1991) Standard Test Method for Unconfined Compressive Strength of Cohesive Soil, Annual book of ASTM Standards, 04.08, Soil and Rock (II), West Consohocken, PA: American Society for Testing and Materials.

ASTM D422-03 (1998) Standard Test Method for Measurement for Particle Size Analysis of Soils, Annual book of ASTM Standards, 04.08, Soil and Rock (II), West Consohocken, PA: American Society for Testing and Materials.

ASTM D4318 (1998) Standard Test Method for Liquid Limit, Plastic Limit and Plasticity Index of Soils, Annual book of ASTM Standards, 04.08, Soil and Rock (II), West Consohocken, PA: American Society for Testing and Materials.

ASTM D854 (1998) Standard Test Method for Specific Gravity of Soils, Annual book of ASTM Standards, 04.08, Soil and Rock (II), West Consohocken, PA: American Society for Testing and Materials.

ASTM D2487 (1998) Standard Classification of Soils for Engineering Purpose (Unified Soil Classification System), Annual book of ASTM Standards, 04.08, Soil and Rock (II), West Consohocken, PA: American Society for Testing and Materials.

ASTM D2435-90 (2003) Standard Test Method for One Dimensional Consolidation Properties of Soils, Annual book of ASTM Standards, 04.09, Soil and Rock (II), pp203-213, West Consohocken, PA: American Society for Testing and Materials.

BS 1377 (1990) Method of test for soils for civil engineering purpose. Classification Tests. British Standards Institution, London.

BS 5930 (1999) Code of practice for site investigations. British Standards Institution, London.